Department of Chemical Engineering

Designing Single Polymer Molecules as Gas Hydrate and Corrosion Inhibitors

Qi Sheng

This thesis is presented for the Degree of

Doctor of Philosophy

of

Curtin University of Technology

March 2018

DECLARATION

To the best of my knowledge and belief this thesis contains no material previously published by any other person except where due acknowledgment has been made.

This thesis contains no material that has been accepted for the award of any other degree or diploma in any university.

Qi Sheng

Signature:

Date: 17/09/2018

ABSTRACT

Corrosion and unwanted gas hydrates formation in subsea natural gas pipelines are two of the major issues that the global gas industry faces. Gas hydrates can cause severe blockages due to the formation of hydrate plugs. Corrosion leads to significant economic loss in terms of prevention, repair and increased lifecycle costs. To manage these issues, hydrate and to date corrosion inhibitors are injected separately to subsea natural gas pipelines. However, they can interact; particularly corrosion inhibitors often depress kinetic hydrate inhibitor performance. The aim of this thesis is to overcome this compatibility problem by developing single polymer molecules that simultaneously prevent hydrate formation and inhibit corrosion. The hypothesis behind this work is: Inclusion of specific motifs like corrosion inhibitors (CIs) onto a single polymer backbone based on well-known chemicals, such as kinetic hydrate inhibitors (KHIs), with the overall molecules providing multi-functionality. In addition, the concentration of KHIs used is significantly higher than CIs', so a single polymer molecule that can inhibit hydrates and corrosion would replace the need for injecting separate inhibitors.

Libraries of single polymer molecules termed as kinetic hydrate and corrosion inhibitors (KHCIs) have been designed, synthesized, and tested with both targets in mind. To achieve this, a new efficient synthetic route was developed instead of using traditional free radical polymerization. These new methods are more efficient and allowed for accurate placement of functional groups onto the target molecules, compared to traditional free radical polymerization, which is currently used for generating most kinetics hydrate inhibitors. The synthetic protocols also target non-toxic chemistry that offers advantages in terms of environmental impact. This approach was initially applied to a commercial polymer Polyacrylamide-co-acrylic acid (PAM-co-AA). PAM-co-AA was modified with various linear and cyclic hydrophobic motifs via this tool. The structure of the resulting materials were then confirmed using acid-base titration, spectroscopy, viscometry, and rheology. The viscosity of the polymers varies over a broad range with those containing larger hydrophobic group showing the highest viscosity, which strongly proves the efficiency of this new synthetic protocol. This method was then extended to two known KHIs

systems of poly(N-isopropylacrylamide)-co-AA (PNIPAM-co-AA) and Poly(vinyl-caprolactam)-co-AA (PVCap-co-AA). These KHI base polymers were synthesized in-house using free radical polymerization and followed by applying the new synthetic protocol to generate libraries of modified polymers. As a result, two controlled libraries of inhibitors with the same molecular weight (Mw), Mw distribution, end groups, and composition along the chain were created successively and characterized via Nuclear Magnetic Resonance (NMR), Gel permeation chromatography (GPC), cloud point, hydrate- and corrosion test. Therein, PNIPAM-based polymers were designed and assembled using motifs including small cyclic groups and alkyl chains to gain better hydrate inhibition performance as the inclusion of pendent group was the key to impact the hydrate surface and inhibit the growth of clathrate. In addition, PVCap-based polymers were synthesized that incorporated known corrosion inhibitor groups onto this base KHI polymer. These specific structures containing active heteroatom centres attached on the backbone of target polymers imparted the corrosion inhibition property and, thus, turned single polymer molecules into multifunctional inhibitors.

Central to these synthetic routes was having a rapid testing method in place that could assess these libraries. This was based on a ranking method using inhibition performance of Structure II (sII)-forming cyclopentane (c-C5) hydrate under atmospheric pressure. Comparison of some commercial KHIs: Luvicap 21W (N-vinylpyrrolidone:N-vinylcaprolactam 2:1 copolymer), Luvicap 55W (N-vinylpyrrolidone:N-vinylcaprolactam 1:1 copolymer), polyvinylpyrrolidone (PVP), poly(N-isopropylacrylamide) (PNIPAM), and polyacrylamide (PAM) was made using this new method, which has been validated against conventional rocking cell measurements. This cost-effective method enables rapid, parallel screening of multiple KHIs with major advantages in time, instrument complexity, safety, and materials. It served as a valuable first screening method for identifying promising candidates among libraries of materials for more rigorous testing. A number of promising candidates were rapidly screened out via this technique from large libraries of PNIPAM-based and PVCap-based modified polymers for further conventional autoclave testing.

Conventional tests in terms of both hydrate and corrosion inhibition performance were conducted to verify the selected candidates. For example, a high-pressure autoclave

was used to assess hydrate inhibition performance of new inhibitors. By determining the hydrate onset time, growth rate, and resistance to flow of new inhibitors compared to three control groups water, Luvicap solution, and polyvinylpyrrolidone (PVP) under various cooling rates (0.25, 0.033, and 0.017 K/min), results showed that the nucleation of hydrate crystals was delayed in the presence of the KHI candidates. The effect of the KHI candidate on the hydrate growth characteristics was also studied by determining the initial growth rate and torque changes with an increasing hydrate fraction in the liquid phase. The obtained results confirmed that the synthesized PVCap-based and PNIPAM-based KHI candidates are comparable to those of commercial KHIs. Additionally, the performance of PVCap-based polymers as corrosion inhibitors for carbon steel in CO_2-saturated brine at ambient temperature using electrochemical analysis were measured. Linear polarization resistance measurement revealed that the maximum efficiency among these polymeric inhibitors was 88.67% at 200 ppm dosage, which are promising results for a first combined kinetic hydrate and corrosion inhibitor (KHCI).

Although there remains a gap in terms of the mode of action and the interaction between kinetic hydrate inhibition and corrosion inhibition including functional groups on single polymer molecules, the concept of using multifunctional polymers that eliminate compatibility issue due to the co-injection of hydrate- and corrosion inhibitors has been proven by this study. A promising candidate as KHCI was screened out through all the tests in this thesis. The approach taken in this thesis has allowed unprecedented control over structure and performance. However, further computational studies could further decipher these effects, which will require advanced computing science to develop a predictive model.

Overall, this work will be of broad interest to the research community and contributes to developing next generation kinetic hydrate and corrosion inhibitors (KHCIs) for the oil and gas industry, which will bring up appealing OPEX/CAPEX savings and desirable improvements in operation.

ACKNOWLEDGEMENTS

This research involves years of concerted effort and enormous amount of help from many people. My sincere appreciation goes to following people, whose guidance and support push forward the work:

- To Colin D. Wood, not only for the opportunity to take up this postgraduate research in CSIRO and Curtin University, but also for his great guidance, encouragement and advice throughout my study. I have been extremely lucky to have a supervisor in CSIRO who is incredible creative and capable to response all my questions so promptly whenever there is a hardship during the research. Great thanks for his help and inspiration.

- To Dr Wendy Tian who is warm-hearted and cared a lot about my life and study during these years. Her professional support on how to use various instruments in CSIRO is really appreciated.

- To Dr Kelly Cristine da Silveira, my friend, it's been great pleasure to work together and also to have fun for after-hours drinking.

- Dr Nuobo Maeda and Dr Celesta Fong for their kind contribution to develop novel high-throughput hydrate screen technique.

- Dr Roger Mulder for his assistance with NMR spectra.

- Professor Rolf Gubner, my supervisor in Curtin University, for welcoming me to corrosion lab and for his assistance to my study and graduation.

- Ms Hoda Ehsani for her great contribution on the experiment of electrochemical analysis in the laboratory of Curtin Corrosion Engineering Industry Centre (CCEIC).

- Ms Lemlem Selomon for offering continued help to solve my application issue related to my project. Many thanks.

- Dr Qinfen Gu of the Australian Synchrotron for his assistance on the Powder Diffraction beamline.

- Mr Barry Halstead, CSIRO Minerals Resources, for his assistance with X-ray powder patterns taken from a laboratory source.

- Professor Malcolm Kelland for proving the commercial KHIs used in this study.

- To my parents, who have always been my inward back-up and drive for accomplishment. Thank you.

- Appreciation is also due to my friends and colleagues in CSIRO for an amazing working atmosphere.

- The funding organization CSIRO and Curtin University for providing resourceful support to this work.

LIST OF PUBLICATIONS REFERRED ORIGINATING FROM THE THESIS

1. **Libraries of modified polyacrylamides using post-synthetic modification**
   By: Kelly Cristine da Silveira; Qi Sheng; Wendy Tian; et al. JOURNAL OF APPLIED POLYMER SCIENCE Volume: 132 Issue: 47 Article Number: 42797 Published: DEC 15 2015
   *This publication is part of Chapter 3
2. **High-throughput Testing of Kinetic Hydrate Inhibitors**
   By: Nobuo Maeda; Celesta Fong; Qi Sheng; et al. ENERGY FUELS Volume: 30 Issue: 7 Published: JUL 13 2016
   *This publication is part of Chapter 6
3. **High throughput synthesis and characterization of PNIPAM-based kinetic hydrate inhibitors**
   By: Kelly Cristine da Silveira; Qi Sheng; Wendy Tian; et al. FUEL Volume: 188 Pages: 522-529 Published: JAN 15 2017
   *This publication is part of Chapter 4 & 6
4. **Simultaneous Hydrate and Corrosion Inhibition with Modified Poly(vinyl caprolactam) Polymers**
   By: Qi Sheng; Kelly Cristine da Silveira; Wendy Tian; et al. ENERGY FUELS Volume 31 Issue: 7 Pages 6721-6731 Published: June 20 2017
   *This publication is part of Chapter 5 & 6 &8
5. **Performance of Poly(N-isopropylacrylamide)-Based Kinetic Hydrate Inhibitors for Nucleation and Growth of Natural Gas Hydrates**
   By: Juwoon Park; Kelly Cristine da Silveira; Qi Sheng; et al. ENERGY FUELS Volume: 31 Issue: 3 Pages: 2697-2704 Published: Feb 20 2017
   *This publication is part of Chapter 7
6. **Kinetic Hydrate Inhibition Performance of Poly(Vinyl Caprolactam) Modified with Corrosion Inhibitor Groups**
   By: Juwoon Park; Hyunho Kim; Qi Sheng; et al. ENERGY FUELS Volume: 31 Issue: 9 Pages: 9363-9373
   *This publication is part of Chapter 7

7. **Evaluation of modified Poly(vinyl caprolactam polymers as corrosion inhibitors for carbon steel in CO2-saturated brine**

   By: Qi Sheng; Hoda Ehsani: Rolf Gubner and Colin D. Wood. Manuscript for Publication (CORROSION)

   *This manuscript is part of Chapter 8

TABLE OF CONTENTS

LIST OF FIGURES

LIST OF TABLES

Chapter 1 INTRODUCTION

1.1 Background

Gas hydrates are solid, ice-like compounds where small molecules such as methane, ethane, propane and carbon dioxide (Sloan and Koh, 2007) are trapped inside cavities formed by a hydrogen-bonded water framework (as shown in Figure 1.1). Typically, gas hydrates contain 85 mol% water and 15 mol% guest(s) when all of the cavities are occupied (Perrin et al., 2013). Most gas hydrates are found in the regions of permafrost and beneath the sea in outer continental margins (Kvenvolden and McMenamin, 1980).

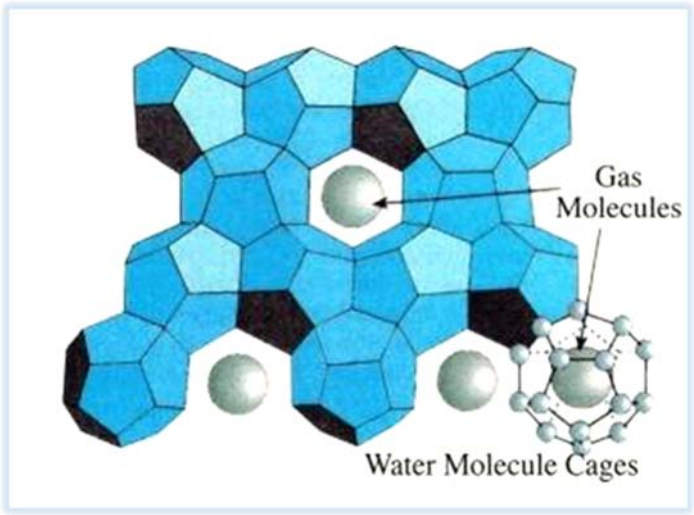

Figure 1. 1 One type of gas hydrate structures (Tohidi Kalorazi, 2008).

On one hand gas hydrates are a largely unexploited natural resource (Sloan, 2003) that have been studied in a range of different areas including gas storage (Sun et al., 2015; Veluswamy et al., 2016; Yang et al., 2016), climate change (Koh et al., 2012), carbon dioxide sequestration (Kim et al., 2016; Kumar et al., 2013), gas separation, desalination (Englezos, 1993), marine sediments (Bidle et al., 1999; Zhang et al., 2007) and the concentration of temperature-sensitive liquids (Huang et al., 1966; Purwanto et al., 2001). On the other hand, they pose a major problem to the oil and gas industry. This was first reported by Hammerschmidt who found that gas hydrate formation could

cause severe blockages in pipelines, and as a result, gas hydrate prevention was introduced (Hammerschmidt, 1934). The formation of gas hydrates in subsea oil and gas flowlines can occur when elevated pressures (more than 0.6 MPa) and low temperatures (less than 300 K) are encountered (Koh, 2002; Sloan, 2003). This problem is exacerbated as exploration and production of oil and gas have been moving into deeper and remote regions (Carroll, 2009; Makogon, 1997; Sloan and Koh, 2007). As a consequence, they restrict gas flow or cause pipeline blockage which presents safety concerns as well as financial impact. Hydrate formation is one of a number of issues, collectively known as flow assurance, which is a major technical problem in offshore energy development (Sloan et al., 2010).

Figure 1.2 shows bulk masses of gas hydrate formed in a gas pipeline. These gas hydrate plugs often block the production facilities and thus cause temporary or even long-term shutdown, leading to enormous financial loss and safety concerns. The removal of hydrate plugs in subsea pipeline is generally difficult and time-consuming (Sinquin et al., 2004).

Figure 1. 2 Massive gas hydrate plug found in the production line (http://continentalshelf.gov/missions/10arctic/logs/aug11/aug11.html).

Considerable investment has, therefore, been committed to avoid pipeline shutdowns including injecting gas hydrate inhibitors (Carroll, 2009; Koh et al., 2012; Sloan, 2000). One potential solution is to remove water prior to transporting the gas in the pipeline

by using a dehydration plant or subsea separator, which requires significant investment as well as logistical issues. Alternatively the temperature of the pipeline could be controlled through insulation and heating (Mokhatab et al., 2007). However, these methods are not always practical and effective as the exploration of oil and gas moves into more challenging environments.

Addition of chemical inhibitors is another route, which is favoured by the oil and gas industry. In terms of hydrates, both methanol and ethylene glycol are well known thermodynamic hydrate inhibitors (THIs). They shift the hydrate formation equilibrium curve towards lower temperatures and higher pressures (Sira et al., 1990; Sloan and Koh, 2007; Wu et al., 2007) and, thus, prevent hydrate formation. Industry practice has relied on the injection of THIs to prevent hydrate formation in subsea flowlines (Ballard, 2006; Lee et al., 2009). However, high dosage rates (up to 50 wt. %) are required, which present economical, logistical, environmental and operational problems. It is estimated that the cost of methanol for hydrate inhibition are at US $220 million per year worldwide (Sloan, 2003). Moreover, storing vast quantities of inhibitors is challenging. For these reasons, new low dosage hydrate inhibitors (LDHIs), which include kinetic inhibitors (KHIs) and anti-agglomerants (AAs), have been developed and that are effective at lower concentrations (0.1-1 wt%) (Kelland, 2006; May et al., 2014; Ree et al., 2016; Sira et al., 1990; Sloan, 2003). They offer economic and logistical advantages over THIs (Kelland, 2006). However, the effectiveness of existing LDHI is limited so there is a need for fundamental studies to develop new materials that are more effective. KHIs and AAs differ in terms of their mode of action, thus, depending on the pipeline conditions, the optimal LDHI can be selected (Perrin et al., 2013). In general, KHIs interfere with the nucleation and growth of hydrate crystal, which delays the formation of hydrates, while AAs allow the formation of hydrates, but they disperse fine hydrate particles to prevent them from forming large blocking masses (Dashti et al., 2015; Kelland, 2006; Tariq et al., 2014). AAs typically require the presence of oil to disperse the hydrate particles that limits their use in the gas dominant flows (Clark et al., 2005). Moreover, they are effective at water cuts <50% and pose a significant environment threat.

KHIs are hydrophilic polymers as the main active ingredient, most of which are vinyl-based polymers with amide or imide groups (Nakarit et al., 2013). These LDHIs can effectively inhibit hydrate formation in the field, however, their application has been

limited due to concerns that they are not effective at low temperatures. In addition, the low cloud point (deposition) temperature associated with some KHIs is also a barrier to the use of various polymeric structures as it causes precipitation of the inhibitor during injection. Typically, the deposition temperature is 5-10 °C above the cloud point temperature. During production in warmer waters (eg., the Gulf of Mexico), the solubility of the polymeric structure is crucial for an efficient inhibition (Kelland et al., 2000). There are also issues associated with their biodegradability, toxicity (Igboanusi and Opara, 2011; Kanu et al., 2014) and incompatibility with corrosion inhibitors, which is the case for most LDHIs. Examples of KHIs include poly(N-vinyl pyrrolidone) (PVP), poly(N-vinylcaprolactam) (PVCap) and related copolymers such as Luvicap 55W (polyvinylcaprolactam/vinyl pyrrolidone, PVCap-PVP, 1:1), and Gaffix VC-7131, which are often the benchmark for developing new KHIs (Kelland, 2006; Koh, 2002; Lucas et al., 2002; Mady and Kelland, 2015; O'Reilly et al., 2011; O'Reilly et al., 2011; Perrin et al., 2013; Sira et al., 1990; Sloan and Earle, 1995; Tariq et al., 2014; Wu et al., 2007). Alternatively, polyacrylamides, such as poly(N-isopropylacrylamide) (PNIPAM) and poly(N-isopropylmethacrylamide) (PNIPMAM), have also been studied, since they can show a strong KHI performance, which is attributed to the amide functionality being attached to a hydrophobic group (Chua et al., 2012a; Chua et al., 2012b; Mady and Kelland, 2014; Perrin et al., 2013).

Corrosion is another significant challenge that the oil and gas industry faces because it accounts for over 50% of pipeline failures (Fu, 2007; Obanijesu et al., 2010). Corrosions of pipelines is generally classified into internal or external corrosion. External corrosion is subject to environmental conditions around pipelines (Kutz, 2015; Mercer and Lumbard, 1995; Obanijesu et al., 2010), while internal corrosion is caused by the pipeline fluids that contain brine, organic acids and acid gases, such as, carbon dioxide and/or hydrogen sulphide, that corrode carbon steel pipelines (Fu, 2007; Hoppe et al., 2006; Jones et al., 2013; Moloney et al., 2009; Moore et al., 2009).

Figure 1. 3 Top of the line corrosion failure

(http://corrosion.curtin.edu.au/research/mining.cfm).

Carbon steels are the main material used in the construction of oil and gas transportation and storage infrastructure (Moussa et al., 2007) due to their relatively low cost and acceptable mechanical properties (Durnie et al., 1999; Geethanjali et al., 2014; Yan et al., 2014; Zhang et al., 2015). However, they are very susceptible to corrosion. Figure 1.3 shows top of the line corrosion failure (internal corrosion) caused by the condensation of water on the top of the pipe in the presence of carbon dioxide and volatile organic acids. The subsequent repair, increased maintenance and even replacement of pipelines due to corrosion issues results in severe economic consequences as well as ecological pollution and safety hazards (Tiu and Advincula, 2015).

Therefore, corrosion inhibitors (CIs) are essential to the oil and gas industry (Arthur et al., 2013; Hoseinzadeh et al., 2014; Jones et al., 2013; Moussa et al., 2007). Corrosion inhibitors, especially film-forming corrosion inhibitors (FFCIs), are prevalent in the oil and gas industry since these molecules interact directly with metal surface. Alternatively, molecules that can neutralize corrosive agents can be employed, examples include ammonia, sodium hydroxide, alkylamines and polyamines (Ting and Crestwood, 1974) or scavengers such as hydrazine and sodium sulphite (Tiu and Advincula, 2015). Film forming corrosion inhibitors are typically organic molecules that contain functional groups with heteroatoms such as nitrogen, sulfur, oxygen,

phosphorus and aromatic rings (Finšgar and Jackson, 2014; Hoseinzadeh et al., 2014; Maege et al., 1998; Moussa et al., 2007; Yan et al., 2014; Zhang et al., 2009).

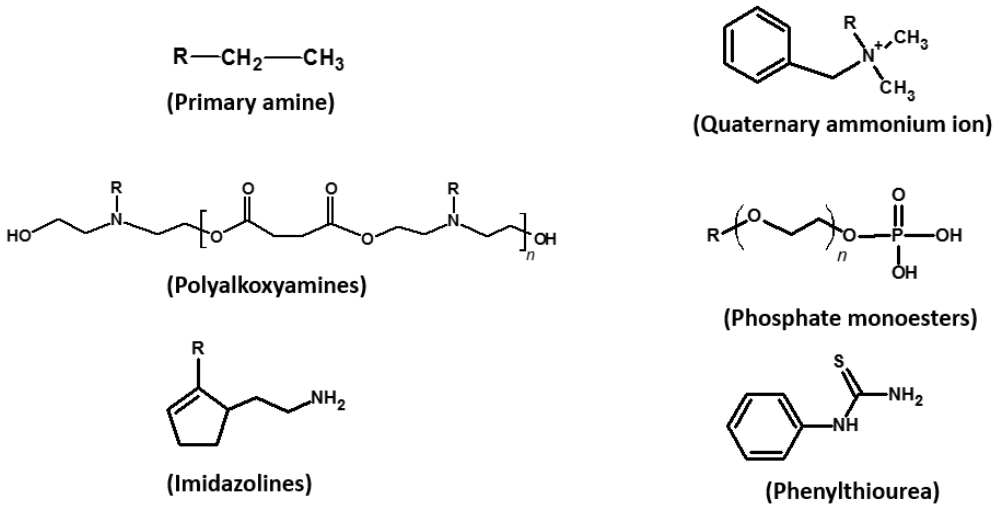

Figure 1. 4 Examples of corrosion inhibitors that contain nitrogen, oxygen, phosphorus, sulfur, and aromatic rings in the functional groups.

These heteroatoms serve as active centres that can absorb onto the metal surface via transferring lone electron pairs so as to protect metals from corrosive agent. They are also common with additional alkyl chains that help with the thickness and strength of protective barrier (Kelland, 2014; Okafor et al., 2009; Palmer et al., 2004; Zhang et al., 2008). In practice, CIs are injected into subsea flowlines along with hydrate inhibitors to maintain flow and to protect the integrity of the pipelines against corrosion (Fu, 2007; Moloney et al., 2009).

As mentioned above, the co-injection of KHIs and CIs often results in compatibility issues and the presence of CI are known to significantly reduce the performance of a KHI or vice versa (Klomp and Mehta, 2007). Limited studies (Clark et al., 2005; Fu, 2007; Hoppe et al., 2006; Jones et al., 2013; Klomp and Mehta, 2007; Moloney et al., 2009; Moore et al., 2009), related to the fundamental mechanism of both chemistries and development of KHI/CI packages, have been conducted to try to address this issue. For example, it has been noted that the performance of KHIs is reduced by up to 50% in the presence of CIs (Jones et al., 2013) and the performance of CIs has a significant

loss at the same time (Klomp and Mehta, 2007; Moloney et al., 2009), while some claim the presence of KHIs were found to have no adverse effect on CIs' performance or to enhance the corrosion inhibition efficiency (Fu, 2007; Moore et al., 2009). Moore et al. (2009) proposed that the incompatibility between KHIs and CIs can be attributed to the competition between the inhibitors for the surface of the hydrate and the pipeline steel, or that the CIs interfere with the ability of KHIs to attach to the surface of hydrate. However, the negative interaction between KHIs and CIs is not well-understood to date. This issue is critical to oil and gas industry, as it means that all KHIs and CIs need to go through validation tests together under simulation conditions before onsite application, which requires significant time and effort (Klomp and Mehta, 2007). Separate tests of KHI and CI are prone to fail in the final application because of unsolved compatibility issues. Therefore, new strategies are required to overcome these issues and to provide a fundamental understanding of the complex mode of action of KHIs and CIs. Hoppe et al. (2009) proposed that it may be possible to design a multifunctional molecule that contains two different ends, one hydrate-philic and one metallo-philic to minimize or eliminate the incompatibility issues. An initial study demonstrated that some KHIs are also potential CIs but this did not involve the design of multifunctional molecules, rather the study tested known KHIs as CIs (Burgazli et al., 2005). Musa et al. reported that copolymers composed of N-vinyl formamide, N-vinyl caprolactam and N-vinyl-2-pyrrolidone have both corrosion and hydrate inhibition properties (Musa et al., 2011). There are few other examples with only the copolymerization of N-vinyl caprolactam and phosphonic acid or vinyl sulfonic acid also show promising results as multi-functional inhibitors (Musa and Lei, 2016).

As such, one possible breakthrough to solve this issue is to develop multi-functional inhibitors that can prevent hydrate and inhibit corrosion simultaneously. The development of appropriate materials with versatile performance to meet different stringent criteria will be of great interest to the future oil and gas industry.

1.2 Aim and objectives

The main aim of this research was to design single polymer molecules that exhibit both hydrate- and corrosion inhibition properties, specifically a kinetic hydrate and corrosion inhibitor (KHCI). This will help to overcome compatibility issues as well as

offer fundamental insights into the mode of action of hydrate and corrosion inhibitors. Consequently, the objectives of the project were:

1. Introducing a high throughput (HTP) synthetic protocols for generating systematic library of target hydrate inhibitors with functionality to which key motifs, e.g., corrosion inhibitor can be coupled;
2. Design and synthesis of novel polymers featuring multi-functionality attributed to specific architectures via this new synthetic protocols, various structure motifs on target polymers can be compared in terms of comparable molecule weight (Mw), Mw distribution, end group and composition;
3. Detailed testing to investigate structure-property relationships
   (a) Development of high throughput KHI ranking method, which is preferably cost effective, high efficacy and without using highly pressurized and potential explosive fuel gases, to identify promising candidates from libraries of materials for more rigorous testing and further optimization.
   (b) Using conventional protocols to access the detail performance of promising KHI candidates.
   (c) Application of high throughput cloud point screen for investigating the impact of structure variations.
   (d) High throughput corrosion screening to rapidly assess the KHCIs for their CI performance.
   (e) Applying industry relevant corrosion testing – electrochemical analysis to distinguish the potential candidates for corrosion inhibition.

1.3 Contents and outline

This thesis is divided into 10 chapters.

In Chapter 2, a general overview of gas hydrates, the technologies used for flow assurance, corrosion and corrosion mitigation, and incompatibility issues of LDHIs and CIs is presented.

In Chapter 3, the introduction of a new synthetic route instead traditional free radical polymerisation: carbodiimide-mediated coupling (CMC) reaction. This new protocol

was utilized on commercial polyacrylamide-co-acrylic acid (PAM-co-AA) polymer as a precursor study.

In Chapter 4, CMC reaction were applied to poly(N-isopropylacrylamide)-co-acrylic acid (PNIPAM-co-AA), which is considered a strong KHI and is structurally analogous to PAM. A library of modified PNIPAM-based KHI polymers was generated. Various characterisations for modified polymers are presented and discussed.

In Chapter 5, CMC reaction were then applied to poly(N-vinylcaprolactam)-co-acrylic acid (PVCAP-co-AA), selection of corrosion motifs were designed and coupled on this base polymers. Libraries of modified PVCap-based KHCI polymers were generated. Various characterisations for modified polymers are presented and discussed.

In Chapter 6, the novel high-throughput (HTP) hydrate screen method is introduced and followed by the studies on screening of KHI candidates among PNIPAM-based KHIs and PVCap-based KHCIs using this technique.

In Chapter 7, high pressure autoclave test results for the most promising KHI candidates are presented (that have been screened by HTP hydrate screen previously). Comprehensive data for KHI evaluation is presented and discussed.

In Chapter 8, two corrosion tests on evaluating the corrosion inhibition performance of KHCIs were conducted and the results are presented.

Finally, the major results are summarised and recommendations for future research are presented in Chapter 9

Chapter 2 LITERATURE REVIEW

2.1 Introduction

This chapter provides a comprehensive review of the literature in terms of gas hydrates and corrosion. The first section provides a fundamental understanding of the microscopic structures of gas hydrates. This is followed by an overview on the kinetics of formation and growth. Then various flow assurance technologies are discussed, focusing on the preferred chemical inhibition methods favoured by industry. Corrosion issues are illustrated next. The fundamental mechanisms of corrosion are introduced, and relevant types of corrosion are summarized, following by chemistries for corrosion inhibitors. Finally, a summary is given of compatibility studies between chemistries used for hydrate and corrosion.

2.2 Gas Hydrates

Gas hydrates, also known as clathrate hydrates, are crystalline, non-stoichiometric compounds that are composed of water and gas (Sloan and Koh, 2007). The gas molecules are encapsulated in cavities formed by hydrogen-bonded water molecules under high pressure and low temperature (Sloan, 2003). Figure 2.1 illustrates three typical clathrate hydrate structures: structure I (cubic), structure II (cubic) and structure H (hexagonal). There also exists other known structures such as structure T (trigonal) found in dimethyl ether (DME) hydrate (Udachin et al., 2001), which is an unusual complex consisting of alternative stacks of structure H and structure II (Udachin and Ripmeester, 1999), and high pressure methane structures MH II and MH III (Loveday et al., 2001). These occur rarely and, therefore, most research is focused on structures I (sI) and II (sII). Pentagonal dodecahedra, denoted 5^{12} (contains 12 pentagon faces), is the common features of these three types of hydrates (Sloan, 2003). A cavity within the structures is formed by hydrogen bonds between water molecules. Within the cavity, small guest molecules are trapped. Van der Waals forces dominate the stabilization of the clathrate hydrate (Loveday et al., 2001), thus there are no strong directional interactions between the guest and host, the guests are free to vibrate and rotate but have limited translational motion (Perrin et al., 2013). To prevent the

hydrogen bonds from breaking, interstices between pentagonal dodecahedra are filled with other cavities to relieve the strain. The 5^{12} cavities are connected either through the vertices (sI) or faces (sII) (Sloan, 2003). As shown in Figure 2.1, sI comprises two 5^{12} cavities and six $5^{12}6^2$ cavities (contains 12 pentagon and 2 hexagonal faces) whereas sII includes sixteen 5^{12} cavities and eight $5^{12}6^4$ cavities (contains 12 pentagon and 4 hexagonal faces). Structure H consists of three 5^{12} cavities, two $4^35^66^3$ (contains 3 square, 6 pentagonal and 3 hexagonal faces), and a very large cavity, denoted $5^{12}6^8$ (contains 12 pentagonal and 8 hexagonal faces). The type of structure formed depends predominantly upon the size of the guest molecules (Koh et al., 2011).

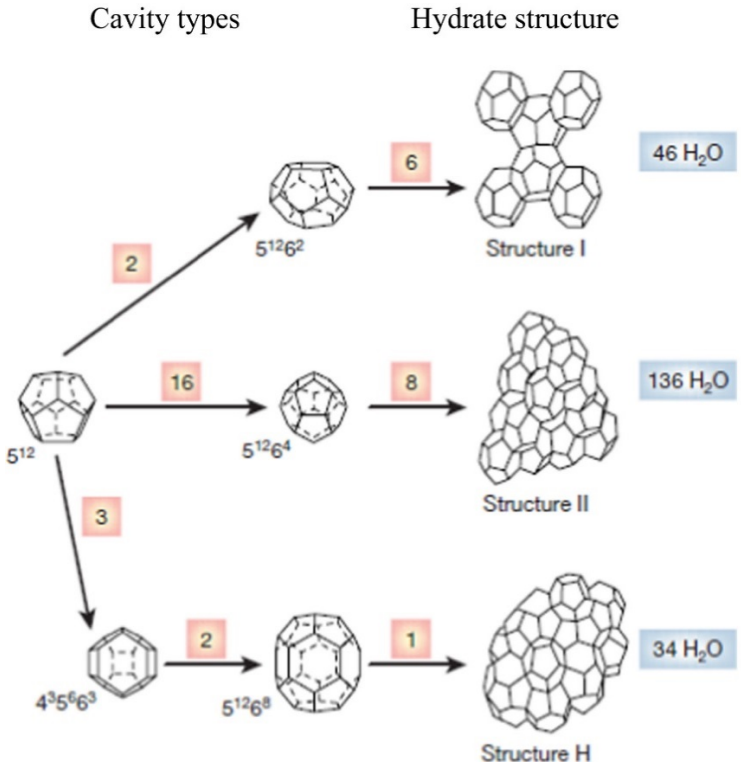

Figure 2. 1 Typical clathrate hydrate structures (English and MacElroy, 2015).

The relationship between the molecule size and structure type has been investigated as it aids the understanding of hydrates. Data regarding cavity radius and molecular diameter or ratios of molecular diameter to cavity diameter are given in Tables 2.1 and 2.2. As can be seen, $5^{12}6^2$ cavities of sI has an average radius of 4.33 Å, which can include molecules with a diameter of 4-5.5 Å, such as methane, ethane, hydrogen sulfide and carbon dioxide. In contrast, $5^{12}6^4$ cavity of sII has an average radius of 4.73

and can hold larger molecules (6-7 Å), such as propane, iso-butane. sH has a significant larger cavity ($5^{12}6^8$) with average radius of 5.71 Å, therefore, the presence of large liquid hydrocarbon molecules (8-9 Å), such as, iso-pentane, 2,2-dimetylbutane, methylcyclohexane and tert-butyl methyl ether, are necessary (Sassen and MacDonald, 1994). In addition, small molecules of methane are also required to occupy smaller cavities in order to form this type of hydrate.

.

Table 2. 1 Cavities of sI, sII and sH hydrate (Sloan, 2003)

Hydrate crystal structure	I		II		H		
Cavity	Small	Large	Small	Large	Small	Medium	Large
Description	5^{12}	$5^{12}6^2$	5^{12}	$5^{12}6^4$	5^{12}	$4^35^66^3$	$5^{12}6^8$
Number of cavities per unit cell	2	6	16	8	3	2	1
Average cavity radius (Å)	3.95	4.33	3.91	4.73	3.91†	4.06†	5.71†
Coordination number*	20	24	20	28	20	20	36
Number of waters per unit cell	46		136		34		

*Number of oxygens at the periphery of each cavity.
†Estimates of structure H cavities from geometric models.

Table 2. 2 Ratios of molecular diameter to cavity diameter for clathrate hydrate former (Sloan and Koh, 2007).

		(Molecular diameter)/(Cavity diameter)			
		Structure I			Structure II
Cavity type	Dia. (Å)	5^{12}	$5^{12}6^2$	5^{12}	$5^{12}6^4$
H_2	2.72	0.533	0.464	0.542	0.408
N_2	4.10	0.804	0.700	0.817*	0.616*
CH_4	4.36	0.855*	0.744*	0.868	0.655
H_2S	4.58	0.898*	0.782*	0.912	0.687
CO_2	5.12	1.000	0.834*	1.020	0.769
C_2H_6	5.50	1.080	0.939*	1.100	0.826
C_3H_8	6.28	1.230	1.070	1.250	0.943*
i-C_4H_{10}	6.50	1.270	1.110	1.290	0.976*
n-C_4H_{10}	7.10	1.390	1.210	1.410	1.070

Regardless of the hydrate structures type, it is considered that one cavity accommodates at most one guest molecule. Exceptions exist when very small guest molecules, such as hydrogen, occupy the cage when two molecules can be accommodated; or four occupants are in one large cavity under unusual high pressure

(Mao et al., 2002). Theoretically, when all cavities are occupied, the three types of hydrates contain a similar concentration of composition: 85 mol% water and 15 mol% guest molecule(s). It is impossible to occupy all cavities, since this would be equal to obtain a perfect crystal. However, general formulas are often written for each hydrate type with all cavities occupied. As a consequence, more water could present in hydrates than predicted by the ideal composition (Ribeiro and Lage, 2008).

2.3 Kinetics of hydrate formation

Gas hydrate formation can be simply described as a crystallization process (Makogon, 1981). The particular nature of the process is time-dependent and involves two distinct kinetic phenomena: nucleation and growth. These processes are influenced by many factors including temperature, pressure, degree of subcooling and the history of the water, etc.(Makogon et al., 2000b). Prior to nucleation and growth, continuous dissolution of gas molecules in liquid water are essential to set a supersaturated environment for the phase transformation to occur. In general, nucleation and growth of hydrates will occur mostly at the gas-water contact interface. This is where most molecular models, with respect to kinetics of hydrate formation, have been focused on (Englezos et al., 1987; Sloan and Koh, 2007).

The gas hydrate formation formula can be expressed by Equation 2.1 (Cox, 1983; Tang et al., 2010) as follows:

$$M\ (g) + nH_2O\ (l) \leftrightarrow M \bullet nH_2O\ (s) \quad (2.1)$$

Where M represents natural gas molecules, n represents mole of water molecules when forming a gas hydrate per one molecule of gas, and M•nH2O represents gas hydrate.

2.3.1 Nucleation

Hydrate nucleation is the process by which a small cluster of water and gas molecules grow and disperse to achieve a critical size. This occurs on a microscopic scale involving hundreds of thousands of molecules with small length and time scales that are difficult to observe experimentally. Current hypotheses for hydrate nucleation are based upon the better-known phenomena of ice nucleation, supercooled water, the

dissolution of hydrocarbons in water, and molecular simulations (Sloan and Koh, 2007; Warrier et al., 2016). Few hypotheses, outlined below, have been put forward to interpret the mechanism of nucleation.

2.3.1.1 Labile cluster hypothesis

This hypothesis was proposed by Sloan et al., (Christiansen and Sloan, 1994). It is termed 'labile cluster' when a gas molecule dissolves in water and causes water molecules to gather around in an ordered form (Christiansen and Sloan, 1994). The corresponding visual model is presented in Figure 2.2, showing the progress of hydrate formation, whereby A represents the condition that no gas molecules are dissolved in the water, and B shows the appearance of labile clusters as the gas molecules dissolve in water. The size of the gas molecules influences the number of water molecules participating in labile cluster formation. Agglomerations of labile clusters form C, which is attributed to hydrophobic bonding (Ben‐Naim, 1975; Franks et al., 1976) formed via the attraction among the gas molecules inside clusters of water. These can either dissipate or agglomerate as long as they are smaller than a certain critical size. As soon as these clusters agglomerate and exceed to the critical size D, intermolecular forces within the cluster begin to prevail and the cluster becomes stable. In other words, a critically sized hydrate nucleus has formed and crystal growth commences (Englezos et al., 1987). It is worth noting that if the system is reheated, the hypothesised process is reversed, and stable gas hydrates are decomposed into liquid and vapour phases.

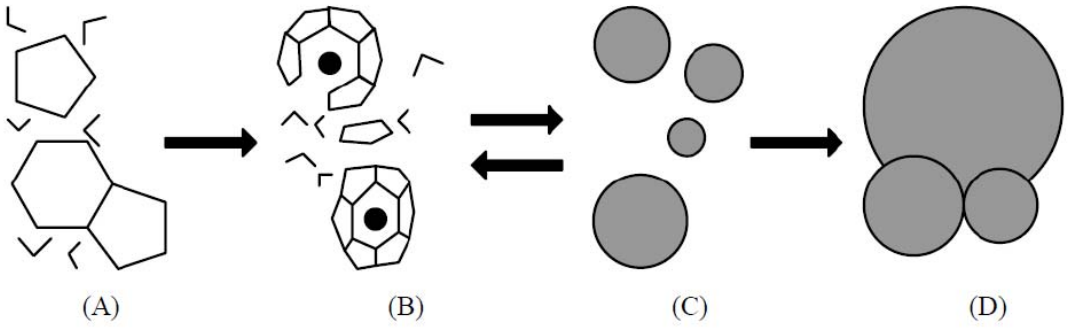

Figure 2. 2 Schematic model of labile cluster hypothesis (Sloan and Koh, 2007).

2.3.1.2 Interfacial nucleation hypothesis

The interfacial nucleation mechanism hypothesis was proposed by Long (Long et al., 1994) and Kvamme (Kvamme, 1996) and can be regarded as a revision of the labile cluster hypothesis. As stated in this hypothesis, gas molecules are transferred to the interface of liquid and gas where nucleation is highly favoured. Water molecules then reorient around these gas molecules followed by cage formation and agglomeration of the labile cluster to a critical size.

2.3.1.3 Local structuring nucleation hypothesis

The local structuring nucleation hypothesis was developed through more recent molecule simulation studies. Radhakrishnan and Trout provided convincing evidence of this hypothesis by utilizing Monte Carlo simulations with a Landau free energy method for CO_2 hydrates, which are known to nucleate at the liquid-liquid interface. (Radhakrishnan and Trout, 2002). In the study, they concluded that the presence of labile clusters is only valid for very dilute concentrations of the hydrophobic solute. Instead, they proposed that the local geometrical arrangement of guest molecules, which resembled clathrate hydrate, would occur by virtue of thermal fluctuations. Water molecules around the guest molecules therewith were perturbed relative to the bulk phase and, providing the guest molecules are in sufficient number, a critical nucleus will form (Perrin et al., 2013).

Moon et al., (2003) conducted an analogous model for methane hydrate nucleation at the methane–water interface, using Molecular-dynamics (MD) simulations (Moon et al., 2003). They presented a 10 ns simulation that showed a rapid ordering of clathrate (with clusters of 280 water molecules) occurring under a methane atmosphere and at moderate subcooling. Full crystallization was not observed in this time frame, however, the nucleation mechanism of methane hydrate was highlighted. Particularly, there was no evidence in the MD simulation that the solvation shell around the dissolved methane molecules formed a clathrate cage, and this study concluded that these simulations were in agreement with the local structuring nucleation hypothesis, but not with the labile cluster model.

In recent studies, however, microsecond MD simulation on methane hydrate nucleation supported the labile cluster hypothesis. It was reported that the hydrate cages, such as 5^{12}, $5^{12}6^2$, $5^{12}6^4$, and other exotic water cages, such as $5^{12}6^3$, were formed as guest molecules interacted with the labile ring structures in water. These cages connect together to form different sI/sII type clusters, which provide the building blocks for hydrate crystal growth (Aman and Koh, 2016; Walsh et al., 2009).

The difference between the local structuring nucleation and the labile cluster hypotheses is remarkable. If it would be possible to determine if the guest ordering is driven by the water or if water-ordering is driven by the guest molecules, this would determine the validity of either hypotheses mentioned above. However, these mechanisms seem to be difficult to separate. When it comes to a practical level, the local structuring model requires a more collective, longer range motion of the guests, whereas the labile cluster approach relies on particle–cluster aggregation for growth (Hawtin et al., 2008).

2.3.1.4 Blob hypothesis

More recently, a new mechanism was proposed by Jacobsen (Jacobson et al., 2010), called the Blob hypothesis. This hypothesis featured both labile cluster and local structuring concepts and involved two distinct steps (mechanism shown in Figure 2.3). First, a reversible step of the formation of blobs took place. The blobs were defined as the long-existing aggregates of guests separated by water molecules. In the blobs, clathrate cages repeatedly nucleated and dispersed until a cluster of cages reached a critical size (about five cages at 0.7 T_m supercooling). As a result of the first step, amorphous clathrates were formed from this process as a metastable intermediate towards the formation of crystalline clathrate. The major difference between a blob and an amorphous clathrate was that in the blob, water molecules are not locked into clathrate cages, whereas in an amorphous crystal, hydrogen-bonded polyhedral cages existed that solidified the structure (Jacobson et al., 2010; Warrier et al., 2016). In addition to the illustration of this novelty mechanism, this study indicated that blobs succeeded in nucleating at the interface although they originated in the bulk, and vice versa, and there was no evident preference for nucleation at the interface. This hypothesis was validated later by Lauricella et al. (Lauricella et al., 2014).

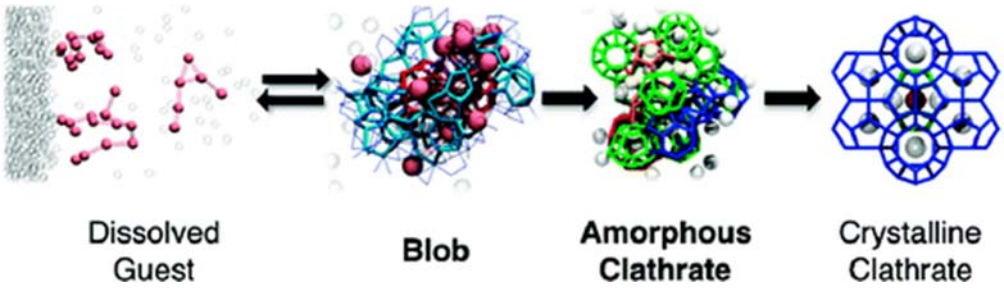

Figure 2. 3 The new proposed 'blob mechanism' (Jacobson et al., 2010).

2.3.2 Growth

Clathrate hydrate growth begins as long as critical sized nuclei are formed. Continuous growth and coalition of crystals eventually forms a solid mass. In this phase, there are three parameters that should be considered. These are the kinetics of crystal growth at the hydrate surface, mass transfer of components to the growing surface, and heat transfer away from the growing surface. Therein mass- and heat transfer are crucial for hydrate growth. A two-step model had been proposed by Englezos et al.(Englezos et al., 1987):

(1) Diffusion of the dissolved gas from the solution bulk to the crystal–liquid interface;

(2) Absorption of gas molecules into the water molecules therein stabilising the hydrate lattice.

This proposed model describes well the experimental data on hydrate growth and is more tenable than the hypotheses on nucleation phenomena. However, a challenge remains to verify the data of hydrate growth through more experiments due to the stochastic nature of hydrate formation. More detailed information on the state-of-the-art for hydrate growth can be found at the literature (Sloan and Koh, 2007).

2.4 Gas hydrate in the oil and gas industry

Gas hydrates were first discovered by Sir Humphrey Davy in 1810 (Koh, 2002) and were identified as a nuisance for oil and gas industry by Hammerschmidt

(Hammerschmidt, 1934). They can be encountered in two stages: drilling and transportation. During deep water drilling, natural gas either from shallow sediments or shutoff of mud circulation can enter the drilling fluid and form hydrate, resulting in the blockage of the pipe and annular clearance and even the cease of drilling operation if the fluid is not hydrate inhibited (Sami et al., 2013). The multiphase hydrocarbon fluid produced at the wellhead will normally be at high pressures and moderate temperatures. As the fluid flows through the pipeline, it becomes colder, thus, pipelines could experience hydrate formation along their length during transportation if the pressures and temperatures fall within hydrate formation zone shown in the Figure 2.4 (Mokhatab and Poe, 2012). Once formed, the solid, non-flowing crystalline matter (as seen in figure 1.2), may lead to the blockages and thus causing production loss and costly operation. Sometimes, it can take months for hydrates to dissociate in large pipelines (Sloan, 2003). Particularly, as the production of oil and gas moves into more hostile environments further from the shore with longer tiebacks, prevention and management of gas hydrates are more challenging than ever. Production facilities may also require the transportation of processed gas/ condensate streams to export facilities through subsea pipelines (Zerpa et al., 2010). As such, industrial hydrate concerns have been focused on flow assurance, which is a major technical problem in offshore development, production and transportation (Moore et al., 2009; Sloan et al., 2010; Tohidi Kalorazi, 2008).

2.5 Technologies used for flow assurance

Flow assurance is an essential aspect of the economic production of oil and gas, especially in deep-water or cold weather conditions. This involves handling many solid deposits, such as wax, scale, asphaltenes, sand, paraffins and especially gas hydrates due to its more frequent occurrence and impact on operation (Gbaruko et al., 2007a; Zerpa et al., 2010). In order to achieve the safe and uninterrupted operation economically from the reservoir to a production facility over the lifetime of a field (Gao, 2008; Jordan et al., 2001; Zerpa et al., 2010), various technologies have been proposed for flow assurance. These are (1) dehydration; (2) depressurization; (3) thermal method (insulation and heating); and (4) chemical injection (THIs and LDHIs) respectively given in the brackets in Figure 2.4.

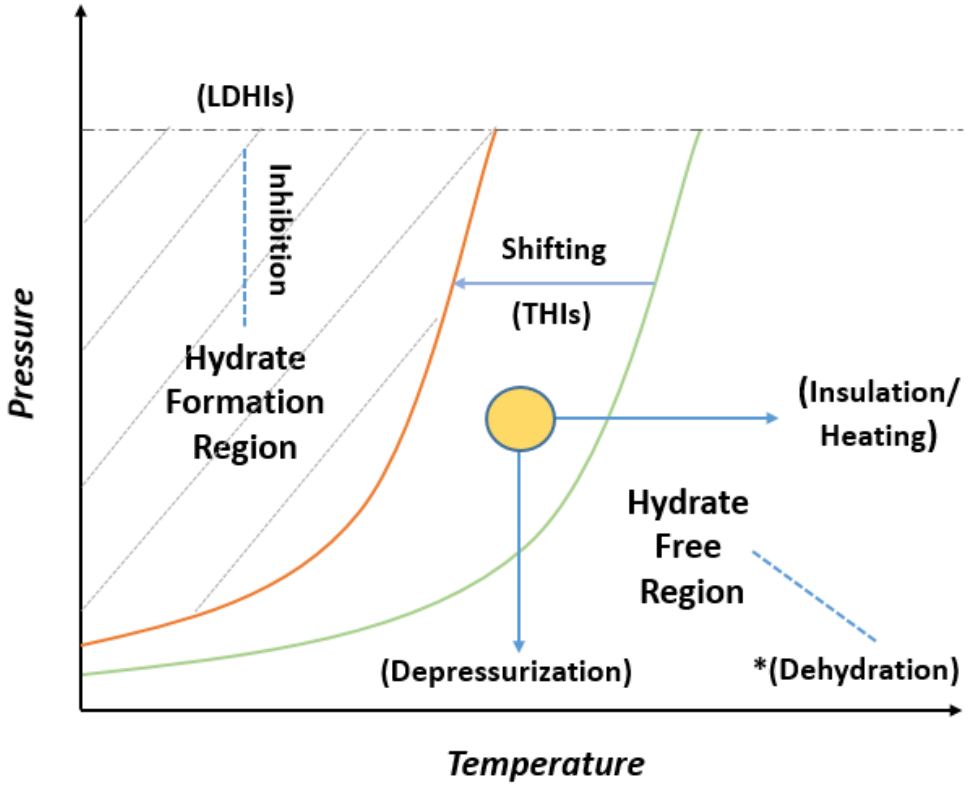

Figure 2. 4 A simplified depiction of hydrate equilibrium curve and flow assurance technologies.

Dehydration is marked by an asterisk in Figure 2.4, since this process not subject to pressure and temperature conditions. As the presence of water is the key to hydrate formation during the extraction of oil and gas, the removal of water prior to transportation by using an offshore dehydration plant or subsea separator is the best preventive strategies. However, these facilities require significant investments as well as a number of logistical issues (Mokhatab et al., 2007). The three most common methods of gas dehydration include liquid desiccant (glycol) dehydration, solid desiccant molecular sieves) and refrigeration. Of the various methods, glycol dehydration is the most common (Igboanusi and Opara, 2011)

Another method to prevent hydrate formation is to manipulate the pressure (P) and temperature (T) conditions out of the hydrate formation region (shown in shadow area) based on the knowledge of hydrate equilibrium curve (HE). The yellow point which is within the hydrate formation region (left of the HE) can be moved into the hydrate free

region (right of the HE) via different techniques including depressurization, heating and/or insulation, etc.

The technique of depressurization aims to lower the pressure below the equilibrium pressure at local temperature so as to manage hydrate formation (Li et al., 2016). However, this results in a low production rate due to the slow dissociation of hydrate (Lee et al., 2010) and it may be not practical when it comes to long and high-pressure gas transmission pipelines. In addition, rapid gas decompression at the wellhead leads to a lower temperature and, thus, could favour the formation of hydrate (Mokhatab and Poe, 2012).

The thermal method targets on keeping the system operating temperature above the hydrate formation threshold (Gbaruko et al., 2007b) via either the conservation and/or introduction of heat. Heat conservation is achieved by insulation, which is common practice for industry (Hunt, 1996). Figure 2.5 illustrates three types of heat conservation by insulation, these are insulation outside the pipe wall, insulation in between the inner and outer pipe, and vacuum the interspace between the inner and outer pipe respectively. This method can be feasible for some subsea applications depending upon the fluid being transported, the tie back distance, and topsides capabilities of host platform. Despite its high capital expense (CAPEX) and technical challenges in preventing the hydrate formation during a long-term shutdown, it generally prevents hydrate formation during normal operation conditions (Mokhatab and Poe, 2012).

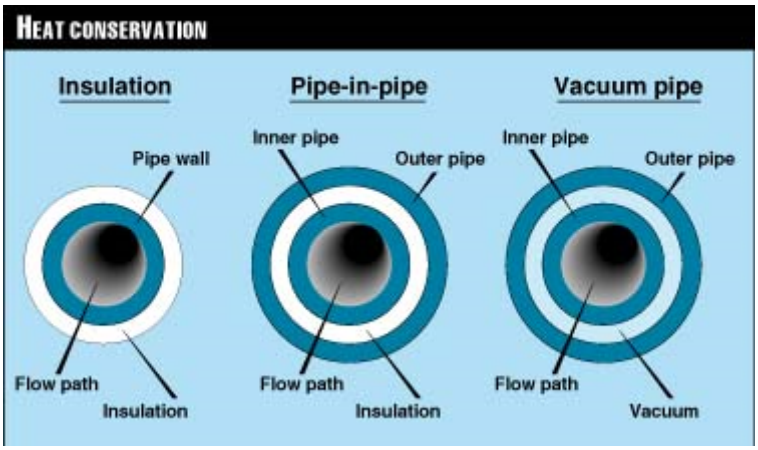

Figure 2. 5 Heat conservation technologies (Hunt, 1996).

The concept of introducing external heat to a pipeline has been suggested as another promising thermal method. For instance, hot fluid circulation using an external hot-water or oil jacket has been commonly accepted by industry. It is flexible for extending the cool down time indefinitely and is capable of warming up a line from seawater temperature to a target operating level. However, there is a limitation in terms of length because the circulation loop system requires storage facilities and significant energy to heat the flow (Denniel et al., 2004). Alternatively, electrical heating is rapidly maturing as a possible solution. This involves direct electrical heating and indirect electrical heating (Lervik et al., 1997). Direct electrical heating is based on induction heating by applying an AC-current directly through the pipeline. Indirect electrical heating system, however, are based on electrical heating elements which are installed on the outer surface of the pipe (Cochran, 2003). It is believed that trace heating, which is one type of indirect electrical heating technology, can provide the highest level of heating efficiency and is workable in bundles and pipe-in-pipe system. Moreover, trace heating can be applied even with very long tie-backs by either using higher voltage or by introducing intermediate power feeding locations (Denniel et al., 2004).

Overall, active heating methods offer a fundamentally different and simpler approach to managing hydrates in deep water subsea flowlines compared to production chemical additives (Pattee and Kopp, 2000). When applying hot fluid circulation and electrical heating technology the industry practice is to combine them with thermal insulation to minimize power requirements (Lervik et al., 1997). Such systems provide environmentally friendly fluid temperature control and enhance the production since there is no time lost by unnecessary operation for hydrate remediation. However, it is still difficult to persuade operators to install the expensive heating system (Mokhatab and Poe, 2012) as this is no complete solution for hydrate prevention.

An alternative method to thermal control P and T is adding thermodynamic hydrate inhibitors. These are able to shift the HE to lower temperatures or higher pressure (green line has been shifting towards red line as can be seen in Figure 2.4). Unlike THIs, LDHIs presented in the hydrate formation region in the Figure 2.4 merely change P and T conditions they have different mode of action in terms of hydration inhibition. More details regarding chemical methods are given in the next section.

2.5.1 Chemicals method to hydrate prevention

A variety of chemical inhibitors are injected into the flowline to prevent hydrate formation via distinct mechanisms. They can be broadly divided into two categories: thermodynamic hydrate inhibitors (THIs) and novel low dosage hydrate inhibitors (LDHIs) including kinetics hydrate inhibitors (KHIs) and anti-agglomerant inhibitors (AAs). Table 2.3 summarizes applications, benefits, and limitations of the chemical inhibitors in a broad sense.

Table 2. 3 Summary of Chemical Inhibitors Applications, Benefits, and Limitations according to (Pickering et al., 2001).

	Thermodynamic	**Kinetic**	**Anti-Agglomerant**
Applications	Multiphase	Multiphase	Multiphase
	Gas & condensate	Gas & condensate	Gas & condensate
	Crude oil	Crude oil (limited)	Crude oil
Benefits	Robust & effective	Lower OPEX/CAPEX	Lower OPEX/CAPEX
	Well understood	Low volumes (<1 wt %)	Low volumes (<1 wt %)
	Predictable	May be environmentally friendly	May be environmentally friendly
	Proven track-record	Non-toxic	Non-toxic
		Tested in gas system	Wide range of subcooling
Limitations	Higher OPEX/CAPEX	Limited subcoolings (<10 °C)	Time dependency
	High volumes (10-60 wt %)	Time dependency	Shutdowns
	Toxic/hazardous	Shutdowns	Restricted to water cuts
	Environmentally harmful	System specific – testing	System specific – testing
	Volatile-losses to vapour	Compatibility	Compatibility
	Salting out	Predication at higher temperature	Limited experience
		Limited experience in oil systems	No predictable models
		No predictable models	

2.5.1.1 Thermodynamic hydrate inhibitors (THIs)

Traditional chemical inhibitors such as methanol (MeOH) and mono-ethylene glycol (MEG) are referred to as thermodynamic hydrate inhibitors (THIs) because of their ability to shift the hydrate equilibrium curve toward higher pressures and lower temperatures. It is suggested that the thermodynamic hydrate inhibitors change the structural organisation of water, which reduces the possibility of the hydrate formation as part of their effect (Makogon et al., 2000b). Specifically, these hydrogen-bonding fluids compete with hydrate for the available water molecules once being injected at the wellhead. (Fu et al., 2001; Koh et al., 2011).

The use of THIs are proven effective technologies for flow assurance and thermodynamic models for predicting the dosage required for hydrate prevention are well developed due to their extensive use for over half a century. Methanol is usually used in non-regeneration systems, whilst glycols are commonly used in continuous processes where the inhibitor is recycled. Methanol is much cheaper compared to ethylene glycol per unit volume, has a lower viscosity and is easier to inject. However, methanol is volatile and some of it is lost into the gas phase, as opposed to the aqueous phase where it should be inhibiting hydrates. Corrosion problems may also result from methanol use because of its high oxygen solubility, which, if not removed prior to injection, will lead to internal corrosion. In addition, the presence of methanol can reduce the efficacy of some corrosion inhibitors (Igboanusi and Opara, 2011). Moreover, methanol adversely impacts the oil and water separation process by reducing the density difference between the hydrocarbon and aqueous phase. Methanol toxicity is an issue, too. High concentrations of methanol and ethylene glycol can also aggravate scaling problems in oilfield brines and halide precipitation in high salinity systems (Frostman et al., 2003).

Overall, the major challenge with THIs is the high dosage requirement for injection (up to 50 wt % of the produced water) and significant attendant costs, including logistics of transportation and storage of large volumes on the facility, as well as decreased production rates (since the THIs take up valuable space inside the pipeline). It is estimated that the worldwide methanol cost for hydrate inhibition in 2011 was about US$220 million annually (Koh et al., 2011). As long as THIs are used in a high enough concentration, hydrate will no longer form at the operating temperature and

pressure. However, often the water production rates, especially when the field is aging, surpass the capacity of the system to inject THIs (Frostman et al., 2003).

2.5.1.2 Low dosage hydrate inhibitors (LDHIs)

In addition to the well-known THIs, which, as stated above, require a high dosage, novel low dosage hydrate inhibitors (LDHIs), such as kinetic inhibitors (KHIs) and anti-agglomerants (AAs), have been developed as the latest tools for flow assurance (Koh et al., 2011). The term LDHI was confined to distinguish these inhibitors from THIs in two main aspects:

(1) Low concentration (0.1-1 wt%) required

(2) Distinctive mechanism of hydrate inhibition

While the use of THIs, such as methanol and glycol, is a proven technology, the operating and capital expenses (OPEX and CAPEX, respectively) for application are significant. The dosage of LDHIs is orders of magnitude lower than methanol or glycol. This provides significant CAPEX savings by eliminating bulky topsides equipment in addition to potential OPEX savings in treatment costs.

These new chemicals have been extensively investigated for more than a decade, in both academia and the petroleum industry, and are rapidly being adopted in the field as a viable alternative thermodynamic inhibitors (Mehta et al., 2002).

Kinetic hydrate inhibitors (KHIs)

The discovery of kinetic hydrae inhibitors (KHIs) is owed to the observation of a certain kind of fish (Winter Flounder) that does not freeze in subzero temperature waters. This unique phenomena led to the finding of antifreeze proteins (AFPs), which bounds to microscopic ice crystals and prevented their subsequent growth (Mehta et al., 2002). These proteins exhibit distinct structural features, such as a regular array of hydrophilic amino acid residues, which are thought to interact with growing surface of an ice crystal. This inspired research into the first generation of synthesized water-soluble amides poly(N-vinyl pyrrolidone) (PVP) conducted at the Colorado School of Mines. It was reported that the hydrate inhibition activity of PVP, with a molecular

weight over 20000, was particular effective in a ball-stop rig test (Perrin et al., 2013). Followed by PVP, the second generation inhibitors poly(N-vinyl caprolatcam) (PVCap) and its copolymers were synthesized. These species were found to outperform the PVP. Nowadays PVP with PVCap and its copolymers are commercially available and are the benchmark for testing the performance of new synthesized polymers.

KHIs are typically water soluble polymers with small cyclic amide groups as the active components (Igboanusi and Opara, 2011). Typical examples of KHIs, including PVP and PVCap, are shown in the Figure 2.6. These KHIs are usually formulated in a solvent along with synergistic products, which are a number of non-polymeric hydrate inhibitors, such as tetrapentylammonium bromide, butoxy-ethanol and certain polyehtermaines that can work as KHI synergists (Kelland, 2006).

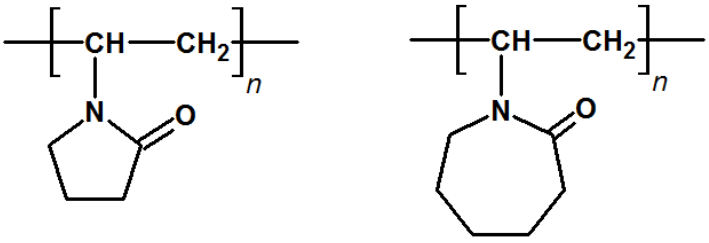

Figure 2. 6 Structures of known KHI PVP and PVCap are shown respectively.

The exact mode of action of KHIs has not been discerned to date even with the modern technology molecular dynamic simulation (MD). Yet it is believed that the polar functional groups of KHI would interact with molecular cages on the hydrate surface to hinder the initial growth and delay the nucleation (Shahnazar et al., 2018) , possibly to a time longer than the residence time of hydrocarbons in the pipeline (Igboanusi and Opara, 2011). This allows the transportation of hydrocarbon/water fluids for a certain period before hydrates start to form. Once this period has lapsed, there is often a very rapid conversion of the remaining water into large hydrate accumulations, usually resulting in a blockage. In the event of a shutdown, if the system is not restarted within the allowable period of time, the pipeline is exposed to a serious hydrate-formation risk (Mehta et al., 2002). The time to the formation of the first hydrate crystals is

called induction time. Hence, KHIs are indeed time-dependent in terms of their application.

In addition to induction time, subcooling is another key factor that determines the efficiency and the applicability of KHIs. It can be defined as the difference between the hydrate equilibrium temperature and the operating temperature at a given pressure (as shown in Figure 2.7). This is the driving force of the kinetics of hydrate formation (Peytavy et al., 2007). All KHIs are limited by subcooling, beyond which they are ineffective. The higher the subcooling, the smaller is the induction time that can be achieved, and, thus, the lower the efficiency of the KHIs. Today available KHIs can prevent gas hydrate formation for days at subcoolings up to 13°C. However most of them can only be used in the subcooling less than 12°C (Igboanusi and Opara, 2011) so they are not a feasible option, particularly in deeper waters with high subcooling.

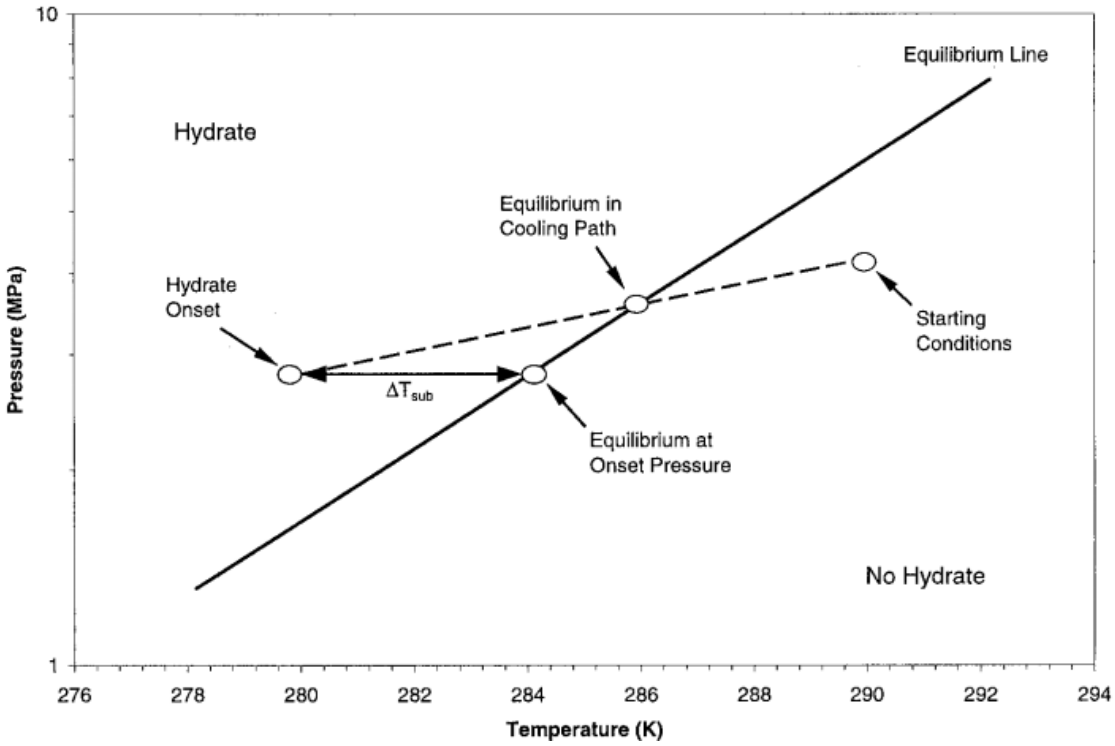

Figure 2. 7 The subcooling (ΔTsub) is the difference between the hydrate equilibrium temperature and the operating temperature at a given pressure (Perrin et al., 2013).

Other factor such as cloud point (the temperature at which the inhibitors becomes cloudy in solution due to polymer aggregation) is also of importance for choosing a suitable LDHIs for a given application.

The development of novel polymers with enhanced performance in terms of subcooling, hydrate inhibition, cloud point, salt tolerance and biodegradability are being more and more important to meet different field requirements. However, very few advancements were made in developing novel potent KHI for the past decade as there are two main hindrances.

First of all, free radical polymerization, a traditional routine method to synthesize KHI is limited in practically. Specifically, chemical structures are confined by this synthesis method. For example, synthesis of a hydrophobic monomer along with a hydrophilic monomer is difficult to achieve since appropriate solvents have to be chosen carefully, since they determine the success of polymerization. Moreover, it is rather difficult for free radical polymerization to incorporate more than two monomers (terpolymer). Even though various target products can be synthesised, it will take a substantial amount of time to tailor the procedures for each individual compound. In addition, the products produced from each study are somewhat not comparable, since the molecular weight is difficult to control by this method, hence, reliable computer models cannot be established.

Secondly, time-consuming validation tests for each produced compound needs to be performed. Traditional experiments for hydrate inhibition performance of inhibitors, such as autoclave testing, takes vast amount of time. In fact, there is a lack of an efficient validation method for screening libraries of new materials.

This study overcame these hindrances by utilising an alternative synthesis method and by developing a novel reliable rapid-screening method for large libraries of new materials.

Anti-Agglomerants (AAs)

Anti-agglomerants (AAs) are another class of low dosage hydrate inhibitors (LDHIs). They act by preventing hydrate crystals from agglomerating into large masses. Instead of eliminating the nucleation of hydrate, they ensure that the hydrate crystals remain

small and well dispersed in the liquid hydrocarbon phase so that low viscosity fluid can be transported without composite hydrate blockage. AAs are thought to have the ability to alter the crystal size of hydrates and the morphology of their agglomerates, as they are usually surfactants containing a head that is attracted to the hydrate and a tail that is dispersed in the liquid hydrocarbon phase. The most efficient among these are certain organic-, quaternary ammonium- and phosphonium salts with one or two long, oleophilic tails (Fu et al., 2001; Igboanusi and Opara, 2011; Mehta et al., 2002).

The applicability of AAs is independent of time or the degree of subcooling, however, they are only effective in the presence of a continuous liquid hydrocarbon phase and their efficacy is subject to water-cuts. At water cuts of less than 50%, no significant increase in fluid viscosity is expected. At higher water cuts, the dispersed hydrate crystals may cause an increase in the viscosity of the liquid hydrocarbon phase and may restrict the flow of the hydrate slurry (Mehta et al., 2002). Therefore, the water-cut for AAs should be below approximately 50% to avoid the difficulty of transportation due to viscous hydrate slurries.

In general, AAs can handle a higher degree of subcooling and sustain a longer shut-in period. However, these chemicals are typically more toxic compared to KHI polymers. There are also many other concerns regarding the application of AAs. For instance, the production problems like contaminated water and emulsion formation; the concerns of erosion, over-pressure, oversize pump operability, increased energy consumption and lack of experience while pumping the resulting hydrate slurries during the operation etc. (Fu et al., 2001).

It has been reported that there are 50-70 field applications of LDHIs worldwide the majority of them related to KHIs by 2005 (Kelland, 2006). As the technology becomes more known, more fields will, most likely, plan to use LDHIs because the CAPEX savings that can be very significant compared to using THIs. In practice, however, the actual performance of a KHI, and to a lesser extent some AAs, depends on the detailed composition of the liquid hydrocarbon phase and other additives, which could also have an effect when mixing. Hence, another hurdle to overcome is combining KHIs with other production chemical additives in a single injection line (Kelland, 2006).

2.6 Corrosion

Corrosion can be generally defined as the gradual deterioration of the material and its properties, typically referred to the metal, as a result of chemical or electrochemical reaction with its environment (Amani and Hjeij, 2015).

Corrosion is normally found in every single stage of production, processing, and transportation of many commercial products and equipment, which represents a major economic problem for most industrialized countries (Tiu and Advincula, 2015). NACE International (International Association of Corrosion Engineers) estimated that $276 billion, roughly 3 % of the US gross domestic product (GDP), was concerned with the cost of corrosion in 2002. Out of that, the oil and gas exploration and production contributes about $1.4 billion (Amani and Hjeij, 2015), which can be further broken down in to $589 million in surface pipeline and facility costs, $463 million annually in downhole tubing expenses, and another $320 million in capital expenditures related to corrosion (Popoola et al., 2013). All in all, costs of corrosion involve CAPEX, OPEX, replacement expenditure and lost revenue (Kermani and Harrop, 1996).

The oil and gas industries contribute to a significant portion in the costs for corrosion, as they are facing the most severe and costly failures due to corrosion. In particular, corrosion connected with operating problems and equipment maintenance can lead to recurrent partial and even total process shutdown and result in huge economics loss (Finšgar and Jackson, 2014).

While cost is an important consequence of inappropriate corrosion control and poor corrosion awareness, of equal importance is the potential impact of corrosion on health, safety and environment (HSE). The leakages and discharges of fluids and gases, which are often flammable, present a potentially serious health and safety hazard. Moreover, the releases of production fluids associated with production additive chemicals, such as scale inhibitors, demulsifies and corrosion inhibitors, may cause contamination of water resources and significant environmental pollution (Kermani and Harrop, 1996).

Since corrosion is involved in every stage of oil and gas production, the materials used for pipeline construction play an important role as they carry liquids and gases over long distances from reservoirs to the final consumers. Over the past few decades there have been many developments in new corrosion resistant alloys (CRAs), such as austenitic stainless steels, duplex stainless steels and super-duplex stainless steels.

However, CRAs largely increase the CAPEX (cost increase by a factor of 4 to 8 per weight) and still have their drawbacks. For instance, some are susceptible to corrosion in media containing large amounts of chloride ions, whilst others are difficult to weld. Therefore, carbon steels in combination with corrosion inhibition and coatings is still the most economically material and are still the most commonly used materials for downhole tubular, flow lines, and transmission pipelines in the oil and gas industry. However, carbon steel materials are highly susceptible to corrosion in most acids (Finšgar and Jackson, 2014). Thus, the use of carbon steel is always combined with corrosion inhibition techniques to mitigate internal corrosion.

2.6.1 Corrosion mechanism

The basic corrosion process, as shown below in the Figure 2.8, is composed of four elements: an anode, a cathode, a cathodic reactant and an electrolyte. The anodic and cathodic sites are areas on the steel surface that differ in electric potential. Therein the anode is the site where the metal loses its electrons and then forms positively charged cations when exposed to a corrosive aqueous environment. The electrolyte is an ion conductive solution due to the presence of charged ions (such as sodium chloride), serving as an indispensable medium for the ionic charge transfer from the anode to the cathode. The cathode, in electrical contact with the anode (anodes and cathodes form on the same steel surface due to minute differences in composition and chemistry in the electrolyte), is the site where the electrons are consumed by the cathodic reactant (Popoola et al., 2013). During this process, the anode undergoes an oxidation reaction and ends up corroding while the cathodic reactant at the cathode is reduced and does not corrode (Amani and Hjeij, 2015).

The electric potential caused by the accumulation of excess electrons generated in the anode will be balanced out at the cathodic site by the reduction of hydrogen ions (in oxygen free environments, such as pipelines), as cathodic reactant, to form hydrogen gas, which is also the typical reaction in acidic solution that contains high concentration of H^+ (Tiu and Advincula, 2015). In the presence of oxygen contamination, the current produced due to oxidation process at the anodic site will also reduce the oxygenated water (oxygen being the cathodic reactant) to form

hydroxyl ions (Tiu and Advincula, 2015). These processes have been illustrated by Equation 2.1-2.5 (Nimmo and Hinds, 2003).

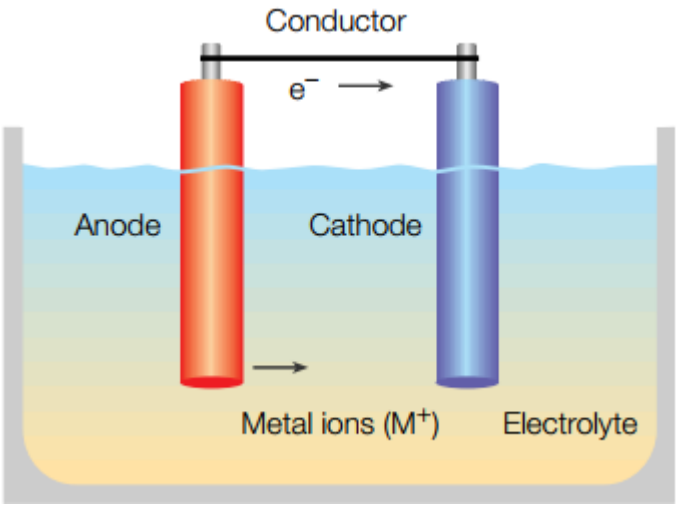

Figure 2. 8 A basic corrosion cell (Brondel et al., 1987).

The anodic reaction for metal is called oxidation reaction (Equation 2.1)

$M \rightarrow M^{n+} + ne^-$ (2.1)

After the metal release free electrons through oxidation reaction, there are four common reduction reaction which takes place at the cathode site (Equation 2.2-2.5, Figure 2.9)

$2H^+ + 2e^- \rightarrow H_2$ (2.2) (hydrogen evolution from acidic solution)

$O_2 + 4H^+ + 4e^- \rightarrow 2H_2O$ (2.3) (oxygen reduction in acidic solution)

$\frac{1}{2}O_2 + H_2O + 2e^- \rightarrow 2OH^-$ (2.4) (oxygen reduction in neutral or basic solution)

$2H_2O + 2e^- \rightarrow H_2 + 2OH^-$ (2.5) (hydrogen evolution from neutral water)

When it comes to the oil and gas industry, however, crude oil and natural gas carries various compounds which are inherently corrosive, such as introduced oxygen, hydrogen sulfide, carbon dioxide, chlorides, organic acids and microorganisms, as well as complex conditions of high temperature and pressure, resulting in more complex corrosion reactions in transmission lines. Since oxygen is not normally not

present, unless it is introduced by injection of water and chemicals, the CO_2 and H_2S corrosion are two main types that industry faces.

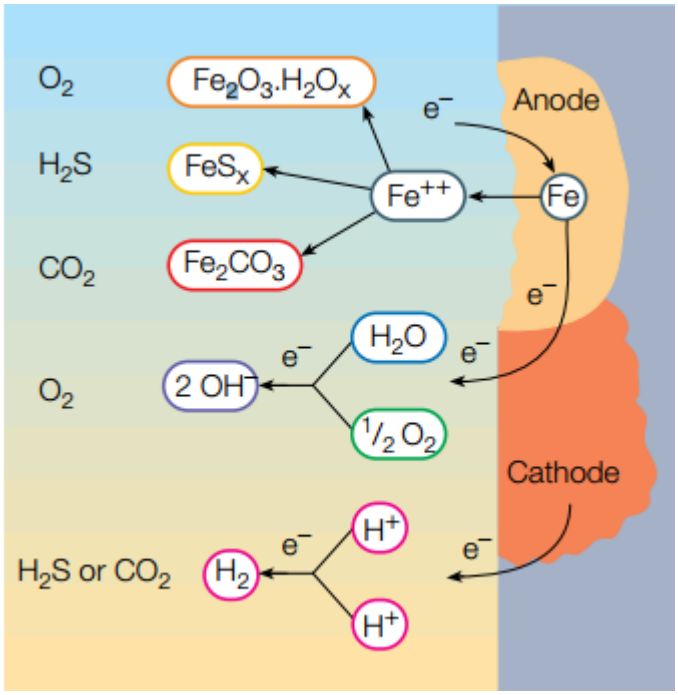

Figure 2. 9 Corrosion on a steel surface (Brondel et al., 1987).

2.6.2 Corrosion inhibition

There is general acceptance by the offshore oil and gas industry that corrosion is impossible to be completely prevented, yet corrosion can be well controlled using appropriate corrosion inhibitors. Corrosion control by chemical inhibition is one of the most mature and developed fields of production chemistry (Jones et al., 2013) and has been successfully applied for more than 50 years (Kelland, 2009). The research and development of effective inhibitors involves many researchers' and chemical vendors' efforts to produce chemistries that can act against corrosion in different oil and gas production systems (Gregg and Ramachandran, 2004). Film forming corrosion inhibitors (FFCIs) are most commonly used for protecting water containing oil and gas pipelines, and will be the focus for this thesis.

2.6.2.1 Film-forming corrosion inhibitors

FFCIs are a type of chemical substances that are highly effective against CO_2 and H_2S corrosion. Like LDHIs, they require a low dosage (typically 50 to 100 ppm based on water cut) when added to a corrosive environment to reduce the corrosion rate of exposed carbon steel. When injecting into the stream of hydrocarbons near to the well head, they form a film inside the pipe wall that slows the cathodic and/or anodic corrosion reactions and thereby protect the metal from corrosion (AlHarooni et al., 2017).

FFCIs can be small molecules or polymers, however, many of them are organic amphiphiles that contain a polar head group and a hydrophobic tail. While, working effectively, little is understood about their inhibitive mechanisms. The polar head groups are thought to interact with iron atoms on the surface and the hydrophobic tails attract liquid hydrocarbons forming an oily film, which further prevents the corrosive aqueous phase from reaching the metal surface. There are some FFCIs without hydrophobic tails can still give good corrosion inhibition by forming the film made up of the inhibitor alone or as iron complexes (Kelland, 2009). These interface inhibitors can be further classified depending on which electrochemical reaction is being blocked: anodic, cathodic or mixed-typed. While anodic inhibitors block the anodic reaction, thus preventing the oxidation reaction, cathodic inhibitors retard the corrosion by inhibiting the reduction of water to hydrogen gas (Obanijesu et al., 2014).

The effectiveness of FFCIs is mainly due to the strength of adsorption to the metal surface, and it can be also affected by the composition of the corrosive environments, shear stress and temperature (Eduok et al., 2016).

FFCIs have been divided into various classes depending on whether their head group contains phosphate, nitrogen, or sulfur, although any given commercial FFCI is composed of complex mixture of chemicals (Duncan et al., 2014).

It is worth mentioning that CIs are often only effective for a particular metallic material in a certain environment. Minor changes in the composition of the solution or alloy can significantly change the inhibition effectiveness (Finšgar and Jackson, 2014). Hence, various conditions need to be taken into consideration when selecting a reliable corrosion inhibitor in practice.

This study is using the efficient synthesis method to add typical FFCI features to the polymer structure of a typical KHI polymer, which turn a single KHI molecules into multifunctional polymers with the aim to address compatibility issues that are outlined in the following section.

2.7 Compatibility studies of KHIs and CIs

As introduced in previous sections, application of KHIs and CIs are solutions for both gas hydrate and corrosion issues. In practice, industry injects these two production chemicals together in just one umbilical line instead of using separate chemical injection lines in order to lower the production costs. The use of combination products may also be favourable because of less overall weight/volume of chemical storage and smaller numbers of storage tanks and application pumps. These are obviously beneficial for operating companies in terms of CAPEX savings and OPEX costs (Clark et al., 2005).

However, during the selection process of a KHI and CI for a North Sea field in the mid 1990's, BP noted that a corrosion inhibitor adversely affected the performance of a KHI. Since then, for fields that use both KHI and CI, Shell carries out all KHI validation tests in the presence of CI (Klomp and Mehta, 2007).

To date, many recent studies (Clark et al., 2005; Frostman et al., 2001; Fu, 2007; Jones et al., 2013; Klomp and Mehta, 2007; Moloney et al., 2009; Moore et al., 2009; Peytavy et al., 2007; Woie, 2011) have confirmed that corrosion and hydrate inhibitors could be incompatible when co-injected. The presence of CI can give rise to adverse effects to the performance of KHI or vice versa.

Klomp et al., (2007) reported that the induction time of some KHIs were considerably shortened in the presence of some CIs during rocking cell tests. The corrosion rate increased by two orders of magnitude immediately after the addition of a KHI in corrosion tests.

Moloney et al., (2009) reported a similar finding of that adverse interactions in some KHI/CI combinations can result in a significant deterioration in the inhibition of both. The corrosion rate of test sample X-65 steel in the presence of a CI and a KHI was more than two orders of magnitude greater than the blank without any chemical present.

Some CIs were not interfered by KHI in terms of general corrosion rate, however, the localised corrosion inhibition was comprised due to the presence of a KHI, which would result in pitting corrosion and asset failure occurring much faster compared to when no chemical was deployed. In addition, the failure of hydrate tests demonstrated an incompatibility of a KHI and CIs in inhibiting hydrate formation and growth. These results confirmed that mutual inference existed between KHI and CI exists in many cases. Furthermore, Moloney et al., conducted the high temperature injection testing as a secondary property evaluation, in which they found out that a KHI and a CI formed globules under high temperature and this effect might result in a deficiency of corrosion or hydrate inhibition due to the incompatibilities.

Woie (2011) indicated interference between these two types of chemistries, too. In this study the KHI Luvicap 55w impacted the performance of the imidazoline CI derivatives negatively with up to 55% in performance loss.

Other studies came to a slightly different conclusion. B. Fu (2007) suggested that the negative impact of CI on the performance of KHI were confirmed in the study using rotating cage apparatus (RCA) experiments whereas the presence of a KHI was found to improve the corrosion inhibition efficiency by being able to reduce the overall rates. Interestingly, the loss of KHI performance could be compensated by the addition of more KHI for some Cis, although this effect was not observed for all CIs.

As Peytavy et al., (2007) claimed in their works, they have never found a positive influence of the presence of CI on the efficiency of KHI, whereas they found both positive and negative effects of the presence of KHI on the CI efficiency.

These studies highlight the fact that while performance testing is an important step in selecting appropriate chemicals for specific applications, the compatibility among production chemicals is crucial and must be taken into consideration, too (Frostman et al., 2001): A CI and a KHI that perform satisfactory on their own, very likely fail the corrosion and the hydrate test protocols when both chemicals are combined (Klomp and Mehta, 2007).

2.7.1 Mechanism of KHI/CI interactions

Moore et al., (2009) proposed two possible mechanisms for KHI/CI interaction:

1. Competition for the surface interface
2. Chemical interaction at a molecule level

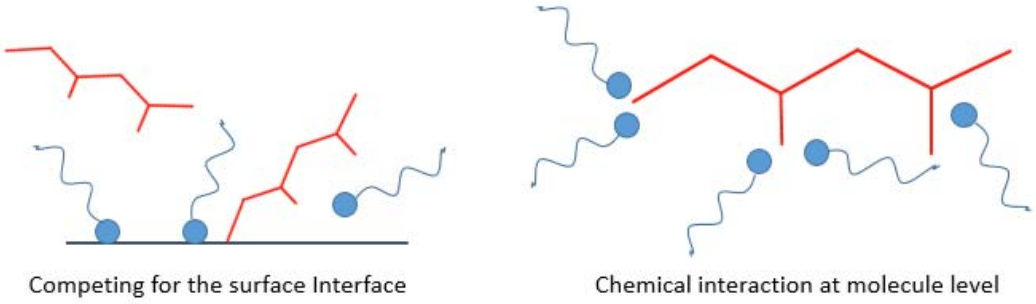

Figure 2. 10 Illustration of two possible mechanisms for KHI/CI interaction (Moore et al., 2009). The KHI polymers were represented in red whereas CI molecules were represented in blue.

Theory 1: Both chemistries are surface-active and take effect via absorption to the surface interface. KHIs are believed to bind to the surface of hydrate crystals in order to prevent the further growth of the structure while CIs absorbs onto the surface of metal to block the reaction sites. If the KHIs absorb onto the metal surface it would impact the CI in terms of forming the protective film. And it will be the same the other way around. If a CI absorb onto the surface of hydrate it would hinder the KHI from interacting the hydrate surface and thus efficiency of a KHI would be compromised.

Theory 2: The KHI polymer, in theory, has anchor points that work by distorting the hydrate structure thereby increasing the amount of energy needed to form hydrates and thus slowing down the reaction kinetics (Moore et al., 2009). As proposed by Makogon et al., (2000) that by absorption onto the hydrate crystal surface KHI polymers force crystals to grow around and between polymer strands and consequently blocking the diffusion of gas to the hydrate surface (Makogon et al., 2000a). If CIs chemically absorb onto the KHI polymers at these anchor points their ability to prevent hydrates would be affected.

Relevant experimental work was performed by Moore et al., (2009) and both mechanisms were proven to a certain extent, which offers better understanding of the interactions between KHI/CI. However, each vendor has its own portfolio of commercially protected active KHIs and Cis formulations, and they are reluctant reveal their KHI/CI formulations, which restricts the development of successful KHI/CI combinations (Klomp and Mehta, 2007).

Inspired by some studies (Burgazli et al., 2005; Hoppe et al., 2006), namely that a few chemistries were discovered that offer both hydrates and corrosion protection, it is believed that it is possible that a specific molecule displays both LDHI and CI properties, which can be achieved by designing molecules having two different functional groups, hydratephillic and metallophillic (Hoppe et al., 2006).

Thus, by developing the next generation of multifunctional inhibitors the compatibility issue may be overcome.

Chapter 3 INTRODUCTION OF CMC REACTION

3.1 Introduction

The traditional free radical polymerization is the state-of-the-art for generating most kinetics hydrates inhibitors (KHIs) currently. However, the KHIs reported to date have different molecular weight, composition or architecture due to the nature of reaction, making it difficult to study KHIs comparatively and systematically. There are also challenges associated with the incorporation of complex monomers using this route. Moreover, the mechanism of inhibition is not fully understood which again poses challenges to designing molecules with significantly improved performance—let alone multifunctional polymer for both hydrate and corrosion inhibition proposed in this thesis. Therefore, a new efficient synthetic route for generating a library of modified polymers instead traditional free radical polymerization was developed. The process is called Carbodiimide-mediated coupling (CMC) reaction. It has been used particularly for synthesis or modification of peptide and protein in biomedical studies (Al-Warhi et al., 2012). Specifically, it is widely used for carboxyl-amine conjugation (Sehgal and Vijay, 1994). CMC are more efficient than traditional free radical polymerization and allow for accurate placement of functional groups, which is favourable for investigating the structure-property relationship. The synthetic protocols also target non-toxic chemistry that offers advantages in terms of the environmental impact large scale production might have.

In this chapter, this method was applied on the commercial polymer Polyacrylamide-co-acrylic acid (PAM-co-AA) as a precursor study for further investigation. PAM-co-AAs were modified with various liner and cyclic hydrophobic motifs via this tool. The resulting materials were then confirmed using acid-base titration, spectroscopy, viscometry, and rheology. The study proves the efficiency of this new synthetic protocols.

3.2 Materials and methods

3.2.1 Materials

All of the chemicals were used without further purification. Purchased from Sigma Aldrich: polyacrylamide-co-acrylic acid partial sodium salt (PAM-co-AA), Mw 520,000, Mn 150,000, typical acrylamide level 80%; N-(3-dimethylaminopropyl)-N'--ethylcarbodiimide hydrochloride (EDC, commercial grade); N-hydroxysuccinimide (NHS, 98%); isopropylamine (isoprop, 99%); cyclopropylamine (cycloprop, 98%); cyclobutylamine (cyclobut, 98%); cyclopentylamine (cyclopent, 99%); cycloheptylamine (cyclohept, 99%); cyclooctylamine (cyclooct, 97%); heptylamine (C7, 99%), dodecylamine (C12, 99%), 1,2-diamino ethane (EDA, >99%); and potassium hydrogen phthalate (KHP, ≥99.95%). Ethanol absolute (ACS) and potassium hydroxide (KOH, 85%) were purchased from Merck, tetrahydrofuran (THF, HPLC grade) from Scharlau and deuterium oxide (D, 99.9%) from Cambridge Isotope Laboratories Inc.

3.2.2 Preparation of modified polymers

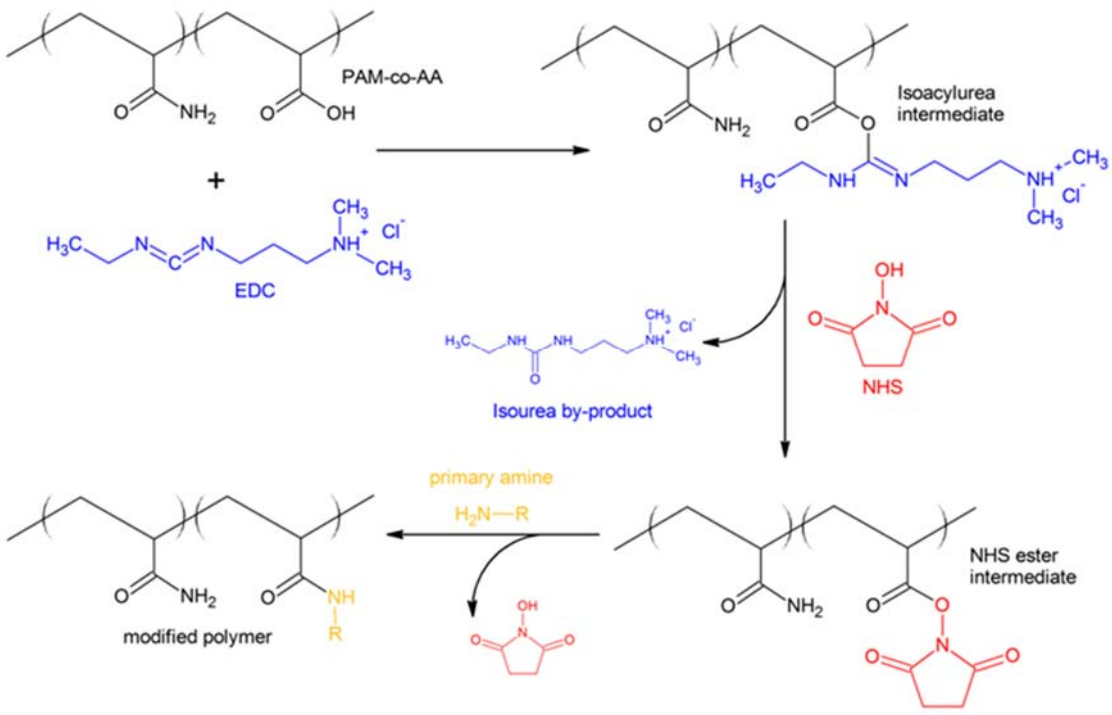

Scheme 3.1 Reaction schematic used for the synthesis of modified polyacrylamides where PAM-co-AA (shown in black) reacts with EDC (shown in blue) and NHS (shown in red) to form an activated polymer (NHS ester intermediate), the NHS is readily replaced with primary amines (shown in yellow) (Silveira et al., 2015)。

The reaction was carried out in open vials in the presence of oxygen at room temperature. EDC was dissolved in distilled water and added to an aqueous solution of PAM-co-AA (15 w/v %), the resulting solution was mixed and the viscosity increased. NHS dissolved in distilled water was then added and the mixture was vigorously mixed. The reaction was left to proceed for a further 3 min; this process activated the polymer to post-synthetic modification. For this study a stock solution of the activated polymer was prepared which was divided into different samples. After this time the requisite amine was added using a syringe (note: isopropylamine and cyclopropylamine are volatile) and the solution was mixed. Representative synthesis conditions are shown in Table 3.1 for a library of modified PAMs prepared at one polymer concentration (15 w/v %), with eight primary amines, at six concentrations. Most of the resulting polymers are soluble in distilled water and the exceptions are indicated in Table 3.1, these are polymers that have been modified with larger groups (C_7 and C_{12}) at high percentages of modification (>5% activation). The molar ratio was 1 AA : 1 EDC : 1 NHS : 1 amine for all samples prepared. For modification levels greater than 5 mol % (determined by the amount of EDC, NHS, and amine) a few drops of THF were slowly added to ensure that the final solution was homogeneous. The resulting polymers were purified by re-precipitating into ethanol, followed by drying under vacuum at 50°C, and then freeze dried.

Table 3. 1 Representative synthesis conditions based on 5 mL of a 15 w/v % PAM-co-AA solution(Silveira et al., 2015).

Activated polymer (%) [a]	Activators		Primary amines [b]							
	EDC (g)	NHS (g)	Isoprop (μL)	Cycloprop (μL)	Cyclobut (μL)	Cyclopent (μL)	Cyclohept (μL)	Cyclooct (μL)	C_7 (μL)	C_{12} (mg)
1	0.0201	0.012	9.1	7.28	9.0	10.1	13.2	14.2	12.0	19.3
2	0.0399	0.024	18.2	14.6	18.0	20.2	26.3	28.5	24.0	38.7[e,f]

5[c]	0.1005	0.06	45.4[d]	36.4[d]	45.0[d]	50.4	65.8	71.1	60.1[g]	96.6[g]
10[c]	0.201	0.12	90.8	72.8	90.0	100.8	131.6	142.2	120.1[g]	193.3[g]
15[c]	0.300	0.18	136.2	109.2	135.0	151.2	197.4	213.3	180.2[g]	289.9[g]
20[c]	0.399	0.24	181.6	145.6	180.0	201.6	263.2	284.5	240.3[g]	386.5[g]

[a] Mol % of polymer repeat units activated with EDC and NHS, 20 mol % is the maximum because the polymer contains 20% acrylic acid (AA), the molar ratio 1AA :EDC : 1NHS.
[b] Polymers are denoted as PAM-amine-x, where x represents the theoretical modification percentage of the polymer by the requisite amine.
[c] To maintain a homogeneous solution after adding the amine at a concentration higher than 5% it was necessary to add THF (0.5 mL - 1.5 mL) to the final solution apart from systems marked (d).
[e] this system was used for further reaction to form a hydrogel by cross-linking through remaining carboxylic acid groups.
[f] PAM-C_{12}-2 was used for the shear thinning rheology test.
[g] polymers are insoluble in water.

3.2.3 Hydrogel synthesis from modified PAM

A hydrogel based on a 2 mol % dodecylamine modified polymer (PAM-C_{12}-2, Table 3.1) was generated by first functionalizing the polymer and subsequently cross-linking. For the hydrogel 0.798 g EDC and 0.48 g NHS was dissolved in 1 mL of distilled water respectively. Then a 10 mL solution of PAM-co-AA (15w/v %) was activated by EDC. After 3 min, NHS was added to the solution and was left for a further 3 min, the final solution is a polymer with full activation (20 mol %). The functionalization was carried out with the addition of 0.0772 g dodecylamine (C_{12}) dissolved in 0.1 mL THF and 0.5 mL of distilled water, the solution was thoroughly mixed. After 3 minutes 0.108 g of 1,2-diaminoethane (EDA) dissolved in 1 mL of distilled water was added to the solution to cross-link the polymer through the remaining activated carboxylic groups that were not reacted with dodecylamine (18 mol %).

3.2.4 Titration of the polymers

The acrylic acid content of the polymers was measured by acid-base titration. The solutions were prepared with approximately 0.4 g of purified polymer. The polymers were left for 24h at room temperature to ensure they were dissolved. The solutions were then titrated against potassium hydroxide (KOH) 0.01N which had been previously standardized with potassium hydrogen phthalate (KHP). Phenolphthalein in ethanol 1 wt% was used as the indicator. The acid number (mg KOH/g of sample) was calculated using the equation (3.1) and (3.2), where:

$$\mathrm{AN} = \frac{\mathrm{Vol}_{KOH} \text{ x N x } 56.1}{\mathrm{W}_{polymer}} \tag{3.1}$$

Vol_{KOH} is the volume of titrant, N is the molar concentration of titrant, 56.1 is the molar mass of KOH, and $\mathrm{W}_{polymer}$ is the mass of polymer in grams.

$$\mathrm{N} = 1000\ \frac{\mathrm{W}_{KHP}}{204.23 \text{ x } \mathrm{Vol}_{KOH}} \tag{3.2}$$

3.2.5 Viscosity determination of polymer solutions

The viscosity measurements were conducted on a vibrational viscometer (Vibro Viscometer, SV-1A), at 25 ± 0.1 °C, using distilled water as standard for calibration. A water jacket was used in conjunction with a refrigerated bath and heat circulator (Thermoline Scientific) to ensure that the samples remain at a constant temperature during the measurements. The polymer solutions were prepared by dissolving the polymers in distilled water for 24 h at room temperature. The samples were left in the system for 15 minutes before the measurement to ensure that the temperature had equilibrated.

3.2.6 Nuclear magnetic resonance

^{1}H NMR spectroscopy was performed on a Bruker Av400 NMR spectrometer using deuterium oxide (D_2O) as solvent and ^{13}C NMR spectroscopy was performed on a Bruker Av500 NMR spectrometer with a 10 mm autotuning and matching broad band observe probe. Samples with concentration of 50 wt% H_2O/D_2O (9:1) were held at 50°C inside the probe. An 83° pulse was used with inverse-gated 1H decoupling using a bilevel waltz-16 decoupling sequence. The acquisition time was 1.08 s and the relaxation delay was 10.0 s, the sum of 11.1 s being greater than 53 the longest T1 measured using an inversion recovery sequence. The data were zero-filled once and exponential multiplication using 5 Hz line broadening was applied prior to Fourier

transformation. The NMR is used for qualitative analysis because it is challenging to accurately determine composition for these polymers using NMR.

3.2.7 Rheology

Rheology was performed using a HR-3 Discovery Hybrid Rheometer (TA Instruments) and a smart swap recessed concentric cylinder geometry with a cup (radius 15mm) and rotor (radius 14mm, and height 42mm). The gap between the bottom of the cup and rotor was set at 4 mm and heating was achieved using Peltier heaters. For measuring Hydrogels: The PAM-co-AA base polymer was activated with EDC and NHS, then the cross-linker was immediately added. 12 ml of the resulting solution was quickly loaded into the measuring geometry. A lid was used to cover the cup to minimize evaporation of the water and to further prevent this mineral oil was poured on the top of the solution and as a result no shrinkage of the hydrogels was observed. Cross-linking was monitored as a function of time and the oscillation frequency was 1 Hz and strain was kept at 0.01%. The experiments were performed for 19.5 hours to ensure the cross-linking reaction was complete which was determined as the plateau in the modulus which occurred before 19.5 hours. Shear thinning testing was performed in a flow sweep mode with the same configuration. The shear rate is from 0.01 to 3500 1/S, using a solution of 12 mL, 5 wt% of PAM-C_{12}-2 (Table 1f) and a solution of PAM-co-AA base polymer (5wt%) were tested.

3.3 Results and discussion

The polymers synthesized were obtained by post-synthetic modification of a precursor poly(acrylamide-co-acrylic acid) with various amines. This was achieved using a carbodiimide mediated coupling reaction (CMC) resulting in a library of modified PAM-based polymers including hydrophobically modified water soluble polymers (HMWSP). All of the polymers possess the same molecular weight but with different functional groups incorporated at controlled concentrations. This flexibility is not possible using free radical polymerization. In the following sections the synthesis and characterization of the polymers is discussed.

3.3.1 Synthesis of modified PAM-libraries

Prior to modification of the PAM-co-AA base polymer it was characterized to determine the concentration of the acrylic acid groups as discussed in one of our previous work (Sheng et al., 2014). The base polymer contains 20 mol% of acrylic acid groups that can be used for modification. The CMC reaction used 1-ethyl-3-(3-dimethylaminopropyl) carbodiimide hydrochloride (EDC) and H-hydroxysuccinimide (NHS) which are routinely used to activate carboxylic acid groups to react with amines to form an amide bond (Scheme 3.1). The EDC reaction results in the formation of an acylurea which undergoes further reaction with NHS to form a more stable NHS intermediate. This NHS-modified group readily reacts with amines to form an amide bond (Valeur and Bradley, 2009). The reactions proceeded at room temperature in aqueous solution and were carried out in open vials. It is worth noting that the side products from the reaction are isourea and NHS so carbodiimide coupling is regarded as a nontoxic transformation (Greim et al., 1998; Park et al., 2002). The primary hazards associated with the amines used to modify the polymers is their corrosiveness, however, as we discuss in the following sections unreacted amines were not detected in the modified polymers. In contrast, free-radical copolymerization uses a number of reagents that can all contribute to toxicity including acrylamide, initiators, and co-monomers. Therefore, the CMC reaction offers an alternative route to generate modified PAM-based polymers that eliminates the use of toxic monomers.

As can be seen from the reaction mechanism (Scheme 3.1) the extent of modification of the polymers can be controlled simply by changing the concentration of the EDC, NHS, and amine. The maximum level of modification is controlled by the amount of acrylic acid in the base polymer. The polymer used in this study contains 20 mol% acrylic acid which is the maximum level of modification. However, there are a broad range of different base polymers that are commercially available or can be synthesized that could be used with this route. For HMWSP the amount of incorporation of hydrophobic groups is typically less than 5 mol% which can be easily controlled using the CMC reaction. However, HMWSP display slow dissolution rates often taking a number of days to dissolve, which impedes their implementation. The solubility of HMWSPs decreases with hydrophobe content, molecular weight, and hydrophobe chain length. This limits the maximum hydrophobe content that can be introduced into a HMWSP. This can be overcome by further hydrolysis of the acrylamide in HMWSP

(Feng et al., 2002; Zhu et al., 2007) to generate charged carboxyl groups to impart better solubility in water (as well as increased viscosity). The resulting polymers are terpolymers containing three structural units including acrylamide, charged carboxyl, and hydrophobic groups. Using the CMC reaction structurally analogous terpolymers were readily generated when <20 mol% modification was carried out due to the carboxyl groups that had not been activated with EDC and NHS which is an important advantage of this route. For free radical routes control over the incorporation of three monomers is extremely challenging. As discussed in the following section the dissolution rates for the polymers synthesized in this study were less than 24 hours.

3.3.2 Characterization of modified PAM-libraries

To determine if the reactions outlined in Table 3.1 were successful detailed characterization of the polymers was carried out including titration of the acid groups, NMR spectroscopy, and viscosity measurements. Figure 3.1 shows the acid number for the polymers as determined using acid-base titration. The acid number represents the mass of potassium hydroxide that is required to neutralize one gram of the polymer.

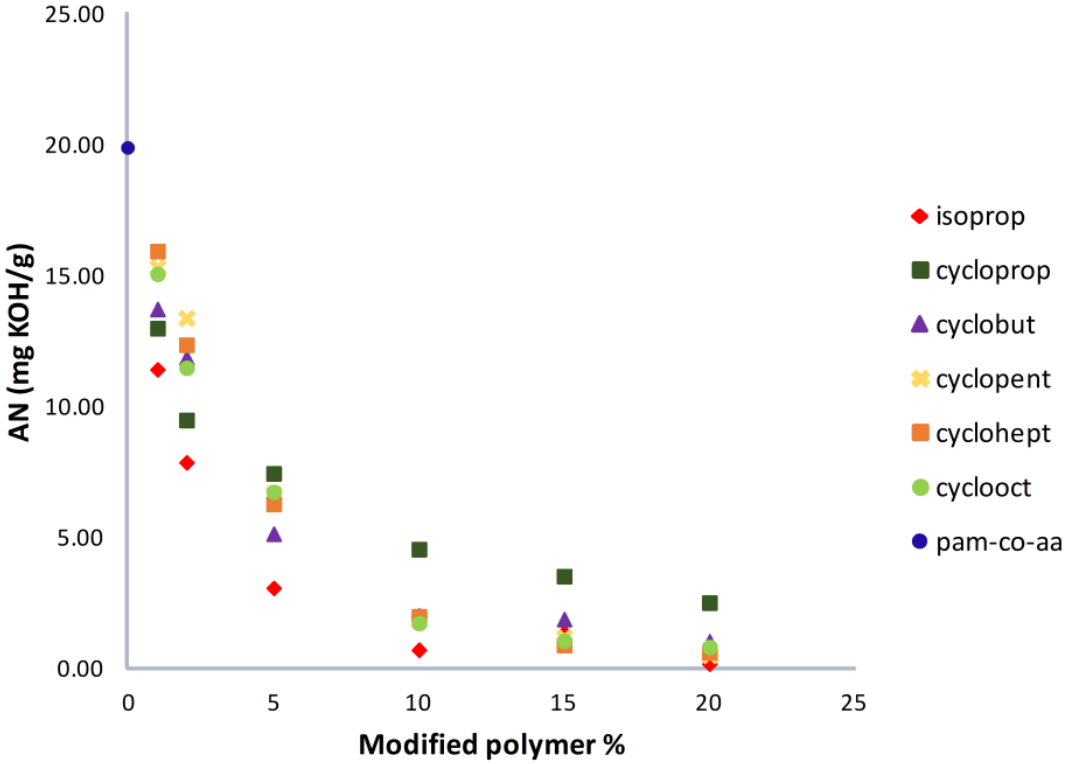

Figure 3. 1 Acid number determined by titration for the PAM-co-AA base polymer and six different functional groups at six different levels of incorporation (Silveira et al., 2015).

The acid number for the base polymer is the highest as shown in blue. As the percentage of modification increased (by using higher concentrations of EDC, NHS, and amine) the acid number decreased. This is due to consumption of the acrylic acid during the modification reaction so the higher the percentage of modification the less acrylic acid is present. The decrease is seen for all the different amine functional groups that were used. The trend for this reduction is also the same for each functional group. However, the acid number is not the same at one percentage of modification across the different functional groups. This is due to inaccuracies when the activated polymer solution was split, in order to improve the accuracy the samples can be prepared separately. In addition, the reactivity of the amines towards the NHS-modified intermediate is different. Alternatively, the solution properties of the resulting polymers vary substantially and the accessibility of the carboxyl groups could be different particularly at elevated pH as the polymers could be contracting. Therefore,

further studies were carried out using NMR spectroscopy to reinforce the successful modification of the polymers.

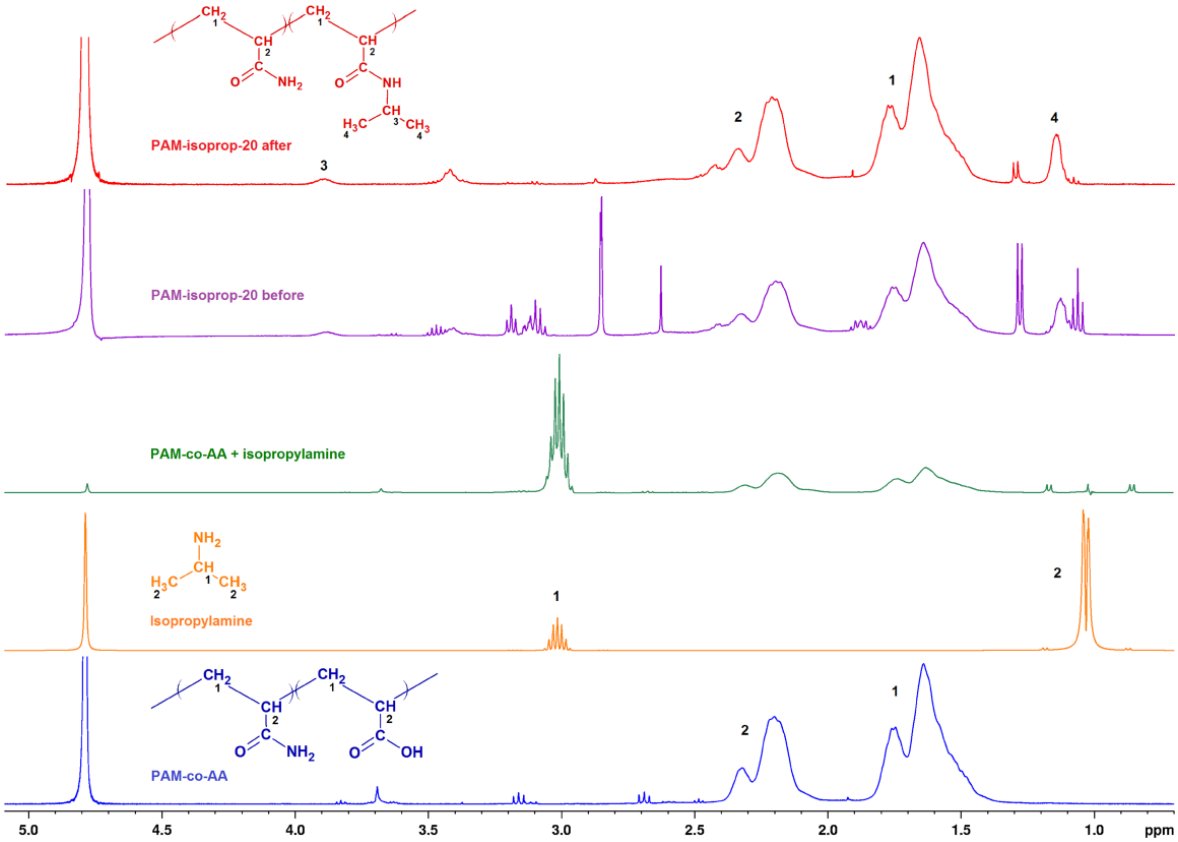

Figure 3. 2 ^{1}H NMR spectra for the base polymer (shown in blue), isopropylamine (shown in orange) which was used to modify the polymer, a mixture of the isopropylamine and base polymer (shown in green without EDC and NHS), and 20% modified polymer before purification (shown in purple), and 20% modified after purification by re-precipitation into ethanol three times (PAM-isoprop-20, shown in red) (Silveira et al., 2015).

^{1}H NMR for the base polymer shows the characteristic peaks for PAM-co-AA and the chemical shifts are highlighted in Figure 3.2. The spectra for isopropylamine (isoprop) and a mixture of the base polymer and isopropylamine are also shown as controls. The peaks for the isoprop can be clearly seen in the mixture with the base polymer. The base polymer was then reacted with isopropylamine using the CMC reaction and the resulting ^{1}H NMR spectra for both the crude (shown in purple) and purified products

(shown in red) are included. As can be seen the spectra for the modified polymer varied substantially from the base polymer and from the mixture of isoprop/PAM-co-AA. The additional peaks present in the spectra have been assigned confirming successful modification of the polymer. For the polymer before purification the additional peaks are due to the non-toxic isourea and NHS side products (NMR spectra shown in Figure 3.3). These side products are removed by re-precipitating the polymer three times.

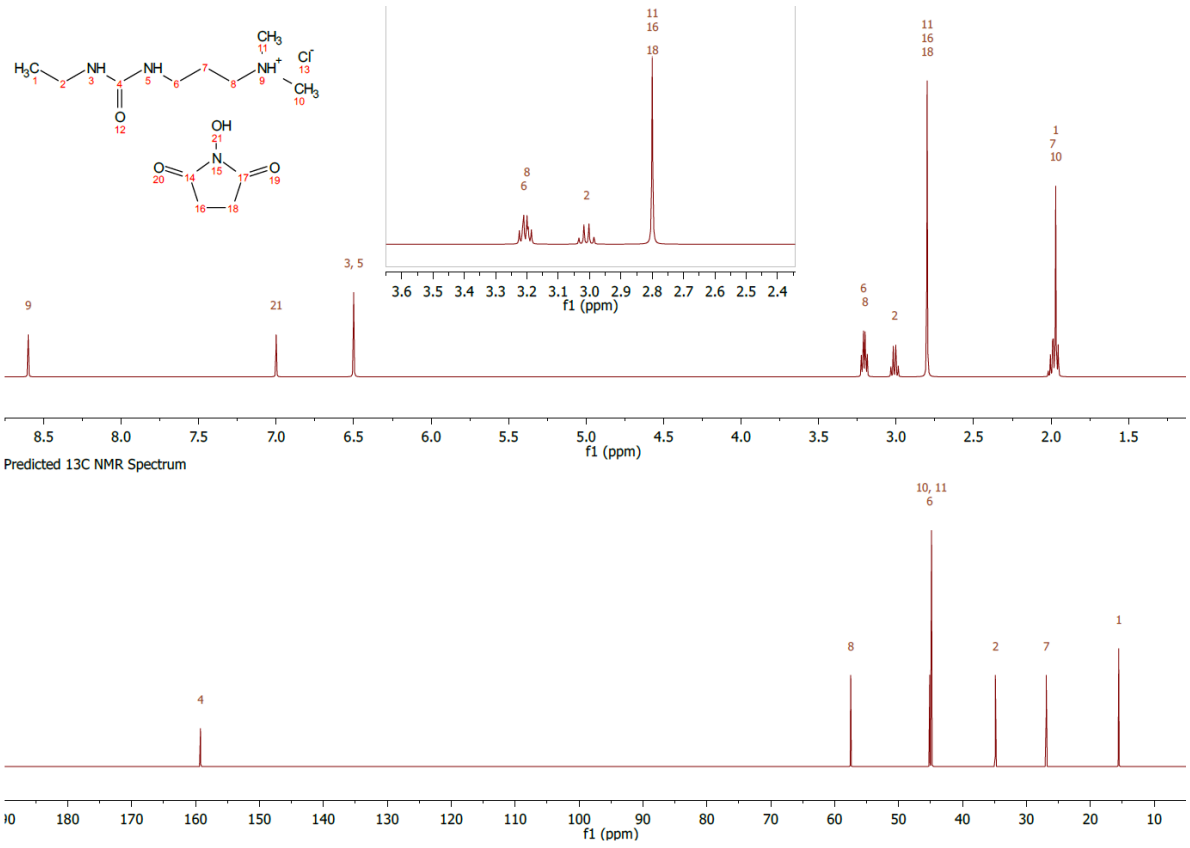

Figure 3. 3 ^{1}H and ^{13}C NMR spectra of the by-products confirming successful modification of the polymer (Silveira et al., 2015).

Figure 3.4 shows ^{13}C NMR spectra for a range of HMWSP and the base polymer. As can be seen the spectra for the base polymer (shown in blue) consists of four major peaks including carbonyl peaks (indicated as C_3 and C_4) and alkyl peaks from the backbone (C_1 and C_2). For the modified polymers the spectra are different with a number of additional peaks which have been assigned to the functional groups incorporated on the modified polymers.

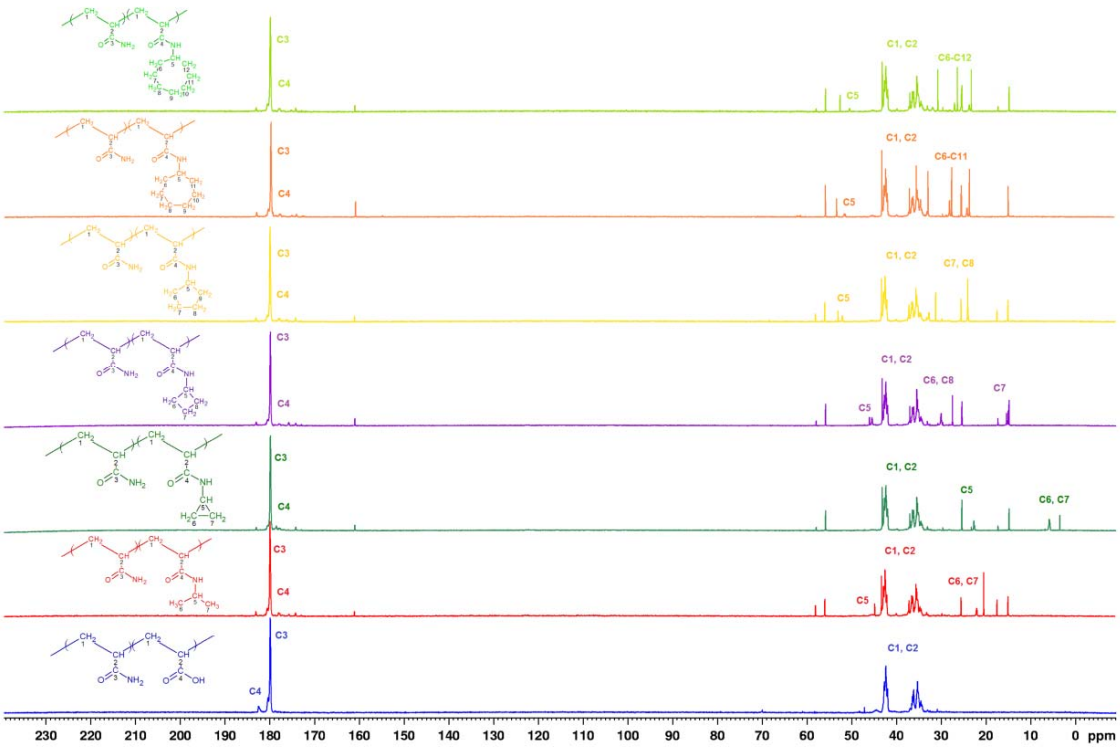

Figure 3. 4 ^{13}C NMR spectra for the base polymer (shown in blue) and 20% modified polymers with different functionality from isopropylamine (PAM-isoprop-20, red), cyclopropylamine (PAM-cycloprop-20, green), cyclobutylamine (PAM-cyclobut-20, purple), cyclopentylamine (PAM-cyclopent-20, yellow), cycloheptylamine (PAM-cyclohept-20, orange) and cyclooctylamine (PAM-cyclooct-20, green), all polymers have been purified by re-precipitation one time (Silveira et al., 2015).

3.3.3 Viscosity

Synthetic water-soluble polymers have been used for a number of years as viscosity enhancers. The ability to controllably place functional groups is essential to maximizing viscosity. Hydrophobic groups can provide the largest enhancements in viscosity as they tend to associate with each other forming intra or intermolecular aggregates which causes a significant increase in the viscosity of the solution. Figure 3.5 shows the viscosity for a range of modified-PAMs at different polymer concentrations, each polymer was modified with 2 mol% of functional groups.

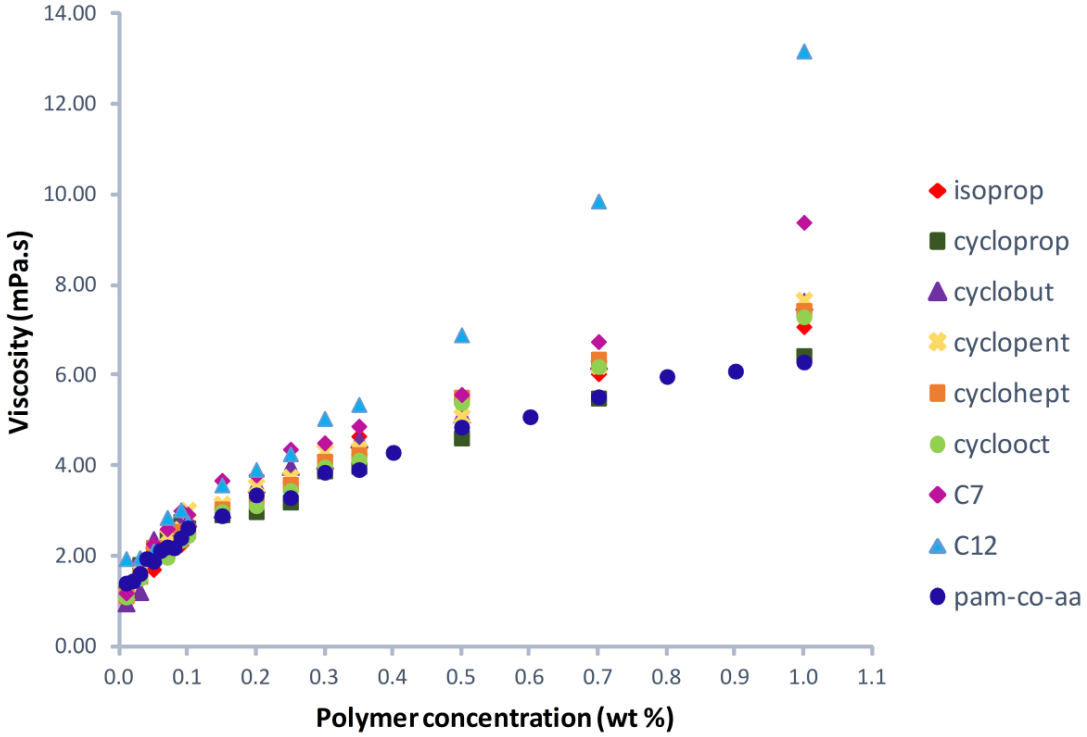

Figure 3. 5 Effect of polymer concentration on the viscosity of a range of modified polyacrylamide-based polymers at 25°C with 2 mol% modification(Silveira et al., 2015).

In the hydrolysed polyacrylamide sample used as the base polymer (PAM-co-AA, Figure 3.5) the modification of the polymer occurs on the acrylic acid groups. Before modification these carboxylate groups cause repulsion of the ionic groups resulting in chain extension, thus the viscosity of a solution with HPAM increases (Needham and Doe, 1987). The solubility of the polymers will also increase due to the presence of these charged groups. We replaced 2 mol% of the acrylic acid with cycloamine groups or longer alkyl chains. Figure 3.5 shows the change in viscosity for all of the resulting polymers which demonstrates that the viscosity is sensitive to the structure of the functional group. As can be seen the inclusion of these groups generally increases viscosity compared to the PAM-co-AA base polymer which is due to hydrophobic interactions. As the polymer concentration is increased the viscosity increases for all of the polymers. The functional group that had the largest effect was the long C_{12} alkyl chain (PAM-C_{12}-2) which is attributed to the enhanced hydrophobic interactions

because this is the most hydrophobic group included. The effect of polymer concentration on the hydrophobic association, and hence viscosity, is higher due to increased intermolecular associations. There is also a variation in the slope of the curves for the C_{12} and C_7 polymers that can be linked to a transition in the concentration regime. This variation occurs at lower concentrations for the C_{12} polymer because the intermolecular interactions are facilitated by the greater length of the pending chains. The C_7 alkyl chain also increased the viscosity whereas the cycloamine groups did not result in a large change in viscosity, this is because these groups are less hydrophobic. The differences in hydrophobicity between the linear and cyclic groups presented here are based on Hansen solubility parameters (Hansen, 2007). Linear hydrocarbon chains contribute only dispersion forces (D), which can be enhanced with increasing size of the molecule (D = 15.3 MPa1/2 for heptane and D = 16.0 MPa1/2 for dodecane), which in turn increases the hydrophobic character of the molecule. Cyclic hydrocarbon chains contribute dispersion forces (D) but also hydrogen bonding (H) (D = 16.4 MPa1/2, H = 1.8 MPa1/2 for cyclopentane and D = 16.8 MPa1/2, H = 0.2 MPa1/2 for cyclohexane for example). It is worth noting that the C7 and C12-modified polymers with 2 mol% modification could also be dissolved quickly because they are terpolymers of acrylamide, acrylic acid, and the functionalized groups. Solubility is typically challenging with polymers containing hydrophobic groups. In any case, the viscosity changes do not relate only to the hydrophobic character of the pendant groups, as can be better observed in the results obtained for the series of 20 mol% substitution. A series of polymers were also prepared with increased level of the hydrophobic groups (20 mol%) to observe the effect of functional group concentration. For HMWSP the maximum concentration that is typically employed is 5 mol% (Kuang and Gao, 2014). However, we modified polymers to 20 mol% to try to react all of the carboxylate groups to generate copolymers containing acrylamide and the functionalized group. The solubility of the resulting polymers in water became challenging as the amount of hydrophobic groups increased. As a result the polymer modified with C_{12} groups at 20 mol% was insoluble in water. This indicates that the reaction was successful as the solubility changed. The polymers that remained soluble had a lower viscosity than the base polymer (PAM-co-AA, Figure 3.6). This is strong evidence that including >5 mol% of hydrophobic groups can actually have a detrimental effect of enhancement of the viscosity. It also demonstrates that the remaining carboxylate groups in the polymers modified with 2

mol% (Figure 3.5) are potentially contributing to the enhanced viscosity seen in Figure 3.4 in comparison to the PAM-co-AA base polymer. Regarding the effect of pendant group structure on the viscosity, the results obtained for this series of 20 mol% substituted groups do not show a direct correlation between the hydrophobicity of the pendant group and viscosity. Once the systems seem to be in a dilute concentration regime and have a high content of pendant groups, there are no intermolecular interactions between the molecules which undergo contraction due to intramolecular hydrophobic interactions. The degree of contraction of the polymer coil is generally associated with the degree of hydrophobicity of the pendant groups. However, it can also be associated with the space for accommodating these groups in the most contracted conformation. Chains containing pendant cyclic groups seem to allow greater contraction of the chain than linear C_7 chains than branched isopropyl groups due to the spatial arrangement established.

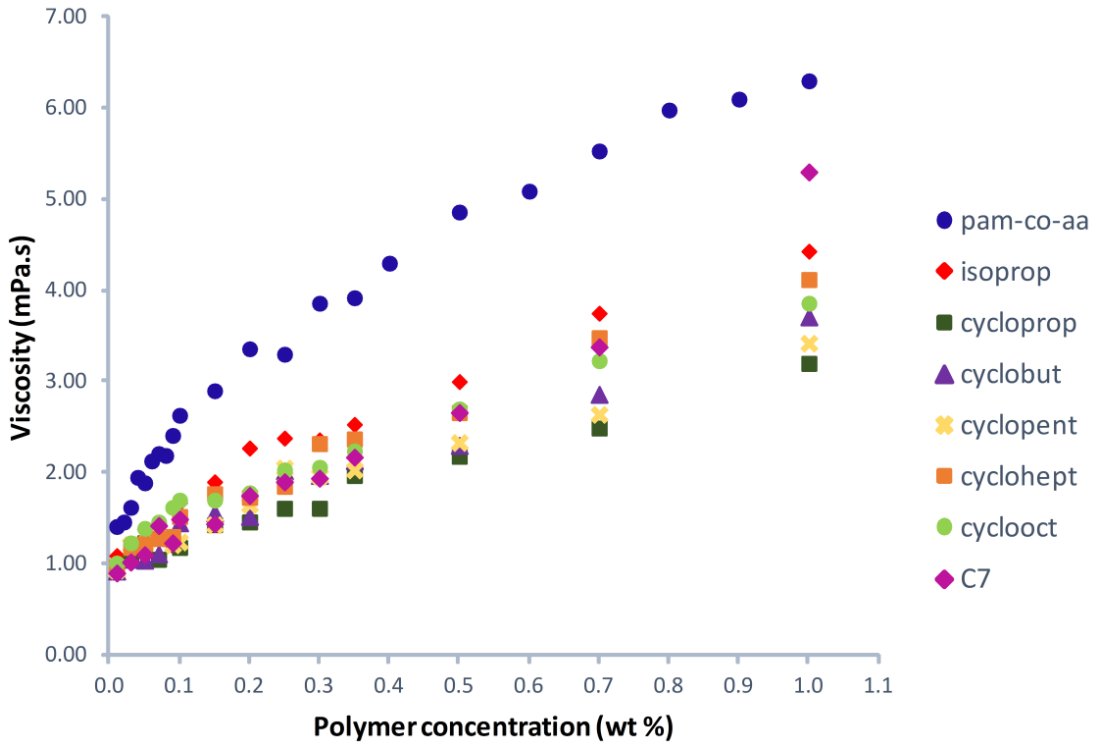

Figure 3. 6 Effect of polymer concentration on the viscosity of a range of modified polyacrylamide-based polymers at 25°C with 20 mol% modification (Silveira et al., 2015).

3.3.4 Rheology

Some polymer solutions show shear thinning under certain conditions which is useful for applications such as drilling fluid where the polymer can suspend cuttings at low shear rate but offer little resistance to flow at high shear rates (Taylor and Nasr-El-Din, 1998). For example, if shear rate is increased the entangled polymer chains unfold resulting in a decrease of viscosity. In addition the higher shear force also reduce the attraction between the polymers chains. However, for polymers that can form micelles the opposite is observed as higher shear rates increase solution viscosity. The PAM-C_{12}-2 (5 wt%) shows a clear shear thinning hydrodynamic behaviour (Figure 3.7) and follows an approximate power law dependence on the shear rate. This suggests that the C_{12} functional groups are well distributed along the polymer chains. In contrast, the base PAM-co-AA polymer (5 wt%) displays shear rate independent viscosity.

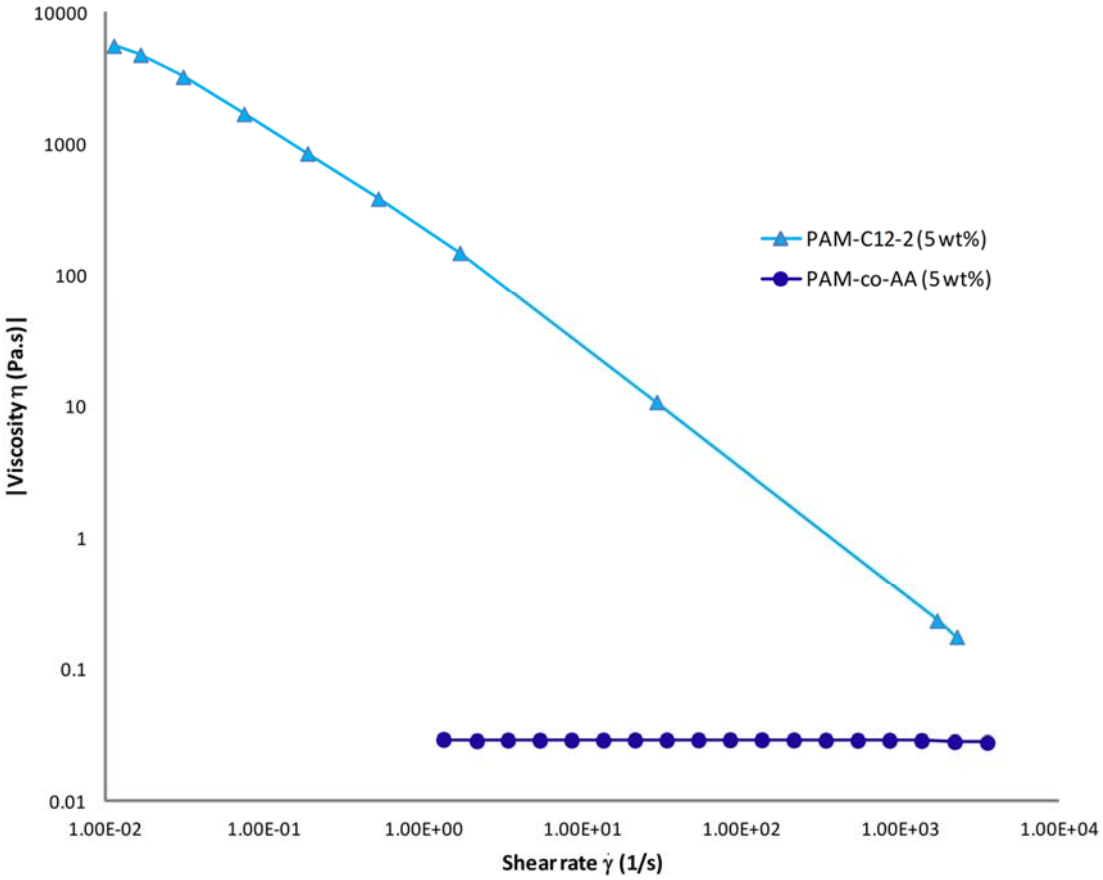

Figure 3. 7 Log-log plot of shear thinning behaviour of modified polymer PAM-C12-2 and the base polymer PAM-co-AA, 5 wt% solutions (Silveira et al., 2015).

3.3.4.1 Hydrophobically modified hydrogel synthesis

To demonstrate the flexibility of this approach a polymer was modified with 2 mol% of C_{12} groups (PAM-C12-2, Table 3.1) and the remaining carboxylate groups were cross-linked with ethylene diamine, we introduced this method in the previous work (Sheng et al., 2014). The reaction was tracked with rheology and a well-developed hydrogel was formed with the storage modulus being higher than the loss modulus (Figure 3.8). The intersection of both curves cannot be observed in Figure 3.8 due to the fast reaction so the cross-linking was occurring as the hydrogel precursor solution was added into the rheometer. Hydrophobically modified hydrogels can often display enhanced toughness (Abdurrahmanoglu et al., 2009) and the gel prepared in this study displays a high storage modulus (>1000Pa).

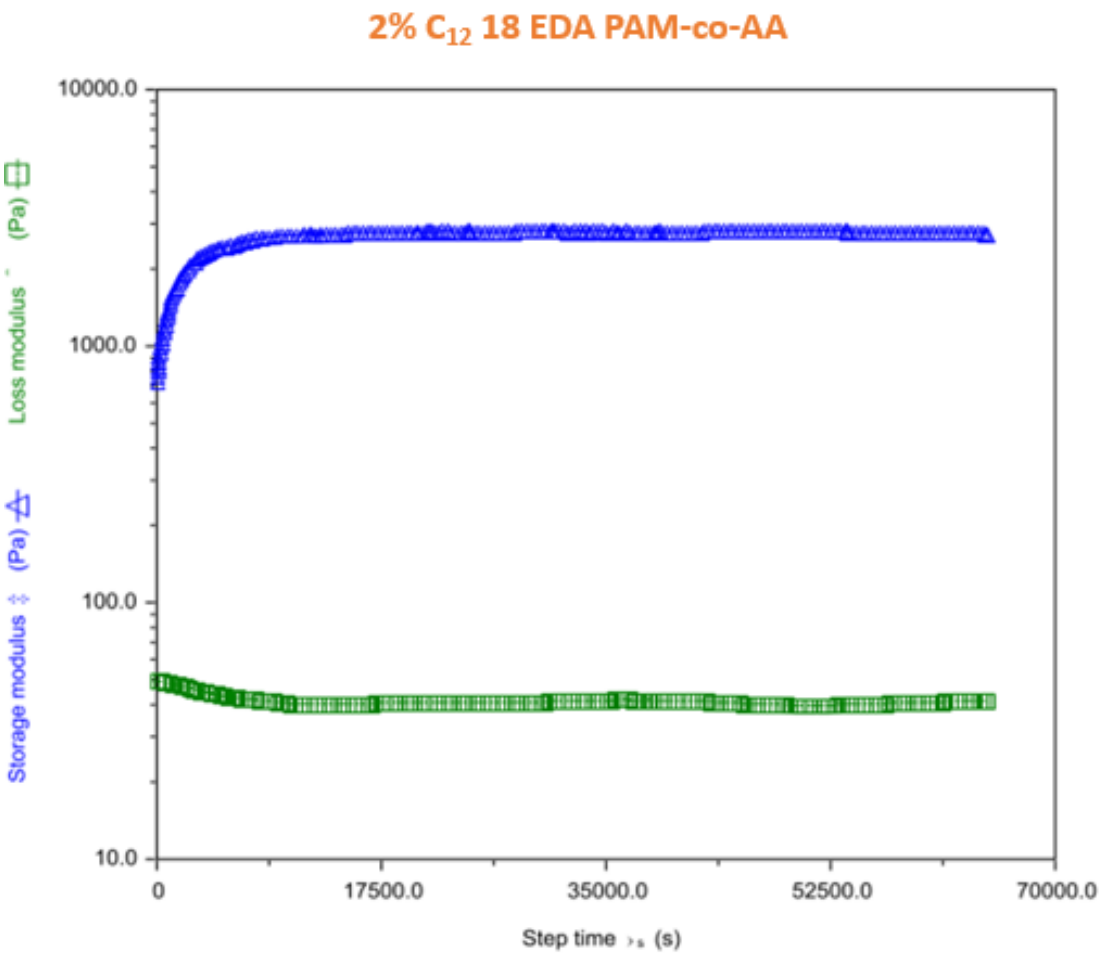

Figure 3. 8 Storage and loss modulus for a hydrogel prepared by cross-linking a 2 mol% C_{12} modified polymer (PAM-C_{12}-2) with ethylene diamine (18 mol%) (Silveira et al., 2015)

3.4 Conclusions

This work demonstrates that functionalized acrylamide-based polymers, including hydrophobically modified water soluble polymers, can be generated using a carbodiimide mediated coupling (CMC) reaction onto an existing PAM-co-AA polymer. This is supported by detailed investigation of the resulting polymers using acid-base titration, NMR spectroscopy, viscosity, and rheology. The reaction converts the acrylic acid in the base polymer to target functional groups which results in a decrease in the acid number. NMR spectroscopy provides further confirmation of the structure of the polymers showing that the CMC reaction is an efficient tool for controlling polymer structure. The viscosity of the resulting polymers is dependent on the structure of the functional group, the level of incorporation, polymer concentration, and the degree of hydrolysis. This provides a handle to fine tune the viscosity and polymers with more hydrophobic groups (C_{12}) gave the highest viscosity. Using the method both copolymers (acrylamide and functional groups) and terpolymers (acrylamide, acrylic acid, and functional groups) can be readily generated. Additional reactions can also be carried out to generate hydrogels by cross-linking the modified polymers with diamines. This flexible CMC post synthetic modification reaction demonstrates a fine control over structure, which is possible to generate a single base polymers with a multitude of functional groups. This also allows for all of the polymers of the same molecular weight. This will be further revealed in the next few chapters where this method was applied to different KHI base polymers.

Chapter 4 SYNTHESIS OF PNIPAM-BASED MODIFIED POLYMERS

4.1 Introduction

As introduced in the chapter 3, CMC reaction has been proved to be a reliable tool for post synthetic modification of commercial PAM-co-AA polymer. In this chapter, a base polymer of poly(N-isopropylacrylamide)-co-acrylic acid (PNIPAM-co-AA) was synthesized via free radical polymerization which was then modified via CMC reaction with functional groups including small cyclic groups through to alkyl chains to investigate the impact of these structure on hydrate inhibition property. This ensured all polymers were from the same base polymers so the M_w and composition was the same. Poly(N-isopropylacrylamide) polymers have been investigated as a strong KHI polymer due to the amide functionality being attached to a hydrophobic group (Chua et al., 2012a; Mady and Kelland, 2014; Perrin et al., 2013). In addition, they are structurally analogues to polyacrylamide polymers (shown in Figure 4.1), which is considered to be feasible for CMC reaction as PAM polymers. In general, by means of CMC reaction, specific functional motifs were added to PNIPAM-co-AA to generate a PNIPAM-based KHI library, the attempt of modification on PNIPAM-based polymers were successful.

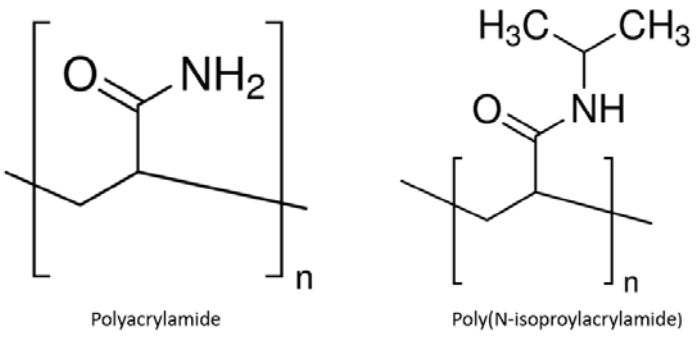

Figure 4. 1 Structure of PAM and PNIPAM polymers.

4.2 Materials and methods

4.2.1 Materials

All reagents were used without purification. The following materials were purchased from Sigma Aldrich: N-(3-dimethylaminopropyl)-N'-ethylcarbodiimide hydrochloride (EDC, commercial grade); N-hydroxysuccinimide (NHS, 98%); cyclopropylamine (cycloprop, 98%); cyclobutylamine (cyclobut, 98%); cyclopentylamine (cyclopent, 99%); cycloheptylamine (cyclohept, 99%); cyclooctylamine (cyclooct, 97%); propylamine (C3, 98%); butylamine (C4, 99.5%); tert-butylamine (C4t, 99.5%); pentylamine (C5, 99%); heptylamine (C7, 99%); octylamine (C8, 99%); potassium hydrogen phthalate (KHP, ≥99.95%); N-isopropylacrylamide (NIPAM, 97%); acrylic acid (with 200 ppm MEHQ, AA, 99%); ethyl acetate (99.8%); azobisisobutyronitrile (AIBN, 98%). Sodium hydroxide (NaOH, 99%); chloridric acid (HCl, 37%) and cyclopentane (c-C5, 98%) were purchased from Merck. Deuterium oxide (D2O, 99.9%) from Cambridge Isotope Laboratories Inc.

4.2.2 Synthesis of PNIPAM-co-AA

In order to produce KHI candidates through post synthetic modification, a base polymer was synthesized that was structurally similar to previous reports for promising KHIs. This ensures that the library is targeted and has the best chance of success and the same approach must be taken with the groups that are coupled onto the polymer. For example, a molecular weight of 10,000 was targeted with approximately 20 mol% of acrylic acid. Before the polymerisation the inhibitor was removed from all monomers by passing through a neutral silica column. NIPAM (60.0 g; 0.53 mol) and AA (10.2 g; 0.14 mol) were dissolved in isopropanol and were added to a round-bottom flask. The reaction was purged with nitrogen for 30 mins and the polymerisation was initiated with AIBN in isopropanol (1.40 g; 8.53 mmol). The total volume of isopropanol was 300 ml (236 g). The temperature was maintained at 60 °C and the reaction was stirred using a magnetic stirrer (930 rpm). After 15 hours the reaction was cooled to room temperature and the solvent was removed under reduced pressure. The reaction mixture was redissolved in distilled water to form a highly viscous solution, which was slowly poured into a large amount of ethyl acetate, the

precipitated polymer was collected and dried under vacuum (at 50 °C, for 24 h). Afterwards the polymer was lyophilized. The reaction yield was approximately 92 % (64 g of final product) which was determined gravimetrically.

4.2.3 Preparation of PNIPAM-based polymers

The post-synthetic modification of the PNIPAM-co-AA was performed in an open container in the presence of oxygen. The protocol for this stage was detailed previously for a commercial polymer PAM-co-AA in Chapter 3. However, for PNIPAM-co-AA polymer it was necessary to carry out the modification in an ice bath to prevent precipitation of the base polymer during the process. An aqueous PNIPAM-co-AA solution was employed (20 w/v %) and for each modification reaction EDC and NHS were prepared to activate the polymer. A series of multicomponent polymers were subsequently generated by reacting the activated polymer with a range of cyclic and linear amines at different modification ratios (molar ratio for all samples was 1 AA : 1 EDC : 1 NHS: 1 amine). Synthesis procedures are shown in Schematic 4.1.

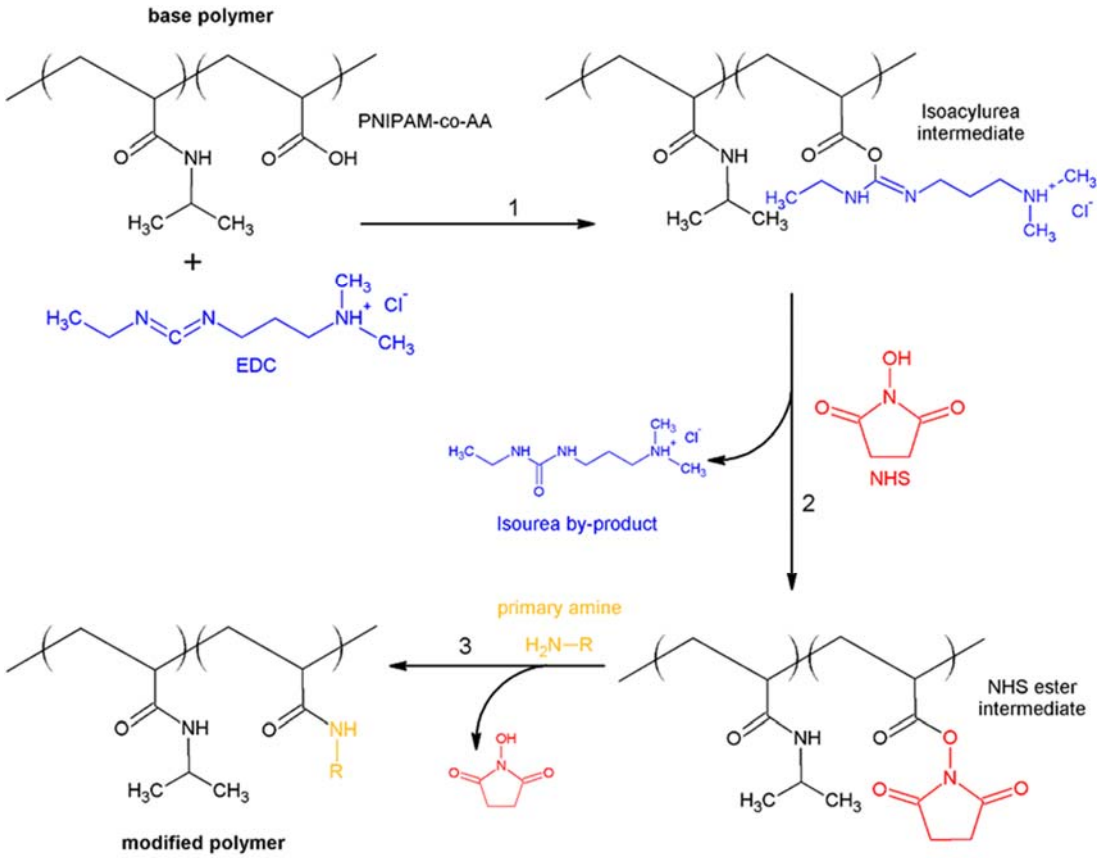

Scheme 4.1 Reaction schematic used for the synthesis of modified poly(N-isopropylacrylamides) where PNIPAM-co-AA reacts with EDC (step 1) and NHS (step 2) to form an activated polymer (NHS ester intermediate), the NHS is readily replaced with primary amines (step 3) (Silveira et al., 2017).

All inhibitor candidates were synthesized using this CMC reaction and were fully characterized. The resulting polymers were dried by lyophilisation. The modified polymers are represented as PNIPAM-amine-%, where different percentage (mol%) of amine was incorporated in a range of 1.5 to 20 mol% the upper limit was determined by the % of AA. Representative synthesis conditions based on polymer solution concentration of 20 w/v % (PNIPAM-co-AA) for all primary amines tested can be found in Table 4.1.

Table 4. 1 Representative synthesis conditions based on polymer solution concentration of 20 w/v % (2.2 g of polymer PNIPAM-co-AA) for all eleven primary amines tested (Silveira et al., 2017).

Primary amines(μL)	**Modification %**		
	1.5 %	3 %	7.5 %
	Activators (g)		
	EDC 0.060 g	EDC 0.12 g	EDC 0.30 g
	NHS 0.036 g	NHS 0.072 g	NHS 0.18 g
Cycloprop (μL)	21.8	43.6	109
Cyclobut (μL)	26.8	53.6	134
Cyclopent (μL)	31	62	155
Cyclohept (μL)	40	80	200
Cyclooct (μL)	43.1	86.2	215.5
C_3 (μL)	25.8	51.6	129
C_4 (μL)	31.1	62.2	155.5
C_4t (μL)	33	66	165

C_5 (µL)	36.4	72.8	182
C_7 (µL)	46.6	93.2	233
C_8 (µL)	52	104	260

4.2.4 Libraries of PNIPAM-based polymers

The structure of the base polymer, PNIPAM-co-AA, was determined using nuclear magnetic resonance (NMR) spectroscopy to confirm successful polymerization (Figure 4.2 and Figure 4.3). The copolymer has 20 mol% of AA and 80 mol% of NIPAM as determined by using ^{13}C NMR spectroscopy. This result was confirmed by titration.

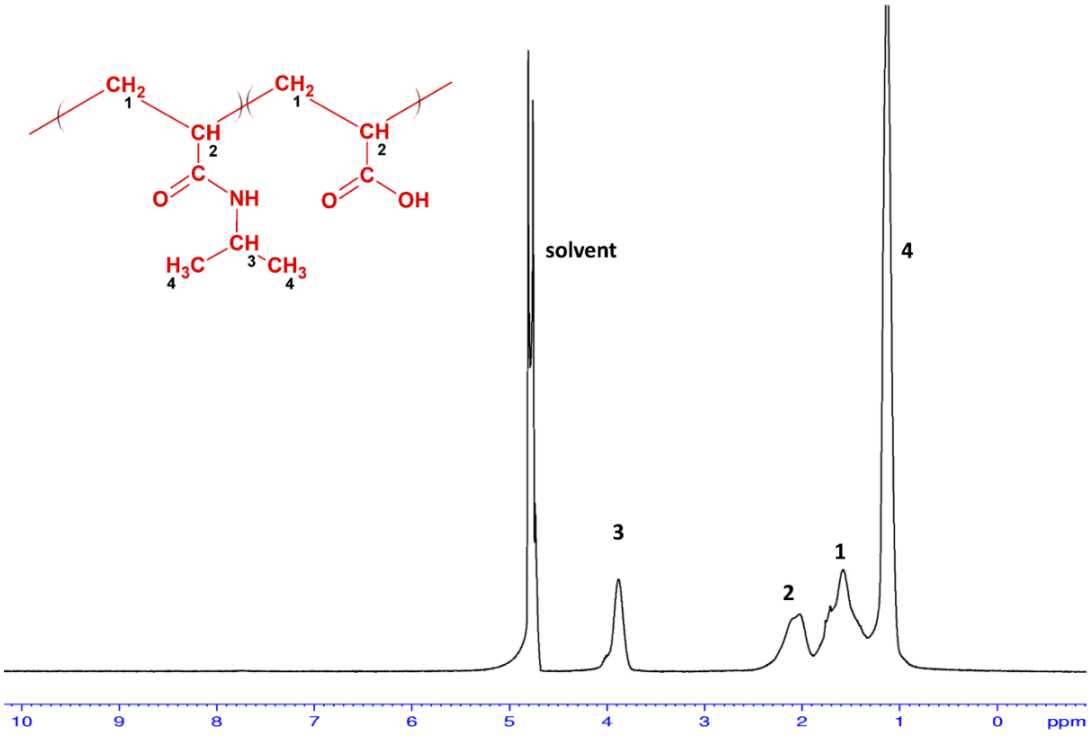

Figure 4. 2 ^{1}H NMR of PNIPAM-co-AA base polymer (Silveira et al., 2017).

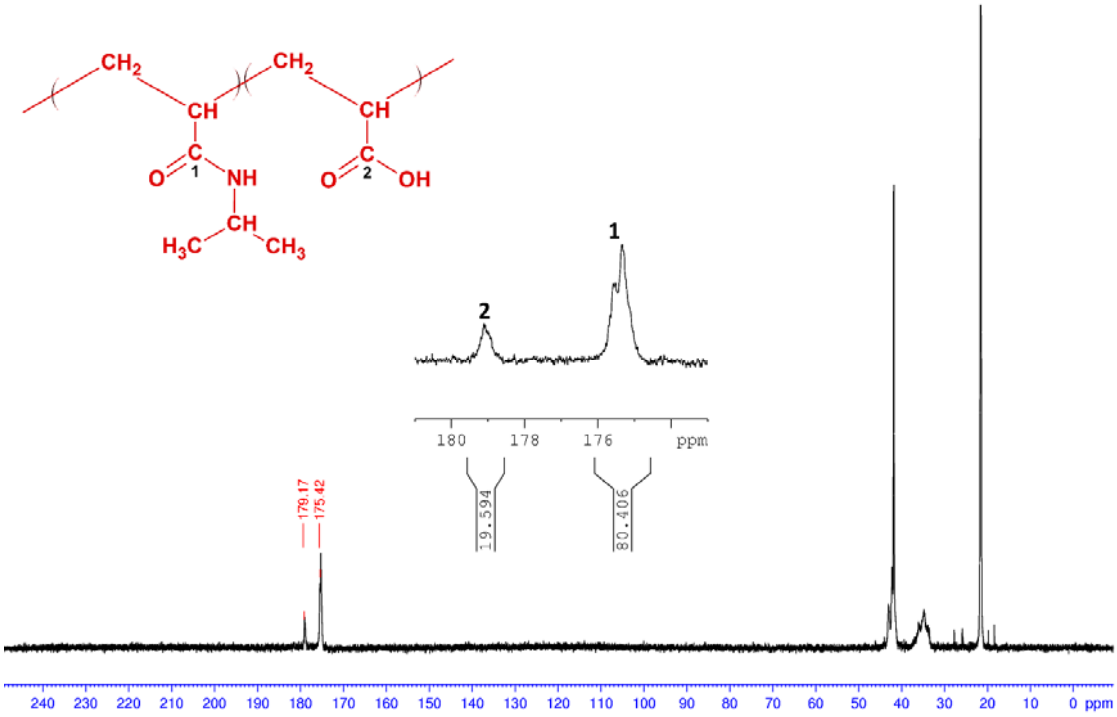

Figure 4. 3 ^{13}C NMR of PNIPAM-co-AA base polymer – composition highlighted: 19.6 mol% of AA and 80.4 mol% of NIPAM (Silveira et al., 2017).

The number average molecular weight (M_n) of PNIPAM-co-AA was found to be 11.5 kDa, with a polydispersity index of 1.79 as measured by gel permeation chromatography (GPC). The modified polymers studied here have similar molecular weight and polydispersity index as can be seen in Figure 4.4 and Table 4.2 (average values: $\bar{M}_n$ 12.5 kDa; $\bar{M}_w$ 24.7; PDI 1.97), which was one of the aims of this study because it removes the effect of Mw on performance.

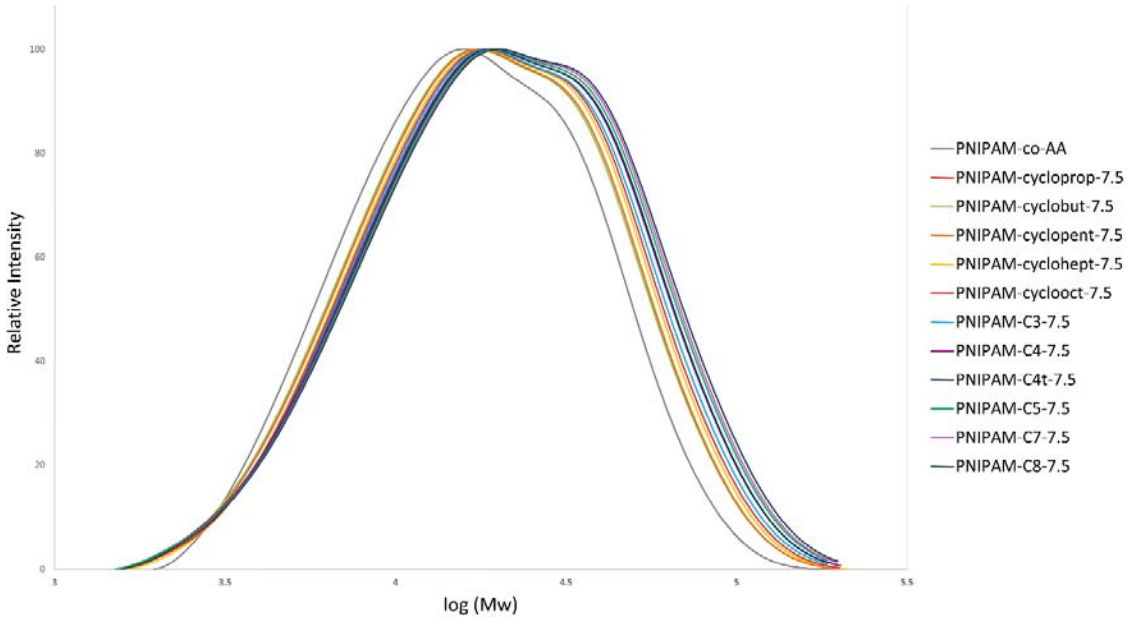

Figure 4. 4 GPC data for KHI candidates with 7.5 mol% of modification – similar molecular weight for all samples achieved using Post Synthetic Modification via CMC reaction (Silveira et al., 2017).

Table 4. 2 GPC data: $\bar{M}_n$, $\bar{M}_w$ and PDI for all modified polymers (Silveira et al., 2017).

Polymer	$\bar{M}_n$	$\bar{M}_w$	PDI
PNIPAM-co-AA	11.50	20.70	1.79
PNIPAM-cycloprop-7.5	11.70	22.70	1.94
PNIPAM-cyclobut-7.5	12.00	23.10	1.93
PNIPAM-cyclopent-7.5	12.20	23.40	1.92
PNIPAM-cyclohept-7.5	12.50	24.20	1.93
PNIPAM-cyclooct-7.5	12.60	24.60	1.95
PNIPAM-C_3-7.5	12.60	25.10	1.99
PNIPAM-C_4-7.5	12.70	25.80	2.02
PNIPAM-C_4t-7.5	12.90	26.00	2.01
PNIPAM-C_5-7.5	12.90	26.60	2.05
PNIPAM-C_7-7.5	13.10	26.90	2.05
PNIPAM-C_8-7.5	13.20	27.40	2.07
Average value	12.49	24.71	1.97

The resulting PNIPAM-based inhibitors were then screened for hydrate inhibition and cloud point. However, in this chapter only cloud point measurements will be discussed. The screening technology and screening result, and autoclave test of modified PNIPAM-based polymers will be illustrated in the following chapters.

4.2.5 Cloud point

For screening the cloud point the polymers were placed in a sample holder that was submerged in a temperature-controlled water bath (Büchi Heating Bath, B-491) and the phase behaviour of each vial was recorded through transparent cap using a webcam (Logitech C920 HD Pro Webcam). Sample solutions with concentration of 0.5 and 1% (w/v) were prepared 24 h before the experiment then added to 5mL sample vials. The base of the vials was painted (red) and the phase behaviour of each system was recorded showing the behaviour of all solutions at the same time, in a temperature range of 25 to 90 °C. The cloud point was determined visually at the point when the solution first became turbid which was determined by a colour change (red to pink). The temperature was increased at a rate of 12 °C/hour. This allowed the temperature of the solutions to stabilize (different locations for the same sample were tested) at the selected temperature. Figure 4.5 shows the apparatus developed for cloud point analysis. Using this method, it is possible to simultaneously measures >100 samples.

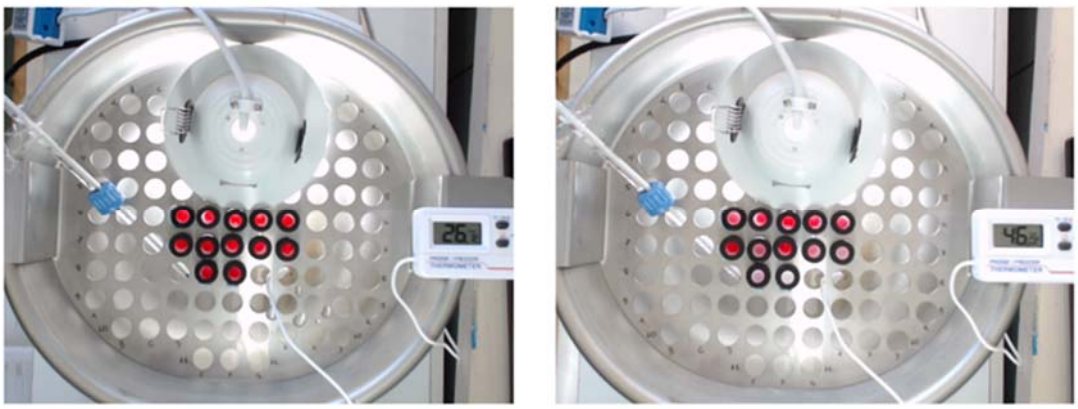

Figure 4. 5 High throughput apparatus for cloud point analysis. Pictures from the top: ongoing analysis at 26 and 46°C, respectively for the same sample set (Silveira et al., 2017).

4.3 Results and discussion

Polymer molecular weight has been shown to be an important parameter influencing KHI efficacy. Low-molecular-weight polymers show improved performance for many classes of polymer other than PVCap (Kelland, 2006, 2009); however, the optimum molecular weight can be different for each polymeric structure. In this study we did not optimize this parameter, but if comparisons are made between different KHIs it is important that the effect of Mw be removed. This is extremely difficult with free-radical polymerization because the Mw and distribution vary widely when the structure of the polymer changes. The molecular weight of the KHI candidates synthesized in this study were fixed because post-synthetically modifying the base polymer ensured that each polymer in the library has similar molecular weight to allow direct comparison of the different functional groups across the library (Figure 4.4). Hence, analysing the impact of polymer structure on performance is crucial for the development of new KHIs. The molecular weight of the polymer is one parameter that affects the performance of a KHIs, however the structural composition has a more profound effect. This is because the KHI performance depends on the interaction of the functional groups with either the water molecules (through hydrogen bonding) or with the gas hydrate cavities (via hydrophobic interactions). The adsorption of a hydrophobic group into a cage at the hydrate surface increases the structure around the cage, which results in a strong adsorption in the surrounding cages which inhibits hydrate growth (Yagasaki et al., 2015). Amide-based with cyclic or acyclic amides, imide or lactams are capable of this and are potential hydrate inhibitors (Kelland, 2006; Perrin et al., 2013; Yagasaki et al., 2015). The post-synthetic modification outlined within has allowed for accurate incorporation of varying functional groups which can start to decipher the complex interactions taking place, this would not be possible with free-radical routes because of variations in Mw, distribution and compositional drift.

4.3.1 Effect of polymer pendant group on the cloud point

Poly(N-isopropylacrylamide) and PNIPAM-based copolymers have been extensively studied because of their thermo-responsive properties. They exhibit a reversible phase transition in aqueous solutions that is observed as turbidity above the lower critical solution temperature (LCST) which is a function of their hydrophilic-hydrophobic

balance. The phase transition, or cloud point, is dependent on the structural characteristics of the PNIPAM polymers. Increasing the cloud point is important for KHI because polymers with very low phase transitions (and consequently deposition points) can precipitate in hot sections of the pipeline, leading to loss of performance (Mady and Kelland, 2014, 2015).

In general, increasing the hydrophobic alkyl chain length lowers the cloud point temperature so it is closely related to the hydrophobicity of the molecule. The functional groups selected for this study allowed for accurate control over the hydrophobicity across the linear, branched and cyclic groups. In order to understand these effects Hansen Solubility Parameters (HSP) have been used to predict molecular affinities, solubility, and solubility-related phenomena (Hansen, 2007). Hydrophobicity is a characteristic that depends on the shape and size of the group considered. Linear hydrocarbon chains contribute only with dispersion forces (δ_D), which can be enhanced by increasing the size of the molecule (δ_D = 13.4 $MPa^{1/2}$ for n-propane, δ_D = 14.1 $MPa^{1/2}$ for n-butane and δ_D = 14.5 $MPa^{1/2}$ for n-pentane, for example), which increases the hydrophobic character of the molecule. Alternatively, branched hydrocarbon chains are less hydrophobic than the corresponding linear structure with the same number of carbon atoms (for example δ_D = 13.7 $MPa^{1/2}$ for iso-pentane). Cyclic hydrocarbon chains contribute with dispersion forces (δ_D) but also hydrogen bonding (δ_H), exhibiting a more hydrophilic character (δ_D = 16.4 $MPa^{1/2}$, δ_H = 1.8 $MPa^{1/2}$ for cyclopentane and δ_D = 16.8 $MPa^{1/2}$, δ_H = 0.2 $MPa^{1/2}$ for cyclohexane for example). All of the groups described above are not N-substituent groups of acrylamide in terms of Hansen solubility parameters; however, they can provide an approximation of their contribution in the final polymer structure. Estimated parameters using this group contribution method for N-substituent groups of acrylamide indicate a small reduction in δ_H and a small increase in δ_D parameter, which can explain the general low hydrophobic character of the structures used in this work. This effect can be observed with the following sequence of substituent groups of acrylamide (Ahmad, 1982): δ_D = 17.1 $MPa^{1/2}$, δ_H = 14.5 $MPa^{1/2}$, δ_P = 2.3 $MPa^{1/2}$ for methyl group; δ_D = 17.3 $MPa^{1/2}$, δ_H = 13.3 $MPa^{1/2}$ δ_P = 2.1 $MPa^{1/2}$ for ethyl group; δ_D = 19.2 $MPa^{1/2}$, δ_H = 12.3 $MPa^{1/2}$, δ_P = 1.9 $MPa^{1/2}$ for isopropyl group; δ_D = 17.6 $MPa^{1/2}$, δ_H = 11.5 $MPa^{1/2}$, δ_P = 1.84 $MPa^{1/2}$ for t-butyl group and δ_D = 17.9 $MPa^{1/2}$, δ_H = 11.5 $MPa^{1/2}$, δ_P = 1.8 $MPa^{1/2}$ for diethyl group. According to HSP estimates for different N-

substituent acrylamides, C_3 has a higher δ_D parameter than C_4t (Ahmad, 1982). The authors did not show the values for C_3 group but using group contribution it would be close to isopropyl parameters, probably slightly higher in terms of δ_D. Additional trends also exist in regard to: Propylamine $\delta_D = 16.9$, $\delta_H = 8.6$, $\delta_P = 4.9$; Isopropylamine $\delta_D = 14.8$, $\delta_H = 6.6$, $\delta_P = 4.4$; Butylamine $\delta_D = 16.2$, $\delta_H = 8.0$, $\delta_P = 4.5$; Diethylamine $\delta_D = 14.9$, $\delta_H = 6.1$, $\delta_P = 2.3$ (Hansen, 2007). Again, a group consisting of 3 carbons has a higher δ_D contribution than 4-carbon group. Therefore, the copolymer PNIPAM-C_3-20 is slightly more hydrophobic, higher δ_D and $\delta(\delta^2 = \delta_D^2 + \delta_H^2 + \delta_P^2)$ than PNIPAM-C_4t-20, which may be resulting in a lower cloud point for PNIPAM-C_3-20 than PNIPAM-C_4t-20 copolymer.

The increasing hydrophobic character observed for the final modified polymers in this study would be expected to reduce the cloud point temperature, due to increasing pendant group content (mol%) and hydrophobic character. However, the results show the opposite trend with an increase in the cloud point temperatures observed for all hydrophobic groups, compared to the base polymer (PNIPAM-co-AA), including groups with large δ_D, and low δ_H such as C_7 and C_8 chains (see Table 4.3).

This apparent inconsistency is rationalised by the presence of side products from the reaction which include isourea and NHS (N-Hydroxysuccinimide). These side products could be causing the change in the cloud points due to a hydrotropic effect on the polymer solubilization in water (Kumar et al., 2014). Hydrotropes have the ability to prevent or control the clouding process in surfactants and polymers. For example, short-chain alkyl benzene sulphonates, alkyl naphthalene sulphonates and sodium salicylate are capable of increasing the cloud points of a nonionic surfactants or a neutral polymer. The hydration of the hydrocarbon backbone of a polymer could also change the cloud point. For example, solubilization of the polymer chain of poly(N-isopropyl acrylamide), occurs as the result of a combination of forces including intermolecular hydrogen bonding, van der Waals interactions and hydrophobic interactions. The difference between the collapsed and solvated states of the polymer was related to a hydrotrope contribution whereby decreasing the hydrophobic interaction, resulted in an increase in the cloud point (Kumar et al., 2014; Roy and Moulik, 2003). Solutes capable of both hydrogen donation and acceptance help to increase solubility. Hydrotropes like urea and N,N-diethyl urea solubilize by altering the nature of the solvent by modifying the ability of the solvent to be involved in

structure formation through intermolecular hydrogen bonding (Dhapte and Mehta, 2015). Urea self-associates into reasonably small clusters, on average 3–4 molecules however, when an organic molecule is added, urea clathrates form (Kunz et al., 2016). The degree of cloud point variation can be different since the hydrotropic effect depends on nature and structure, as well the capacity of the hydrotrope agent to promote an interaction with the polymer chain. There is clearly a complex interplay between polymers groups in solution and this complexity increases in the presence of hydrotropes. The outlined discussions offer some explanation to this trend but further studies would be required in order to elucidate these effects and post-synthetic modification is a viable method to probe these complex effects. Despite these complex effects as seen in Figure 4.6 the outlined method offers control over the cloud point over 50 °C.

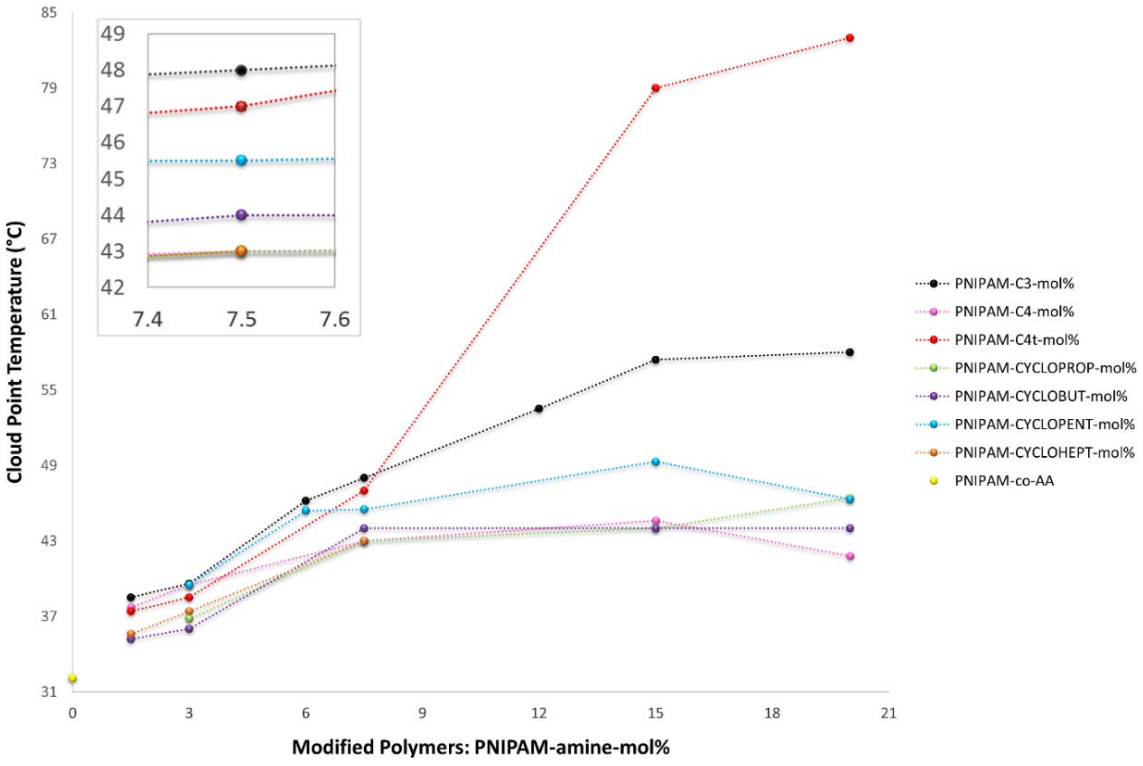

Figure 4. 6 Cloud point for KHI candidates synthesized by carbodiimide mediated coupling (CMC) (samples with 1 wt % water solution). The continuous lines are added as a guide (Silveira et al., 2017).

Initially samples with 7.5 mol% of polymer modification were studied for all of the cyclic and linear amines described above. Based on hydrate and cloud point screening all pendant groups demonstrated higher cloud points than the unmodified polymer (T ≥ 43 °C), and showed promising inhibitor performance. As a result, additional polymers were prepared that were modified up to 20 mol% (see Table 4.3).

Table 4. 3 Cloud point values for all modified polymers(Silveira et al., 2017).

Modified Polymer	**Solution Concentration wt%**	**Cloud Point (°C)**
PNIPAM-co-AA	1	32.1
PNIPAM-co-AA + 7.5 % by-products	1	31.4
PNIPAM-co-AA + 15 % by-products	1	29.7
PNIPAM-co-AA + 20 % by-products	1	29.3
PNIPAM-C_3-7.5	1	48
PNIPAM-C_4-7.5	1	43
PNIPAM-C_4t-7.5	1	47
PNIPAM-C_5-7.5	1	41
PNIPAM-C_7-7.5	1	36
PNIPAM-C_8-7.5	1	26.6
PNIPAM-CYCLOPROP-7.5	1	43
PNIPAM-CYCLOBUT-7.5	1	44
PNIPAM-CYCLOPENT-7.5	1	45.5
PNIPAM-CYCLOHEPT-7.5	1	43
PNIPAM-CYCLOOCT-7.5	1	42

PNIPAM-co-AA	0.5	33
PNIPAM-C_3-7.5	0.5	51
PNIPAM-C_4-7.5	0.5	44.5
PNIPAM-C_4t-7.5	0.5	49
PNIPAM-C_5-7.5	0.5	42
PNIPAM-C_7-7.5	0.5	38
PNIPAM-C_8-7.5	0.5	34.5
PNIPAM-CYCLOPROP-7.5	0.5	45
PNIPAM-CYCLOBUT-7.5	0.5	45.5
PNIPAM-CYCLOPENT-7.5	0.5	47
PNIPAM-CYCLOHEPT-7.5	0.5	45.5
PNIPAM-CYCLOOCT-7.5	0.5	44
PNIPAM-C_3-1.5	1	38.5
PNIPAM-C_3-3	1	39.6
PNIPAM-C_3-6	1	46.2
PNIPAM-C_3-7.5	1	48
PNIPAM-C_3-12	1	53.5
PNIPAM-C_3-15	1	57.4
PNIPAM-C_3-20	1	58
PNIPAM-C_4-1.5	1	37.7
PNIPAM-C_4-3	1	39.5
PNIPAM-C_4-7.5	1	43
PNIPAM-C_4-15	1	44.6
PNIPAM-C_4-20	1	41.8

PNIPAM-C4t-1.5	1	37.4
PNIPAM-C4t-3	1	38.5
PNIPAM-C4t-7.5	1	47
PNIPAM-C4t-15	1	79
PNIPAM-C4t-20	1	83
PNIPAM-CYCLOPROP-1.5	1	34.7
PNIPAM-CYCLOPROP-3	1	36.8
PNIPAM-CYCLOPROP-7.5	1	43
PNIPAM-CYCLOPROP-15	1	44
PNIPAM-CYCLOPROP-20	1	46.4
PNIPAM-CYCLOBUT-1.5	1	35.2
PNIPAM-CYCLOBUT-3	1	36
PNIPAM-CYCLOBUT-7.5	1	44
PNIPAM-CYCLOBUT-15	1	44
PNIPAM-CYCLOBUT-20	1	44
PNIPAM-CYCLOPENT-3	1	39.5
PNIPAM-CYCLOPENT-6	1	45.4
PNIPAM-CYCLOPENT-7.5	1	45.5
PNIPAM-CYCLOPENT-15	1	49.3
PNIPAM-CYCLOPENT-20	1	46.3
PNIPAM-CYCLOHEPT-1.5	1	35.6
PNIPAM-CYCLOHEPT-3	1	37.4
PNIPAM-CYCLOHEPT-7.5	1	43

As shown in Figure 4.6, the polymers (PNIPAM-amine-mol%) containing C_3, C_4, C_4t, cycloprop, cyclobut, cyclopent and cyclohept groups show an increase in cloud point with increasing modification up to 15 mol% compared to the base polymer (shown in yellow). Polymers based on butylamine (C_4) and cyclopentylamine (cyclopent) had maximum cloud points (44.6 and 49.3 °C) at 15 mol% of functionalization, respectively. Polymers with cycloprop, C_3 and C_4t groups showed an increase in cloud point temperature response as the hydrophobic content of the chain (variable mol%) increased up to 20 mol%. Based on these data it is likely that a higher cloud point could be reached with increased pendant group content but the maximum modification that could be achieved with the base polymer in this study is 20 mol% which is the acrylic acid content. Overall the hydrophobic content (variable mol%) of a specific pendant group appears to have a stronger effect on the cloud point compared to the overall hydrophobicity of the molecule for the same group of KHIs. Therefore, the difference between the hydrophobic effects of the pendant groups studied here is small, but the impact upon the cloud point is pronounced. This demonstrates the utility of post-synthetic modification in modulating cloud point which can be difficult using free-radical polymerization.

4.4 Conclusions

Libraries of kinetic hydrate inhibitors (KHIs) were synthesized using a high-throughput post-synthetic modification methodology of a precursor poly(N-isopropylacrylamide-co-acrylic acid) with various amines. All of the polymers possess similar molecular weight but with different functional groups incorporated at controlled concentrations. This is the first truly systematic structure-property study for KHIs. This is also interesting to researchers investigating on PNIPAM. Some of these modified polymers have a cloud point that is higher than some leading KHIs, which is advantageous for injection into hot fluids. It is also flexible enough to accurately control cloud point of the polymers which is relevant to natural gas transport but areas where PNIPAM is employed. The study also highlights interesting effects of side products from the reaction which would likely be present during application which include the strong change in cloud point.

Chapter 5 SYNTHESIS OF PVCAP-BASED MODIFIED POLYMERS

5.1 Introduction

After the successful of modification on PAM-co-AA and PNIPAM-co-AA polymers, poly(N-vinylcaprolactam) based polymers were being synthesized using the same efficient protocol. As the aim of this work was to design single polymer molecules that exhibit both hydrate and corrosion inhibition, specifically a kinetic hydrate and corrosion inhibitor (KHCI), a systematic library of multifunctional polymers were generated by modifying a poly(N-vinylcaprolactam)-co-acrylic acid (PVCap-co-AA) polymer with key functional groups including Taurine, (2-Aminoethyl)trimethylammonium chloride hydrochloride (ATCH), 1-(3-Aminopropyl)imidazole (APIM) and (Aminomethyl)phosphonic acid (AMPA). These contain heteroatom centres that can bind via electron pairs that is a key structural feature for corrosion inhibition. Moreover, addition of a dodecyl hydrocarbon chains with and without pendant amine groups onto the polymers backbone were also investigated. This study is promising to help to overcome compatibility issues as well as offer fundamental insights into the mode of action of hydrate and corrosion inhibitors.

5.2 Materials and methods

5.2.1 Materials

All of the chemicals were purchased from Sigma Aldrich: N-vinylcaprolactam (VCap; 98%); acrylic acid (AA, contains 200ppm, MEHQ as inhibitor, 99%) was used after being filtered through a neutral activated alumina column; 2-2'azobisisobutyronitrile (AIBN, 99%) was purified by recrystallization from methanol, dried under vacuum and stored at 4°C; N-(3-dimethylaminopropyl)-N'-ethylcarbodiimide hydrochloride (EDC, commercial grade); N-hydroxysuccinimide (NHS, 98%); taurine (≥99%); (2-aminoethyl)trimethylammonium chloride hydrochloride (ATCH, 99%); 1-(3-aminopropyl)imidazole (APIM, ≥97%); dodecylamine (C_{12}, 99%); 1,12-diaminododecane (diaminoC_{12}, 98%). Ethanol absolute (ACS), 2-propanol (IPA,

≥99.8%), sodium hydroxide (NaOH, ≥99%), hydrochloric acid (HCl,≥30%), cyclopentane (≥98%) and buffer solution pH 4.00(citric acid/sodium hydroxide/hydrogen chloride) were purchased from Merck, tetrahydrofuran (THF, HPLC grade) from scharlau, deuterium oxide (D2O, 99.9%) from Cambridge Isotope Laboratories Inc. and (aminomethyl)phosphonic acid (AMPA, 98%) from Apollo Scientific Inc.

5.2.2 Synthesis of PVCap-co-AA

The poly(VCap-co-AA) copolymer was prepared by free radical copolymerization of VCap with AA in the presence of AIBN as an initiator (see in Scheme 5.1). VCap and AA (feed ratio=82.5 mol% : 17.5 mol%) were dissolved in IPA with total monomer concentration of 33wt%. 2mol% of AIBN was then added to resulting solution. The mixture was purged with nitrogen for 30 min and then heated to 70 °C under constant stirring (1000 rpm) for 24 h under nitrogen. After this time the solvent was removed by rotary evaporation. The product was washed several times by MilliQ water to remove residual initiator and monomer and dried completely under vacuum.

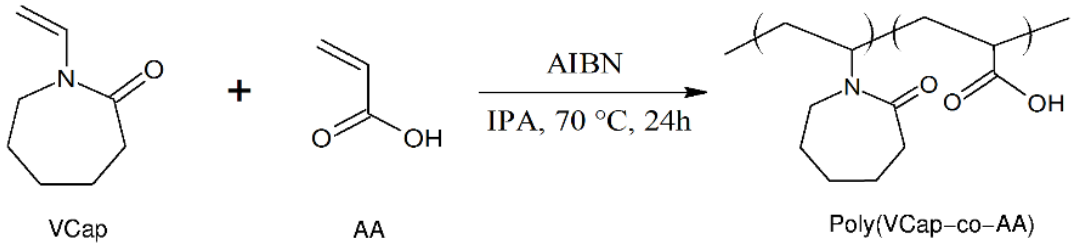

Scheme 5.1 Synthesis of the base Poly(VCap-co-AA) copolymer (Sheng et al., 2017).

5.2.3 Preparation of PVCap-co-Na AA

The base polymer (PolyVCap-co-AA) was insoluble in neutral water at ambient temperature which can be attributed to the formation of hydrogen bonding between amide groups and protonated carboxylic groups (Shtanko et al., 2003). In order to overcome this the solution was neutralized to increase solubility after which the

polymer could be characterized and the post-synthetic modifications performed. The carboxylic acid groups of copolymers were neutralized by sodium hydroxide thus turning Poly(VCap-co-AA) into Poly(Vcap-co-Na AA) which increases solubility in water. The exact amount of NaOH used for neutralization had been calculated based on the determination and analysis of acidic comonomer units via titration and nuclear magnetic resonance spectroscopy (NMR). The pH test strips were also used to confirm the resulting solution was neutral after the reaction. The resulting polymers were then freeze dried and were prepared as a stock solution.

5.2.4 Preparation of PVCap-based KHCI polymers

This step is virtually the same as preparation of PNIPAM-based polymer as introduced in the chapter 4 because it was so effective. Hence, the detail of procedures have been omitted. It is worthy to mention that this reaction was carried out in open vials in the presence of oxygen at a low temperature (approx. 0°C) to ensure that the solutions were below the cloud point of the polymers. Synthesis procedures are shown in Scheme 5.2.

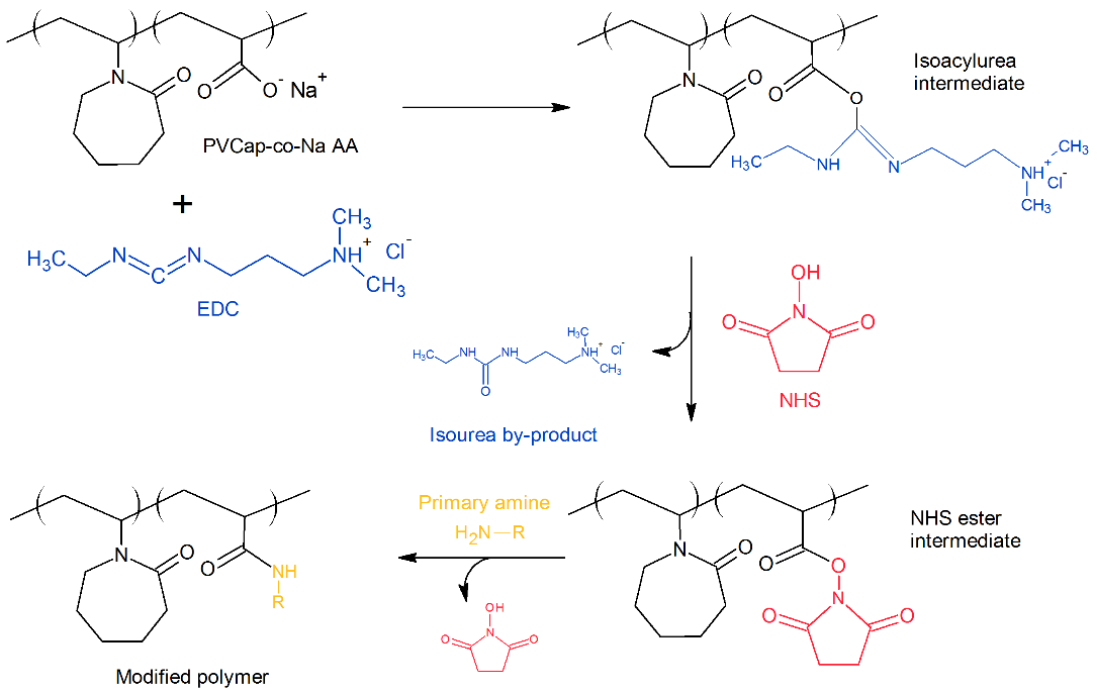

Scheme 5.2 Reaction schematic used for the synthesis of modified polymer where the carboxylate group of poly(VCap-co-Na AA) (shown in black) activated by EDC (shown in blue) and NHS (shown in red) forms a stable conjugation with primary amines.

Representative synthesis conditions are shown in Table 5.1 for an array of structurally unique, modified PVCap polymers prepared at one polymer concentration (20w/v%) with several functional amines (Sheng et al., 2017).

Table 5. 1 Representative Synthesis Conditions based on 5ml of a 20w/v% Poly(VCap-co-Na AA) solution (Sheng et al., 2017).

	Activators		**Primary Amines** [b]											
Activated polymer (%) [a]	**EDC (g)**	**NHS (g)**	**Taurine (g)**	**Taurine C_{12}(g)** [c]	**Taurine DiaminoC$_{12}$(g)** [c,d]	**ATCH (g)**	**ATCH C_{12}(g)** [c]	**ATCH Diamino C_{12}(g)** [c,d]	**APIM (g)**	**APIM C_{12}(g)** [c]	**APIM Diamino C_{12}(g)** [c,d]	**AMPA (g)**	**AMPA C_{12}(g)** [c]	**AMPA DiminoC$_{12}$(g)** [c,d]
20	0.2946	0.1768	0.1923			0.2691			0.1923			0.1706		
18	**0.2964**	**0.1768**		**0.1731**	**0.1731**		**0.2421**	**0.2421**		**0.1730**	**0.1730**		**0.1536**	**0.1536**
+				**0.0284**	**0.0616**		**0.0284**	**0.0616**		**0.0284**	**0.0616**		**0.0284**	**0.0616**
2														

Activators (EDC and NHS) and amines are dissolved in 0.5 mL of water.

Amines: Taurine (≥99%); (2-Aminoethyl)trimethylammonium chloride hydrochloride (ATCH); 1-(3-Aminopropyl)imidazole (APIM); (aminomethyl)phosphonic acid (AMPA); Dodecylamine (C_{12}); 1,12-Diaminododecane (DiaminoC_{12})

[a] mol% of polymer repeat units activated with EDC and NHS, 20 mol% is the maxium because the polymer contains 20% sodium carboxylate group (1Na AA: 1EDC: 1NHS). The reaction either with C_{12} amines or C_{12} diamines is conducted after the modification of other amines to aviod random polymers.

[b] Polymers are denoted as PVCap-amine-X or PVCap-amine-X-amine-Y, where X or Y represents the theroretical modication percentage of the polymer by the requisite amine.

[c] C_{12} amine and C_{12} diamine are insoluble in water so an additional 0.5 mL of THF was added.

[d] excess amount of diamine was required to avoid alternative cross-linking reaction which will form hydrogel at a rapid speed.

5.3 Results and discussion

5.3.1 Synthesis and characterization of KHI base polymer

The starting base polymer was synthesized by free radical copolymerization of VCap with AA in the presence of AIBN as an initiator (Scheme 5.1). PVCap is a known KHI so the aim of this study was to use this as a base polymer onto which known corrosion inhibitor groups are coupled using an efficient chemical modification via the AA group. The molecular weight of base polymer in this work was targeted around 10,000 because this is in the line with other studies (Chua et al., 2012a) and the molecular weight of the synthesized polymer (PVCap-co-AA) was 12 KDa as characterized by GPC in dimethylacetamide (DMAc, Figure 5.1).

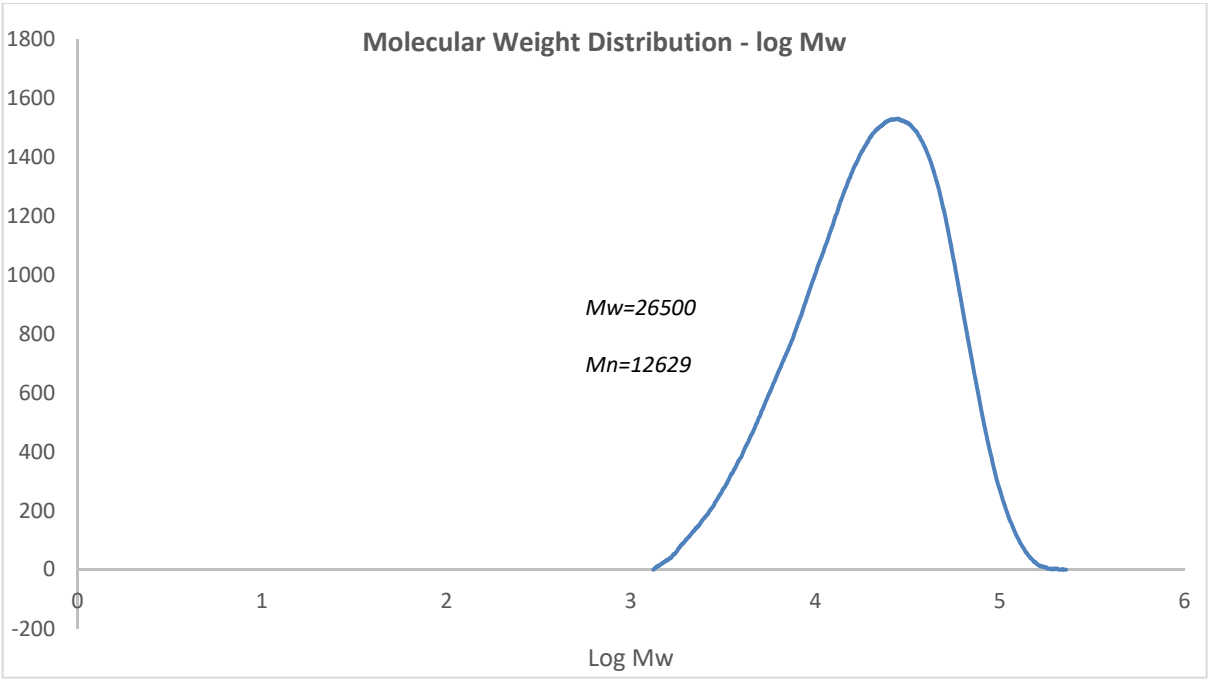

Figure 5. 1 The molecular weight of poly(VCap-co-AA) copolymer by GPC measurement (Sheng et al., 2017).

This molecular weight is in line with other KHIs because the molecular weight can affect the performance of KHIs (Kelland et al., 2000). Additional molecular weights were not investigated because the aim of the study was to remove molecular weight effects across a broad sample set so the impact of different structural groups on performance can be decoupled from Mw. Once the optimum structure is identified then molecular weight can be optimized using this approach.

The polymer was characterized with ^{1}H NMR spectroscopy (Figure 5.2), ^{13}C NMR (Figure 5.3) and titration which confirmed that the acrylic acid content was 20mol%. The titration used NaOH for neutralization and the acid content was calculated at 20mol%.

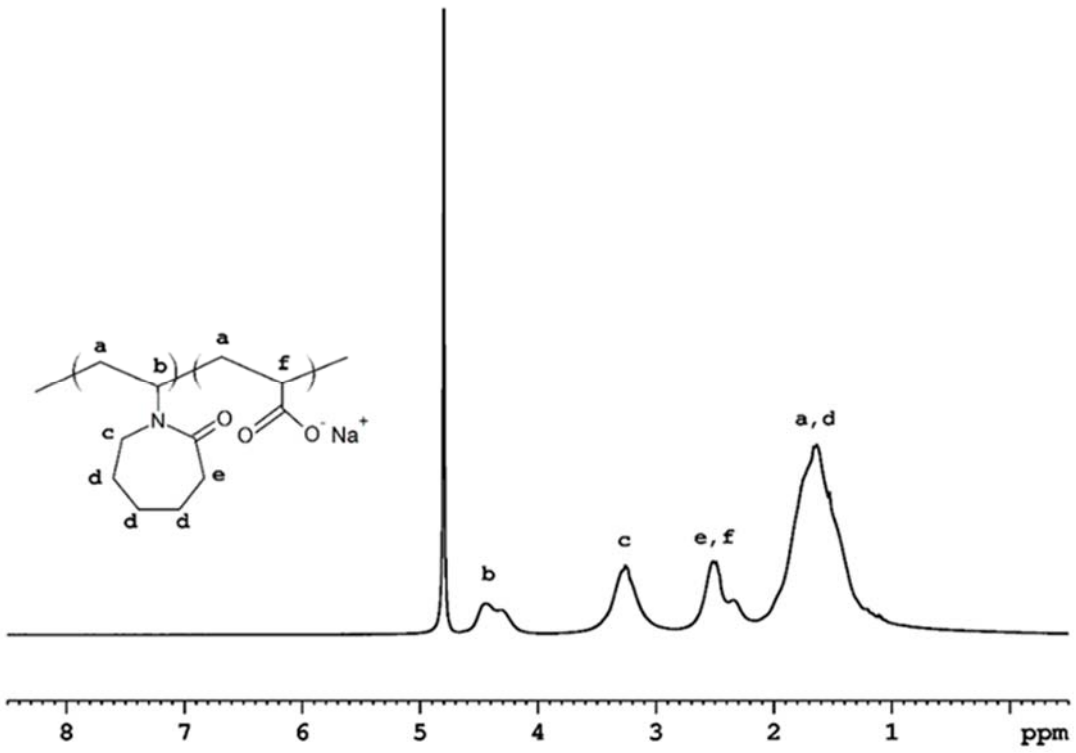

Figure 5. 2 ^{1}H NMR of poly(VCap-co-Na AA) copolymer in D_2O (Sheng et al., 2017).

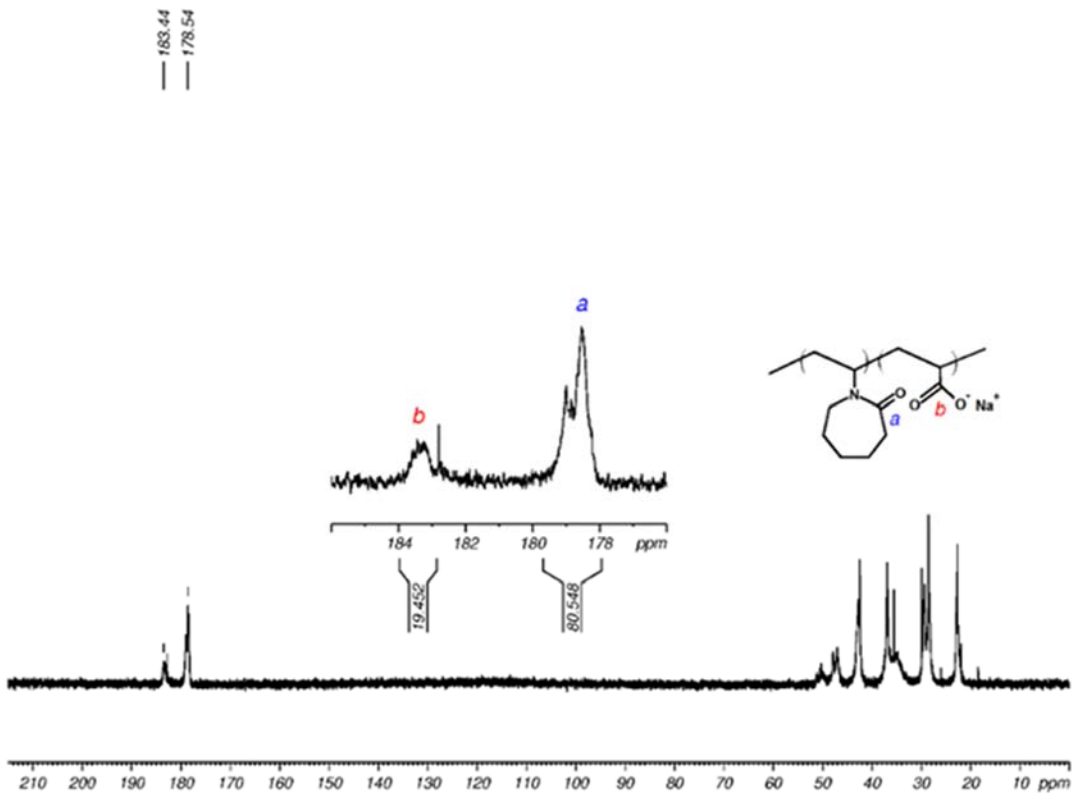

Figure 5. 3 ^{13}C NMR spectra of poly(VCap-co-Na AA) copolymer in D_2O composition highlighted: 19.4 mol% of Na AA and 80.5 mol% of VCap (Sheng et al., 2017).

The modification of the base polymer was confirmed with ^{1}H NMR (Figure 5.4, blue curve) and ^{13}C NMR (Figure 5.5) and as can be sen the spectra clearly changed after modification with APIM (Figure 5.4, green curve) and dodecyl chains (Figure 5.4, yellow curve). The spectrum of the starting materials that are used for modification are also included (Figure 5.4, red curve, imidazole, and Figure 5.4, purple curve, dodecylamine), and as can be seen, the resonances for the modified polymers (green and yellow) are substantially different to the base polymer and starting materials with additional peaks across the whole range that have been assigned. In terms of the ^{13}C NMR, the signal from the sodium acrylate disappears after modification which is strong evidence of successful reaction.

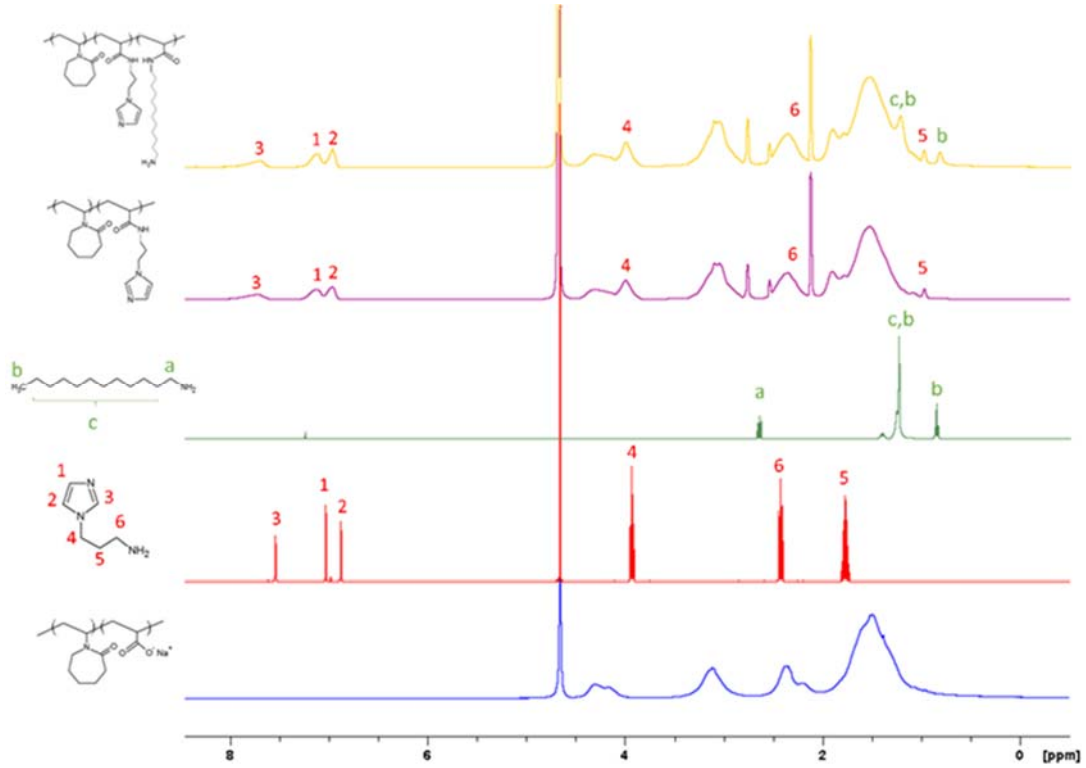

Figure 5. 4 ^{1}H NMR spectra of PVCap-APIM-20 & PVCap-APIM(18)-C_{12} in D_2O (Sheng et al., 2017)

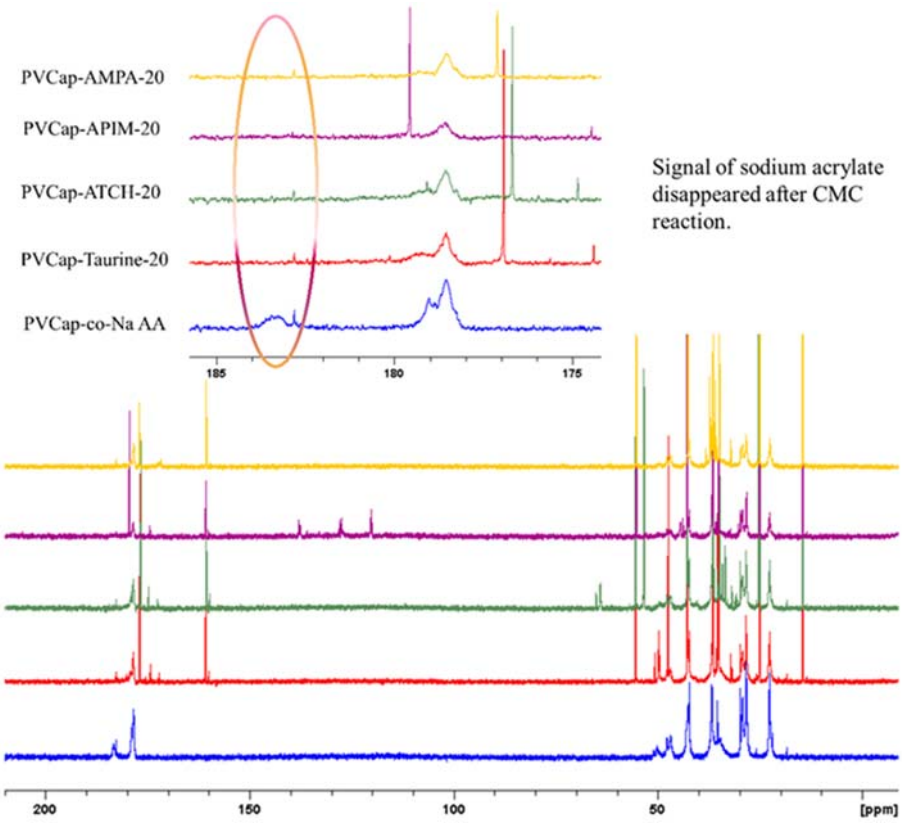

Figure 5. 5 ^{13}C NMR spectra of modified polymers in D_2O, as shown in the focused area, signal of sodium acrylate disappeared after modification which confirmed the transformation of sodium acrylate to target structure was complete after CMC reaction (Sheng et al., 2017).

5.3.2 Synthesis of PVCap-based KHCI polymers

A library of modified PVCap-based polymers which carry kinetic hydrate inhibitor groups and corrosion inhibitors groups were obtained by post-synthetic modification, specifically a carbodiimide mediated coupling reaction (CMC) (Scheme 5.1). This method has been described in detail for modified polyacrylamide structure and modified poly(N-isoproplacrylamide) (PNIPAM) in the previous chapter.

As discussed the polymers consist of 20 mol% of the sodium carboxylate content which can be used for modification. To achieve the optimized KHCI all of the carboxylate units were reacted and three groups of novel KHCI were designed and synthesized as shown in Scheme 5.2.

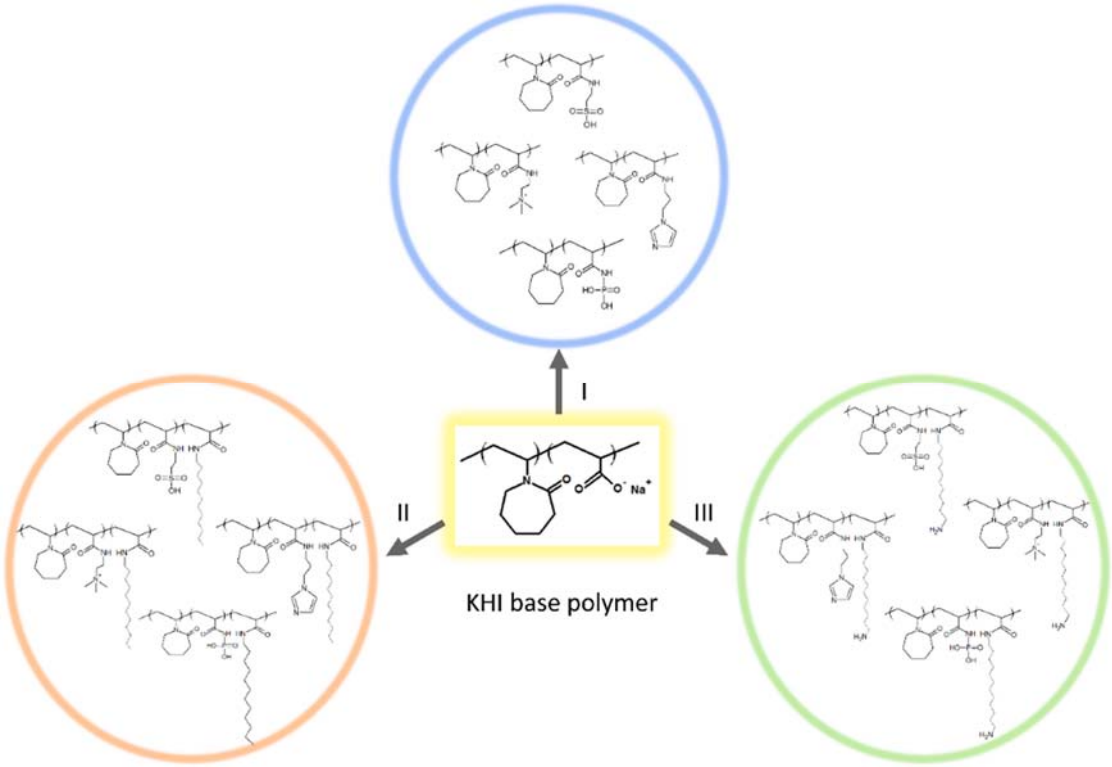

Scheme 5.2 I. 20mol% Modified with CI amines (blue); II. 2mol% addition of $C1_{12}$ amines (orange); III. 2mol% addition of C_{12} diamines (green) (Sheng et al., 2017).

For Group I, all of the sodium carboxylate groups were modified with imidazoline, quaternary ammonium, phosphate and sulfonic acid groups which are among the main classes of corrosion inhibitors (Fuchs-Godec, 2006; Hatch and Ralston, 1969; Hluchan et al., 1988; Hoseinzadeh et al., 2014; Meakins, 1963; Musa and Lei, 2016; Zhang et al., 2008; Zhang et al., 2009).

The mode of action of these corrosion inhibitor groups is to absorb onto metal surfaces, but they can also interact with the growing hydrate surfaces, but they can also interact with the growing hydrate surface. This contributes to the compatibility issues between KHIs and CIs as their mode of action is similar. As such there is substantial overlap with the chemistry of antiagglomerants and corrosion inhibitors. For example, quaternary ammonium groups are found in corrosion inhibitors and antiaglglomerants. This demonstrates that corrosion groups will interact with hydrates. In terms of the single polymer molecules presented in this study the presence of the corrosion groups is likely to increase the interaction of the inhibitor with the metal surface but also the hydrate. The extent to which the groups contribute to hydrate and corrosion

performance requires accurate control over polymer structure so it is important to minimize variations in molecular weight, composition, and end groups. The method presented in this thesis allows for these parameters to be normalized across the inhibitors.

In order to compare the effect of pendant substituent on different KHCI structures, for group II and III, 18 mol% of the carboxylate units were modified with the same four structures mentioned above and the remaining 2 mol% was modified with C_{12} amine and C_{12} diamine. Corrosion inhibitors typically contain an alkyl chain so 2 mol% of C_{12} groups were included to enhance corrosion inhibition. This hydrophobic substituent helps to form a protective barrier once the "active centre" of the KHCI has attached onto the metal surface and thus prolongs the de-absorption process. The pendant amine group can also enhance the corrosion inhibition when the amine head at a hydrophobic chain serves as an anchor site to the surface (Al-Sabagh et al., 2013; Martínez et al., 2009).

5.3.3 Cloud point

The cloud points for all of the polymers were determined using the same method introduced in the last chapter, and the results are presented in Tables 5.2 and Table 5.3. As can be seen the cloud point for all of the polymers does not change substantially as the polymers are modified. All of the polymers display a cloud point that is in line with other PVCap-based polymers that have been reported (Kelland et al., 2000; Mady and Kelland, 2015; Musa et al., 2011). This is despite the fact that the structure of the polymers has changed as confirmed by NMR spectroscopy. This suggests that the cloud point is dominated by the VCap groups in the polymer since the ratio of this structural group in the polymer is 80%. This is in line with other studies where the cloud point of PVCap-based polymers did not change substantially when N,N-dimethylhydrazidoacrylamide (DMHAM) was incorporated into the polymers which is a polar monomer. For example, the authors found that PVCap had a cloud point of 34 °C and when DMHAM was incorporated the cloud point did not change when the ratio of DMHAM:VCap was 1 : 9. By changing the ratio of DMHAM:VCap to 1:4 the cloud point increased to 40 °C which is in line with the data presented here. Alternatively, the presence of by-products from the CMC reaction (urea and NHS)

could be effecting the cloud point so the cloud point for the base polymer was measured in the presence of varying concentrations of the side products which were added to a solution of the purified base polymer (Table S3), and as can be seen, the side products did not change the cloud point.

Table 5. 2 Cloud point of KHCI polymers (Sheng et al., 2017).

Polymer	T_{cp} (°C)
PVCap-co-Na AA	34
PVCap-ATCH-20	37
PVCap-ATCH(18)-C_{12}(2)	37
PVCap-ATCH(18)-DiaminoC_{12}(2)	37
PVCap-Tau-20	37
PVCap-Tau(18)-C_{12}(2)	37
PVCap-Tau(18)-DiaminoC_{12}(2)	37
PVCap-APIM-20	37
PVCap-APIM(18)-C_{12}(2)	37
PVCap-APIM(18)-DiaminoC_{12}(2)	37
PVCap-AMPA-20	39
PVCap-AMPA(18)-C_{12}(2)	40
PVCap-AMPA(18)-DiaminoC_{12}(2)	37

Table 5. 3 Cloud point for base polymers with the presence of by-product generated in CMC reaction in different ratio (5%, 10% and 20%) (Sheng et al., 2017).

Polymer	T_{cp} (°C)
PVCap-co-Na AA	34
PVCap-co-Na AA (5% by-product)	34
PVCap-co-Na AA (10% by-product)	34
PVCap-co-Na AA (20% by-product)	34

5.4 Conclusions

Using the outlined method the structure and properties of the polymers can be modulated over a broad range. Polymers based on poly(VCap-co-AA) onto which

modification with taurine, ATCH, APIM, and AMPA as well as a dodecyl (C_{12}) alkyl chain were generated successfully. A libraries of novel KHCIs were characterized by gel permeation chromatography, titration, proton NMR and carbon NMR. The further investigation of the key property such as hydrate and corrosion inhibition of these KHCIs will be discussed in the following chapters.

Chapter 6 HIGH-THROUGHPUT HYDRATE SCREEN TECHNOLOGY

6.1 Introduction

As demonstrated in the previous chapters, two libraries of KHI-based modified polymers via CMC reaction were successfully generated. To further characterize the hydrate inhibition property of these polymers, a novel and efficient method must be applied correspondingly. This chapter will illustrate a newly developed technology for ranking commercial available KHI inhibitors. This ranking was validated against the more conventional rocking cell method. After the validation of our new hydrate screen protocol, two libraries of novel polymers were then screened via this high-throughput hydrate (HTP) hydrate technology. Some promising candidates were picked out for more rigorous conventional test.

6.2 Innovation of HTP hydrate screen

It is well known that the efficacy ranking of KHIs can be derived from a range of conventional experimental techniques; autoclaves (Del Villano and Kelland, 2011; Duchateau et al., 2009a), stirred batch reactors (Duchateau et al., 2012), rocking cells (Mady and Kelland, 2014; May et al., 2014), High Pressure-Automated Lag Time Apparatus (Maeda, 2014; Maeda et al., 2011) and flow loop (Di Lorenzo et al., 2014). These instruments typically measure the induction times at constant subcoolings and/or the maximum achievable subcoolings during constant cooling ramps. They require flammable gases, high pressures and further require long data accumulation times. The amount of sample required for testing is also large which renders the use of the conventional technique challenging for precious inhibitors such as anti-freeze proteins (Sharifi et al., 2014; Walker et al., 2015).

These conventional protocols have proven to be a bottleneck for new materials development in this area in that a large number of expensive instruments are required for parallel screening of multiple inhibitors. Structure is central to the development of a knowledge base that will lead to the understanding required for control and prediction of hydrate formation. Efficient design of high performance advanced

materials requires a thorough understanding of structure-property relationships that is currently hindered by the current conventional evaluation protocols. As astronomical numbers of combinations are theoretically possible in the design of a polymeric KHI and recent advances in high-throughput synthesis allow this broad experimental space to be explored, a cost effective method for the rapid, parallel screen of potential KHIs is desirable, which preferably does not involve handling of highly pressurized and potentially flammable/explosive fuel gases.

High throughput techniques have been routinely employed by the pharmaceutical industry and biological research community for decades and translation of this philosophy to materials research has occurred in recent years (Mulet et al., 2013; Pyzer-Knapp et al., 2015; Tse et al., 2012). Discovery and optimisation typically follow several stages that progressively narrow the parameter space in question. In the initial phase, coarse characterisation of the essential properties is performed to identify promising compositions, reaction conditions or structures. In subsequent phases, the selected property is characterised more precisely and thoroughly; reiteration of this process leads to new materials discovery with a knowledge of structure-property correlations (Figure 6.1).

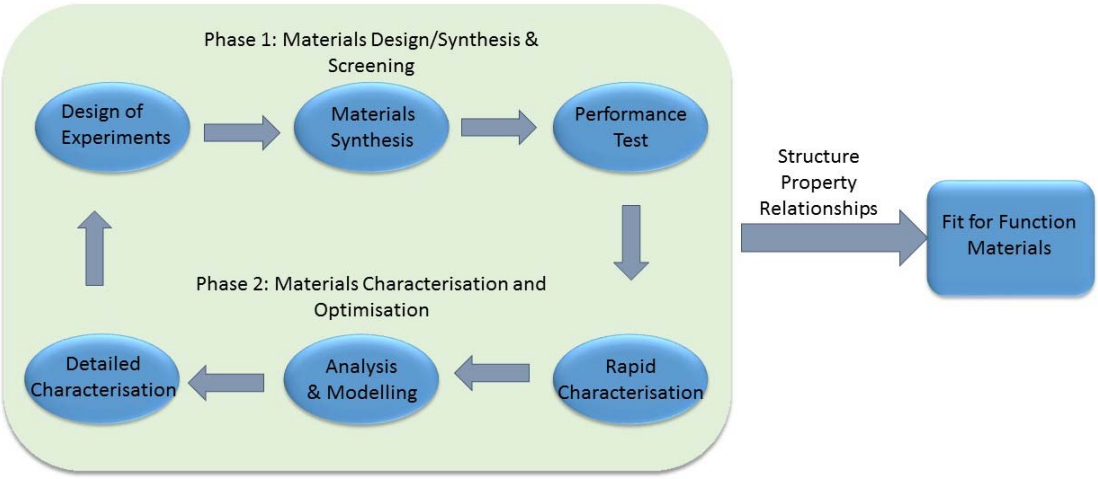

Figure 6. 1 Ideal Combinatorial and high throughput workflow for the discovery of new materials (Maeda et al., 2016).

This study aims to develop a rapid screening method for ascertaining KHI efficiency based upon the observation of the inhibition of hydrate formation of Structure II (sII)-

forming cyclopentane (c-C5) hydrate under atmospheric pressure. It has been shown that the efficacy ranking of the KHIs based on the use of c-C5 hydrate did not completely match from that obtained using natural gas hydrates (Dirdal et al., 2012). Nevertheless, the rankings were broadly similar to each other and hence c-C5 could still serve as a useful first screening method which can be used to identify promising candidates for more rigorous testing. Within the context of Figure 1, the screen is Phase 1 of the new materials discovery and optimisation workflow. For this purpose, some commercially available KHIs were screened and ranked, and this ranking validated against the more conventional Rocking Cell method which used natural gas which also forms sII hydrates. Thus the comparison between the conventional techniques and the proposed method is two-fold; the equipment used for the testing and the chemicals that act as guests.

Specifically, the comparative efficiency of some commercial and well-known KHIs: Luvicap 21W, Luvicap 55W, polyvinylpyrrolidone (PVP), poly(N-isopropylacrylamide) (PNIPAM), and polyacrylamide (PAM) included as a weak KHI to make sure not all strong performing , as well as the common THI, MEG were screened and ranked using the model sII-hydrate forming cyclopentane (Table 6.1).

Table 6. 1 List of KHIs used in the study (Maeda et al., 2016).

KHI name	Mw (g/mol)	Supplier
Luvicap 55W	2000-4000	BASF
Luvicap 21W	21000	BASF
Polyvinylpyrrolidone (PVP) K15	9000	Ashland Chemical Co.
Poly(N-isopropylacrylamide) (PNIPAM)	8500	Synthesized in-house (Mady and Kelland, 2014)
Polyacrylamide (PAM)	5000000	Sigma - Aldrich

Natural gas as a guest also form sII hydrates. Tetrahydrofuran (THF) and cyclopentane (c-C_5) however, are among the several guests that form sII hydrates at atmospheric pressure and above 273.16 K and these have been used as model hydrate formers (Dirdal et al., 2012; Ripmeester and Davidson, 1977; Sun et al., 2002). The thermodynamic equilibrium dissociation temperature, T_{eq}, of THF hydrate and c-C_5 hydrate is 277.5K and 280.8K, respectively (Dirdal et al., 2012; Sun et al., 2002). c-C_5 hydrate thus offers more room for sub-cooling above the ice point; it is also sparingly soluble in water and so is a more appropriate analogue for natural gas than THF, which is miscible with water at all proportions.

6.2.1 Materials and methods

6.2.1.1 Materials

The KHIs tested were (1) Luvicap 21W: 34.6wt.% VP:VCap 2:1 in H2O (from BASF), low Mw 2000-4000 Da, (2) Luvicap 55W, 53.8wt.% in water (from BASF): VP:VCap 1:1 copolymer, Mw = 21000 Da, (3) polyvinylpyrrolidone PVP K15 (from Ashland Chemical Co.), Mw = 9000 Da, (4) poly(N-isopropylacrylamide), PNIPAM, Mw = 8500 Da (Synthesized in-house (Mady and Kelland, 2014)) and (5) polyacrylamide-co-acrylic acid, PAM, Mw = 5000000 Da (Sigma-Aldrich). Mono-ethylene-glycol (MEG) was purchased from Sigma Aldrich (purity > 99.8%) and used as received. Cyclopentane was purchased from Merck (purity > 98%) and used as received. For each KHI to be tested, a dilution series of the KHI aqueous solutions was prepared using water from a Millipore unit (> 18.2 MΩ resistivity). The range of concentrations of the dilution series was at least two orders of magnitude and the range covers the typical KHI dosage of 0.5wt%.

6.2.1.2 High-Throughput hydrate testing of kinetic hydrate inhibitors

0.5ml of each KHI solution was placed in a separate vial (2 ml) and was frozen using dry ice and 0.1ml of liquid cyclopentane was added to each frozen KHI solution. The mixed solution was then placed inside a constant temperature water bath which was in turn housed in a refrigerator (3-3.5 °C; Figure 6.2).

Figure 6. 2 Schematic illustration of the high-throughput KHI performance screening setup (Maeda et al., 2016).

Typically it took less than an hour for the whole solution to be thawed. Continuous monitoring of the progress of hydrate formation was recorded using a webcam (Logitech C920 HD Pro Webcam). A control comprising water + cyclopentane (without a KHI) was always monitored in parallel.

The so-called "memory effect" is a commonly used strategy to increase the reproducibility of the measurements related to intrinsically stochastic nucleation events (Duchateau et al., 2009b). The memory effect refers to observations that gas hydrates form easier or faster from water obtained by the dissociation of gas hydrates or melting of ice (Sefidroodi et al., 2013; Sloan and Koh, 2007; Sowa and Maeda, 2015). In this instance this would require that each KHI solution be heated to a few degrees above the thermodynamic equilibrium dissociation temperature, $T_{eq'}$ of the c-C_5 hydrate after seeding with ice, and then cooling the solution back to below $T_{eq'}$. However, such a protocol would introduce additional experimental parameters to be controlled, and given that the purpose of our protocol was a fast and crude screening

method of a large number of KHIs, we decided to adopt the direct ice seeding method (Makogon, 1981; Sloan and Fleyfel, 1991; Stern et al., 1996). Since the ice seeding effectively ensures the nucleation of c-C_5 hydrate, there is a risk that we may accidentally rule out a promising nucleation inhibitor based on its poor performance as a growth inhibitor.

6.2.1.2 Powder diffraction

To verify that the hydrate was being formed in these experiments, X-ray diffraction was performed on the powder diffraction beamline at the Australian Synchrotron (Wallwork et al., 2007), at an X-ray energy of ~13 keV. Each sample was placed in a 1.0 mm diameter borosilicate capillary and data was collected over the 2θ range of ~2-82°.

Pawley analyses were performed on the data using the Bruker TOPAS™ V5 program. The background signal was described using a combination of Chebyshev polynomial linear interpolation function, 1/x function, and a broad pseudo-Voight function to describe the background due to the capillary itself. Cell parameters, peak full width at half maximum and peak scale factors were all refined.

A representative XRD pattern is shown in Figure 6.3 for cyclopentane hydrate formed, in this case in the presence of PVP. The crystal structure has cubic symmetry with space group Fd3m and lattice parameter a $\approx$ 1.735 nm, consistent with sII structure for these clathrates where cyclopentane is the guest molecule (Sloan and Koh, 2007). Here the sampling time was a few minutes for a given sample and the measurement commenced within a few minutes of mounting of a frozen sample, so the ice peaks are present together with the sII structure in Figure 6.3. For the high throughput cyclopentane hydrate measurements each frozen KHI solution was taken out of the freezer and transferred to a bath inside a refrigerator and cyclopentane was added at time = 0 (see above). Therefore the XRD measurements closely mimic an early stage of the high throughput cyclopentane hydrate measurements (time < 1 hour).

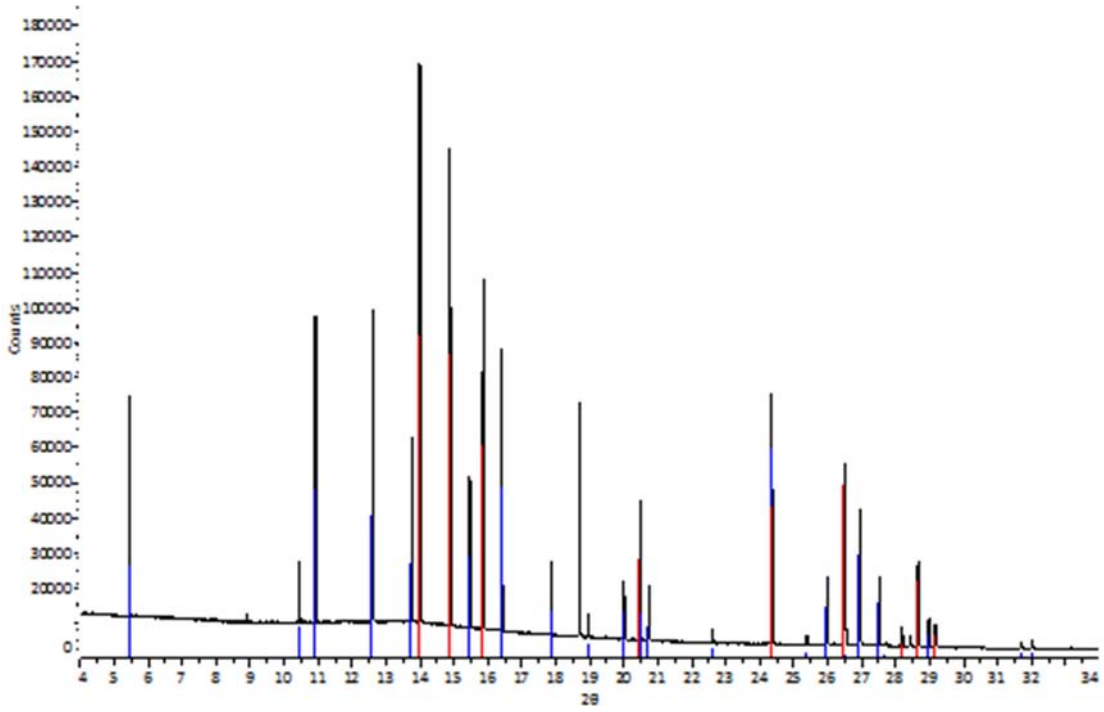

Figure 6. 3 An example synchrotron powder X-ray diffractogram for the hydrate structure formed in the presence of a KHI, in this case PVP. The clathrate is sII (blue lines) with lattice parameter a=1.735 nm. Red lines indicate the presence of ice (Maeda et al., 2016).

6.2.1.3 Rocking cell method in collaboration with University of Stavanger

Rocking cell kinetic hydrate inhibition experiments were carried out in five parallel high pressure steel cells of volume 40ml. The equipment (RC5 unit) was supplied by PSL Systemtechnik, Germany. Each cell contained a steel ball. The cells were placed in a temperature-controlled cooling bath. The gas composition used, which gives a Structure II hydrate as the most thermodynamically-stable phase, is given in Table 6.2.

Table 6. 2 Composition of Synthetic Natural Gas (SNG) used for the rocking cell measurements (Maeda et al., 2016).

COMPONENT	MOLE %
METHANE	80.67
ETHANE	10.20
PROPANE	4.90
ISO-BUTANE	1.53
N-BUTANE	0.76
N_2	0.10
CO_2	1.84

Each cell had its own temperature and pressure sensor. The temperature in each of the cells was measured individually and to an accuracy of ±0.1 °C. The pressure was measured with an accuracy of ±0.2 bar.

The test procedure used a "constant cooling" method whereby cooling is carried out at a constant rate of 1 °C/h. At the start of each experiment the pressure was approximately 76 bar. The equilibrium temperature (T_{eq}) at this pressure was 20.2 °C ±0.05 °C, determined by a series of standard laboratory dissociation experiments warming at 0.025 °C/h for the last 3-4 °C (Gjertsen and Fadnes, 2000; Tohidi et al., 2000).

The constant cooling test procedure was as follows:

1. 20 ml of distilled water with dissolved KHI was added to each cell. The concentration of each KHI was 5000 ppm.

2. Air in the cells was removed using a combination of vacuum pumping and filling with the sample gas to 2 bar. The process was then repeated.

3. The cell was pressurized to 76 bar and rocked at 20 rock/minute at an angle of 40°.

4. The cells were cooled from 20.5 °C at a rate of 1 °C/hr down to 2 °C whilst logging the pressure and temperature for each individual cell, as well as the temperature of the cooling bath.

Fresh samples were used for each repeat measurement (each KHI solution was discarded after a single cooling ramp and not re-used for more than one test). The average onset temperature, T_o, and the average temperature at which rapid hydrate formation takes place, T_a, were measured from eight tests for each KHI. We did not

observe any bias between the five cells, i.e. no one cell gave consistently worse or better results than the others. The standard deviation was in the range of 5-7% for both T_o and T_a. In this constant cooling ramp method, the lower the T_o (and usually the T_a), the better the performance of the KHI. A typical graph of pressure and temperature data versus time for one of the steel rocking cells in shown in Figure 6.4.

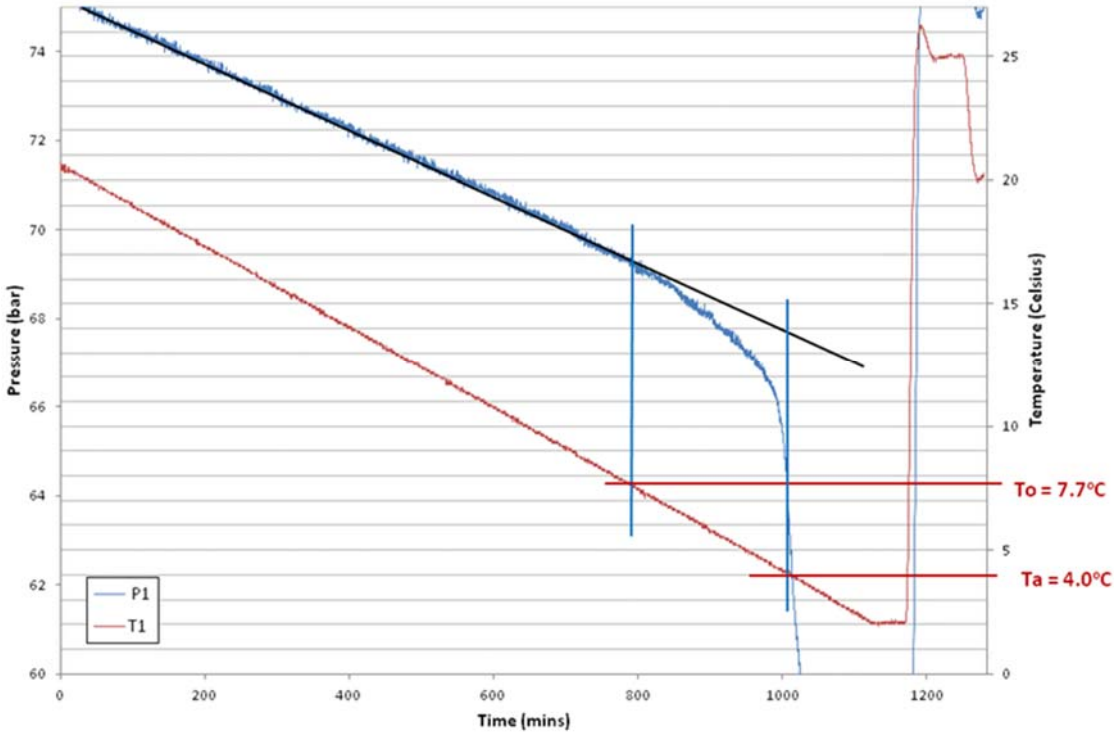

Figure 6. 4 An example temperature–pressure profile which shows the onset temperature T_o, and the temperature at which rapid hydrate formation takes place, T_a, of a rocking cell measurement (Maeda et al., 2016).

A more thorough investigation of the reproducibility at various test conditions in this multi-cell rocker rig has been reported (Lone and Kelland, 2013).

6.2.2 Results and discussion

6.2.2.1 High-throughput hydrate testing of commercial kinetic hydrate inhibitors

The amount of c-C_5 hydrate formation increased with the time for a given sub-cooling – i.e., the longer a sample was left at a subcooled state the more likely the cyclopentane hydrate nucleated. For a systematic comparison, we selected an arbitrary cut-off time at which the inhibition performance of KHIs could be assessed. For a given cut-off time, we measured the threshold KHI concentration above which the KHI became effective in inhibiting the formation of cyclopentane hydrate. This threshold KHI concentration was then used as a measure of the efficacy of the KHI in that the lower the threshold concentration the better performing the KHI. For the results shown below we used 20 hours as the cut-off time. This selection is arbitrary but is long enough for hydrate formation to have taken place.

At least three batches of samples were prepared for each concentration of each KHI. Despite the ice seeding at the beginning of the sample preparation, some variability in the cyclopentane hydrate formation was inevitable. Nevertheless, the repeatability was good in that (1) the KHI efficacy ranking remained unchanged and (2) we found no instance in which a higher concentration sample of a given KHI provided a poorer inhibition effect than a lower concentration sample of the same KHI at the same cut-off time.

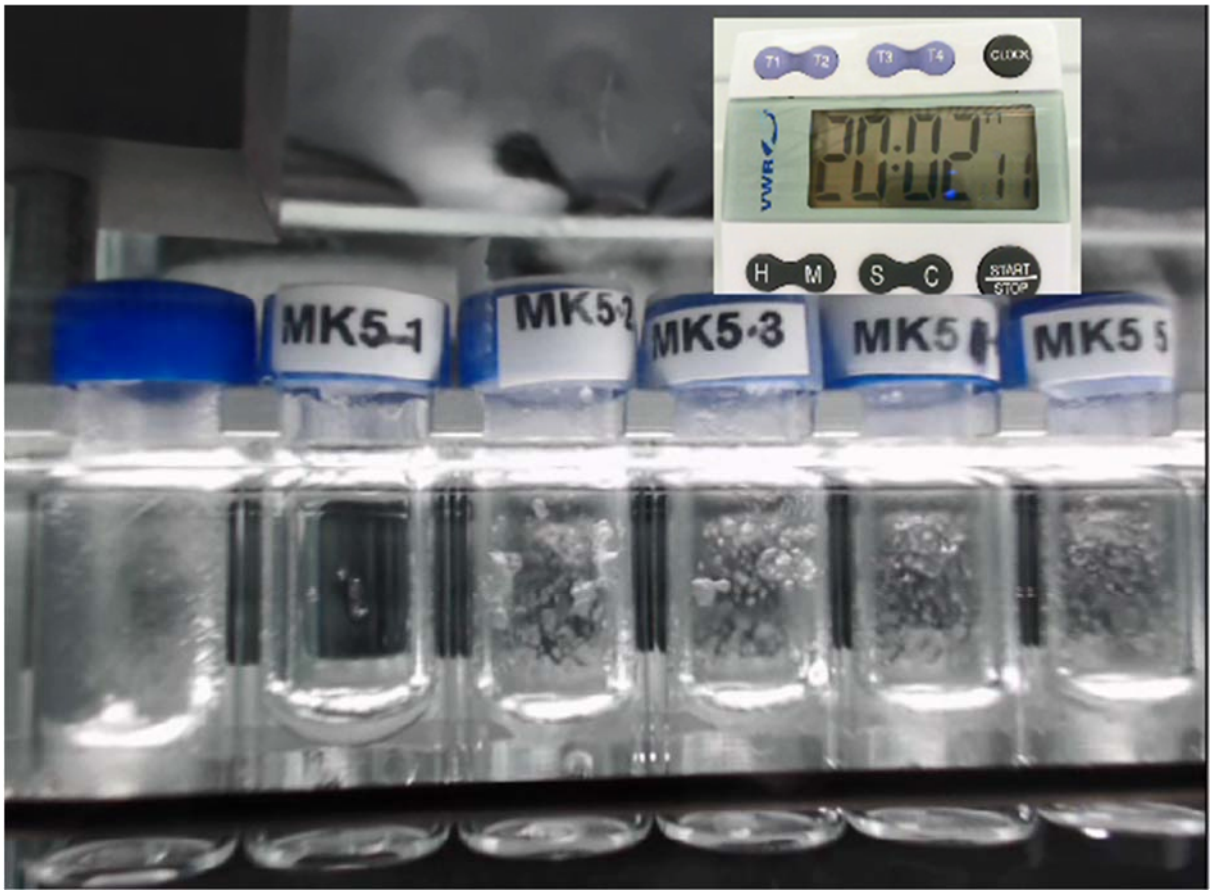

Figure 6. 5 Example photograph of a dilution series of Luvicap 21W after a cut-off time of 20 h. The vials shown are, from left to right, blank, 0.3wt%, 0.15wt%, 0.03wt%, 0.015wt% and 0.003wt%, respectively. The threshold concentration of Luvicap 21W after a cut-off time of 20 hours was 0.3wt% (Maeda et al., 2016).

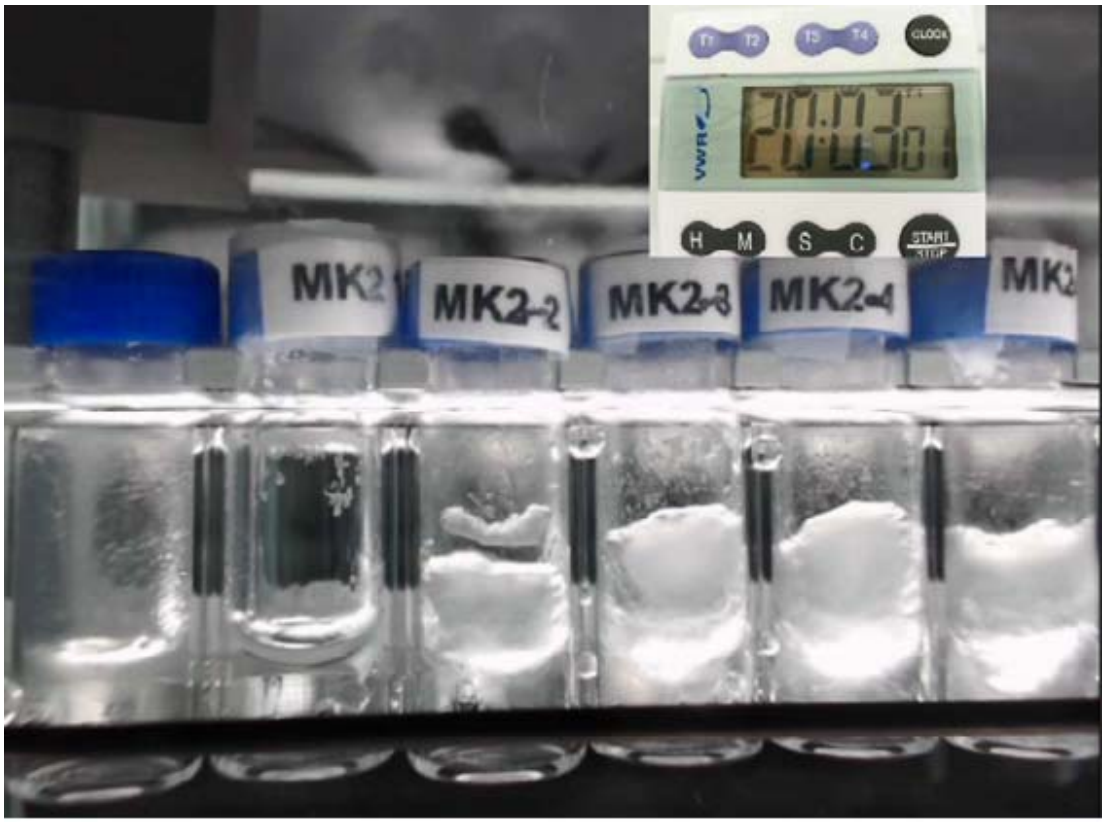

Figure 6. 6 Example photograph of a dilution series of Luvicap 55W after a cut-off time of 20 h. The vials shown are, from left to right, blank, 0.wt%, 0.25wt%, 0.05wt%, 0.025wt% and 0.005wt%, respectively. The threshold concentration of Luvicap 21W after a cut-off time of 20 hours was 0.5wt% (Maeda et al., 2016).

Figure 6. 7 Example photograph of a dilution series of PNIPAM after a cut-off time of 20 h. The vials shown are, from left to right, blank, 1wt%, 0.5wt%, 0.1wt%, 0.05wt% and 0.01wt%, respectively. The threshold concentration of Luvicap PNIPAM after a cut-off time of 20 hours was 1wt% (Maeda et al., 2016).

Figure 6. 8 Example photograph of a dilution series of PVP after a cut-off time of 20 h. The vials shown in the top panel are, from left to right, blank, 1wt%, 0.5wt%, 0.1wt%, 0.05wt% and 0.01wt%, respectively. The vial shown in the bottom panel are, from left to right, 10wt%, 5wt%, 3wt%, 2wt%, 1wt% and blank, respectively. The threshold concentration of PVP after a cut-off time of 20 hours was 2wt% (Maeda et al., 2016).

Figure 6. 9 Example photograph of a dilution series of PAM after a cut-off time of 20 h. The vials shown in the top panel are, from left to right, blank, 1wt%, 0.5wt%, 0.1wt%, 0.05wt% and 0.01wt%, respectively. The vial shown in the bottom panel are, from left to right, 10wt%, 5wt%, 3wt%, 2wt%, 1wt% and blank, respectively. The threshold concentration of PAM after a cut-off time of 20 hours was >10wt% (Maeda et al., 2016).

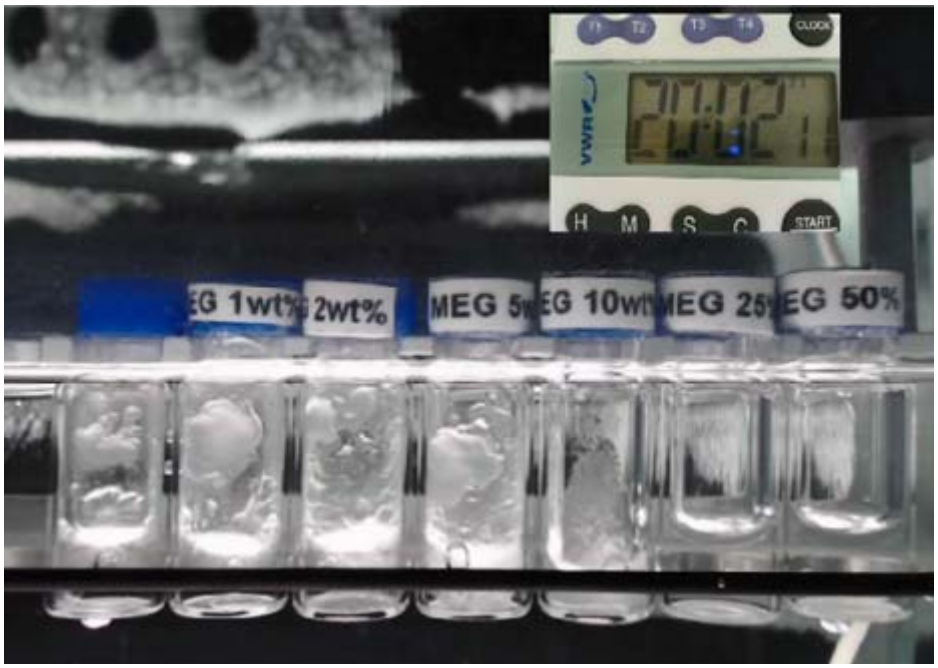

Figure 6. 10 Example photograph of a dilution series of ethylene glycol (MEG) after a cut-off time of 20 h The vials shown are, from left to right, blank, 1wt%, 2wt%, 5wt%, 10wt%, 25wt%, and 50wt%, respectively. The threshold concentration of MEG after a cut-off time of 20 hours was 25wt% (Maeda et al., 2016).

Figures 6.5-6.10 show that the threshold concentration at 20 hours of cut-off time was 0.3 wt% for Luvicap 21W, 0.5 wt% for Luvicap 55W, 1 wt% for PNIPAM and > 1 wt% for PVP (1 wt % PVP solution did not always inhibit the formation of c-C_5 hydrate at 1wt%, as the top and the bottom panel show). For PAM, even the highest concentration of 10 wt% was not sufficient. These results are summarized in Table 3.

Table 6. 3 The threshold concentration C_t (wt %) of KHIs above which the KHI inhibited cyclopentane hydrate formation, after the cut-off time of 20 hours at 4 °C (Maeda et al., 2016).

KHI	C_t
Luvicap 21W	0.3
Luvicap 55W	0.5
Poly(N-isopropylacrylamide); PNIPAM	1
Polyvinylpyrrolidone; PVP K15	2
Polyacrylamide; PAM	>10

On basis of these results, we conclude that the efficacy ranking of these five KHIs is;

Luvicap 21W ≥ Luvicap 55W > PNIPAM ≥ PVP > PAM

To further demonstrate that the rapid c-C_5 hydrate screening method is capable of detecting hydrate inhibition, we also measured a dilution series of mono ethylene glycol (MEG). Figure 6.10 shows the dilution series of MEG. It can be seen that only concentrations of 25wt% or higher inhibited c-C_5 hydrate formation for 20 hours at 3-3.5°C. This MEG result is for the sole purpose of demonstrating that the proposed method can detect hydrate inhibition at sufficiently high concentrations of MEG, as expected. No quantitative and/or industrial implications should be inferred from the threshold concentrations of the KHIs or from that of MEG.

6.2.2.2 Rocking cell method

The results for the same five KHIs, but now tested in the rocking cells, are summarized in Table 6.4.

Table 6. 4 Results of the standard constant cooling ramp method (1 K/hour) in steel rocking cells[a] (Maeda et al., 2016).

KHI	T_o (°C)	T_a (°C)
Blank	17.2	16.5
Luvicap 55W	4.3	3.8
Luvicap 21W	5.5	4.7
Poly(N-isopropylacrylamide) (PNIPAM)	6.9	6.1
Polyvinylpyrrolidone (PVP) K15	11.0	10.9
Polyacrylamide (PAM)	17.1	16.5

[a]The concentration of each KHI was 5000ppm. The average onset temperature, To, and the average temperature at which rapid hydrate formation takes place, Ta, were measured from 8 tests for each KHI. The standard deviation was in the range of 5-7%.

As expected, the polyacrylamide showed no activity as a KHI. Although it is water-soluble and contains strong hydrogen-bonding amide groups, it has no hydrophobic functionality, which is essential for good KHI performance. PVP K15 is the next worse KHI tested. It is water-soluble at all temperatures 0-100 °C at the test concentration of 5000 ppm and thus has no cloud point. The ring methylene groups in PVP do impart some hydrophobicity enabling the polymer to have some activity as a KHI .(Kelland, 2006, 2011).

PNIPAM and the VP:VCap copolymers are all more hydrophobic than PVP, exhibiting cloud points in solution (Kelland and Iversen, 2010). Luvicap 21W has a higher proportion of the VP monomer than Luvicap 55W and was therefore expected to perform worse as a KHI.

As can be seen, the ranking from T_o and that from T_a matched with each other. In either case, the efficacy ranking of these five KHIs are;

Luvicap 55W > Luvicap 21W > PNIPAM > PVP > PAM

6.2.2.3 Comparison of the two methods

There is a rather minor difference between the two rankings in that the rapid c-C_5 hydrate screening method ranked Luvicap 21W ahead of Luvicap 55W in contrast to the rocking cell method. The rest of the efficacy ranking was the same from both methods.

Luvicap 21W and Luvicap 55W are both highly effective KHIs which are structurally similar to each other. It is not surprising that the rapid c-C5 hydrate screening method was not sensitive enough to discern the two. This limitation that the method is not capable of discriminating the performance of structurally similar KHIs suggests that it can only serve as the first screening of a family of mutually similar KHIs from other polymer groups.

The rapid c-C_5 hydrate screening method is an optical method and does not detect any microscopic c-C_5 hydrate formation, let alone nucleation. Therefore, that the efficacy ranking from this method was in broad agreement with the rocking cell method suggests that a large part of the inhibition effect of the KHIs comes from the growth inhibition of c-C_5 hydrate. We note that unlike in rocking cells / stirred autoclaves, the samples in the rapid c-C_5 hydrate screening method are quiescent. Stirring could facilitate the growth of gas hydrate by at least 2 mechanisms; (1) create new aqueous-guest interfaces at which gas hydrate can form, (2) dissipate the latent heat that arises from the formation of gas hydrate. Thus the quiescent samples in the new method is expected to deter the growth of c-C_5 hydrates compared with stirred systems. It follows that any new KHIs that show poor inhibition performance from the rapid c-C_5 hydrate screening method are not worth subjecting to further, more rigorous testing.

Even though the use of ice seeding is convenient in inducing c-C_5 hydrate formation with certainty, the nucleation and growth mechanisms of c-C_5 hydrates may not be the same as in the absence of any ice. Nevertheless, our results suggest that the difference is not drastic enough to significantly alter the efficacy ranking of KHIs. Despite the coarse nature of the screen, this method has enabled fast parallel screening of KHIs. It is not designed as a replacement for detailed hydrate tests so the aim was accomplished.

6.2.3 Conclusions

There is a demand for new kinetic hydrate inhibitors that are cost effective and efficient. To date, the techniques available for evaluating the efficiency of KHIs are a bottleneck for new materials development. We have adopted a high throughput philosophy to parallel screen the KHIs so that we can begin to build a more comprehensive understanding of structure-property relationships. This method utilizes cyclopentane hydrate to screen KHIs under atmospheric pressure. Ice seeding was used to enable rapid screening, which could accidentally rule out a promising nucleation inhibitor on the basis of its poor performance as a growth inhibitor. Nevertheless, the observed efficacy performance ranking of the selected KHIs compares well with rocking cell data as described above.

Despite its simplicity, this method has sufficiently replicated the same broad trends identified by more rigorous testing using conventional techniques. The advantages of this method lies in its significant improvement with respect to the following important points:

- Time: Multiple samples can be screened in parallel with a typical experimental duration of 24 h.
- Safety: The experimental setup does not require elevated pressures or noxious gases, as it uses cyclopentane at subcoolings of 3-4 degrees.
- Materials: A small amount of material required, viz 0.5ml of KHI solution.

This method could serve as a useful first screening method which can be used to identify promising candidates for more rigorous testing.

6.3 HTP hydrate screen of PNIPAM-based KHI polymers

6.3.1 Methodology

Sample solutions with concentrations of 0.01%; 0.05%; 0.1%; 0.5–1.0% (w/v) were prepared at room temperature 24 h in advance. This range of concentrations covers the typical KHI dosage of 0.5 wt%. Subsequently, 1 mL of each solution was frozen using dry ice and cyclopentane (c-C_5) was then added in the ratio of 1:5 (0.2 ml of c-C_5 per

sample). The vials were returned to the dry ice to ensure the polymer phase was frozen. All samples were quickly transferred to a sample holder which was located in a water bath stored in a refrigerator at 3–3.5 °C. It took less than an hour for the solution to thaw. After this time the hydrate formation was recorded using time lapse images every 30 s (over 24 h). A comparison was made between control samples with no polymer added (water + cyclopentane) and various solution concentrations of the synthesized polymers. For each repeat measurement the samples were freshly prepared. The aim was to explore the efficiency of KHI candidates in different concentrations, based on the fact that a good inhibitor can prevent or slow down the formation of hydrate crystals even at low concentration

6.3.2 Results and discussion

The post-modification route is able to rapidly generate large libraries of KHIs and testing these libraries in a reasonable timeframe is not possible with conventional hydrate testing protocols. Therefore, High Throughput (HTP) Hydrate tests were carried out to assess all of the KHI. The KHIs were compared under identical test conditions and each sample was measured in triplicate. Cyclopentane (c-C_5) was used as a model hydrate to evaluate polymers as potential KHIs, because c-C_5 form hydrates at atmospheric pressure, it is immiscible with water and forms structure II hydrates, the same as formed in oil and gas production systems. Controls with no polymer were also measured (only water and cyclopentane).

All experiments were initially carried out at a polymer concentration of 1 wt% (Figure 6.11) with 7.5 mol% modification and the KHIs were classified according to their performance.

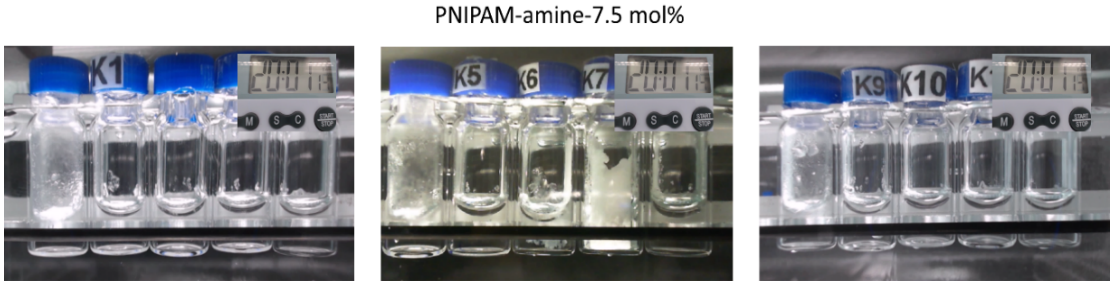

Figure 6. 11 High Throughput (HTP) Hydrate Screen results using 1 wt% polymer solutions of modified PNIPAM-amine with 7.5mol% modification: preliminary selection using visual hydrate amount as a parameter, at 20 hours of experiment. From the left: control sample; base polymer (PNIPAM-co-AA); PNIPAM-C_3-7.5; PNIPAM-C_4-7.5; PNIPAM-C_4t-7.5; control sample; PNIPAM-C_5-7.5; PNIPAM-C_7-7.5; PNIPAM-C_8-7.5; PNIPAM-cyclobut-7.5; control sample; PNIPAM-cyclopent-7.5; PNIPAM-cyclohept-7.5; PNIPAM-cyclooct-7.5; PNIPAM-cycloprop-7.5 (Silveira et al., 2017).

As expected for systems where hydrate forms the volume of hydrate increased with time – i.e., the longer a sample was left at a sub-cooled state the more likely the cyclopentane hydrate formed. In order to systematically compare samples a constant time was selected (20 h) at which the inhibition performance of all samples could be visually evaluated. After 20 h, the performance of the KHIs was compared with stronger inhibitors being effective at lower concentrations. Therefore, weak KHIs did not inhibit hydrate formation at 1 wt% and for each KHI a dilution series was tested and compared to other KHIs across the same dilution range. The lowest polymer concentration where the KHI is effective at inhibiting hydrate is termed as the threshold polymer concentration which was used to determine the efficacy of the KHIs relative to others in the library. With the exception of polymers containing more hydrophobic groups (C_5, C_7, C_8 and cyclooct), samples made with 7.5 mol% of modification showed a noticeable inhibition effect, using 1 wt% polymer solutions. After running a dilution series the performance of these polymers based on the threshold concentration is: cyclopent ≈ C_3 ≈ C_4t ≈ PNIPAM-co-AA > cycloprop ≈ C_4 ≈ cyclobut > cyclohept. A more accurate classification can be made when working with different conditions, for example, polymer concentration and functional group content. In general, the performance of KHIs can be difficult to reproduce, giving a

slightly different result each time, even for standard protocols like rocking cells or autoclave experiments due to the stochastic nature of hydrate formation in a small cell (Chua et al., 2012a).

The leading KHIs were also tested at lower sample concentrations (0.5 and 0.1 wt%) and representative images are shown in Figures 6.12 (Figures 6.13-6.14 show additional results).

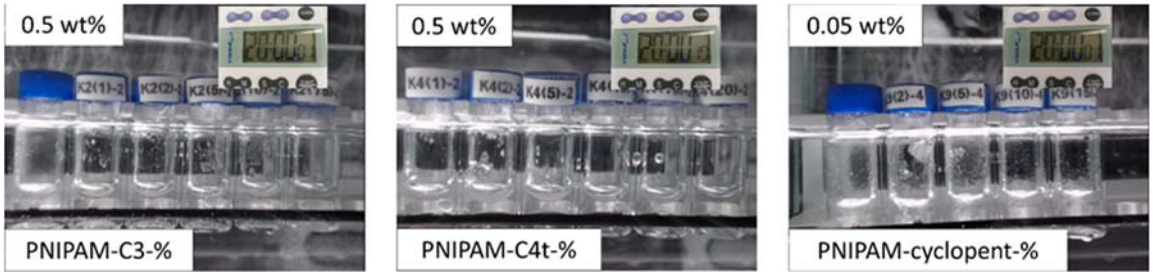

Figure 6. 12 Threshold concentration comparison for PNIPAM-C_3-mol%, PNIPAM-C_4t-mol% and PNIPAM-cyclopent-mol% libraries performing in different concentration (Silveira et al., 2017).

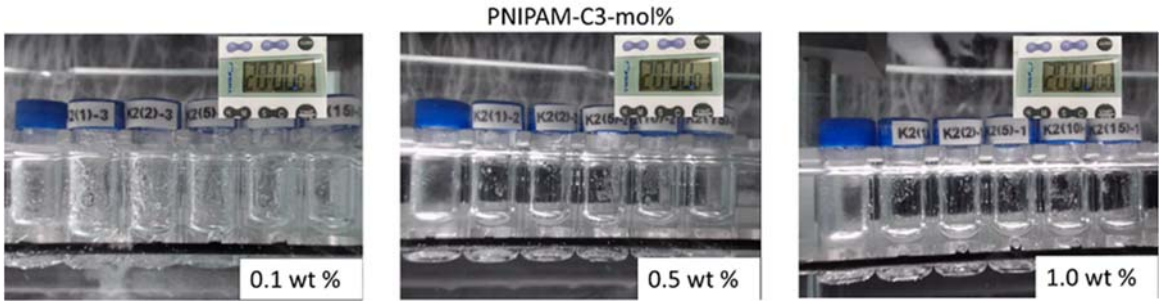

Figure 6. 13 PNIPAM-C_3-mol% polymers at different concentrations (0.1 – 1 wt%) and variable modification degrees. From the left: control solution; PNIPAM-C_3-1.5mol%; PNIPAM-C_3-3mol%; PNIPAM- C_3-7.5mol%; PNIPAM- C_3-15mol% and PNIPAM- C_3-20mol% (Silveira et al., 2017).

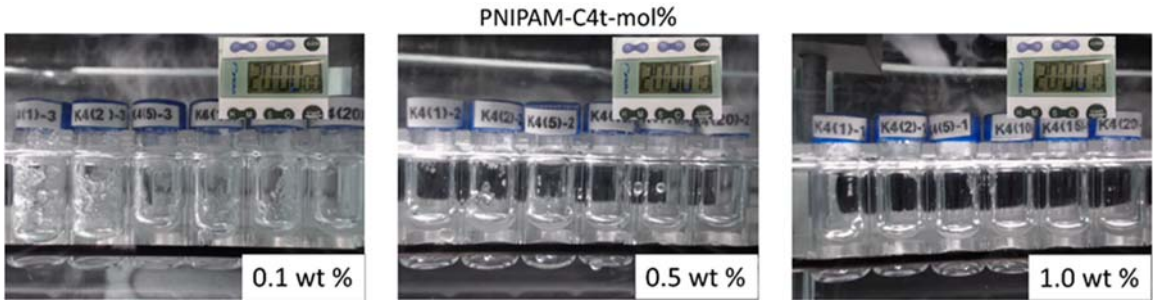

Figure 6. 14 PNIPAM-C_4t-mol% polymers at different concentrations (0.1 – 1 wt%) and variable modification degrees. From the left: PNIPAM-C_4t-1.5mol%; PNIPAM-C_4t-3mol%; PNIPAM-C_4t-7.5mol%; PNIPAM-C_4t-15mol% and PNIPAM-C_4t-20mol% (Silveira et al., 2017).

They were PNIPAM-C_3 (left), -C_4t (centre) and -cyclopent (right) polymers with different degrees of modification (mol%). The concentration of the C_3 modified polymers were 0.5 wt%, for C_4t it was 0.5 wt% and cyclopent it was 0.1 wt%. For cyclopent-functionalized polymers they were also tested at lower concentrations (0.01 and 0.05 wt%). As can be seen there is minimal hydrate formation at varying degrees of modification, even at these low polymer concentrations, which indicates these are effective KHIs. Typically, this would not be the case for weak KHIs such as PAM (Figure 6.9).

In general, based on the screening method the performance of the synthesized KHIs are comparable or better than commercial KHIs such as Luvicap 21W or Luvicap 55W (Figures 6.5 and Figure 6.6, respectively). When compared to other KHIs like PVP K15 and PNIPAM 8.5k the performance of the synthesized KHIs was significantly improved. Clearly modification of the polymers is contributing to the KHI performance by increasing the hydrophobic content (mol %). This is linked to a higher surface area of the pendant group and can be rationalised qualitatively as a steric hindrance effect in preventing hydrate formation (Qin et al., 2015). By accurately controlling the polymer structure across the library these effects are clearer because we have removed variations in the structure and Mw that would be present with a conventional KHIs library synthesized by free radical routes.

Cloud point measurements were also determined because it is believed that high performance KHI tends to have relative low cloud point. However, based on these

libraries of KHIs, the results showed that the cloud point of the copolymer/terpolymer did not correlate to inhibitor performance (Table 6.5).

Table 6. 5 Experimental results for PNIPAM-C_3, PNIPAM-C_4t and PNIPAM-cyclopent polymers in terms of cloud point and threshold concentration which is the lowest concentration at which the inhibitor is effective, the lower the concentration the better the performance (Silveira et al., 2017).

Polymer	Cloud Point (°C)	Threshold Concentration (wt%)
PNIPAM-C3-1.5	38.5	0.5
PNIPAM-C3-3	39.6	0.5
PNIPAM-C3-7.5	46.2	0.5
PNIPAM-C3-15	57.4	0.1
PNIPAM-C3-20	58.0	0.1
PNIPAM-C4t-1.5	37.4	0.5
PNIPAM-C4t-3	38.5	0.5
PNIPAM-C4t-7.5	47.0	0.1
PNIPAM-C4t-15	79.0	0.1
PNIPAM-C4t-20	83.0	0.1
PNIPAM-cyclopent-3	39.5	0.1
PNIPAM-cyclopent-7.5	45.5	0.1
PNIPAM-cyclopent-15	49.3	0.05
PNIPAM-cyclopent-20	46.3	0.05

For example, materials with similar cloud points and percentage of modification PNIPAM-cyclopent- 7.5 (cloud point 45.5 °C) and PNIPAM-C_3-7.5 (cloud point 46.2 °C) have different hydrate inhibition with PNIPAM-cyclopent-7.5 being effective

at lower concentration (0.1 wt%) compared to PNIPAM-C_3-7.5 (0.5 wt%). Therefore, the change in polymer structure has the most profound effect on the hydrate inhibition.

In the case of PNIPAM-cyclopent polymers, the 5-membered ring in the polymer chain may be able to disrupt the formation of hydrate crystals because of an optimized interaction with the pentagonal faces of the building block ($5^{12}6^5$). This assists with the inhibition process for the same reason that poly(vinylcaprolactam) (PVCap) is claimed to function as a KHI. The amide groups of the polymer can be adsorbed on the hydrate crystal surface which can prevent interactions with water molecules which can delay the hydrate growth (Koh et al., 2002; Perrin et al., 2013).

The hydrate inhibition of the leading three KHIs from this study was compared with commercial inhibitors based on their threshold concentration using the HTP Hydrate Screen and they ranked as follows:

PNIPAM-cyclopent-20 (0.05 wt%) > PNIPAM-C_4t-20 (0.1 wt%) ≈ PNIPAM-C_3-20 (0.1 wt%) > Luvicap 21W (0.3 wt%) > Luvicap 55W (0.5 wt%) > PNIPAM 8.5k (1 wt%) > PVP K15 (2 wt%) ≥no additive.

The KHIs synthesized in this study show promising performance compared to commercial samples in terms of the hydrate screening method. It is important to note that the threshold concentration is a guide for performance based on the screen and the actual amounts do not correspond to that increase in performance. As such, this is a first approximation and more detailed testing is required. However, it is clear that accurately controlling polymer structure can fine tune performance and methods that can do this offer a route to overcome the limitations of commercial KHIs.

The HTP screen is sensitive enough to compare samples within a KHI subset (eg., PNIPAM-C_3) where each polymer has the same functional group:

PNIPAM-C_3-20 (0.1 wt%) ≈ PNIPAM-C_3-15 (0.1 wt%) > PNIPAM-C_3- 1.5 (0.5 wt%) ≈ PNIPAM-C_3-3 (0.5 wt%) ≈ PNIPAM-C_3-7.5 (0.5 wt%) > Luvicap 55W (0.5 wt%) ≥ no additive.

The effect of polymer concentration was also investigated and generally increasing KHI concentration decreases hydrate formation and the HTP hydrate screen confirmed this was the case with the KHIs synthesized in this work. For example, the results for cyclopent products (Figure 6.15 show that the hydrate content (at 20 h) is lower at

higher KHI concentration (0.01 up to 1 wt%). This further reinforces that the HTP hydrate screening method is effective as a first screen to assess large KHI libraries.

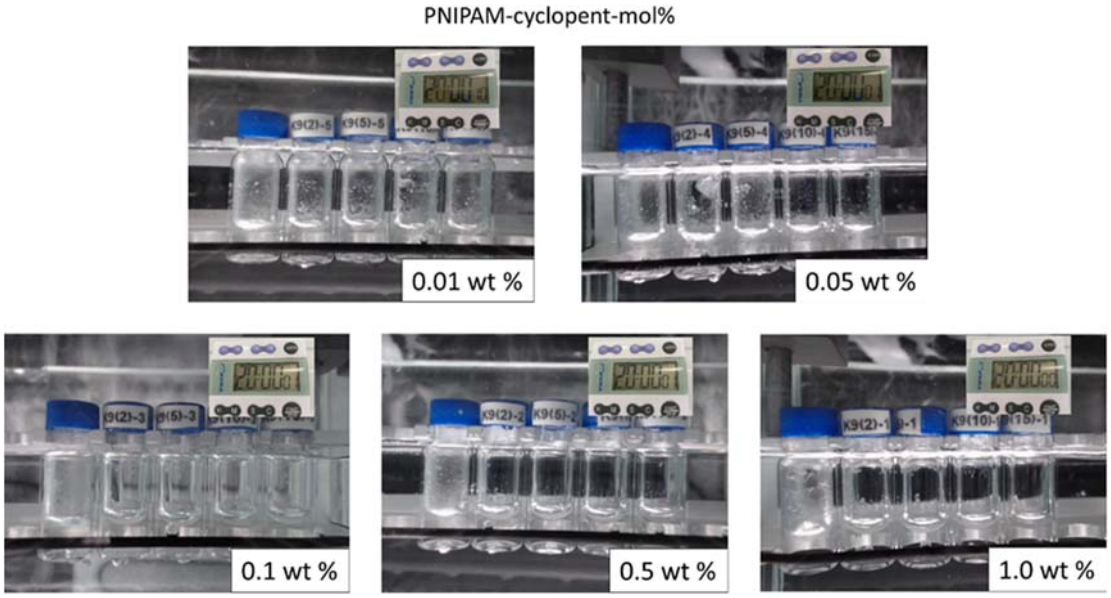

Figure 6. 15 PNIPAM-cyclopent polymers performing in different concentration (0.01 – 1 wt%). In this sequence: Control solution; PNIPAM-cyclopent-3mol%; PNIPAM-cylopent-7.5mol%; PNIPAM-cyclopent-15mol% and PNIPAM-cyclopent-20mol% (Silveira et al., 2017).

6.3.3 Conclusions

The polymer synthesized with cyclopentane groups demonstrated strong KHI performance at lower concentrations (0.01 and 0.05 wt%) and a significant change in cloud point which indicates that CMC modification is very successful at controllably introducing groups that can modulate performance. Clearly, the modified polymers are more advantageous for injection into hot fluids than some leading KHIs without compromising the hydrate inhibition performance. Moreover, PNIPAM-C_4t, PNIPAM-cyclopent and PNIPAM-co-AA were picked out from libraries of modified polymers by our HTP hydrate screen technology for more rigorous test.

6.4 HTP hydrate screen of PVCap-based KHCI polymers

6.4.1 Results and discussion

To evaluate the hydrate inhibition performance of these KHCIs the HTP hydrate screen using cyclopentane hydrate was conducted as introduced in the previous sections.

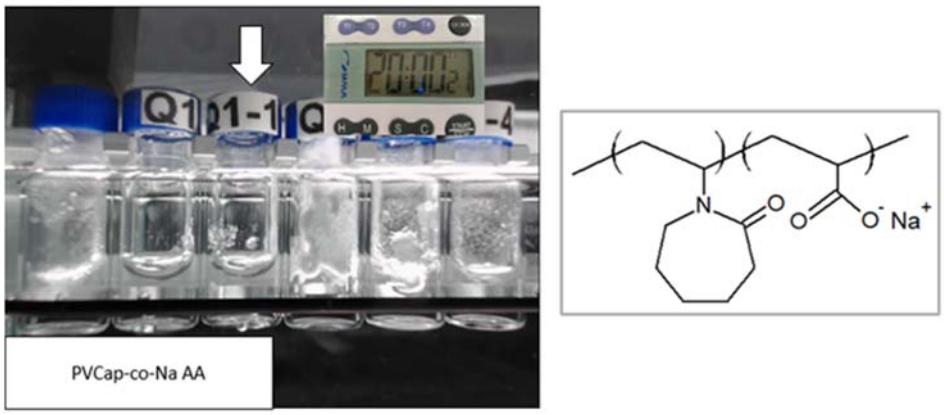

Figure 6. 16 Dilution series of Poly(VCap-co-Na AA) after a cut-off time of 20 hours. The vials shown are, from left to right, blank (no inhibitor), 1wt%, 0.5wt%, 0.1wt%, 0.05wt% and 0.01wt%, respectively. The threshold concentration of Poly(VCap-co-Na AA) after a cut-off time of 20 hours was 0.5 wt% (Sheng et al., 2017).

Figure 6.16 shows the hydrate screening for the base polymer at a range of concentrations. A control sample (no inhibitor, left image) shows that after the 20 hours screen time significant hydrate can be seen. When the base polymer was added the hydrate was inhibited when higher concentrations were used but when the concentration was below 0.5 wt% hydrate was formed. As such the threshold concentration for the base polymer is 0.5 wt%.

The threshold concentration of new inhibitors modified by taurine, ATCH, APIM and AMPA respectively were determined. For the taurine modified series, the ranking was taurine DiaminoC_{12} > taurine > taurine C_{12} (Figure 6.17) while for the APMA series modification did not affect the threshold concentration of 0.5 wt% (Figure 6.20). Notably, the incorporation of ATCH and APIM molecules has a positive effect on hydrate inhibition, with similar rankings in the order ATCH (APIM) > ATCH

diamino-C_{12} (APIM diaminoC_{12}) > ATCH C_{12} (APIM C_{12}) (Figure 6.18 and Figure 6.19). This strongly suggests that ATCH and PIM when combined with PVCap can have positive effects on hydrate performance. This can be explained by considering the structure of these groups because ATCH is based on a quaternary ammonium group which is a key component in antiagglomerant chemistries. The quaternary ammonium group functions by interacting strongly with the hydrate, and this explains why the ATCH can improve the hydrate performance. The APIM was also effective at improving the hydrate performance, and this group also contains nitrogen atoms but is not extensively studied as an antiagglomerant. The results presented here suggest that APIM when combined in a single polymer molecule show improved hydrate inhibition. Therefore, this route can be used to modulate the structure and performance of the inhibitors compared to the base polymer. Based on the HTP hydrate screen the inclusion of ATCH and APIM may have a positive synergistic effect that does not compromise the KHI performance. In general, 2 mol% addition of a long hydrocarbon chain has a significant negative effect on the hydrate inhibition. The inclusion of C_{12} diamine was supposed to have a different impact on the whole KHCI structure compared to C_{12} amine due to an extra amine head by the end of hydrocarbon chain. This amine head is believed to have more affinity for surface. In this study, apparent difference can be seen through the hydrate screen. The long C_{12} chain with amine head had a less adverse effect than C_{12} did and in the case of taurine modified series it seemed to help with the overall performance. This could be due to the interaction between amine head and hydrate surface, somehow interrupting the hydrate nucleation and growth process. For the phosphate-containing series (AMPA, Figure 6.20) the performance was similar to the base polymer despite the addition of a long hydrocarbon chain.

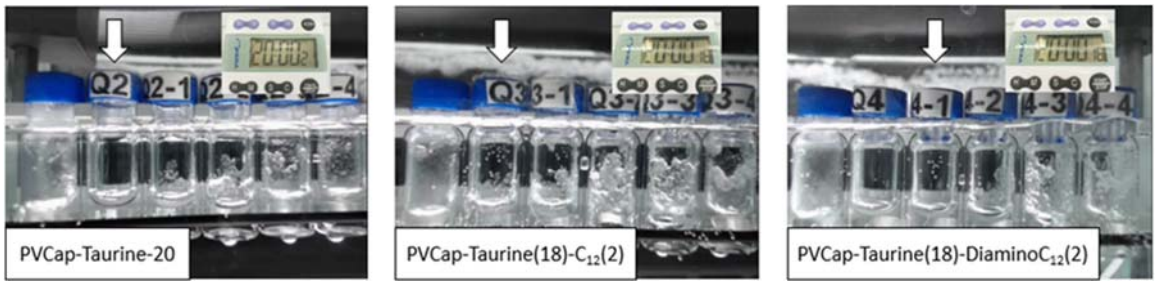

Figure 6. 17 Dilution screening for Taurine modified series after 20 hours. The threshold concentrations after a cut-off time of 20 hours were 1 wt%, 1 wt%, 0.5 wt% in sequence (Sheng et al., 2017).

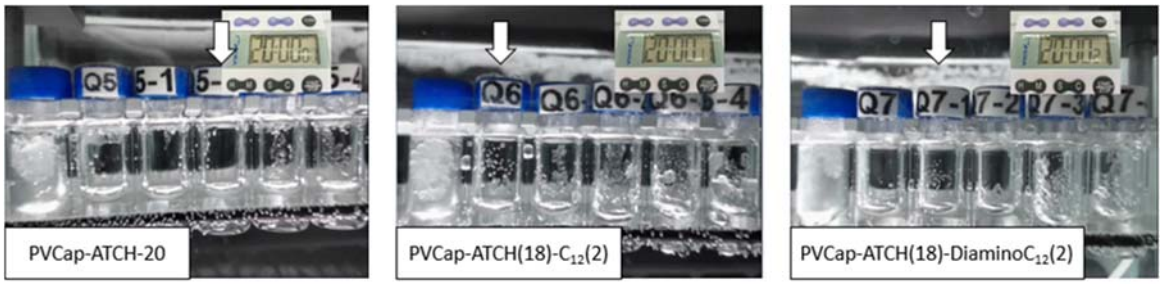

Figure 6. 18 Dilution screening for ATCH modified series after 20 hours. The threshold concentrations after a cut-off time of 20 hours were 0.1 wt%, 1 wt%, 0.5 wt% in sequence (Sheng et al., 2017).

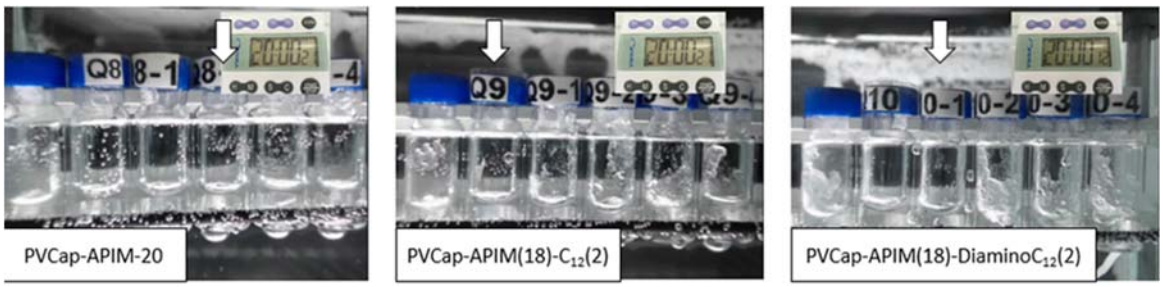

Figure 6. 19 Dilution screening for APIM modified series after 20 hours. The threshold concentrations after a cut-off time of 20 hours were 0.1 wt%, 1 wt%, 0.5 wt% in sequence (Sheng et al., 2017).

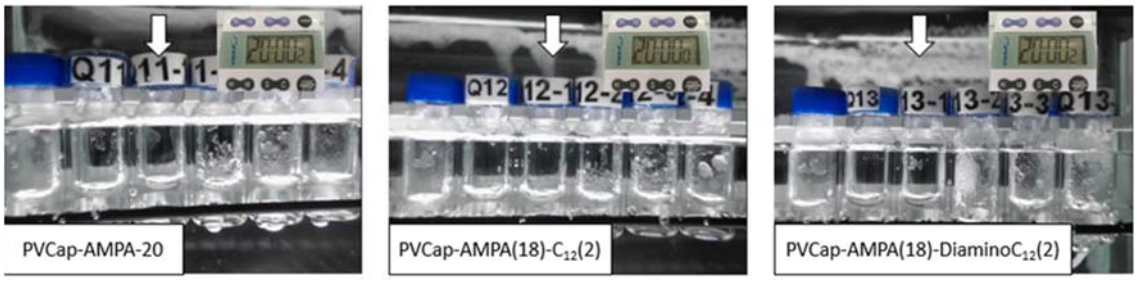

Figure 6. 20 Dilution screening for AMPA modified series after 20 hours. The threshold concentrations after a cut-off time of 20 hours were 0.5 wt%, 0.5 wt%, 0.5 wt% in sequence (Sheng et al., 2017).

To gain an insight into how polymer modification and structure influences KHCI performance, the APIM modified KHCIs is discussed. Figures 6.16 and 6.19 show the threshold concentration after 20 hours which was determined as 0.5 wt% for the base polymer, 0.1 wt% for PVCap-APIM-20, 1 wt% for PVCap-APIM(18)-C_{12}(2) and 0.5 wt% for PVCap-APIM(18)-DiaminoC_{12}(2). Accordingly, the ranking based on the result is:

PVCap-APIM-20 > base polymer ≥ PVCap-APIM(18)-DiaminoC_{12}(2) > PVCap-APIM(18)-C_{12}(2).

As shown in the figures, PVCap-APIM-20 outperforms the base polymer in terms of inhibiting hydrate growth and formation. A concentration of 0.1 wt% PVCap-APIM-20 is effective while the concentration of base polymer needed to be 0.5wt% to inhibit hydrate. This indicates that the modified imidazole structure, a nitrogen-containing heterocyclic ring, has played a role in changing the mode of action and effectiveness of the base polymer. Imidazole is regarded as a corrosion inhibitor, depending on the metal surface it binds, the five-membered ring may also be interacting with the surface of the hydrate and thus interrupts the hydrate formation process. This apparent improvement suggests that the inclusion of this functionality has a good synergistic effect on hydrate inhibition.

PVCap-APIM(20)-C_{12}(2) contains a dodecyl (C_{12}) hydrophobic alkyl chain and is ineffective at inhibiting hydrate formation even at 1wt%. Although such a hydrophobic pendant has been shown to enhance corrosion inhibition, in this case hydrate inhibition was not demonstrated compared to the base polymer. This may be due to the fact that

with the increased amphilphilic character of the pendant C_{12} alkyl chain resulting in self-association of the polymers which can prevent association with the growing hydrate interface to prevent effective inhibition or they could be promoting hydrate. AA molecules promote formation so we may not see that in these tests, it would show up as a failure but the nature of the test is KHI not AA. So these polymers may be useful as an anti-agglomerants (AAs) which is under investigation.

PVCap-APIM(18)-DiaminoC_{12}(2) has a similar performance as the base polymer but is inferior to PVCap-APIM-20. Once again this is rationalised with respect to potential self-association of the C_{12} alkyl chain. The more compact and complex steric conformation may account for the reduction of the efficiency compared to PVCap-APIM-20.

6.4.2 Conclusions

Using a HTP hydrate screen together with weight loss measurements for corrosion (this test is discussed in detail in the chapter 8), we propose the PVCap-APIM-20 and PVCap-ATCH-20 are two promising KHCIs. This is a concept-of-proof study, and the performance of the inhibitors is further validated in subsequent chapters.

Chapter 7 AUTOCLAVE TESTING

7.1 Introduction

Few promising KHI candidates from two libraries of modified polymers have been selected via HTP hydrate screen technology. However, the stochastic nature of hydrate nucleation induces scattering of the experimental results, demanding more investigation on a larger scale, and more rigorous test that is relevant to field application needs to conduct. Experimental devices for testing and screening of KHIs for gas hydrate systems, from laboratory scale to pilot scale, have evolved over the years, the autoclave is one of the most commonly used apparatus (Ke and Kelland, 2016) (shown in Figure 7.1).

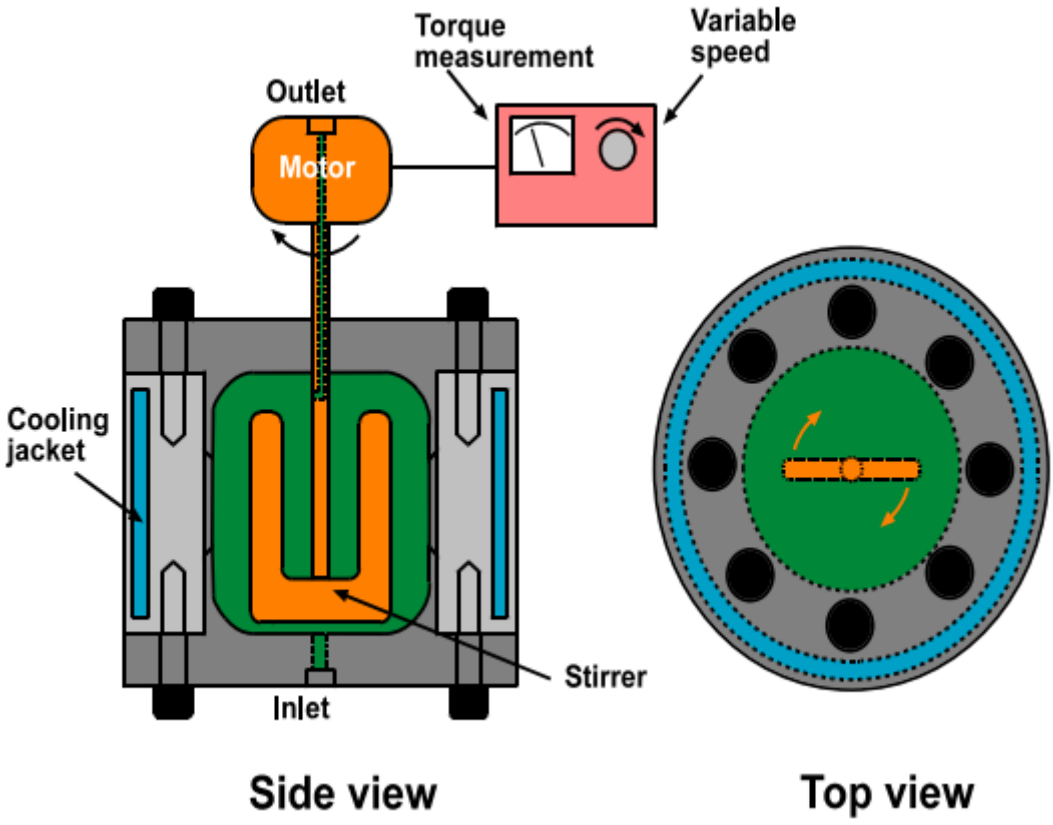

Figure 7. 1 A schematic diagram of high-pressure autoclave apparatus (Tohidi, 2014)

The performance of KHIs has been evaluated by measuring the subcooling temperature, which represents the temperature difference between the theoretical

hydrate equilibrium temperature and the measured hydrate formation temperature at the corresponding pressure.

The performance test for KHIs has generally been carried out with a cooling of the KHI candidate solution at a constant rate and a measurement of the hydrate onset time, which indicates how long the hydrate formation is delayed in the presence of the KHI candidate. The cooling of the hydrocarbon mixture in a subsea flowline will be affected by the seawater temperature, the flowrate and the insulation materials for the subsea flowline; however, most of the performance tests for KHIs have been carried out with a fixed cooling rate or under isothermal conditions (Ree et al., 2016; Ree et al., 2015).

It is still challenging to transfer the laboratory test result into conditions relevant to field operations; thus, there have been many attempts to develop advanced test protocols to screen the KHI candidates. However, there is scarce literature studying the effect of varying the cooling rate on the performance of KHIs. Moreover, recent work by Anderson et al. (Anderson et al., 2011) suggested that KHIs disturb the gas capture into hydrate cages by their adsorption into the growing hydrate crystals, and this directly affects the growth of the hydrate as well as its nucleation. Along with the measurement of the hydrate onset temperature, a catastrophic growth temperature was measured to indicate the way that the KHIs effectively suppressed the growth of the hydrate crystals (Anderson et al., 2011; Ree et al., 2016; Ree et al., 2015); however, the growth of hydrate crystals involves a more complex process of hydrate particle growth and their agglomeration, which ultimately forms the solid hydrate plug. In the proposed mechanism for hydrate particle agglomeration, a hydrate shell forms on the water droplets and then the cohesive interaction between the hydrate shell-covered particles results in the formation of multi-particle aggregates (Akhfash et al., 2013; Joshi et al., 2013). It seems that the agglomeration of hydrate particles can be prevented by avoiding multi-particle aggregation; however, controlling the growth rate of hydrate is challenging, because the mass transfer for hydrate formation is too fast to avoid the sintering and cohesion of the hydrate shell-covered water droplets. Joshi et al.(Joshi et al., 2013) suggested that hydrate particles will aggregate faster when the hydrate fraction in the liquid phase is larger than 10−20 vol %, which is supported by high-pressure autoclave studies by Akhfash et al., (Akhfash et al., 2013; hoon Sohn et al., 2015). These results indicate that the performance of a KHI must be investigated

with the amount of hydrate and the resulting resistance to flow to evaluate its performance as a potential crystal growth inhibitor.

In this chapter, detailed studies of high-pressure autoclave testing on PNIPAM-based KHI polymers and PVCap-based KHCI polymers are presented. The performance of these candidates were investigated with a holistic investigation on both nucleation and growth of hydrates as follows: (1) measuring the hydrate onset time with a varying cooling rate in the nucleation stage and then (2) measuring the torque changes of the fluids as a function of the hydrate fraction in the growth stage. When a holistic investigation was employed, a more effective characterization of the candidate inhibitors was possible. In general, the conventional test was in good agreement with HTP screen method to some extent, suggesting the performance of these modified polymers can be evaluated with holistic investigation on nucleation and growth of hydrate crystals.

7.2 Performance of PNIPAM-based KHI polymers

This study investigated the natural gas hydrate inhibition performance of three poly(N-isopropylacrylamide) (PNIPAM)-based KHIs [poly(Nisopropylacrylamide- co-acrylic acid (PNIPAM-co-AA), poly(N-isopropylacrylamide-co-cyclopentylamine (PNIPAM-co-Cp), and poly(N-isopropylacrylamide-co-tert-butylamine (PNIPAM-co-C_4t)] by determining the hydrate onset time, growth rate, and resistance to flow using a high-pressure autoclave. These data are compared to three control groups [water, Luvicap solution, and polyvinylpyrrolidone (PVP)] under various cooling rates (0.25, 0.033, and 0.017 K/min). The results show that the nucleation of hydrate crystals was delayed in the presence of the KHI candidates as assessed using the onset time at different cooling rates. The effect of the KHI candidate on the hydrate growth characteristics was also studied by determining the initial growth rate and torque changes with an increasing hydrate fraction in the liquid phase. The results obtained confirmed that the synthesized PNIPAM-based KHIs showed a high subcooling temperature, which is comparable to those of commercial KHIs. The modification of the base polymer (PNIPAM-co-AA) improves the kinetic inhibition performance for PNIPAM-co-C_p (13.9, 12.5, and 7.8 K for 0.25, 0.033, and 0.017 K/min cooling rates, respectively) but results in decreased performance for PNIPAM-co-C_4t (9.6, 9.9, and

7.6 K for 0.25, 0.033, and 0.017 K/min cooling rates, respectively). After the hydrate onset, PNIPAM-co-C_4t showed a slower growth rate and more stable torque during the hydrate formation than PNIPAM-co-C_p, suggesting its potential role as a crystal growth inhibitor.

7.2.1 Materials and methods

7.2.1.1 Materials

All reagents were used without purification. PNIPAM-co-AA and its modified polymers were synthesized in-house as introduced in previous chapter. Luvicap and polyvinylpyrrolidone (PVP) were used as commercial inhibitors. Luvicap EG HM was supported by BASF, and PVP [K-15, molecular weight (M_w) = 9000 Da] was obtained from Ashland Chemical Co. An artificial natural gas (90.0 mol % CH_4, 6.0 mol % C_2H_6, 3.0 mol % C_3H_8, and 1.0 mol % n-C_4H_{10}) was supplied by Special Gas (Korea). Deionized water (purity of 99.99 mol %) was obtained from OCI.

7.2.1.2 Hydrate formation kinetic experiments

All of the experiments were conducted using a high-pressure autoclave equipped with a magnetically coupled stirrer with an anchor-type impeller. The reactor was constructed out of 316 SUS. A total of 80 mL of liquid was loaded into the reactor, which has a total volume of 360 mL, and the total liquid consisted of a 60:40 volume ratio of water and hydrocarbon (in this work, decane). After the liquid was loaded, the cell was flushed 3 times using natural gas to remove any residual air. Then, the autoclave was placed in the circulating bath (RW 2040G, Jeio Tech). For the continuous stirring of the liquid in the cell, the anchor-type impeller was placed on a shaft and connected to a motor (BLDC 90). The cell was pressurized to 120 bar with a syringe pump at 24 °C, and the contents were stirred at 600 rpm to ensure that the liquid was saturated with the natural gas. The fluids at 600 rpm speed are in a turbulent regime with an approximate Reynolds number of 32 000. Once the pressure and temperature became stable, the cell was cooled to the target temperature of 4 °C with various cooling rates (0.25, 0.033, and 0.017 K/min) using a constant cooling method under isochoric conditions. The temperature was maintained at 4 °C for 10 h, followed

by ramping up to 28 °C, where the temperature was retained for 3 h to dissociate the hydrate and eliminate any residual hydrate structures. It is worth noting that the dissociation temperature is below the measured cloud point for the polymers; therefore, they remain soluble under these conditions. The temperature, pressure, and torque were measured using a PT 100 Ω (±0.15 °C), a transducer (0−200 bar, ±0.1 bar), and a torque sensor (TRD-50KC, ±0.3%), respectively. The temperature, pressure, and torque were logged using a data acquisition system. Five experiments were repeated for each PNIPAM-based KHI (total of 15) to average the hydrate onset time, subcooling temperature, and hydrate volume fraction. The other 15 experiments for the three control systems, pure water + decane mixture, 0.5 wt % PVP solution + decane mixture, and 0.5 wt % Luvicap solution + decane mixture, were carried out for a direct comparison to the 15 experiments for the PNIPAM-based KHI systems (0.5 wt % PNIPAM-co-AA solution + decane mixture, 0.5 wt % PNIPAM-co-Cp solution + decane mixture, and 0.5 wt % PNIPAM-co- C4t solution + decane mixture).

7.2.2 Results and discussion

7.2.2.1 Hydrate onset characteristics at different cooling rates

Once the fluid temperature becomes lower than the hydrate equilibrium temperature, hydrate nuclei would be formed instantly from the thermodynamic point of view; however, there needs to be a driving force to initiate the nucleation. The primary function of kinetic hydrate inhibitors is to delay the nucleation of hydrate crystals under the given subcooling condition. Therefore, the hydrate onset characteristics were analyzed according to the hydrate onset time and subcooling temperature. In the constant cooling experiments, the hydrate nucleation point was determined by the rapid gas decrease from the hydrate formation. Table 7.1 presents the mean value and standard deviation over five repeat trials for the subcooling temperature (ΔT_{sub}) and the hydrate onset time (t_{onset}) at different cooling rates.

Table 7. 1 Hydrate Onset Conditions for 0.5 wt % PNIPAM-Based KHIs and Control Systems[a] (Park et al., 2017b).

PNIPAM derivative	cooling rate (K/min)	subcooling temperature (K)	onset time (min)
PNIPAM-*co*-AA	0.25	14.1 (0.1)	80.4 (2.0)
	0.033	7.6 (0.1)	241.6 (0.9)
	0.017	7.1 (0.3)	436.2 (21.0)
PNIPAM-*co*-Cp	0.25	13.9 (0.9)	71.0 (8.6)
	0.033	12.5 (0.1)	389.4 (2.4)
	0.017	7.8 (0.8)	481.6 (47.8)
PNIPAM-*co*-C_4t	0.25	9.6 (0.6)	54.5 (5.4)
	0.033	9.9 (1.0)	311.4 (1.1)
	0.017	7.6 (1.1)	468.8 (65.6)
pure water	0.25	4.7 (0.6)	20.4 (2.1)
	0.033	3.3 (0.1)	104.4 (3.9)
	0.017	3.3 (0.1)	200.8 (4.7)
Luvicap	0.25	11.6 (0.2)	83.8 (5.2)
	0.033	11.4 (0.9)	353.2 (26.3)
	0.017	7.9 (0.9)	484.8 (56.2)
PVP	0.25	12.5 (1.2)	73.9(10.3)
	0.033	10.2 (0.5)	323.0 (11.9)
	0.017	8.5 (0.1)	548.5 (2.6)

[a]The standard deviation of the subcooling temperature and onset time is shown in parentheses.

The subcooling temperature is a significant factor presenting the required thermal driving force for the nucleation of hydrate crystals; thus, it can be a criterion for the estimation of the kinetic inhibition performance of the potential KHI candidate. The concentration of the KHI candidate was 0.5 wt % in aqueous phase, as in the control groups. The increase of the cooling rate indicates that high thermal energy was applied over a certain period, resulting in a different hydrate nucleation point. For pure water, the subcooling temperature changes from 3.3 to 4.7 K with an increasing cooling rate, while the onset time decreases from 200.8 to 20.4 min. The addition of Luvicap and PVP increases the subcooling temperature as well as the onset time, clearly indicating

that the polymer structure acts on the hydrate nucleation process. The synthesized PNIPAM-base KHIs also increased the subcooling temperature and onset time compared to pure water.

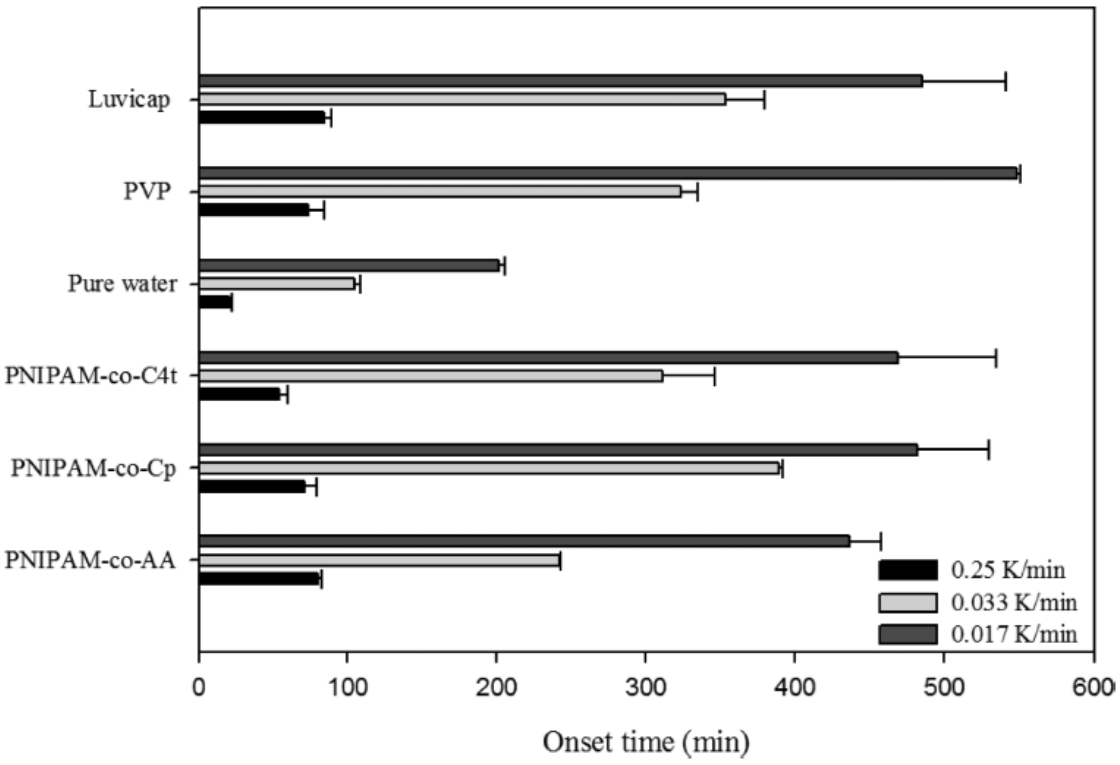

Figure 7. 2 Hydrate onset time comparison between the PNIPAM-based KHIs, commercial KHIs (Luvicap and PVP, 0.5 wt %), and water system. Error bars indicate the standard deviation (Park et al., 2017b).

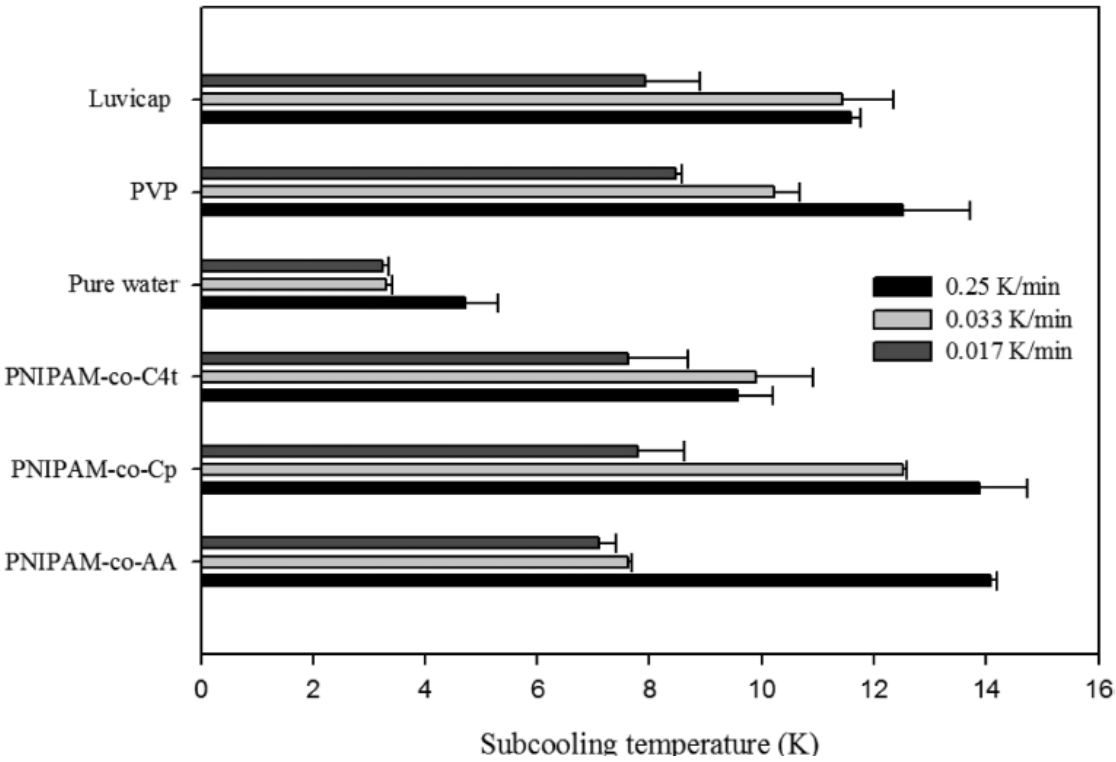

Figure 7. 3 Hydrate subcooling temperature comparison between the PNIPAM-based KHIs, commercial KHIs (Luvicap and PVP, 0.5 wt %), and water system. Error bars indicate the standard deviation (Park et al., 2017b).

Figures 7.2 and Figure 7.3 showed the comparison of the hydrate onset time and subcooling temperature between the PNIPAM-based KHIs and the control group. The PNIPAM-co-AA solution showed subcooling temperatures of 14.1, 7.6, and 7.1 K with the cooling rates of 0.25, 0.033, and 0.017 K/min, respectively; furthermore, the onset times were 80.4, 241.6, and 436.2 min. For the PNIPAM-co-Cp system, the subcooling temperatures were 13.9, 12.5, and 7.8 K with the cooling rates of 0.25, 0.033, and 0.017 K/min, respectively; moreover, the onset times were 71.0, 389.4, and 481.6 min. The modification of the base polymer structure, PNIPAM-co-AA, with Cp enhanced the kinetic inhibition performance at the cooling rate of 0.033 K/min. For the PNIPAM-co-C_4t, the subcooling temperatures were 9.6, 9.9, and 7.6 K and the onset times were 54.5, 311.4, and 468.8 min, respectively. We also included PNIPAM-co-AA modified with C_4t, PNIPAM-co-C_4t, which adversely affected the performance of PNIPAM-based KHI, where the subcooling was higher than that in pure water but lower than that in PNIPAM-co-AA solution.

In comparison to the performance of PNIPAM-based KHIs, the commercial KHIs, both Luvicap and PVP, showed a high subcooling temperature and long onset time. For a fast cooling rate of 0.25 K/min, the subcooling temperature of PVP solution was 12.5 K and slightly less than that of PNIPAM-co-AA and PNIPAM-co-Cp. When the cooling rate was reduced to 0.033 K/min, Luvicap solution showed the subcooling temperature of 11.4 K; however, the value was still less than that of PNIPAM-co- Cp. For a slow cooling rate of 0.017 K/min, the subcooling temperatures for KHI candidates were obtained at around 8.0 K, except PNIPAM-co-AA solution. As seen in Figures 7.2 and Figure 7.3, the variation of the subcooling temperature was less than 50% at the studied cooling rate ranges; however, the onset time increased almost 7 times with decreasing the cooling rate. Thus, the subcooling temperature might need to be evaluated along with the onset time.

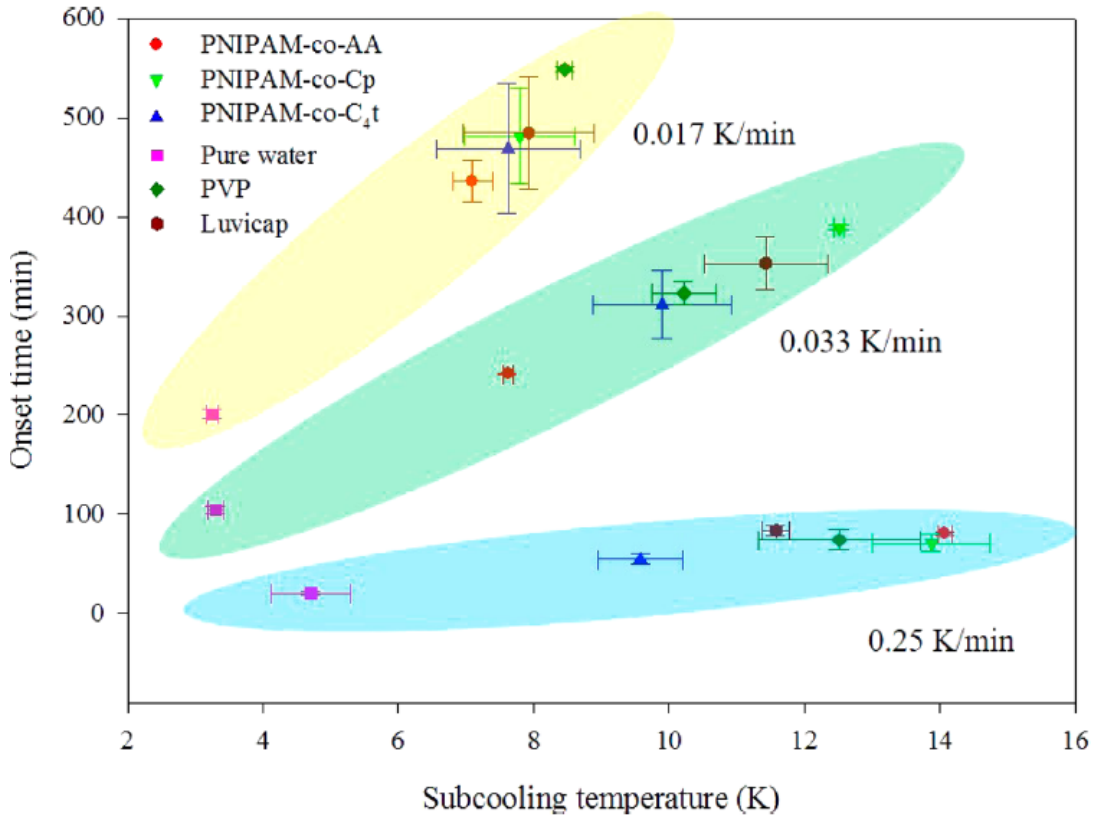

Figure 7. 4 Hydrate onset time as a function of the subcooling temperature of PNIPAM-based KHIs with various cooling rates: 0.25 K/min (yellow region), 0.033 K/min (green region), and 0.017 K/min (blue region) (Park et al., 2017b).

Figure 7.4 shows the hydrate onset time as a function of the subcooling temperature with various cooling rates. The leading KHI would result in a high subcooling temperature and long hydrate onset time. For the application of KHI for offshore fields, the maximum value for the subcooling temperature is the maximum difference between the seawater temperature and hydrate equilibrium temperature of hydrocarbon fluid, while the maximum value for the onset time is the longest duration of hydrocarbon fluid inside the subsea flowlines. In this work, the maximum subcooling temperature came from the target cooling temperature, 277.15 K, and the hydrate equilibrium temperature, 293.15 K. The maximum onset time was 600 min from the start of the experiment.

For the cooling rate of 0.25 K/min, the obtained onset time showed a linear increase with increasing the subcooling temperature depending upon the added KHIs. Pure water showed the shortest onset time of 20.4 min and the lowest subcooling temperature of 4.7 K, while PNIPAM-co-AA showed the longest onset time of 80.4 min at the highest subcooling temperature of 14.1 K. The performance of PNIPAM-co-Cp was close to the base polymer, and Luvicap was next. When reducing the cooling rate to 0.033 K/min, the linear relationship shifted to a lower hydrate risk area as a result of increased onset time. The performance of PNIPAM-co-Cp was the best in this cooling rate, and Luvicap followed. For the cooling rate of 0.017 K/min, commercial KHIs, Luvicap and PVP, performed better than PNIPAM-based KHIs with a slight difference.

As seen in Figure 7.4, the performance of KHIs cannot be simply judged from the measured subcooling temperature and would be better evaluated from the relationship between the subcooling temperatures versus the onset time. Moreover, the cooling rate also affects the relationship. Figure 7.4 suggests that the cooling rate of 0.033 K/ min maintains a high subcooling temperature and long onset time, thus, the performance of KHIs placed in the low-risk plane. A fast cooling rate of 0.25 K/min induces a short onset time, whereas a slow cooling rate of 0.017 K/min results in a low subcooling temperature. These results suggest that the insulation design for offshore flowlines may affect the performance of the deployed KHI which must be considered in pipeline design.

Our previous work (section 6.3) adopting a HTP hydrate test showed stochastic hydrate formation for PNIPAM-co-AA but confirmed an indicative inhibition performance. Modification of the polymers contributed to the inhibition performance by increasing the hydrophobic content in the polymer structure. In this chapter, we confirmed again the performance of the PNIPAM-based KHIs with quantitative analysis of hydrate onset time and subcooling temperature. The PNIPAM-based KHIs and the commercial KHI have different functional groups, and the structure and percentage of each group varies the adsorbing behaviours on the hydrate cage, thereby inducing a delayed hydrate nucleation. These phenomena would come from different functional groups in each PNIPAM-based KHI. It is well-known that commercial KHIs, such as PVCap and PVP, have a polyethylene backbone that is linked to the pendant groups of one branch (five- or seven-membered ring), including the amide group, and that the pendant groups enter the hydrate cage when the KHI absorbs on the hydrate crystal with the polymer backbone stretching along the hydrate crystal surface. By modification of the structure of PNIPAM-co-AA, the surface area of the pendant group would change, which can result in steric hindrance in terms of hydrate formation. The change in the polymer structure also affects the cloud point of the polymer, as shown in section 4.2.5, therefore, using this synthetic method, the performance of the KHIs can be modulated in terms of hydrate performance and cloud point.

7.2.2.2 Hydrate growth characteristics at different cooling rates

After the hydrate onset, hydrate particles quickly consumed dissolved gas molecules in the liquid phase and grow further with mass transfer of gas molecules from the vapour phase to the liquid phase. The hydrate plug formation would occur when the hydrate fraction in the liquid phase was large enough to accompany the agglomeration and bedding of the hydrate particles. The resistance to flow as a result of the agglomeration and bedding of hydrate particles became evident with the hydrate fraction in the liquid phase of more than 0.10. KHI molecules may inhibit the hydrate growth by attaching on the surface, thus reducing the growth rate in the early stage of the hydrate formation process.

In this chapter, the performance of crystal growth inhibition for the PNIPAM-based KHIs (PNIPAM-co-AA, PNIPAM-co-Cp, and PNIPAM-co-C4t) was investigated at different cooling rates and compared to the control groups (pure water, Luvicap solution, and PVP solution). The hydrate volume fraction was estimated from the gas consumption during the formation process, and the amount of gas consumed for hydrate formation was calculated from the pressure difference between the experimental and calculated pressures with the postulation that no hydrate is formed (Ke et al., 2011; Seo et al., 2009). This procedure has been suggested as a method for the hydrate formation studies in a flow wheel (Hemmingsen et al., 2008) and in autoclave systems (Cha et al., 2013; Del Villano and Kelland, 2011; Duchateau et al., 2009b; Sloan, 2010). The hydration number was assumed to be 6.5 (Seo et al., 2009). The growth rate was estimated from the consumed amount of gas, while the formation proceeds linearly in the early stage. The hydrate fraction in the liquid phase at 100 min after the hydrate onset and the value at the end of each cycle are calculated to present the hydrate fraction in early and last stages of the experiment. Table 7.2 presents the average values and standard deviation of the growth rate, hydrate fraction at 100 min, hydrate fraction at 600 min, and water conversion to hydrate at 600 min.

Table 7. 2 Hydrate formation kinetic characteristics under 0.5 wt % PNIPAM-Based KHIs[a] (Park et al., 2017b).

	cooling rate (K/min)	growth rate (volume fraction/min)	hydrate volume fraction at 100 min	hydrate volume fraction at 600 min	water conversion (%)
PNIPAM-*co*-AA	0.25	1.2×10^{-3}	0.11 (0.02)	0.32 (0.03)	45.8 (3.9)
	0.033	0.3×10^{-3}	0.02 (0.00)	0.18 (0.02)	25.6 (2.4)
	0.017	0.2×10^{-3}	0.02 (0.01)	0.18 (0.01)	25.7 (1.5)
PNIPAM-*co*-Cp	0.25	6.0×10^{-3}	0.25 (0.01)	0.39 (0.03)	56.9 (4.1)
	0.033	3.8×10^{-3}	0.20 (0.01)	0.33 (0.03)	47.2 (5.3)
	0.017	0.2×10^{-3}	0.02 (0.01)	0.28 (0.02)	40.2 (3.1)
PNIPAM-*co*-C_4t	0.25	7.7×10^{-3}	0.24 (0.02)	0.42 (0.02)	62.3 (3.9)
	0.033	2.4×10^{-3}	0.24 (0.05)	0.54 (0.08)	81.3 (13.5)
	0.017	3.6×10^{-3}	0.14 (0.15)	0.47 (0.06)	69.2 (10.2)
pure water	0.25	8.9×10^{-3}	0.43 (0.02)	0.50 (0.02)	74.0 (3.9)
	0.033	14.7×10^{-3}	0.38 (0.03)	0.49 (0.02)	72.5 (3.7)
	0.017	6.5×10^{-3}	0.35 (0.01)	0.45 (0.02)	66.5 (2.8)
Luvicap	0.25	4.9×10^{-3}	0.20 (0.06)	0.40 (0.06)	58.9 (9.8)
	0.033	3.8×10^{-3}	0.13 (0.01)	0.38 (0.03)	55.8 (4.2)
	0.017	0.2×10^{-3}	0.03 (0.02)	0.38 (0.04)	55.2 (6.5)
PVP	0.25	6.4×10^{-3}	0.29 (0.03)	0.38 (0.02)	55.7 (3.8)
	0.033	7.8×10^{-3}	0.32 (0.02)	0.44 (0.02)	64.9 (2.6)
	0.017	10.1×10^{-3}	0.31 (0.01)	0.43 (0.04)	63.3 (6.5)

[a]The standard deviation of the hydrate volume fraction at 100 and 600 min and water conversion is shown in parentheses.

(a)

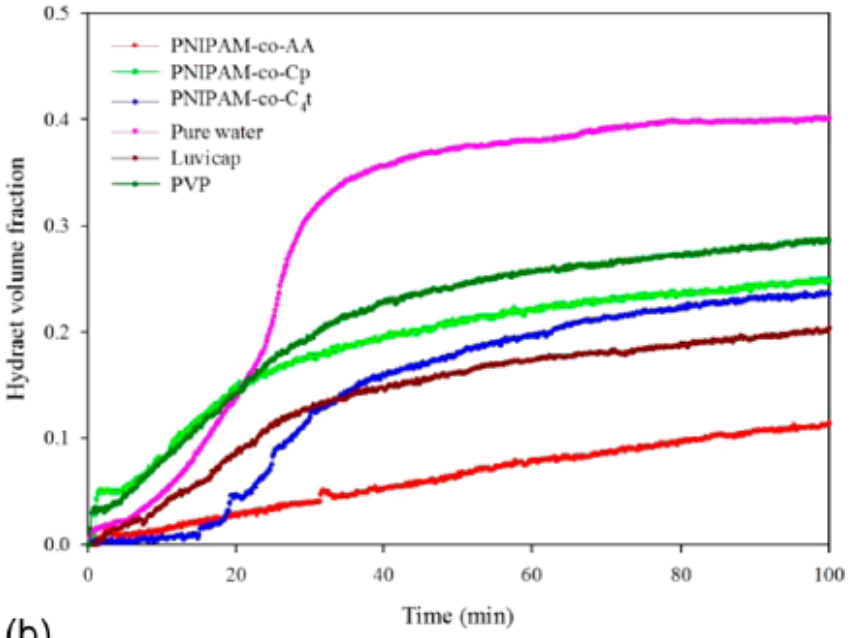
PNIPAM-co-AA
PNIPAM-co-Cp
PNIPAM-co-C4t
Pure water
Luvicap
PVP
Hydract volume fraction
Time (min)

(b)

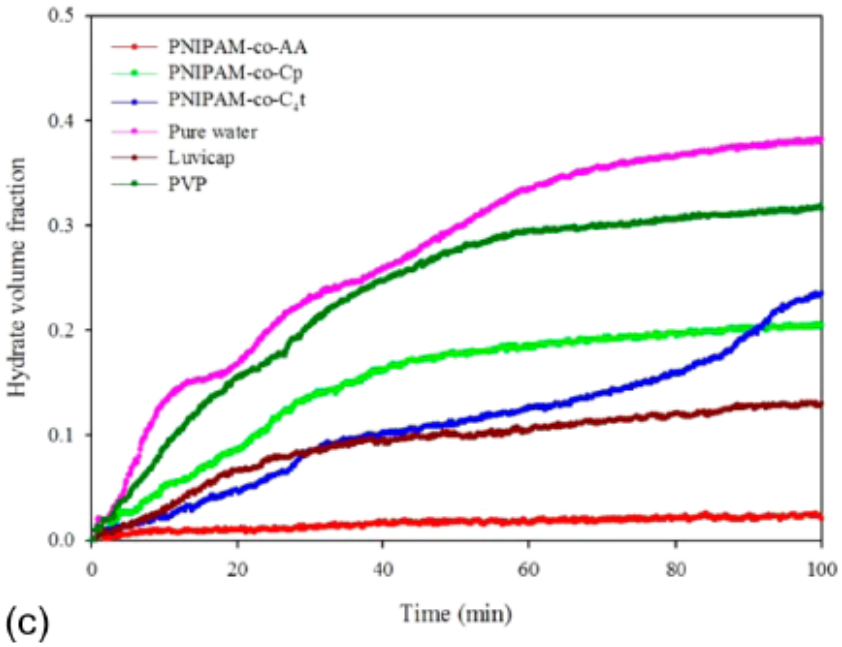
PNIPAM-co-AA
PNIPAM-co-Cp
PNIPAM-co-C4t
Pure water
Luvicap
PVP
Hydrate volume fraction
Time (min)

(c)

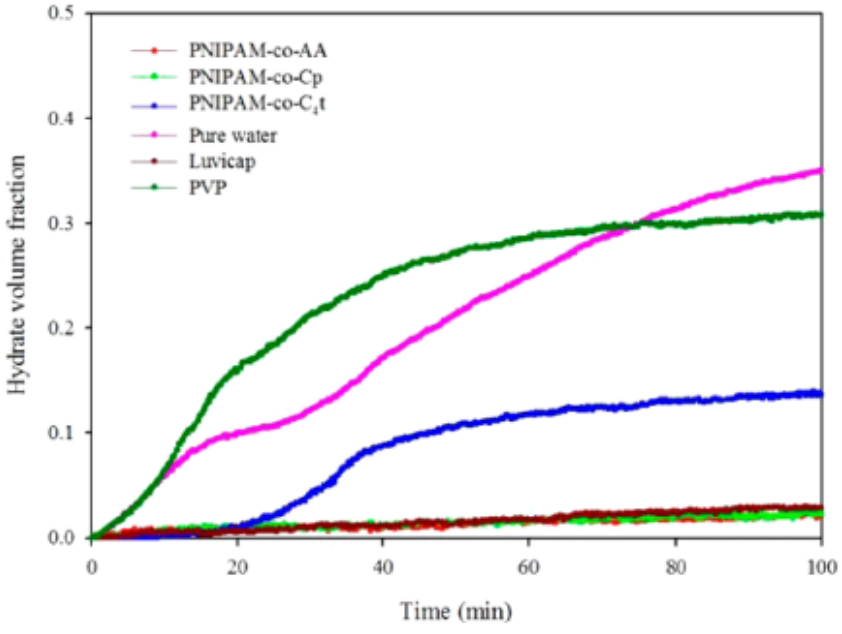
PNIPAM-co-AA
PNIPAM-co-Cp
PNIPAM-co-C4t
Pure water
Luvicap
PVP
Hydrate volume fraction
Time (min)

Figure 7. 5 Comparison of hydrate growth for PNIPAM-based KHIs, commercial KHI (Luvicap and PVP, 0.5 wt %) solutions, and pure water under cooling rates of (a) 0.25 K/min, (b) 0.033 K/min, and (c) 0.017 K/min (Park et al., 2017b).

Figure 7.5 shows the growth of hydrate for 100 min after the onset at each cooling rate. For every cooling rate, pure water showed fast hydrate growth compared to other KHI-added systems. The hydrate fraction reached 0.43 at 100 min with an initial growth rate of 0.0089 volume fraction/min and increased slightly more to 0.50 at 600 min at fast cooling of 0.25 K/min. The addition of PVP reduces the initial growth rate of 0.0064 volume fraction/min, and the hydrate fraction at 100 min was 0.29. Luvicap performed better with the initial growth rate of 0.0049 volume fraction/min and the hydrate fraction of 0.13 at 100 min. The base polymer PNIPAM-co-AA outperformed Luvicap, showing the initial growth rate of 0.0012 volume fraction/min and the hydrate fraction of 0.11 at 100 min.

However, modification of the structure into PNIPAM-co-Cp and PNIPAM-co-C4t showed a growth rate of 0.0060 and 0.0077 volume fraction/min, respectively, and the resulting hydrate fraction was 0.24 and 0.25, respectively. As seen in Figure 7.5a, the growth curve for PNIPAM-co-Cp and PNIPAM-co-C4t solutions was placed between PVP and Luvicap. PNIPAM-co-C4t showed a very slow growth period during the first 15 min; however, fast growth was followed soon after. It can be concluded that the base polymer PNIPAM-co-AA outperformed commercial KHIs in terms of crystal growth inhibition; however, further modification adversely affects its performance. This is important because it highlights which functional groups can improve KHI performance. The trends are more accurate than using other synthetic routes (e.g., free-radical copolymerization) because this approach generates all polymers with a similar MW and the same composition and end groups.

Similar results were obtained for cooling rates of 0.033 and 0.017 K/min. For the initial growth after the onset, PVP has the fastest growth rate at slow cooling of 0.017 K/min and is even faster than that of pure water until the volume fraction of 0.3. The hydrate growth rate of the other systems is slower than that of pure water. The modified polymers, PNIPAM-co-Cp and PNIPAM-co-C4t, performed better than PVP and close to Luvicap a commercial KHI. The base polymer PNIPAM-co-AA was the best

performing inhibitor. The initial growth rate was 0.003 and 0.002 volume fraction/min at a cooling rate of 0.033 and 0.017 K/min, respectively. The hydrate fraction was 0.02 at 100 min and reached 0.18 at 600 min, which was about half of the fraction obtained in Luvicap solution. The modification of the base polymer increased the cloud point and enhanced the nucleation inhibition performance; however, it was not straightforward to the performance for the crystal growth inhibition.

Figure 7.5 suggested that the cooling rate also affected the performance of KHIs significantly during the formation process. The rapid cooling of the system would induce relatively higher subcooling temperatures, leading to an excess energy supply for the hydrate formation; therefore, the larger temperature difference of the solution under faster cooling rates was more favourable to the fast hydrate growth than under slower cooling rates. Insulation of subsea flowlines would decrease the cooling rate and would help to reduce the hydrate growth, as seen in Figure 7.5c. This was true for PNIPAM-based KHIs and Luvicap; however, PVP showed the increase of the initial growth rate from 0.0064 to 0.0101 volume fraction/min when reducing the cooling rate from 0.25 to 0.017 K/min. As shown in the previous section, PVP performed well to inhibit the hydrate onset; however, once the hydrate crystals started to grow, its performance as a crystal growth inhibitor was not as effective as others. More investigation must be carried out to understand the role of functional groups in KHIs during the formation process.

To investigate the relation between the hydrate volume fraction and the resistance to flow, the torque with the hydrate growth was measured. Panels a−c of Figure 7.6 showed that the measured torque changes during the hydrate formation for PNIPAM-based KHIs and control groups at different cooling rates. The resistance to flow is a qualitative parameter to estimate the flowability of hydrocarbon fluid to keep transporting the hydrate particles without forming the hydrate plug. As the sintering and bedding of hydrate particles occurs, lower flowability of the hydrocarbon fluid would result in torque increases. As seen for pure water in panels a−c of Figure 5, torque started to increase when the hydrate fraction increased more than 0.10 in the liquid phase, suggesting that the agglomeration of hydrate particles would occur for a larger hydrate fraction in the liquid phase than 0.10. The growth rate of pure water became faster with an increased torque after the 0.15 hydrate fraction, as seen in panels

a and b of Figure 7.6, which means that the hydrate that had formed in the system changed from homogeneous to heterogeneous.

The hydrate growth and torque changes for PNIPAM-based KHIs showed different patterns than commercial KHIs. PNIPAM-co-Cp and PNIPAM-co-C_4t indicated that torque increases once the hydrate volume fraction increased more than 0.10. When the cooling rate was 0.017 K/min, the PNIPAM-co-AA system represented the smallest growth rate and torque value with the least hydrate volume fraction, followed by the PNIPAM-co-Cp system, as presented in Figure 7.6c. The PNIPAM-co-C_4t system showed a plateau, but a sudden increase during the hydrate fraction reached the moment of 0.10. Overall, the base polymer PNIPAM-co-AA was the best to suppress the torque increase during the hydrate formation, but its modification into PNIPAM-co-CP and PNIPAM-co-C_4t did not help to control the increase of resistance to flow. More investigation will be carried out in the near future to understand the role of KHIs during the agglomeration and bedding of hydrate particles during the formation process.

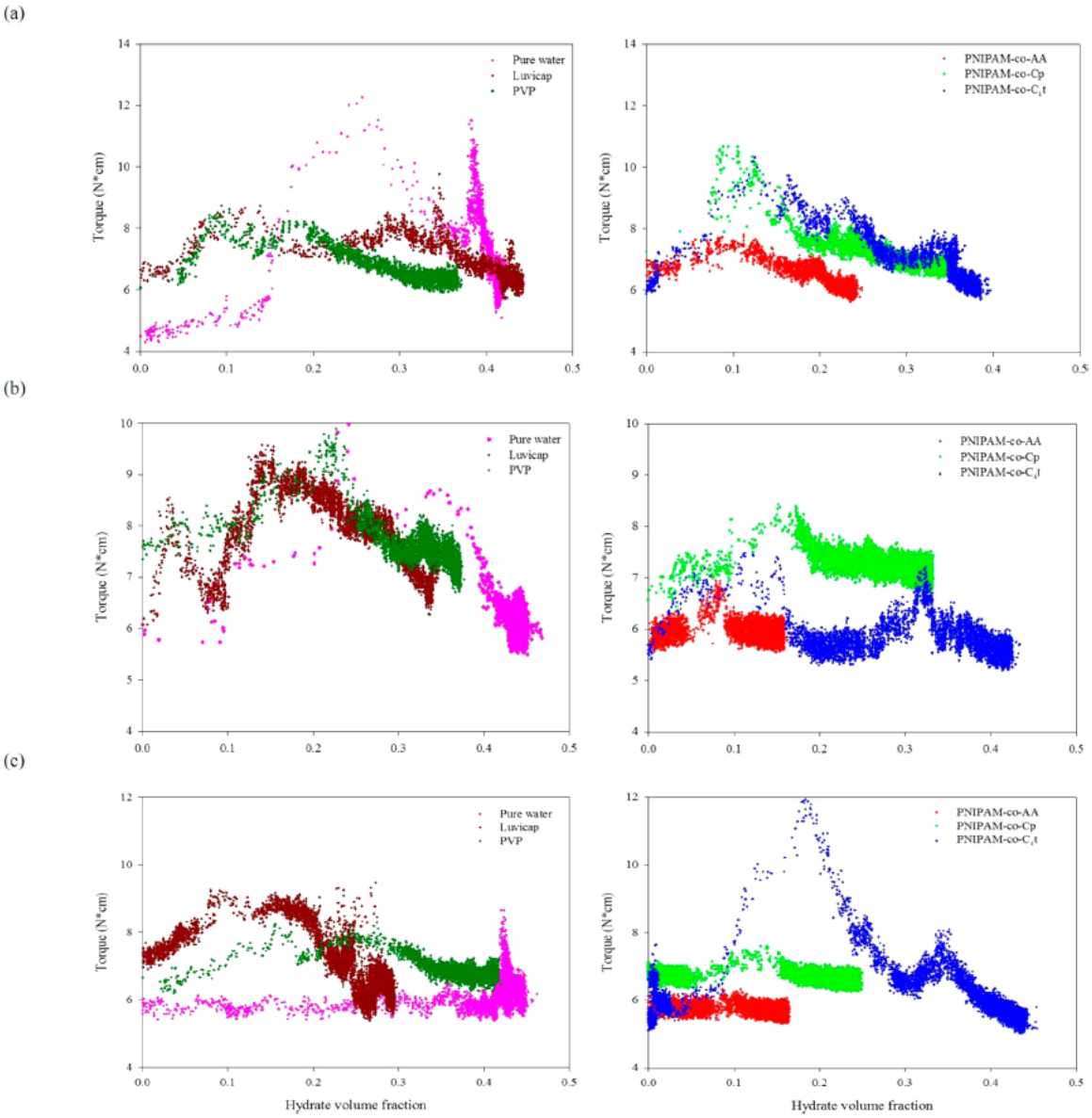

Figure 7. 6 Relationship between the hydrate fraction and torque in a representative cycle for PNIPAM-based KHIs, commercial KHI (Luvicap and PVP, 0.5 wt %) solutions, and pure water under cooling rates of (a) 0.25 K/min, (b) 0.033 K/min, and (c) 0.017 K/min (Park et al., 2017b).

7.2.3 Conclusions

These above sections investigated the hydrate inhibition performance of three PNIPAM-based KHIs (PNIPAM-co-AA, PNIPAM-co-Cp, and PNIPAM-co-C4t) by determining the hydrate onset time, its growth rate, and resistance to flow using a high-pressure autoclave. A comparison to three control groups (water, Luvicap solution,

and PVP solution) was also performed at various cooling rates (0.25, 0.033, and 0.017 K/min). The modification of the base polymer structure, PNIPAM-co-AA, with Cp enhanced the kinetic inhibition performance at the cooling rate of 0.033 K/ min. For the PNIPAM-co-C_4t, the subcooling temperatures were 9.6, 9.9, and 7.6 K and the onset times were 54.5, 311.4, and 468.8 min, respectively. The modification with C_4t adversely affected the performance of PNIPAM-based KHIs, where the subcooling was higher than that in pure water but lower than that in PNIPAM-co-AA solution. The obtained results confirmed that the synthesized PNIPAM-based KHIs presented a high subcooling temperature, which is comparable to those of commercial KHIs. The obtained subcooling temperature was plotted with the hydrate onset time, which suggested that the cooling rate of 0.033 K/min maintains a high subcooling temperature and long onset time, thus, the performance of KHIs placed in the low-risk plane. Using the cooling rate to determine the performance of KHI candidates is a new approach. After the hydrate onset, PNIPAM-co-C_4t showed a slow growth rate, but a stable torque during the hydrate formation was achieved with PNIPAM-co-Cp, suggesting that the base polymer PNIPAM-co-AA showed the best performance as a crystal growth inhibitor. These results suggested that the performance of PNIPAM-based KHIs were able to be evaluated with the holistic investigation on nucleation and growth of hydrate crystals.

7.3 Performance of PVCap-based KHCI polymers

Multifunctional polymers were designed and synthesized that contain both a kinetic hydrate inhibitor and corrosion inhibitor groups. This was achieved by modifying a copolymer of vinyl caprolactam and acrylic acid (PVCap-co-AA) where the acid groups were converted to known corrosion inhibitor groups including imidazole (APIM) and quaternary ammonium (ATCH) moieties. Their performance as kinetic hydrate inhibitors was evaluated using the same method as with PNIPAM by determining the hydrate onset time, growth rate, and resistance to flow using a high pressure autoclave.

The experimental results show that both PVCap-co-APIM and PVCap-co-ATCH were able to delay hydrate nucleation; however, PVCap-co-APIM was better than PVCap-co-ATCH. The performance of new KHICIs was evaluated and compared with that of

a commercial KHI, Luvicap, with three different cooling rates: for high and medium cooling rates, Luvicap delayed hydrate nucleation for a longer time compared to the new KHICIs. At low cooling rate, one of the KHICIs (PVCap-co-APIM) showed better performance than Luvicap. PVCap-co-APIM also performed better than Luvicap and PVCap-co-ATCH in decreasing the hydrate growth rate. Hydrate growth rate and resistance to flow were also studied during the hydrate formation to investigate the effect of the inhibitors on the growth of hydrate particles in the liquid phase. PVCap-co-APIM successfully suppressed hydrate growth in the early stage of hydrate formation, whereas PVCap-co-ATCH resulted in fast growth of the hydrate phase. For all of the studied cooling rates, PVCap-co-APIM showed stable resistance to flow even with increasing hydrate fraction in the liquid phase; however, PVCap-co-ATCH showed a torque surge in the early stage of hydrate formation when a fast cooling rate was used, which suggests that the ATCH group has a negative effect on the hydrate inhibition performance. These results provide a proof-of-concept that the modified PVCap-co-APIM, or related structures, that contain both kinetic hydrate inhibitor and corrosion inhibitor groups can be used as multifunctional inhibitors for offshore oil and gas fields.

7.3.1 Materials and methods

7.3.1.1 Materials

The distilled water and decane (purity: 99%) were purchased from OCI (Korea) and Sigma-Aldrich, respectively. The water and decane were used without further purification. The synthetic natural gas (CH4: 90 mol %, C2H6: 6 mol %, C3H8: 3 mol %, n-C4H10: 1 mol %) was supplied by Special Gas (Korea). Luvicap EG HM was supplied by BASF. PVCap-based KHIs were synthesized in house. Among the synthesized KHCIs, PVCap-co-APIM (20) and PVCap-co-ATCH (20) were selected to further evaluate via the advanced inhibitor test methodology as they showed low threshold concentration from HTP screening as well as low weight loss from the corrosion coupon test (see detail in chapter 8). Figure 7.7 presents the structures of PVCap based KHIs tested in this work.

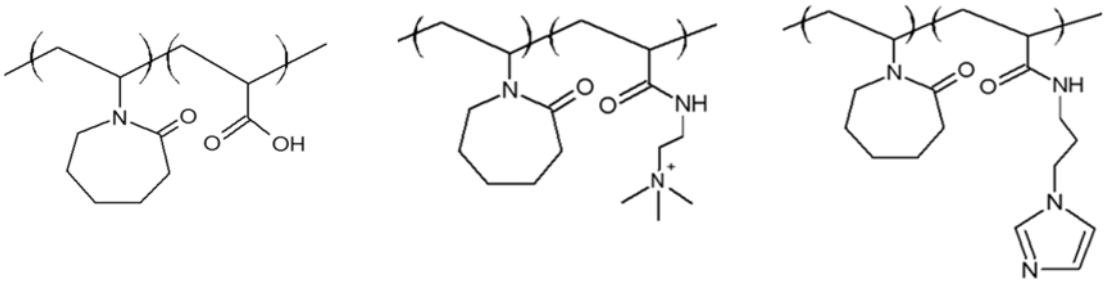

Figure 7. 7 Structures of PVCap-based KHIs: (from left) PVCap-co-AA, PVCap-co-ATCH, and PVCap-co-APIM (Park et al., 2017a).

7.3.1.2 Hydrate inhibition performance evaluation

All experiments were conducted using the same apparatus and method as introduced in the previous section 7.2. For comparison, pure water and Luvicap solution were selected as control groups. The concentration of PVCap derivatives (PVCap-co-AA, PVCap-co-ATCH (20), and PVCap-co-APIM (20)) was 0.5 wt % based on the aqueous phase for all experiments.

Performance of PVCap-based KHIs was evaluated by measuring the subcooling temperature. Three different cooling rates (0.25, 0.033, and 0.017 K/min) were applied to simulate the different insulation status of subsea flowlines. The role of PVCap-based KHIs during the hydrate nucleation and growth stage was investigated to evaluate their performance.

7.3.2 Results and discussion

7.3.2.1 Kinetic inhibition performance of PVCap-Based KHCIs

The mean value and standard deviation over three repeat trials for the subcooling temperature (ΔT_{sub}) and the hydrate onset time (t_{onset}) of PVCap-based KHIs are presented in Table 7.3.

Table 7. 3 Subcooling temperature and onset time from hydrate formation experiments with 0.5 wt % PVCap- Based KHIs solution[a] (Park et al., 2017a).

PVCap-based KHIs	cooling rate (°C/min)	ΔT_{sub} (K)	t_{onset} (min)
PVCap-*co*-AA	0.017	8.5 (0.1)	540.2 (5.6)
	0.033	8.4 (0.2)	284.5 (2.0)
	0.25	9.5 (1.1)	52.1 (7.4)
PVCap-*co*-ATCH	0.017	7.7 (0.3)	473.5 (13.7)
	0.033	7.6 (0.2)	246.0 (1.9)
	0.25	8.4 (0.6)	41.9 (3.8)
PVCap-*co*-APIM	0.017	8.3 (1.1)	517.4 (69.3)
	0.033	9.0 (0.3)	290.5 (5.9)
	0.25	9.7 (0.1)	42.5 (0.8)
pure water	0.017	3.3 (0.1)	200.8 (4.7)
	0.033	3.3 (0.1)	104.4 (3.9)
	0.25	4.7 (0.6)	20.4 (2.1)
Luvicap	0.017	7.9 (0.9)	484.8 (56.2)
	0.033	11.4 (0.9)	353.2 (26.3)
	0.25	11.6 (0.2)	83.8 (5.2)

[a]The standard deviation of the subcooling temperature and onset time is shown in parentheses. Data for pure water and Luvicap solution were from preivous PNIPAM section.

For pure water, ΔT_{sub} was 3.3 °C, while t_{onset} was 200.8 min at a slow cooling rate of 0.017 °C/min. With increasing cooling rate (0.033 °C/min), the ΔT_{sub} was maintained 3.3 °C and t_{onset} was decreased to 104.4 min. For the highest cooling rate of 0.25 °C/min, ΔT_{sub} was 4.7 °C and t_{onset} was 20.4 min. These results suggested that the subcooling temperature was less affected by changing the cooling rate, whereas the hydrate onset time was highly affected.

Figure 7.8 shows the comparison of the subcooling temperature between the PVCap-based KHIs and the control groups including pure water and a Luvicap solution. The 0.5 wt % PVCap-co-AA showed ΔTsub of 9.8, 8.4, and 8.5 °C with the cooling rates of 0.25, 0.033, and 0.017 °C/min, respectively, indicating the synthesized PVCap-co-AA performed well as a kinetic hydrate inhibitor. The commercial KHI, Luvicap,

showed better performance than PVCap-co-AA at cooling rates of 0.25 and 0.033 °C/min; however, it showed similar performance at 0.017 °C/min. When the base polymer was modified with corrosion groups, PVCap-co-APIM, a slightly enhanced performance was observed as seen from the increased ΔTsub to 9.7, 9.0, and 8.3 °C with the cooling rates of 0.25, 0.033, and 0.017 °C/min, respectively. However, for PVCap-co-ATCH, ΔTsub was decreased slightly compared to the base polymer at every cooling rate studied in this work.

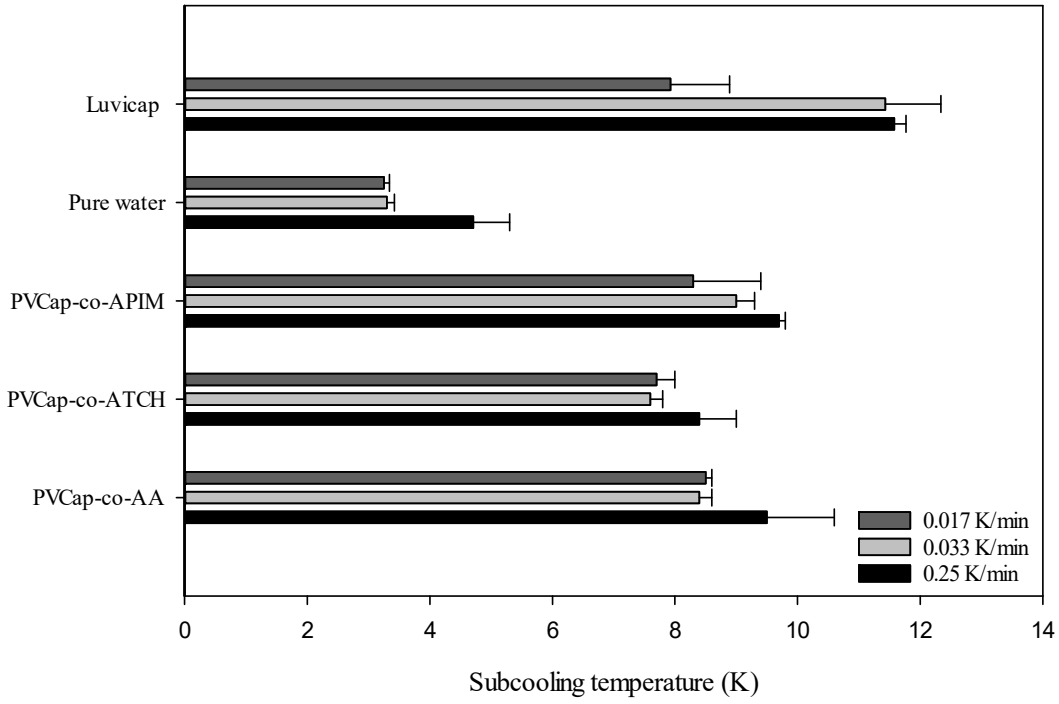

Figure 7. 8 Subcooling temperature of PVCap-co-AA, PVCap-co-ATCH, and PVCap co-APIM. Pure water and Luvicap solution were studied to provide comparison. Error bars indicate the standard deviation (Park et al., 2017a).

Figure 7.9 shows the t_{onset} as a function of ΔT_{sub} with varying cooling rates. For a fast cooling rate of 0.25 K/min, Luvicap showed the best performance with a difference in subcooling of 1.9 °C. PVCap-co-APIM and PVCap-co-AA were close, while PVCap-co-ATCH showed the lowest performance (Luvicap > PVCap-co-APIM ≈ PVCap-co-AA > PVCap-co-ATCH). When the cooling rate was reduced to 0.033 °C/min, Luvicap again showed the best performance when compared to the base PVCap-co-

AA and modified polymers. PVCap-co-APIM was better than others, but the subcooling difference between PVCap-co-APIM and Luvicap was 2.4 °C, which was calculated to 72.7 min from the cooling rate. PVCap-co-ATCH showed the lowest subcooling temperature (Luvicap > PVCap-co-APIM > PVCap-co-AA > PVCap-co-ATCH). For a slow cooling rate of 0.017 °C/min, PVCap-co-AA showed the best performance, closely followed by PVCap-co-APIM. The performance of PVCap-co-ATCH and Luvicap was less than the above (PVCap-co-AA > PVCap-co-APIM > Luvicap $\approx$ PVCap-co-ATCH). The difference between the highest performing (PVCap-co-AA) and the lowest (PVCap-co-ATCH) KHIs was only 0.8 °C. Overall, the synthesized polymers performed less than the commercial polymer under fast and median cooling rates; however, two of them showed slightly better performance under slow cooling. The commercial KHI polymer does not carry any corrosion groups, so it is unlikely to act as a corrosion inhibitor.

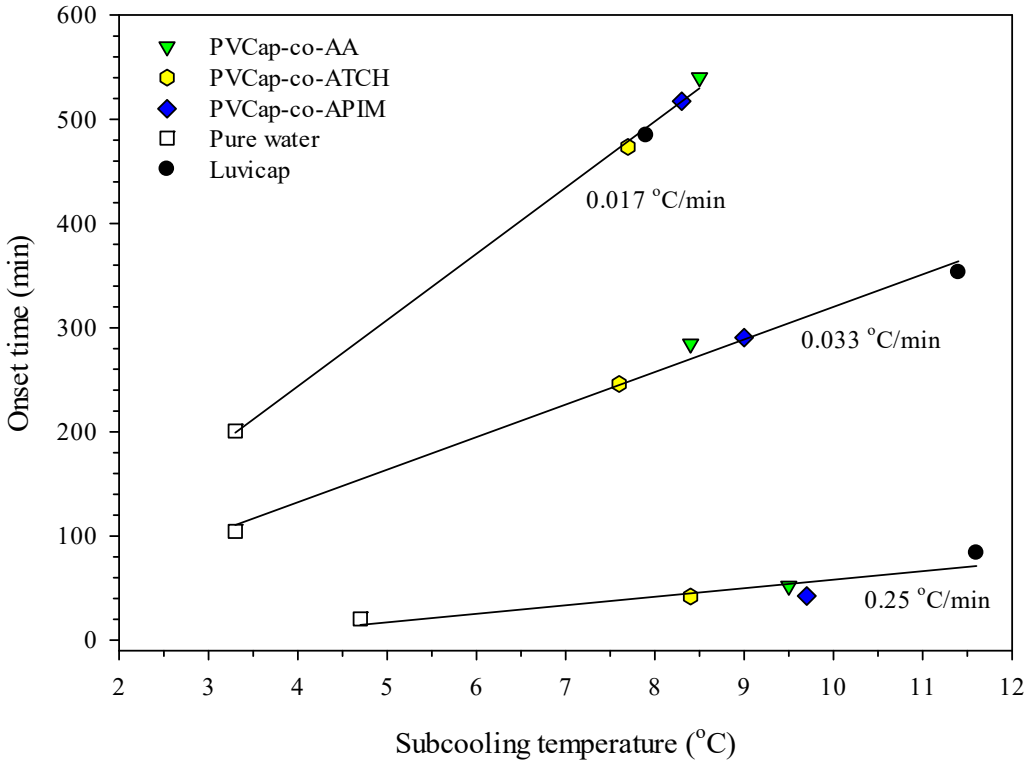

Figure 7. 9 Hydrate onset time as a function of the subcooling temperature for PVCap-based KHIs with varying cooling rates: 0.25, 0.033, and 0.017 K/min. Solid lines indicate linear regression of the measurements (Park et al., 2017a).

In our previous work as shown in section 6.4.1, a high-throughput hydrate test showed the low threshold concentration, 0.5 wt % for the base polymer and 0.1 wt % for the modified polymer with ATCH and APIM. This work expands the test for kinetic hydrate inhibition by measuring hydrate onset time and subcooling temperature under mixing, at elevated pressure with natural gas, and while varying the cooling rate. As discussed in Figure 7.9, PVCap-co-APIM showed better inhibition performance than the base polymer and PVCap-co-ATCH at fast and slow cooling. However, for the slow cooling rate, the base polymer, PVCap-co-AA, performed better than both modified polymers. PVCap-co-ATCH showed the lowest performance among the tested KHIs. These results suggest that the performance of the PVCap-based KHIs obtained from subcooling temperatures and onset times can vary from that of the high-throughput hydrate test. Previous work by Dirdal et al. also found the results of testing a range of KHIs using cyclopentane at atmospheric pressure correlated fairly well with tests carried out by trichlorofluoromethane in high pressure stirred autoclaves, but there were some notable exceptions (Dirdal et al., 2012). KHI performance tests using cyclopentane at atmospheric pressure can be carried out in relatively short duration and for many KHI samples. However, for the qualified KHI candidates, comprehensive investigation must be carried out using the reliable experimental apparatus and conditions that can simulate the production of hydrocarbon fluids in subsea flowlines.

7.3.2.2 Hydrate growth characteristics in the presence of KHIs and KHCIs

Measurement of the subcooling temperatures clearly indicated that the modified polymers structure can display both kinetic hydrate inhibition and corrosion inhibition performance during the nucleation stage of hydrate crystals. Recent studies suggest that the KHIs also affect the growth of hydrate crystals and provide an additional delay time until the formation of a hydrate plug (Chua et al., 2012a; Lucas et al., 2002; O'Reilly et al., 2011; Perrin et al., 2013). In order to study the role of PVCap-based KHIs during the hydrate growth stage, the growth rate and resistance-to-flow were investigated by estimating the hydrate fraction from the change in pressure and torque.

Table 7.4 presents the initial growth rate (r_{ini}), late growth rate (r_{late}), maximum torque (τ_{max}), hydrate fraction at maximum torque (Φ_{trans}), hydrate fraction at 600 min (Φ_{final}),

and water conversion to hydrate at 600 min (x_{conv}). As seen in Figures 7.10−7.12, the hydrate fraction increased rapidly in the early stage of hydrate formation, but soon reached an inflection point from which the hydrate fraction increases slowly. We presented the hydrate growth rate in the early stage of hydrate formation as the initial growth rate; then the late growth rate indicated the hydrate growth rate after reaching the inflection point. The change in torque with respect to hydrate fraction was used to locate the maximum torque and the corresponding hydrate fraction. Recent studies suggest that torque changes indicate resistance to the hydrocarbon flow due to the agglomeration and bedding of hydrate particles (Aman et al., 2014; Kim et al., 2014). In this work, decane was mixed with water in the liquid phase at 600 rpm, where decane droplets were dispersed homogeneously. As the volume of water in the liquid phase was 60%, the continuous phase was water in this work. The decane droplets would be dispersed in water phase while bulk hydrate particles were formed and grew; this might form a liquid bridge which accelerates the agglomeration of hydrate particles. The PVCap-based KHCIs would be absorbed to the surface of growing hydrate particles as they are dissolved in the water phase. Their ability to inhibit hydrate growth would result in a low hydrate fraction as well as dispersed hydrate particles without causing high resistance to flow.

Table 7. 4 Hydrate formation characteristics in 0.5 wt% PVCap-Based KHI solutions while varying cooling rate (Park et al., 2017a).

Cooling rate	System	r_{ini} (min^{-1})	r_{late} (min^{-1})	τ_{max} (N cm)	Φ_{trans}	Φ_{final}	x_{conv} (%)
0.017 °C/min	PVCap-co-AA	0.0034	0.0001	8.4	0.04	0.27	38.94
	PVCap-co-ATCH	0.0071	0.0004	9.1	0.12	0.38	54.93
	PVCap-co-APIM	0.0017	0.0004	8.1	0.13	0.31	44.62
	Pure water	0.0063	0.0003	9.2	0.42	0.45	66.53
	Luvicap	0.0003	0.0005	11.7	0.23	0.30	43.65
	PVCap-co-AA	0.0014	0.0004	7.9	0.03	0.22	31.37

0.033 °C/min	PVCap-co-ATCH	0.0101	0.0003	8.9	0.13	0.34	49.93
	PVCap-co-APIM	0.0025	0.0004	8.4	0.11	0.33	47.79
	Pure water	0.0164	0.0004	10.3	0.07	0.49	72.50
	Luvicap	0.0037	0.0005	9.9	0.12	0.36	52.39
0.25 °C/min	PVCap-co-AA	0.0020	0.0004	7.8	0.03	0.27	38.25
	PVCap-co-ATCH	0.0121	0.0010	17.8	0.07	0.42	62.56
	PVCap-co-APIM	0.0077	0.0006	7.4	0.15	0.43	62.99
	Pure water	0.0103	0.0003	13.9	0.25	0.43	64.04
	Luvicap	0.0051	0.0007	9.3	0.09	0.45	66.87

Figure 7.10 shows the increase of hydrate volume fraction as a function of time for 300 min after the hydrate onset for each system when the cooling rate was 0.017 °C/min. For pure water, hydrate formation can be observed when the subcooling temperature was 3.3 °C and the initial growth rate was 0.0063 min^{-1}. As seen in Figure 7.10a, the hydrate growth curve showed an inflection point at approximately 100 min when the hydrate fraction was close to 0.4. Then, the hydrate fraction kept increasing to 0.42, where the torque started to rise and showed a maximum of 9.2 N cm. After the inflection point, the late growth rate was 0.0003 min^{-1} and the final hydrate fraction was 0.45, suggesting that the growth rate was very slow after the inflection point. For Luvicap solution, the initial growth rate was 0.0003 min^{-1} and the late growth rate was 0.0005 min^{-1}. The torque quickly increased with increasing hydrate fraction unlike pure water; then it showed severe fluctuation when the hydrate fraction was larger than 0.20. The maximum torque was 11.7 N cm at a hydrate fraction of 0.23. The final hydrate fraction was 0.30, which is significantly lower than that of pure water; however, the torque changes, i.e., resistance to flow, suggests a high risk of hydrate blockage formation for Luvicap solution, although the hydrate growth rate was low.

The base polymer (PVCap-co-AA) showed an initial growth rate of 0.0034 min^{-1}, but in 50 min, the growth rate became 0.0001 min^{-1}. The maximum torque was 8.4 N cm

at a hydrate fraction of 0.04; however, the baseline torque was at around 7 N cm. The base polymer successfully retarded the growth of hydrate particles and inhibited the agglomeration of hydrate particles. Addition of the ATCH group to the base polymer, PVCap-co-ATCH, showed the initial growth rate of 0.0071 min^{-1} and maximum torque of 9.1 at a hydrate fraction of 0.12. The late growth rate was 0.0004 min^{-1}, and the final hydrate fraction was 0.38. For PVCap-co-APIM, the initial growth rate was 0.0017 min^{-1} and the maximum torque was 8.1 N cm at a hydrate fraction of 0.13. The late growth rate was 0.0004 min^{-1}, and the final hydrate fraction was 0.31. These results suggest that both ATCH and APIM groups showed good compatibility with the VCap group in preventing high resistance to flow when the cooling rate was 0.017 °C/min. However, the ATCH showed higher initial growth rate and hydrate fraction than that of APIM, indicating better inhibition performance of APIM.

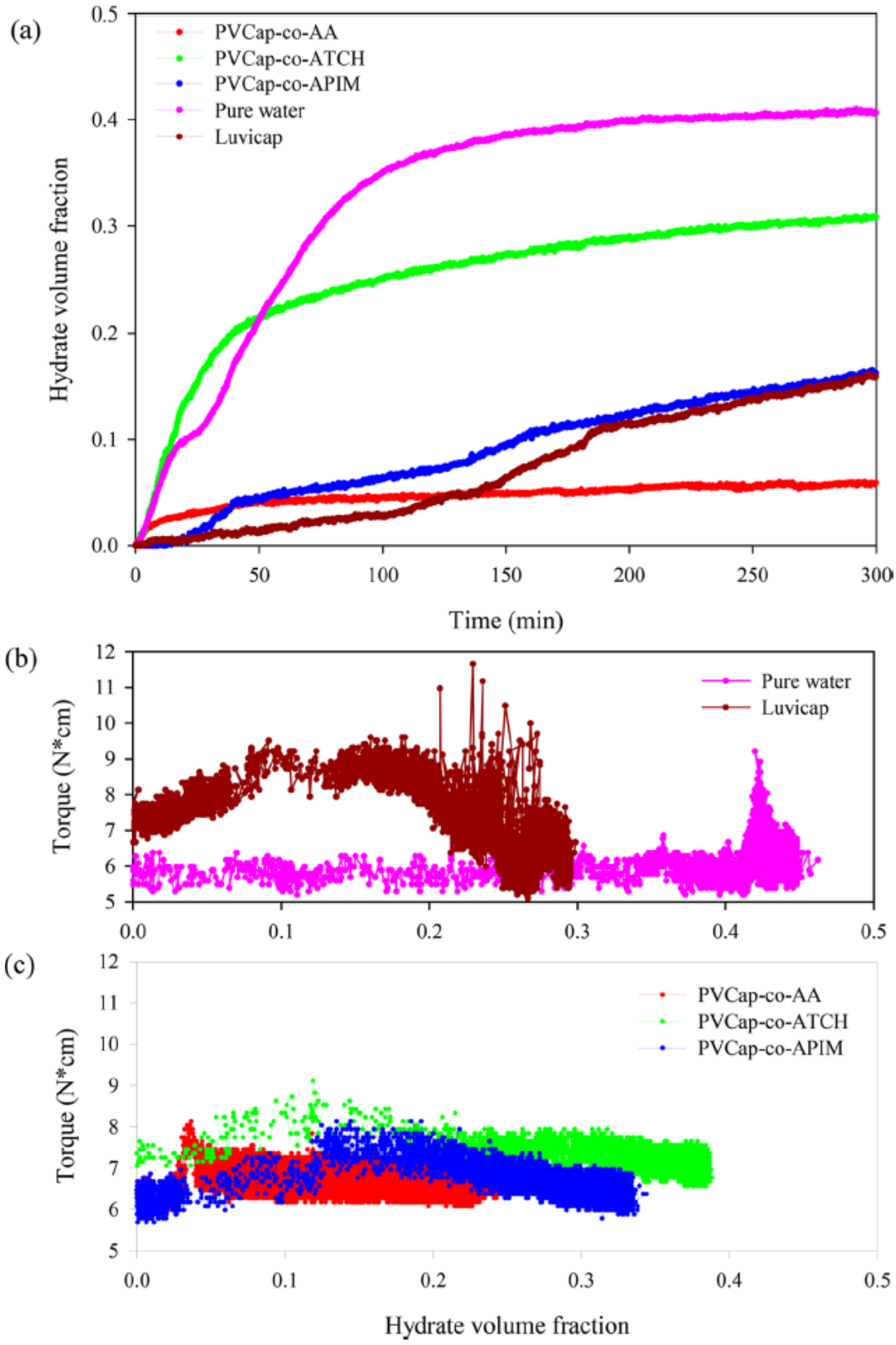

Figure 7. 10 Hydrate growth and corresponding torque changes for PVCap-based KHIs at a cooling rate of 0.017 °C/min. (a) Hydrate volume fraction in liquid phase as a

function of time. (b) Torque changes for pure water and Luvicap solution. (c) Torque changes for PVCap-based KHIs (Park et al., 2017a).

Figure 7.11 presents the hydrate growth curves as a function of time and the torque changes with hydrate fraction for each system at a cooling rate of 0.033 °C/min. The initial growth rate increased for most systems due to increased subcooling temperature. For pure water, the initial growth rate was 0.0164 min^{-1}, which was a 2.6 times higher rate than that of 0.017 °C/ min. Interestingly, the maximum torque was 10.3 N cm in the early stages of hydrate formation when the hydrate fraction was 0.07. The torque fluctuated and involved a stepwise increase of hydrate phase as seen in Figure 7.10a until the inflection point was observed at around 90 min and hydrate fraction of 0.35. Since the inflection point, the late growth rate decreased to 0.0004 min^{-1} and the torque fluctuated slightly.

As seen in Figure 7.11c, addition of PVCap-co-AA based KHIs showed stable torque along with increase of hydrate fraction. The maximum torque was 7.9, 8.9, and 8.4 N cm at hydrate fractions of 0.03, 0.13, and 0.11 for PVCap-co-AA, PVCap-co-ATCH, and PVCap-co-APIM, respectively. As the baseline torque value was about 7 N cm, only a slight increase was observed during hydrate growth. For PVCap-co-ATCH, the initial growth rate was 0.0101 min^{-1}, which was close to that of pure water. Due to early occurrence of the inflection point, a lower hydrate fraction was obtained in the presence of PVCap-co-ATCH than in pure water. However, its growth rate was faster than that of PVCap-co-AA and PVCap-co-APIM, thus there may be a risk of hydrate blockage formation if the functional group for hydrate inhibition became ineffective.

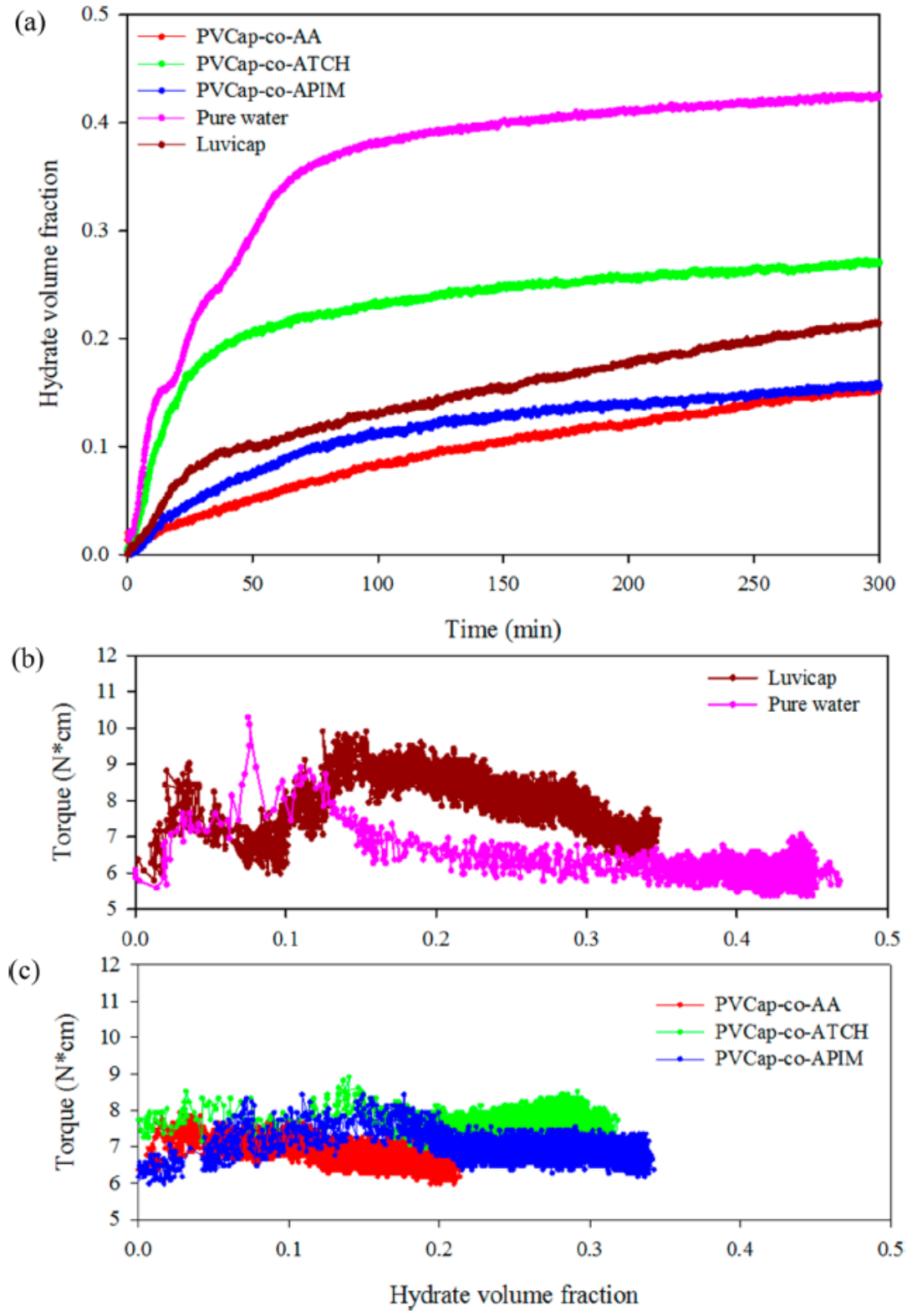

Figure 7. 11 Hydrate growth and corresponding torque changes for PVCap-based KHIs at a cooling rate of 0.033 °C/min. (a) Hydrate volume fraction in liquid phase as a function of time. (b) Torque changes for pure water and Luvicap solution. (c) Torque changes for PVCap-based KHIs (Park et al., 2017a).

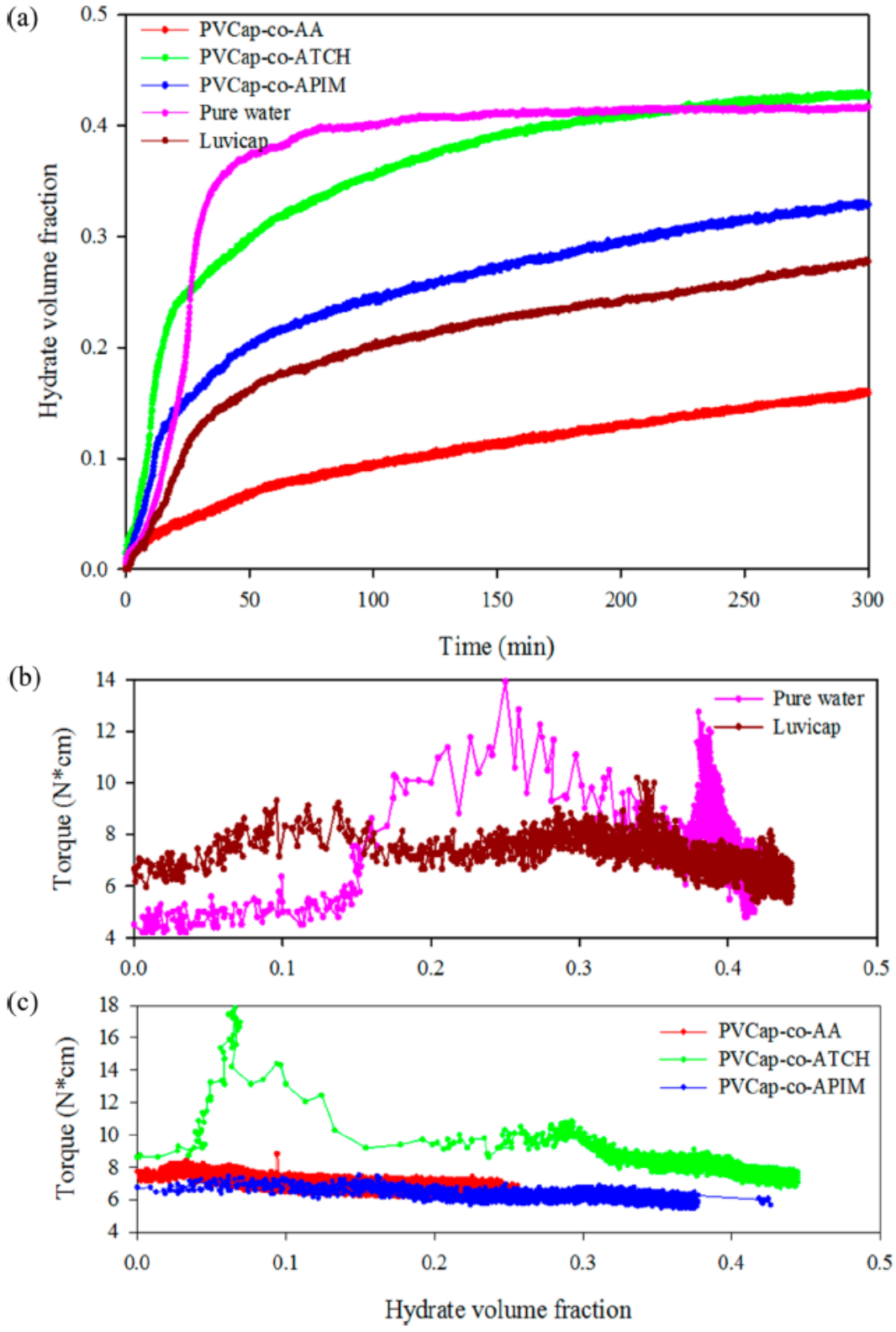

Figure 7. 12 Hydrate growth and corresponding torque changes for PVCap-based KHIs at a cooling rate of 0.25 °C/min. (a) Hydrate volume fraction in liquid phase as a function of time. (b) Torque changes for pure water and Luvicap solution. (c) Torque changes for PVCap-based KHIs (Park et al., 2017a).

Figure 7.12 shows hydrate growth curves and torque changes for PVCap-co-AA based KHIs at a cooling rate of 0.25 °C/min. Similar results were obtained in that the initial growth rate was faster for PVCap-co-ATCH, 0.0121 min^{-1}, than the growth rate of PVCap-co-APIM, which was 0.0077 min^{-1}. PVCap-co-AA showed the lowest initial growth rate, 0.0020 min^{-1}. The late growth rates after the inflection points were about 0.0004min^{-1} for PVCap-co-AA, 0.0010 min^{-1} for PVCap-co-ATCH, and 0.0006 min^{-1} for PVCap-co-APIM. The initial growth rate for pure water was 0.0103 min^{-1}, and the late growth rate was 0.0003 min^{-1}, while the addition of Luvicap reduced the initial growth rate to 0.0051 min^{-1}, and the late growth rate of 0.0007 min^{-1}. PVCap-co-ATCH showed almost no hydrate inhibition performance from the hydrate growth rate and the hydrate fraction. For pure water, the maximum torque was 13.9 N cm at a hydrate fraction of 0.25, whereas PVCap-co-ATCH solution showed a maximum torque of 17.8 N cm at a hydrate fraction of 0.07. PVCap-co-APIM showed similar hydrate growth rate and hydrate fraction to those of Luvicap, and the associated torque changes indicated a minimum resistance to flow compared to other KHIs. It clearly showed the hydrate growth became fast and more hydrate was formed in the presence of the ATCH group, suggesting the incompatibility of the ATCH group against the VCap group for hydrate inhibition. Table 7.5 summarizes the performance of KHI polymers on hydrate growth at each cooling rate.

Table 7. 5 Performance of PVCap-Based KHI solutions while varying cooling rate (Park et al., 2017a).

variables	cooling rate (°C/min)	ranking
Initial growth rate	0.017	PVCap-*co*-ATCH ≫ PVCap-*co*-AA > PVCap-APIM > Luvicap
	0.033	PVCap-*co*-ATCH ≫ Luvicap > PVCap-APIM > PVCap-*co*-AA
	0.25	PVCap-*co*-ATCH ≫ PVCap-*co*-APIM > Luvicap > PVCap-*co*-AA
max. torque	0.017	Luvicap > PVCap-*co*-ATCH > PVCap-*co*-AA ≈ PVCap-*co*-APIM
	0.033	Luvicap > PVCap-*co*-ATCH > PVCap-*co*-APIM > PVCap-*co*-AA
	0.25	PVCap-*co*-ATCH > Luvicap > PVCap-*co*-AA > PVCap-*co*-APIM
hydrate fraction at transition	0.017	Luvicap > PVCap-*co*-APIM ≈ PVCap-*co*-ATCH ≫ PVCap-*co*-AA
	0.033	PVCap-*co*-ATCH ≈ Luvicap ≈ PVCap-*co*-APIM > PVCap-*co*-AA
	0.25	PVCap-*co*-APIM > Luvicap > PVCap-*co*-ATCH > PVCap-*co*-AA
Hydrate fraction at 600 min	0.017	PVCap-*co*-ATCH > PVCap-*co*-APIM ≈ Luvicap > PVCap-*co*-AA
	0.033	Luvicap > PVCap-*co*-ATCH ≈ PVCap-*co*-APIM > PVCap-*co*-AA
	0.25	Luvicap ≈ PVCap-*co*-APIM ≈ PVCap-*co*-ATCH ≫ PVCap-*co*-AA

Hydrate blockage formation would occur when the hydrate particles agglomerate and segregate from the continuous phase to deposit on the wall. Without hydrate inhibitors, increasing cooling rate resulted in a rapid increase in the hydrate fraction, which will increase the possibility of agglomeration and bedding of hydrate particles. In Figures 7.10-7.12, increasing hydrate fraction involves a steady increase or fluctuation of torque, i.e., high resistance to flow. Therefore, the role of the KHI during the hydrate formation process would be to suppress the hydrate growth rate, which results in a low hydrate fraction in the liquid phase for extended periods. In this work, the performance of PVCap-co-AA, the base polymer before modification, could reduce the hydrate growth to maintain stable torque with increasing hydrate fraction. By modifying the AA group with APIM, PVCap-co-APIM showed a slight increase of hydrate growth rate compared to PVCap-co-AA, but stable torque was observed for all cooling rates. The modification with ATCH, PVCap-co-ATCH, resulted in rapid hydrate growth compared to other PVCap-based KHIs, and a surge in torque was observed in the early stages of hydrate formation. Figure 7.13 shows the torque surge in PVCap-co-ATCH solution.

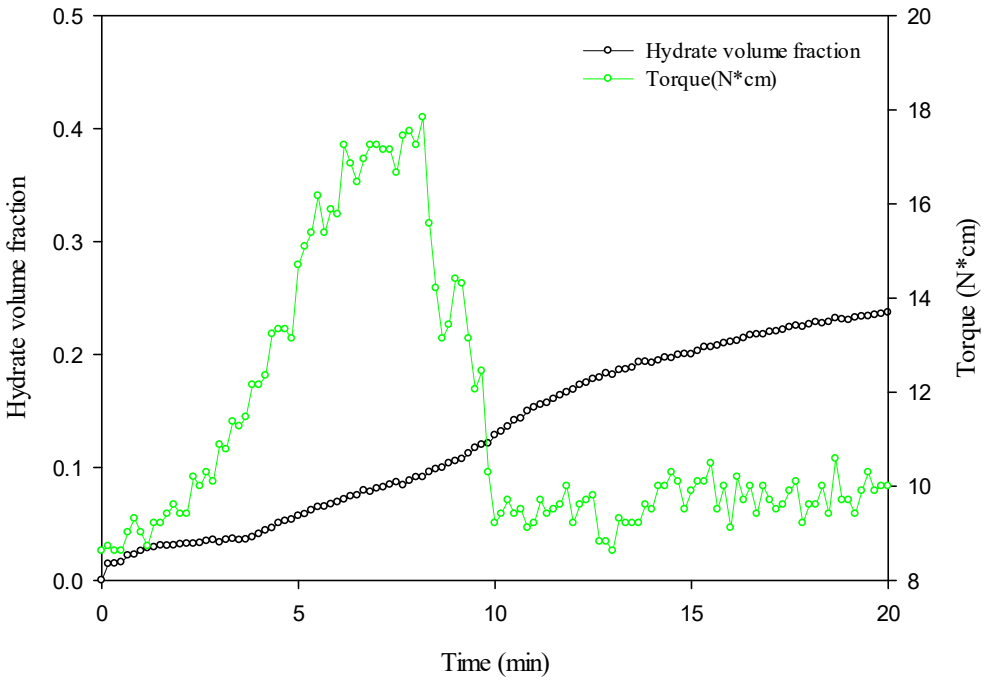

Figure 7. 13 Hydrate fraction increase and torque changes as a function of time for PVCap-co-ATCH solution in early stage of hydrate formation (Park et al., 2017a).

After the hydrate onset, the hydrate fraction reached only 0.03 when torque started to rise; then a maximum torque of 17.8 N cm was observed when the hydrate fraction reached 0.09. Recent studies suggest that the resistance to flow resulted from agglomeration and bedding of hydrate particles which became evident with the hydrate fraction in the liquid phase was more than 0.10 (Akhfash et al., 2013; Aman et al., 2014; Kim et al., 2014). However, the modification to PVCap-co-ATCH resulted in high resistance to flow in the early stage of hydrate formation, which would increase the risk of hydrate blockage when hydrate formation begins. Unlike PVCap-co-APIM, PVCap-co-ATCH was only effective to delay the hydrate onset and was not able to prevent the hydrate plug formation as seen from fast hydrate growth and high resistance to flow.

Our previous work of HTP hydrate screen (section 6.4.1) suggested that the modification of PVCap-co-AA with APIM or ATCH groups showed effective corrosion inhibition performance. From the high pressure autoclave tests in this chapter, the PVCap-co-APIM showed the best combination of lowering hydrate nucleation while suppressing the growth rate while maintaining the torque during hydrate formation process. Its modification with ATCH showed adverse effects on hydrate inhibition performance, suggesting the incompatibility between this hydrate inhibitor group and this corrosion group.

7.3.3 Conclusions

This chapter investigated the hydrate inhibition performance of PVCap-based KHIs (PVCap-co-AA, PVCap-co-ATCH, and PVCap-co-APIM) by determining the hydrate onset time, growth rate, and resistance-to-flow using a high pressure autoclave. First, the subcooling conditions were determined for PVCap-based KHIs solutions and the results were compared to those of pure water and Luvicap solution at various cooling rates (0.25, 0.033, and 0.017 °C/min). PVCap-APIM and PVCap-co-AA were close, while PVCap-co-ATCH showed the lowest performance when the cooling rate was increased from 0.017 to 0.25 °C/min. For delaying hydrate formation, Luvicap again showed better performance than the base PVCap-co-AA and modified polymers, although the performance of Luvicap diminished than the modified polymers at 0.017 °C/min (Luvicap > PVCap-co-APIM ≈ PVCap-co-AA > PVCap-co-ATCH).

For the growth stages, the modification of the base polymer with APIM, PVCap-co-APIM, enhanced the kinetic hydrate inhibition performance. The initial growth rate was less than that in pure water and PVCap-co-ATCH solution. The hydrate fraction increased slowly while maintaining a stable torque. The modification with ATCH adversely affected the kinetic inhibition performance of PVC-based KHI, where the initial growth rate was faster than that of other PVCap-based KHIs and a high hydrate fraction was obtained. For a fast cooling rate, 0.25 °C/min, a surge in torque was observed in the early stage of hydrate formation, suggesting a high risk of hydrate blockage formation upon hydrate onset. These results suggest that the multifunctional polymer was successfully designed and synthesized by incorporating corrosion inhibitor groups, APIM, onto a known kinetic hydrate inhibitor, VCap. Their efficacy was able to be evaluated with the holistic investigation on nucleation and growth of hydrate phase in the liquid phase.

Chapter 8 CORROSION MEASURMENT

8.1 Introduction

This chapter investigates the corrosion inhibition performance of a systematic library of PVCap-based KHCI polymers following the evaluation of the hydrate inhibition property discussed in the previous chapters. Weight-loss measurement, and linear polarization resistance (LPR) measurements were conducted. The results acquired from the two different methods are variable to some extent, however, they reveal that the specific key structure that plays a role in contributing corrosion inhibition property of a KHCI polymer. Moreover, its corresponding compatibility that is with a KHI functionality moiety, is valuable to decipher the structure-property relationship when designing a multifunctional polymer.

8.2 Materials and methods

8.2.1 Materials

Hydrochloric acid (HCL, ≥ 30%) and Sea salts were purchased from Sigma Aldrich. Novel KHCIs including: PVCap-co-AA; PVCap-taurine-20, PVCap-taurine(18)-C_{12}, PVCap-taurine(18)-diaminoC_{12}; PVCap-ATCH-20, PVCap-ATCH(18)-C_{12}, PVCap-ATCH(18)-diaminoC_{12}; PVCap-APIM-20, PVCap-APIM(18)-C_{12}, PVCap-APIM(18)-diaminoC_{12}; PVCap-AMPA-20, PVCap-AMPA(18)-C_{12}, PVCap-AMPA(18)-diaminoC_{12} were synthesized in-house (Chapter 5) and were tested for corrosion inhibition performance.

8.2.2 Corrosion weight-loss measurement

Carbon steel coupons were (12 mm in diameter and 1 mm in thickness) polished and then washed with water and ethanol prior to rinsing and drying with distilled water. The coupons were then exposed to 10 ml 2 M HCl with or without 500 ppm (0.05 wt %) polymer for 120 h in open glass vials. At specific time intervals, the coupons were withdrawn from the solutions and weighted after being rinsed by ethanol and

distilled water. The immersion tests were repeated 5 times to test the reproducibility. It is important to note that this method may not remove mineral scale or corrosion deposits on the surface of the coupons. It is a method to assess the performance of inhibitors relative to others.

8.2.3 Electrochemical measurements

The electrochemical tests were performed using rotating cylinder electrode (RCE) test setup in a three-electrode system. The carbon steel rotating cylinder electrode (RCE) was used as the working electrode (WE). A platinum mesh electrode was used as a counter electrode (CE) and a silver-silver chloride electrode (Ag/AgCl) 3.5 M was used as a reference electrode (RE). After the initial de-aeration of the test solution with CO_2, the carbon steel cylinder (WE) was immersed in the test solution and rotated at 1000 rpm, which is equivalent to about 3 Pa wall shear stress. Each test was repeated at least twice to ensure reproducibility of the results.

Electrochemical measurements were commenced by monitoring open circuit potential (OCP) for 15 minutes in sea water using VMP3 Multi-channel potentiostat (Bio-Logic Science Instruments). Then, the blank corrosion rate of each experiment was measured for 80 minutes with 20 minutes interval using linear polarization resistance technique (LPR). This was to make sure that the blank corrosion rate is reproducible in all experiments. Potential range was ± 10 mV vs OCP at a scan rate of 0.167 mV/s.

After 80 minutes of baseline corrosion rate measurement, the inhibitor was added and the LPR corrosion rate was continuously measured. The polymer solution was prepared beforehand in 5 ml of water to ensure it was fully dissolved and then injected into the bulk solution. The corrosion rate was monitored for another 400 minutes.

The corrosion current densities were calculated from the estimated polarization resistance (R_p) obtained from the slope of the applied potential and the resulting current density curve ($\Delta E/\Delta i$). The measured R_p value is inversely related to the corrosion current density through the Stern-Geary Equation:

$i_{corr} = B/R_p$

where R_p is the polarization resistance obtained from the LPR plot in Ohm.

B is the empirical polarization resistance constant. The estimated B value in this work is 26 mV/decade of current.

i_{corr} is the corrosion current density in A/cm^2.

The corrosion rate in mm/y is then determined from the estimated corrosion current densities (i_{corr}) using following equation:

$$\mathrm{CR}\left(\frac{\mathrm{mm}}{\mathrm{yr}}\right) = 3.27\ 10^6 \text{ x icorr x Ew/d}$$

where i_{corr} is the corrosion current density in A/cm^2, Ew is the equivalent weight of 1030 carbon steel in g/equivalent and d is the density in g/cm^3 of 1030 carbon steel.

The % inhibition efficiency (IE) from LPR test results was calculated using the following equation:

$$\mathrm{IE\%} = \frac{i_{corr}(\mathrm{uninhibited}) - i_{corr}(\mathrm{inhibited})}{i_{corr}(\mathrm{uninhibited})} \times 100$$

where i_{corr} (uninhibited) and i_{corr}(inhibitor) are the corrosion current densities in μA/cm^2 from the non-inhibited and inhibitor-containing test solution, respectively.

The 1 litre of test solution was prepared by dissolving 4 w/v% sea salt (composition listed in Table 8.1) in ultra-pure water (Mili-Q system, resistivity 18.2 MΩ. cm). In the inhibited tests corrosion inhibitors were added in the concentration of 200 ppm (ppm by weight). CO_2 gas (oxygen content <10ppb) was used at atmospheric pressure to saturate the test solution for at least two hours prior to the immersion of the test

specimen. The gas was continuously sparged into the solution during the experiment to keep the system deaerated. All the experiments were carried out at ambient temperature.

1030 grade carbon steel cylinders were machined from parent rod material with an area of approximately 3 cm^2. Chemical composition of the test material is given in Table 8.2. Prior to each experiment, carbon steel cylinders were polished with silicon carbide (SiC) paper to 600-grit. The test sample was degreased and sonicated in ethanol, dried with nitrogen and mounted on the specimen holder.

Table 8. 1 Sea salt composition (Sigma Aldrich) (Kadiri, 2010)

Components	**Concentration (mg/L)**
Chloride	19290
Sodium	10780
Sulphate	2660
Magnesium	1320
Potassium	420
Calcium	400
Carbonate	200
Boron	5.6
Bromide	56
Iodide	0.24
Fluoride	1.0

Table 8. 2 Chemical composition by weight % of cylindrical specimen used in this study.

Element	C	Mn	P	Si	S	Ni	Mo	Cr	Mo	Sn	Al	Fe
Content (wt %)	0.37%	0.80%	0.012%	0.28%	0.001%	0.012%	0.004%	0.098%	0.004%	0.004%	0.01%	balance

8.3 Results and discussion

8.3.1 Corrosion performance as measured by weight loss

Weight loss measurements for metal coupons in a corrosive fluid were used to rank the performance of KHCI polymers as corrosion inhibitors. The inhibition efficiency of the polymers was determined by many factors such as the solution composition, temperature, structure, and dosage being used. A 2 M HCL solution was used as extreme acidic environment to rapidly assess the polymer to identify leading structures because without any inhibitor this resulted in 18.1% weight loss. While oxygen containing HCl is not representative of actual pipeline conditions, where the fluid would contain CO_2 and possibly hydrogen sulphide, hydrochloric acid is sufficiently aggressive to result in significant corrosion without any inhibitor. The mechanism of corrosion inhibition should still be due to film formation. The concentration used was 500 ppm (0.05 wt %) at which the solution of surfactant-like inhibitors (C_{12}-based polymers) should achieve the maximum efficiency according to the critical micellar concentration theory. As known the surface coverage does not increase when a certain concentration is reached so the monolayer, micelle, or multilayers will form (Free, 2002; Jovancicevic et al., 1999).

Figure 8.1 shows the weight loss percentage of carbon steel coupons with different KHCI polymers under the same conditions. A significant reduction of weight loss was observed for the developed inhibitors compared to the case without inhibitor or PVCap without corrosion groups. The weight loss % of the best performing polymer APIM C_{12} in the test was 0.62 wt % compared to 18.12 wt % for the control. PolyVCap (shown in black) was also included as a known KHI and this demonstrated some corrosion inhibition which can be attributed to the nitrogen containing caprolactam ring which could be absorbing on the metal surface. The green column represents APIM-based modified polymers which appear to be the optimal anticorrosion inhibitors, though the ATCH-based modified polymers are also promising. APIM C_{12} therein reaches the maximum protection for the carbon steel. This can be explained by multifunctional action of the surfactant-like polymer APIM C_{12} which contains a metallo-philic head and hydrophobic side chain. The imidazole ring contains three possible anchoring sites that are active for bonding: pyridine like nitrogen atom, pyrrole like nitrogen atom, and aromatic ring (Zhang et al., 2009) that provide stable

physical absorption with metal surface. This in combination with a long hydrophobic chain that promotes polymer self-association above its CMC can assist to retard corrosion. APIM diaminoC_{12} by contrast is more effective than APIM but less effective than APIM C_{12}, this may be attributed to the surface competition between imidazole and amine head.

In the case of ATCH C_{12}, ATCH diaminoC_{12}, taurine C_{12}, and AMPA C_{12} the performance was not improved. This may be due to the hydrocarbon side chain changing the steric conformation of the polymer to hinder the absorption process of the active centre. Another possibility for Taurine C_{12} and AMPA C_{12} could be that low cloud points of these two KHCIs occurred after being applied in acidic environment. In general, AMPA modified polymers perform relatively better than those modified with Taurine which is in good agreement with the prediction that inhibition efficiency should be in the order: S < P regarding very similar structure (alkyl chain length) (Hoseinzadeh et al., 2014). This accelerated corrosion test is a relative comparison between inhibitors which are compared to controls without inhibitor and further corrosion testing should also be carried out. Therefore, additional corrosion testing such as polarization, impedance (EIS) needs to be carried out.

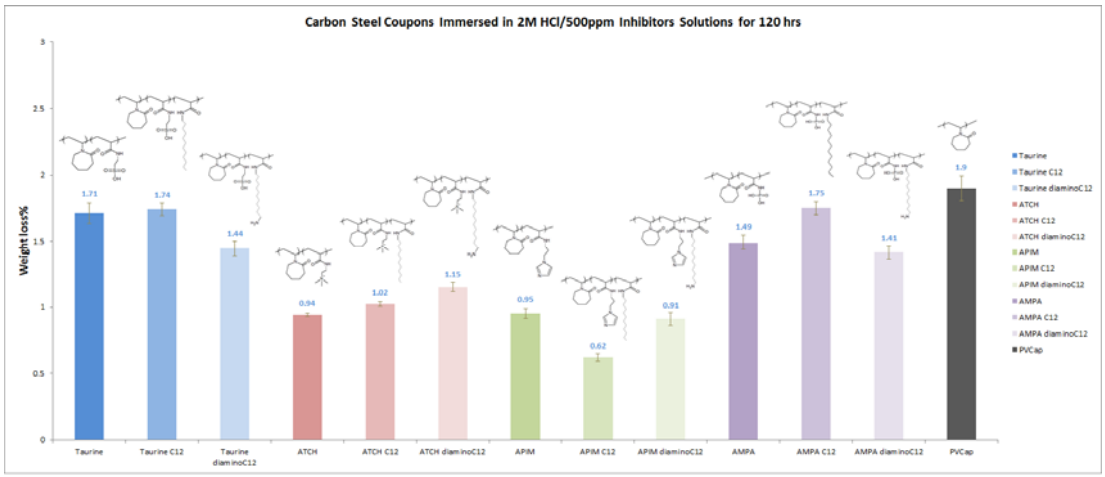

Figure 8. 1 Weight loss percentage of carbon steel in 2 M HCl in the presence of different polymers. Weight loss % of the blank coupon was 18.12% (Sheng et al., 2017).

8.3.2 KHCIs evaluated by LPR

The corrosion of carbon steel in the presence of novel KHCIs has been further investigated by linear polarization resistance measurement. KHCIs that contain same domain corrosion inhibitors have been shown in Figure 8.2-8.5 respectively. The graph presenting a relationship between inhibition efficiency IE (%) and time (min) was plotted according to calculated data including values of R_p (Ohm), i_{corr} (µA/cm2) and CR (mm/yr). A significant change in terms of corrosion inhibition efficiency can be observed after the addition of inhibitors. The highest inhibition efficiency among all of the KHCIs was 88.67% by PVCap-APIM(18)-C_{12}(2) and the performance of PVCap-ATCH(18)-C_{12}(2) was comparable at an efficiency of 88.07%, which is reasonably in good agreement with the result from weight-loss screen. Table 8.2 summarizes the overall performance of KHCIs in LPR measurement.

Table 8. 3 Ranking of all KHCIs in the Gravimetric screen and linear polarization measurement arranged in descending order.

Gravimetric screen KHCI Polymer (500ppm)	**LPR measurement KHCI Polymer (200ppm)**	**Inhibition Efficiency % (Read at 500mins)**
PVCap-APIM(18)-C_{12}(2)	PVCap-APIM(18)-C_{12}(2)	88.7
PVCap-APIM(18)-diaminoC_{12}(2)	PVCap-ATCH(18)-C_{12}(2)	88.1
PVCap-ATCH(20)	PVCap-Taurine(18)-C_{12}(2)	83.8
PVCap-APIM(20)	PVCap-APIM(18)-diaminoC_{12}(2)	83.0
PVCap-ATCH(18)-C_{12}(2)	PVCap-Taurine(18)-diaminoC_{12}(2)	68.0
PVCap-ATCH(18)-diaminoC_{12}(2)	PVCap-AMPA(18)-diaminoC_{12}(2)	59.8

PVCap-AMPA(18)-diaminoC$_{12}$(2)	PVCap-AMPA(18)-C$_{12}$(2)	36.6
PVCap-Taurine(18)-diaminoC$_{12}$(2)	PVCap-ATCH(20)	28.9
PVCap-AMPA-20	PVCap-APIM(20)	26.2
PVCap-taurine(20)	PVCap-AMPA-20	7.1
PVCap-Taurine(18)-C$_{12}$(2)	PVCap-ATCH(18)-diaminoC$_{12}$(2)	-0.9
PVCap-AMPA(18)-C$_{12}$(2)	PVCap-taurine(20)	-7.1

8.3.2.1 Effect of structure

The mode of action of KHCIs can be described in two steps: (1) the adsorption of functional moiety on the metal surface (2) and followed by the retardation of cathodic and/ or anodic electrochemical corrosion reactions. The initial step ascribes to the presence of heteroatoms such as nitrogen, sulfur, oxygen, phosphorus and aromatic rings. These 'active centers' exhibiting strong affinity for the metal surface can adsorb on the metal simultaneously by displacing water molecules on the surface and providing a film barrier to the dissolution of metal in electrolyte (Arthur et al., 2013; Dariva and Galio, 2014). The transferring of lone pairs of electrons from the inhibitor to metal leads to the forming of chemisorption bond as well as the coordinate covalent bond. As a result, corrosion was retarded. The efficiency of inhibitor varies a lot and may depend on steric configuration, electron density of donor atoms, type and number of anchor site for bonding (Dariva and Galio, 2014; Gece, 2008) in terms of controlled carbon steel sample and same electrolyte solution.

This can be illustrated by Figure 8.2-8.5, all KHCIs show different inhibition behavior when adding into acidic and brine solution. As the addition of effective inhibitor would cause a decrease in corrosion rate immediately, the plot data started from the addition point which is defined as time zero presented in the figures. In fact, PVCap polymers modified with 20 mol% of taurine, AMPA, ATCH and APIM all exhibited poor inhibition performance in the LPR test which is contrary to the weight-loss

measurement. This is possibly due to high shear stress combined with bubbling CO_2 gas. The severe condition reduces the time window for the contact of interface and thus results in less absorption. Comparatively, despite the more corrosive environment, weight loss measurement was taken under a relatively static condition for absorption which changes the final result. However, simple comparison for PVCap-Tau-20, PVCap-AMPA-20, PVCap-ATCH-20 and PVCap-APIM-20 can still deduce the same ranking as in weight loss measurement that APIM>=ATCH>AMPA=taurine. APIM is among the class of nitrogen-bearing organic compounds with effective corrosion inhibition potential due to the unique electronic π-orbital characters and electron density around their basic N-heteroatoms. These N-heteroatoms serve as active adoption sites where the probability of electron pair transfer to metallic orbitals is high. Simply put, it is composed of a five membered ring containing two nitrogen atoms. This structure provides three possible reactive sites for bonding: pyridine like nitrogen atom, pyrrole like nitrogen atom and aromatic ring whereas ATCH, AMPA, taurine only has one. Moreover, APIM belongs to imidazoles which represent an environmental-friendly class of corrosion inhibitors for pipeline steels (Eduok et al., 2016).

It turned out that PVCap-APIM-20 shown in Figure 8.5 have a highest efficiency in the first place among others though there were a reduction in performance as time went on.

Despite the inhibition efficiency of these four KHCIs was unsatisfactory, significant improvements can be observed with additional long hydrophobic chain in most case except PVCap-ATCH(18)-diaminoC_{12}(2). For instance, in an extreme case of PVCap-tau-20 the general corrosion rate was promoted as shown in Figure 8.2. PVCap-tau-20 drops to negative value from the beginning point of injection whereas the efficiency of PVCap-Tau(18)-C_{12}(2) and PVCap-Tau(18)-diaminoC_{12}(2) rise up to 83.75 % and 67.97% respectively by the end of test. For the case of PVCap-APIM(18)-C_{12}(2) the inclusion of long hydrophobic chain maximized the performance to 88.67% which was the highest efficiency can be observed among all KHCIs. This can be explained by the long hydrophobic tail drives the polymer molecules to the surface as well as acting as extra barrier to water and corrosive environment (Edwards et al., 1994), which stabilizes the polymer molecules for further chemisorption and thus enhances the performance. The effect of C_{12} pendant on performance is superior to C_{12} amine

pendant as can be concluded from Table 8.2 This may due to the surface competition between corrosion inhibitor groups and C_{12} amine head as it can serve as another anchor site to the surface. This can explain why inclusion of C_{12} amine pendant can have an either positive or negative impact on polymers with different steric structures and heteroatoms.

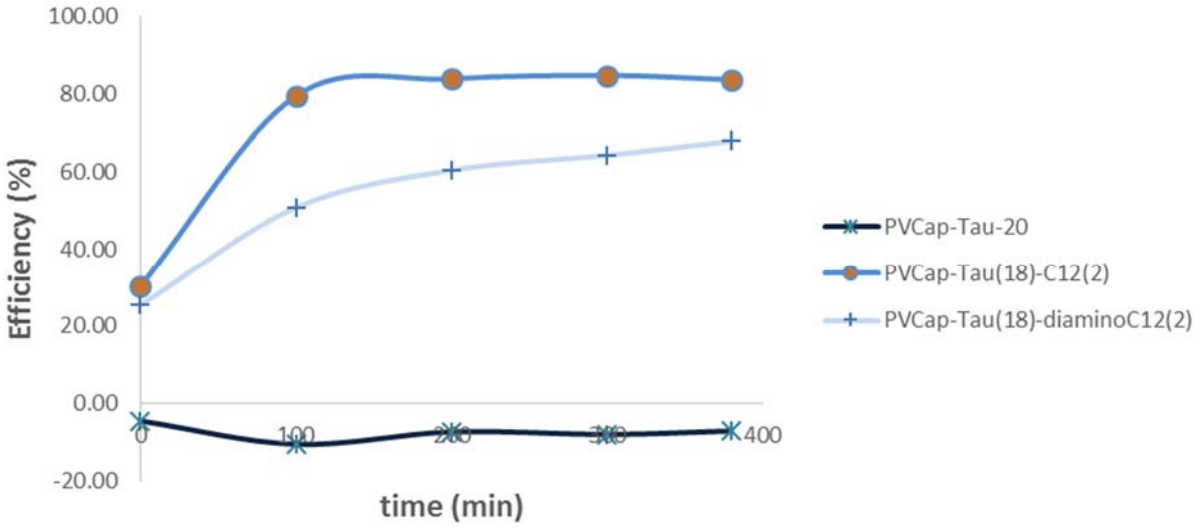

Figure 8. 2 Inhibition efficiency plot of PVCap-Tau-20, PVCap-Tau(18)-C_{12}(2) and PVCap-Tau(18)-DiaminoC_{12}(12) after addition.

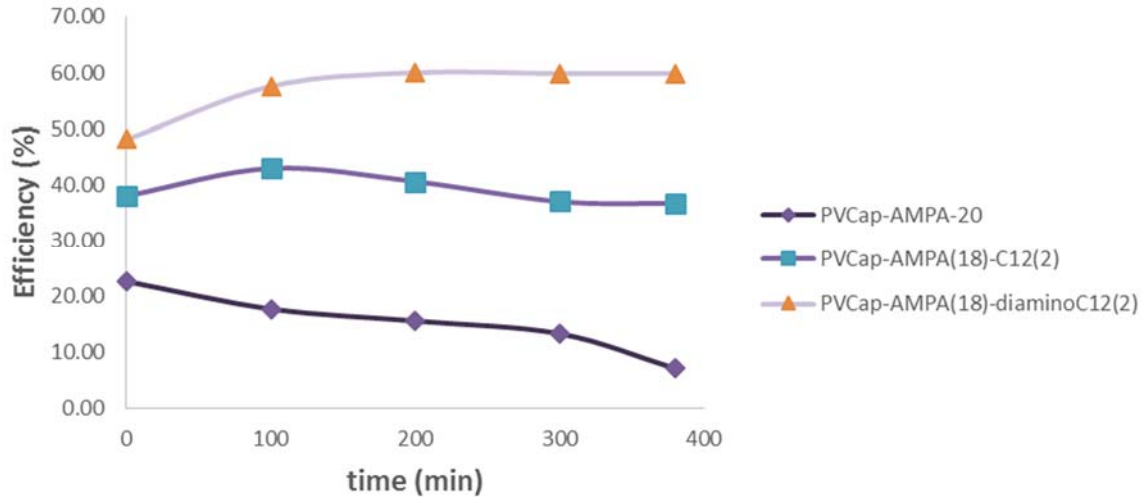

Figure 8. 3 Inhibition efficiency plot of PVCap-AMPA-20, PVCap-AMPA(18)-C_{12}(12) and PVCap-AMPA(18)-DiaminoC_{12}(2) after addition.

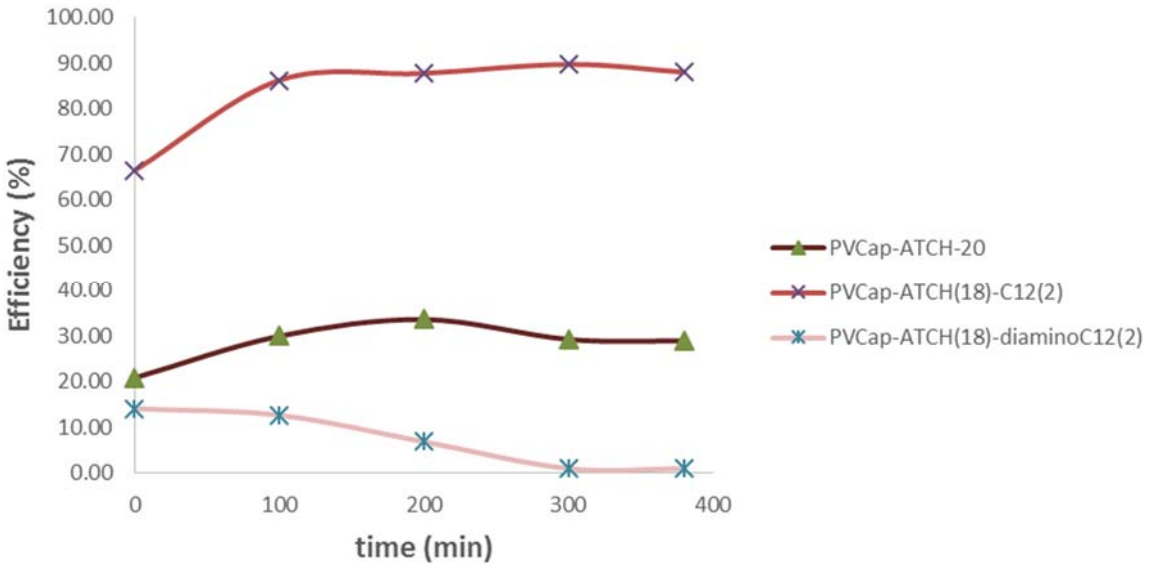

Figure 8. 4 Inhibition efficiency plot of PVCap-ATCH-20, PVCap-ATCH(18)-C_{12}(2) and PVCap-ATCH(18)-DiaminoC_{12}(2) after addition.

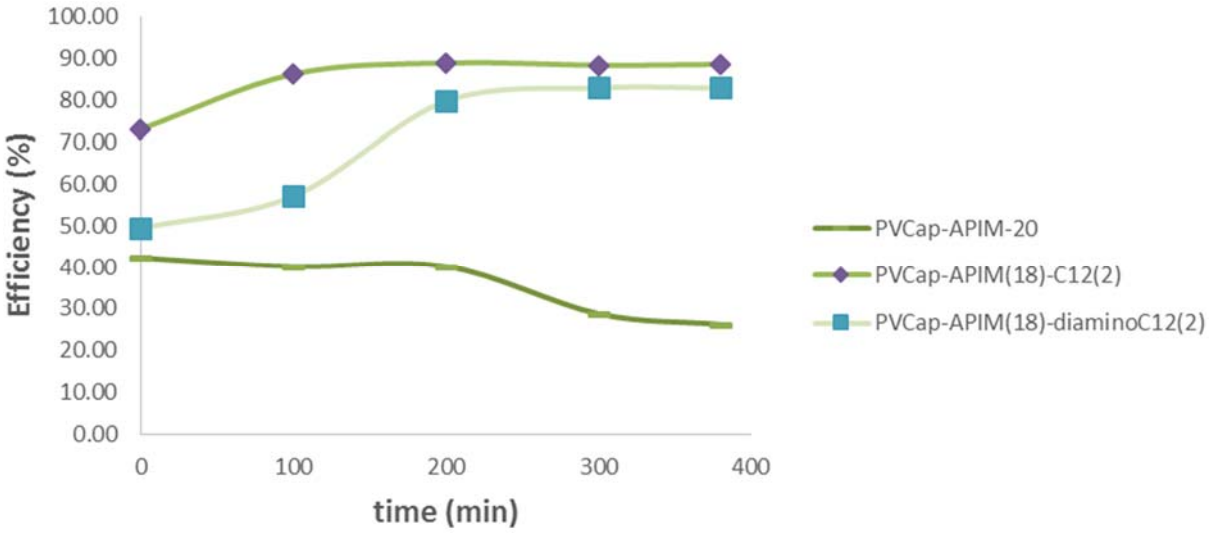

Figure 8. 5 Inhibition efficiency plot of PVCap-APIM-20, PVCap-APIM(18)-C_{12}(2) and PVCap-APIM(18)-DiaminoC_{12}(2) after addition.

8.3.2.2 Effect of time

The performance of KHCIs was evaluated at every 20 mins over the whole test. It is noticeable that the tendency of efficiency is varying with increased immersion time. As observed in Figure 8.2-8.5, most KHCIs reach a relatively high efficiency around

100 min and then there was a divergence of the tendency. In order to distinct the effect of time for absorption, typical tendency plots (Figure 8.6-8.8) were given. Clearly, those without long hydrophobic tail exhibit a significant downtrend afterwards whereas surfactant-like KHCIs went in a slow and steady upward trend until the end of test.

This reveals that the initial step of adsorption may mainly due to physical blockage of PVCap polymer segments and partial chemisorption of corrosion functional groups. As the flow continues, de-adsorption process was promoted and thus performance decreased. For KHCIs with additional long chain pendant, the adsorption process was stabilized and performance increased gradually by the end as the bonding of corrosion inhibitor groups were complete.

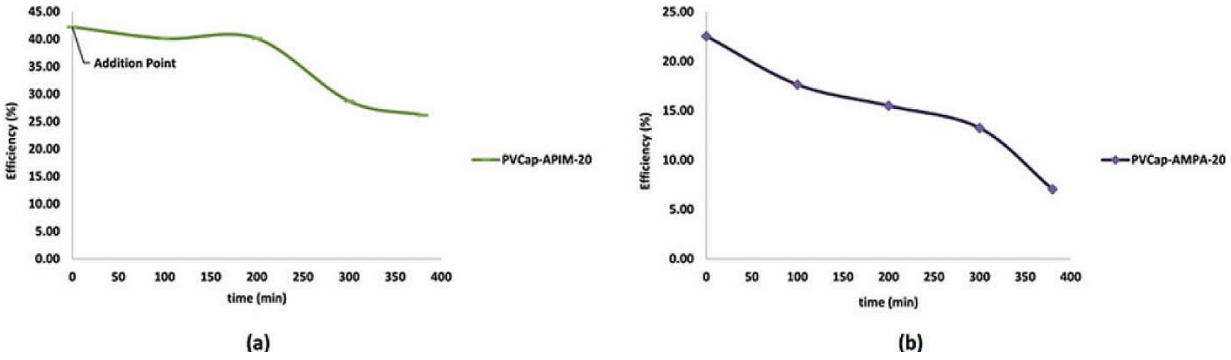

Figure 8. 6 Tendency plot of PVCap-APIM-20 (a), PVCap-AMPA-20 (b) after addition.

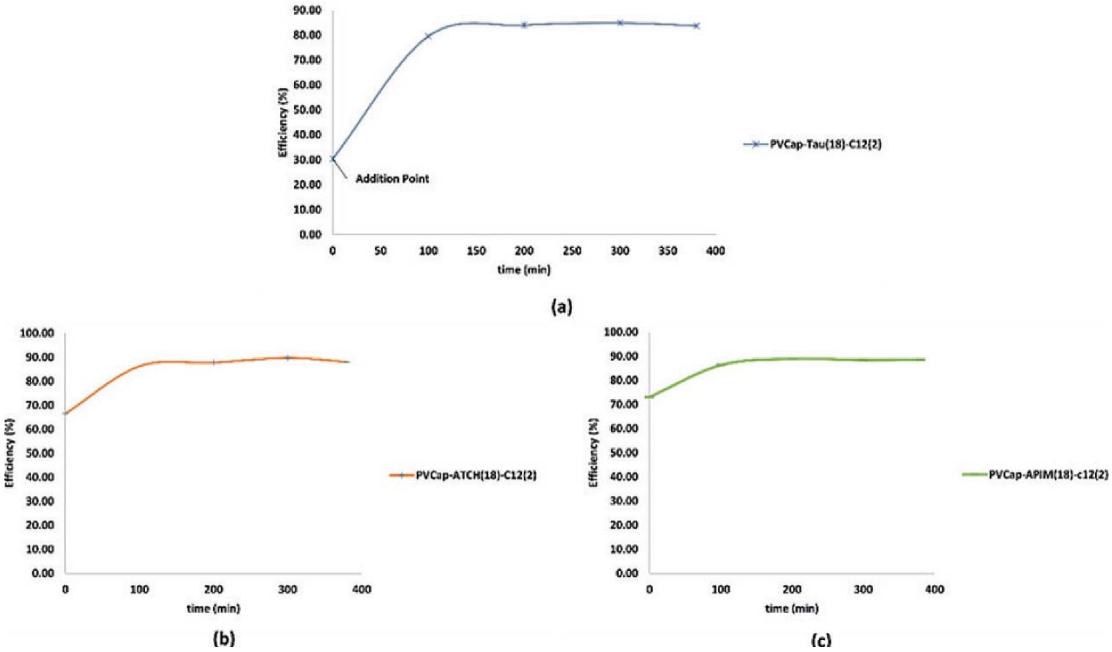

Figure 8. 7 Tendency plot of PVCap-Tau(18)-C_{12}(2) (a), PVCap-ATCH(18)-C_{12}(2) (b), and PVCap-APIM(18)-C_{12}(2) (c) after addition.

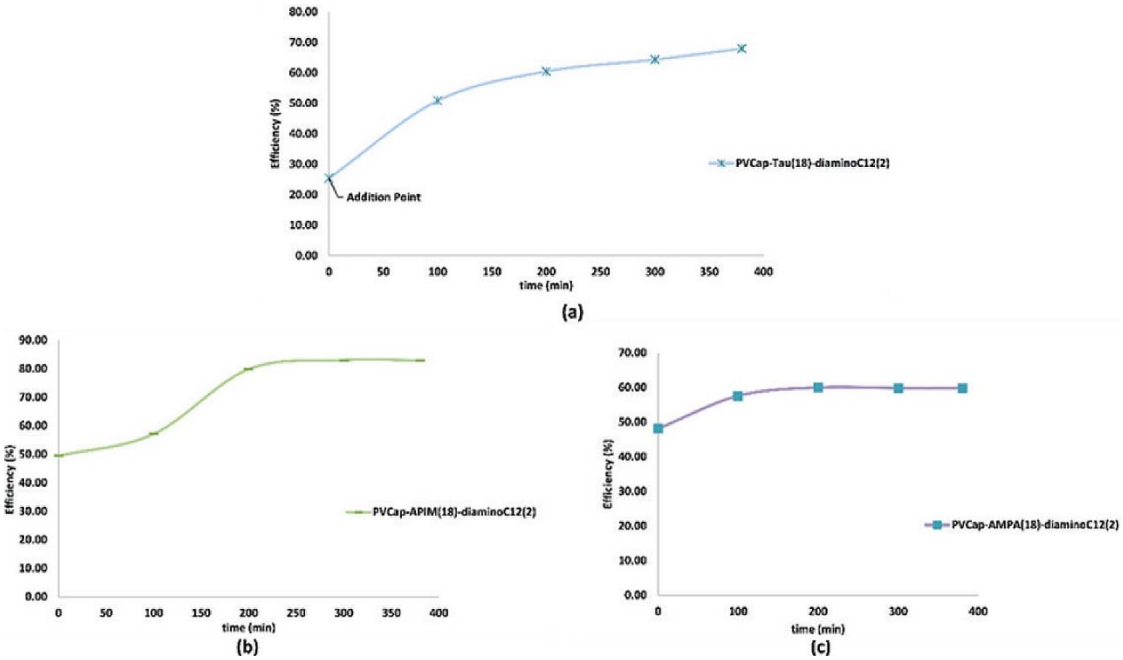

Figure 8. 8 Tendency plot of PVCap-Tau(18)-diaminoC_{12}(2) (a), PVCap-APIM(18)-diaminoC_{12}(2) (b), and PVCap-AMPA(18)-diaminoC_{12}(2) (c) after addition.

8.3.2.3 Effect of concentration

Figure 8.9 illustrates the effect of inhibitor concentration as a function of time by comparing the efficiency of PVCap-APIM-20 and PVCap-APIM(18)-C_{12}(2) at the dosage of 200 ppm and 500 ppm respectively. It has been observed that the inhibition efficiency did not increase with increasing concentration. The final efficiency read at 480 min were virtually the same for both samples, which indicated that the maximum efficiency of these KHCIs was at or less than the dosage of 200 ppm.

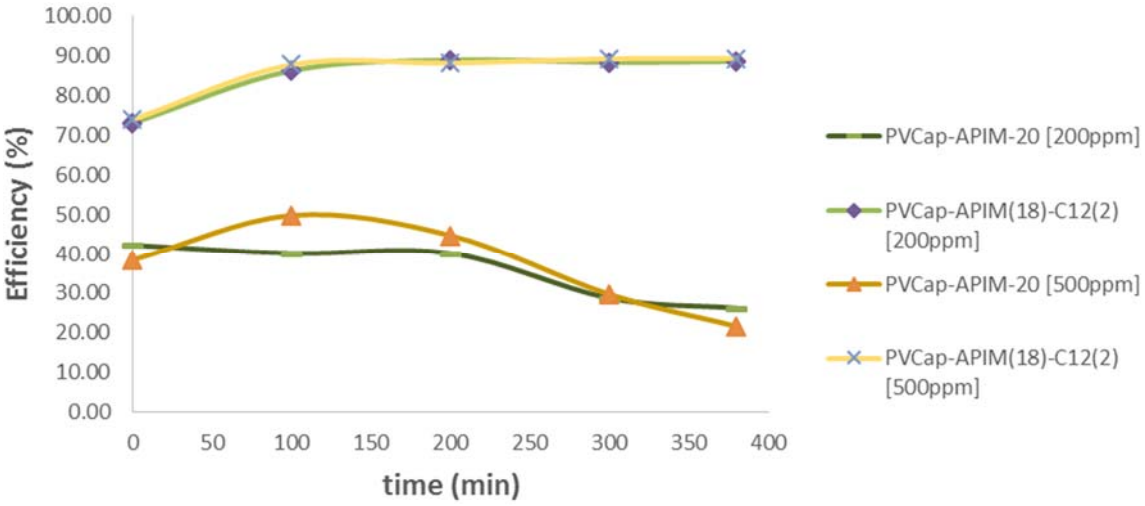

Figure 8. 9 Inhibition efficiency plot of PVCap-APIM-20, PVCap-APIM(18)-C_{12}(2) deployed at 200ppm and 500ppm respectively after addition.

8.4 Conclusions

A library of KHCIs were evaluated using a weight-loss screen and linear polarization measurement. On the whole, the addition of KHCIs results in a reduction in general corrosion rate indicating the success of this proof-of-concept. In most case, all KHCIs with pendant substituents show a dramatically increase in performance than those with merely APIM, ATCH, taurine and AMPA structure. The best candidate among all KHCIs is PVCap-APIM(18)-C_{12}(2) which has a maximum efficiency of 88.67% at 200ppm dosage.

Chapter 9 CONCLUSIONS AND RECOMMANDATIONS

From the studies presented in the previous chapters, the following conclusions are made:

CMC reaction is potent tool to develop and investigate novel materials including but not limited to KHIs, AAs or multifunctional KHCIs for industry. As illustrated in chapter 3, 4 & 5, this high efficient method has been successfully applied to generate libraries of target polymers in respect of modified PAM polymers, modified PNIPAM polymers, and modified PVCap polymers with accurate control of $M_{w,}$ M_w distribution, end groups, and composition. The characterization of NMR, GPC, viscosity, titration, cloud point, and key performances concerning hydrate and corrosion inhibition have been conducted and prove the success of this method, which is more advantageous than traditional free radical polymerization to understanding the fundamental mechanisms of a material in terms of structure-property relationship.

The newly developed HTP hydrate screen is also a worthy highlight. This method realized the time-saving and visualization screen for KHI evaluation, which is indeed a breakthrough compared to traditional KHI ranking method such as rocking cell and autoclaves. HTP hydrate screen allows rapid first hand screen for picking up outstanding KHIs among libraries of polymers. These candidates can be further tested via more rigorous conventional tool, which will be board of interest and boost the development of new materials that are beneficial for oil and gas industry.

As concluded by HTP screen and autoclave testing, PNIPAM-co-AA is an outstanding KHI. When modified with Cyclopent, the kinetic inhibition performance were enhanced at the cooling rate of 0.033 K/ min while modification with C_4t adversely affected the performance. These synthesized PNIPAM-based KHIs presented a high subcooling temperature, which is comparable to those of commercial KHIs. Moreover, modification of the structure of PNIPAM-co-AA can result in steric hindrance in terms of hydrate formation, which can change the polymer structure and also affect the cloud point of the polymer, suggesting the performance of the KHIs can be modulated in terms of hydrate performance and cloud point. PVCap-co-AA is also comparable to

commercial KHIs. At the nucleation stage, the PVCap-co-APIM showed slightly better performance performed than the commercial polymer under slow cooling rates while PVCap-co-ATCH showed the lowest performance. For the growth stages, again, APIM corrosion enhanced the kinetic hydrate inhibition performance. The hydrate fraction increased slowly while maintaining a stable torque. The modification with ATCH adversely affected the kinetic inhibition performance of PVC-based KHI, where the initial growth rate was faster than that of other PVCap-based KHIs and a high hydrate fraction was obtained. This is reasonable because corrosion groups often possess surfactants properties and surfactants have been established to aid hydrate formation. However, this suggests that PVCap-co-ATCH may be possible to work as AAs when the dosage is high.

As shown by weight-loss screening and LPR corrosion measurements, APIM and ATCH corrosion groups exhibit strong corrosion inhibition properties when incorporated into PVCap polymers, and the substitution of C_{12} alkyl chains greatly increases their potential for corrosion inhibition in both test. However, there is a divergence of results that these KHCIs modified with APIM or ATCH performs fairly well in weight loss screen whereas poor performance of them can be observed in LPR, though their performance greatly enhanced with alkyl chain version. This could be due to different acid environment condition, and strong and continuous flow condition that can disrupt the absorption process.

In summary, the results indicate that APIM are the only promising structure for PVCap-based KHCIs, which can balance hydrate and corrosion inhibition well. However, substitution of alkyl chains may be required to be incorporated into the polymer chains, which will adversely affect the hydrate inhibition performance whilst enhancing the corrosion inhibition performance. Apparently, designing single polymer molecules is more complex than blending inhibitors, but the compatibility issues that are often encountered between KHIs and CIs when mixed warrants to further research this approach.

Based on our findings our recommendation for future work would be:

1. Using CMC reaction as a tool for symmetrically study on libraries of new materials.
2. Applying HTP hydrate screen as the first screen for all newly developed KHIs.
3. APIM structure is promising structure that can well enhance the hydrate inhibition of VCap and impart corrosion inhibition properties in the meantime, which is capable of overcoming the compatibility issue. However, a small percentage of synergistic structure (preferable avoiding long alkyl chain) is required to work with APIM, and VCap functional moiety to reach the maximum corrosion inhibition efficiency.

APPENDIX OF COPYRIGHT FORMS

Copyright information related to;

Libraries of modified polyacrylamides using post-synthetic modification

By: Kelly Cristine da Silveira; Qi Sheng; Wendy Tian; et al. JOURNAL OF APPLIED POLYMER SCIENCE Volume: 132 Issue: 47 Article Number: 42797 Published: DEC 15 2015

JOHN WILEY AND SONS LICENSE TERMS AND CONDITIONS

Feb 22, 2018

This Agreement between Mr. QI SHENG ("You") and John Wiley and Sons ("John Wiley and Sons") consists of your license details and the terms and conditions provided by John Wiley and Sons and Copyright Clearance Center.

License Number	4294010754383
License date	Feb 22, 2018
Licensed Content Publisher	John Wiley and Sons
Licensed Content Publication	Journal of Applied Polymer Science
Licensed Content Title	Libraries of modified polyacrylamides using post-synthetic modification
Licensed Content Author	Kelly Cristine da Silveira,Qi Sheng,Wendy Tian,Elizabete Fernandes Lucas,Colin D. Wood
Licensed Content Date	Aug 28, 2015
Licensed Content Pages	1
Type of use	Dissertation/Thesis
Requestor type	Author of this Wiley article
Format	Print and electronic
Portion	Full article
Will you be translating?	No
Title of your thesis / dissertation	Designing Single Polymer Molecules as Gas Hydrate and Corrosion Inhibitors
Expected completion date	Feb 2018
Expected size (number of pages)	200
Requestor Location	Mr. QI SHENG 16 SOUTHDOWN AVE GLEN WAVERLEY, VIC 3150

Copyright information related to;

High-throughput Testing of Kinetic Hydrate Inhibitors

By: Nobuo Maeda; Celesta Fong; Qi Sheng; et al. ENERGY FUELS Volume: 30 Issue: 7 Published: JUL 13 2016

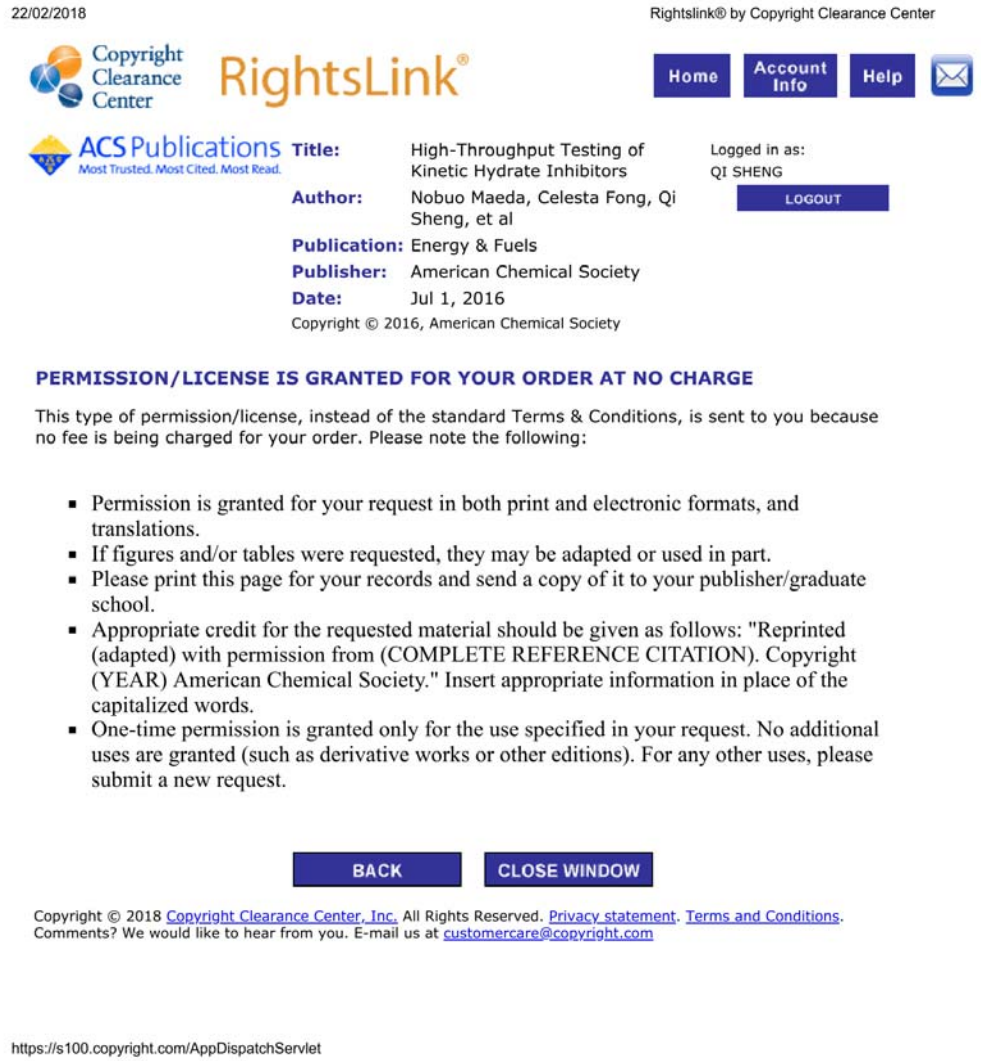

22/02/2018 Rightslink® by Copyright Clearance Center

Copyright Clearance Center RightsLink®

Home | Account Info | Help

ACS Publications Most Trusted. Most Cited. Most Read.

Title: High-Throughput Testing of Kinetic Hydrate Inhibitors

Author: Nobuo Maeda, Celesta Fong, Qi Sheng, et al

Publication: Energy & Fuels

Publisher: American Chemical Society

Date: Jul 1, 2016

Copyright © 2016, American Chemical Society

Logged in as: QI SHENG

LOGOUT

PERMISSION/LICENSE IS GRANTED FOR YOUR ORDER AT NO CHARGE

This type of permission/license, instead of the standard Terms & Conditions, is sent to you because no fee is being charged for your order. Please note the following:

- Permission is granted for your request in both print and electronic formats, and translations.
- If figures and/or tables were requested, they may be adapted or used in part.
- Please print this page for your records and send a copy of it to your publisher/graduate school.
- Appropriate credit for the requested material should be given as follows: "Reprinted (adapted) with permission from (COMPLETE REFERENCE CITATION). Copyright (YEAR) American Chemical Society." Insert appropriate information in place of the capitalized words.
- One-time permission is granted only for the use specified in your request. No additional uses are granted (such as derivative works or other editions). For any other uses, please submit a new request.

BACK | CLOSE WINDOW

Copyright © 2018 Copyright Clearance Center, Inc. All Rights Reserved. Privacy statement. Terms and Conditions.
Comments? We would like to hear from you. E-mail us at customercare@copyright.com

https://s100.copyright.com/AppDispatchServlet

Copyright information related to;

High throughput synthesis and characterization of PNIPAM-based kinetic hydrate inhibitors

By: Kelly Cristine da Silveira; Qi Sheng; Wendy Tian; et al. FUEL Volume: 188 Pages: 522-529 Published: JAN 15 2017

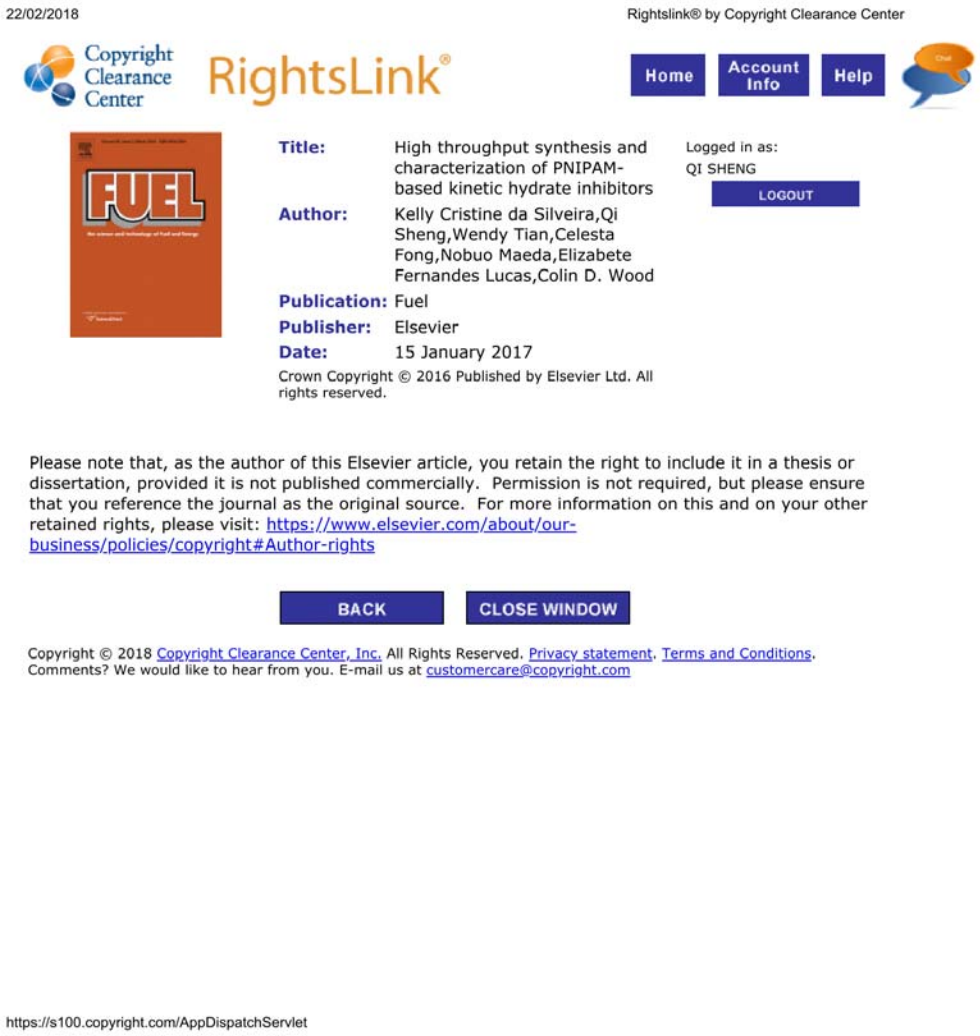

22/02/2018 Rightslink® by Copyright Clearance Center

Copyright Clearance Center RightsLink®

Home | Account Info | Help

Title: High throughput synthesis and characterization of PNIPAM-based kinetic hydrate inhibitors

Author: Kelly Cristine da Silveira,Qi Sheng,Wendy Tian,Celesta Fong,Nobuo Maeda,Elizabete Fernandes Lucas,Colin D. Wood

Publication: Fuel

Publisher: Elsevier

Date: 15 January 2017

Crown Copyright © 2016 Published by Elsevier Ltd. All rights reserved.

Logged in as: QI SHENG

LOGOUT

Please note that, as the author of this Elsevier article, you retain the right to include it in a thesis or dissertation, provided it is not published commercially. Permission is not required, but please ensure that you reference the journal as the original source. For more information on this and on your other retained rights, please visit: https://www.elsevier.com/about/our-business/policies/copyright#Author-rights

BACK CLOSE WINDOW

Copyright © 2018 Copyright Clearance Center, Inc. All Rights Reserved. Privacy statement. Terms and Conditions. Comments? We would like to hear from you. E-mail us at customercare@copyright.com

https://s100.copyright.com/AppDispatchServlet

Copyright information related to;

Simultaneous Hydrate and Corrosion Inhibition with Modified Poly(vinyl caprolactam) Polymers

By: Qi Sheng; Kelly Cristine da Silveira; Wendy Tian; et al. ENERGY FUELS Volume 31 Issue: 7 Pages 6721-6731 Published: June 20 2017

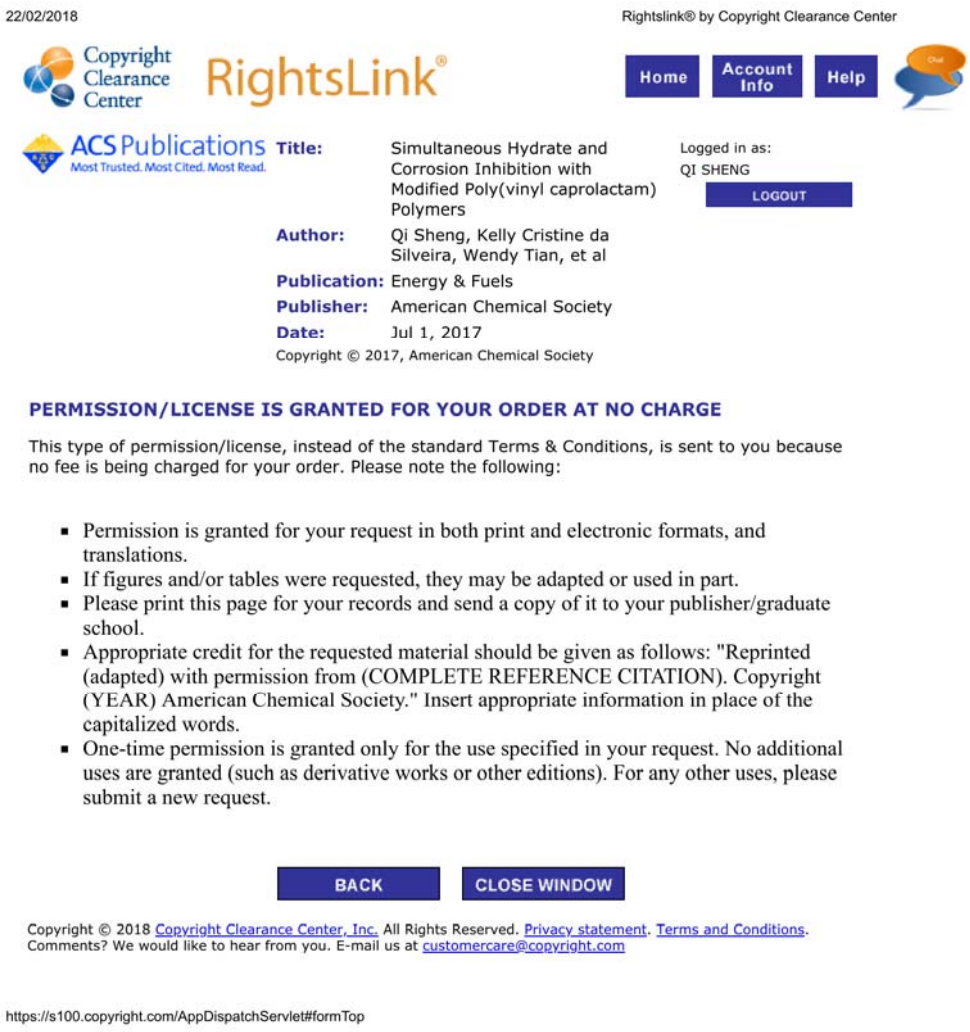

22/02/2018 Rightslink® by Copyright Clearance Center

Copyright Clearance Center RightsLink®

Home | Account Info | Help

ACS Publications Most Trusted. Most Cited. Most Read.

Title: Simultaneous Hydrate and Corrosion Inhibition with Modified Poly(vinyl caprolactam) Polymers

Author: Qi Sheng, Kelly Cristine da Silveira, Wendy Tian, et al

Publication: Energy & Fuels

Publisher: American Chemical Society

Date: Jul 1, 2017

Copyright © 2017, American Chemical Society

Logged in as: QI SHENG

LOGOUT

PERMISSION/LICENSE IS GRANTED FOR YOUR ORDER AT NO CHARGE

This type of permission/license, instead of the standard Terms & Conditions, is sent to you because no fee is being charged for your order. Please note the following:

- Permission is granted for your request in both print and electronic formats, and translations.
- If figures and/or tables were requested, they may be adapted or used in part.
- Please print this page for your records and send a copy of it to your publisher/graduate school.
- Appropriate credit for the requested material should be given as follows: "Reprinted (adapted) with permission from (COMPLETE REFERENCE CITATION). Copyright (YEAR) American Chemical Society." Insert appropriate information in place of the capitalized words.
- One-time permission is granted only for the use specified in your request. No additional uses are granted (such as derivative works or other editions). For any other uses, please submit a new request.

BACK CLOSE WINDOW

Copyright © 2018 Copyright Clearance Center, Inc. All Rights Reserved. Privacy statement. Terms and Conditions.
Comments? We would like to hear from you. E-mail us at customercare@copyright.com

https://s100.copyright.com/AppDispatchServlet#formTop

Copyright information related to;

Performance of Poly(N-isopropylacrylamide)-Based Kinetic Hydrate Inhibitors for Nucleation and Growth of Natural Gas Hydrates

By: Juwoon Park; Kelly Cristine da Silveira; Qi Sheng; et al. ENERGY FUELS Volume: 31 Issue: 3 Pages: 2697-2704 Published: Feb 20 2017

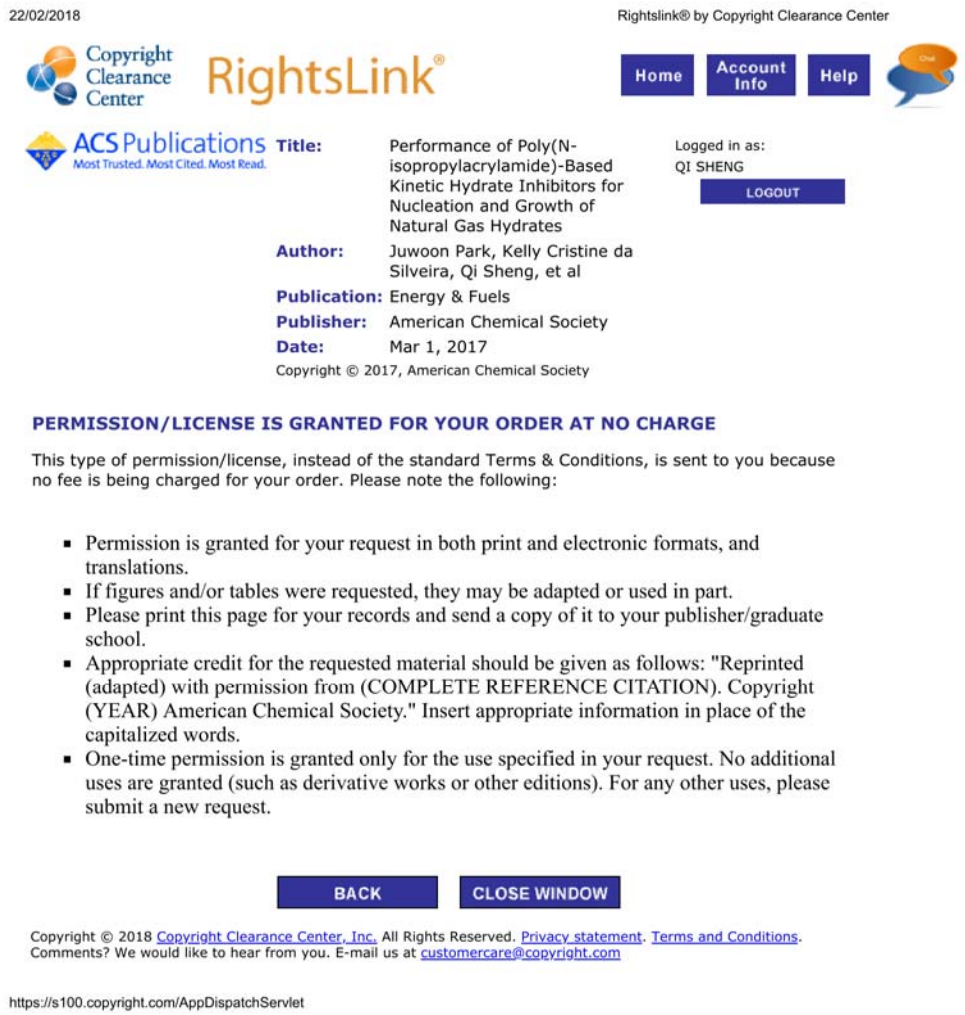

22/02/2018 Rightslink® by Copyright Clearance Center

Copyright Clearance Center RightsLink®

Home | Account Info | Help

ACS Publications Most Trusted. Most Cited. Most Read.

Title: Performance of Poly(N-isopropylacrylamide)-Based Kinetic Hydrate Inhibitors for Nucleation and Growth of Natural Gas Hydrates

Author: Juwoon Park, Kelly Cristine da Silveira, Qi Sheng, et al

Publication: Energy & Fuels

Publisher: American Chemical Society

Date: Mar 1, 2017

Copyright © 2017, American Chemical Society

Logged in as: QI SHENG

LOGOUT

PERMISSION/LICENSE IS GRANTED FOR YOUR ORDER AT NO CHARGE

This type of permission/license, instead of the standard Terms & Conditions, is sent to you because no fee is being charged for your order. Please note the following:

- Permission is granted for your request in both print and electronic formats, and translations.
- If figures and/or tables were requested, they may be adapted or used in part.
- Please print this page for your records and send a copy of it to your publisher/graduate school.
- Appropriate credit for the requested material should be given as follows: "Reprinted (adapted) with permission from (COMPLETE REFERENCE CITATION). Copyright (YEAR) American Chemical Society." Insert appropriate information in place of the capitalized words.
- One-time permission is granted only for the use specified in your request. No additional uses are granted (such as derivative works or other editions). For any other uses, please submit a new request.

BACK CLOSE WINDOW

Copyright © 2018 Copyright Clearance Center, Inc. All Rights Reserved. Privacy statement. Terms and Conditions.
Comments? We would like to hear from you. E-mail us at customercare@copyright.com

https://s100.copyright.com/AppDispatchServlet

Copyright information related to;

Kinetic Hydrate Inhibition Performance of Poly(Vinyl Caprolactam) Modified with Corrosion Inhibitor Groups

By: Juwoon Park; Hyunho Kim; Qi Sheng; et al. ENERGY FUELS Volume: 31 Issue: 9 Pages: 9363-9373

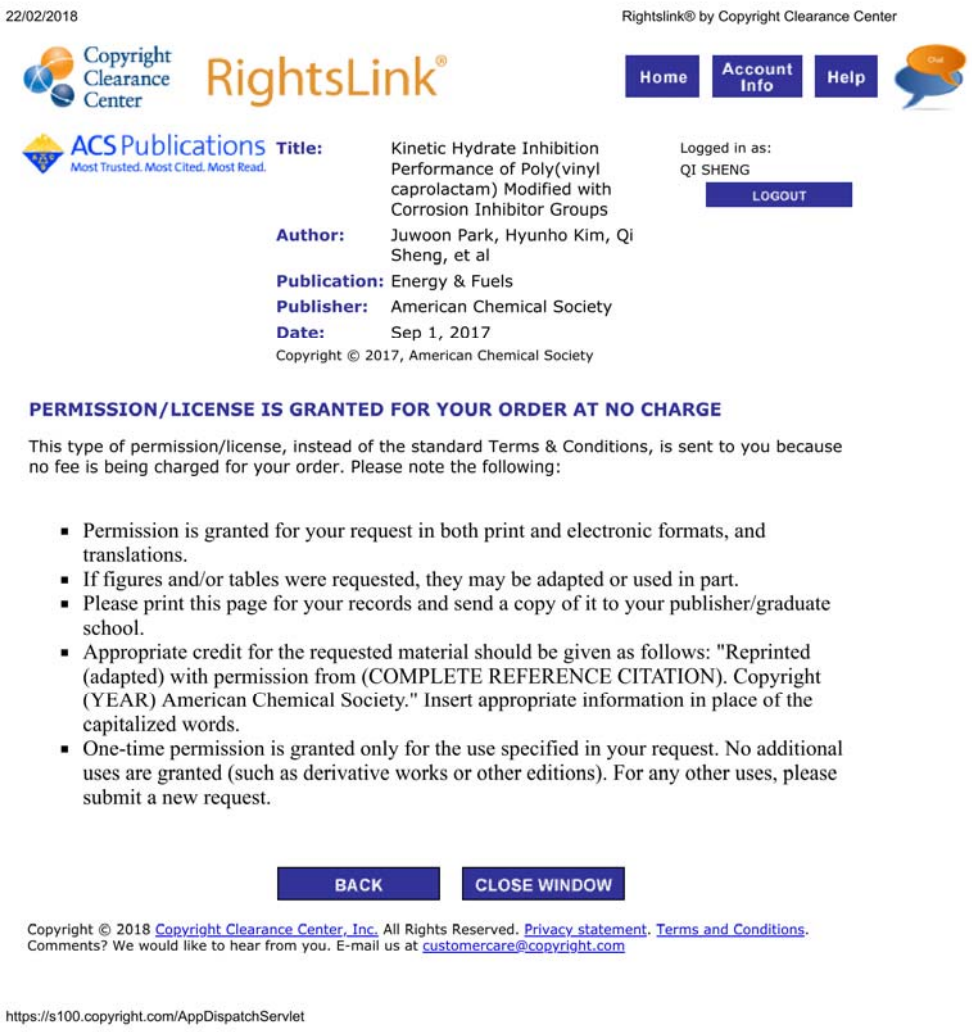

22/02/2018 Rightslink® by Copyright Clearance Center

Copyright Clearance Center RightsLink®

Home | Account Info | Help

ACS Publications Most Trusted. Most Cited. Most Read.

Title: Kinetic Hydrate Inhibition Performance of Poly(vinyl caprolactam) Modified with Corrosion Inhibitor Groups

Author: Juwoon Park, Hyunho Kim, Qi Sheng, et al

Publication: Energy & Fuels

Publisher: American Chemical Society

Date: Sep 1, 2017

Copyright © 2017, American Chemical Society

Logged in as: QI SHENG

LOGOUT

PERMISSION/LICENSE IS GRANTED FOR YOUR ORDER AT NO CHARGE

This type of permission/license, instead of the standard Terms & Conditions, is sent to you because no fee is being charged for your order. Please note the following:

- Permission is granted for your request in both print and electronic formats, and translations.
- If figures and/or tables were requested, they may be adapted or used in part.
- Please print this page for your records and send a copy of it to your publisher/graduate school.
- Appropriate credit for the requested material should be given as follows: "Reprinted (adapted) with permission from (COMPLETE REFERENCE CITATION). Copyright (YEAR) American Chemical Society." Insert appropriate information in place of the capitalized words.
- One-time permission is granted only for the use specified in your request. No additional uses are granted (such as derivative works or other editions). For any other uses, please submit a new request.

BACK CLOSE WINDOW

Copyright © 2018 Copyright Clearance Center, Inc. All Rights Reserved. Privacy statement. Terms and Conditions.
Comments? We would like to hear from you. E-mail us at customercare@copyright.com

https://s100.copyright.com/AppDispatchServlet

REFERENCES

Abdurrahmanoglu, S., Can, V., & Okay, O. (2009). Design of high-toughness polyacrylamide hydrogels by hydrophobic modification. *Polymer, 50*(23), 5449-5455.

Ahmad, H. (1982). Solubility parameter of acrylamide series polymers through its components and group contribution technique. *Journal of Macromolecular Science—Chemistry, 17*(4), 585-600.

Akhfash, M., Boxall, J. A., Aman, Z. M., Johns, M. L., & May, E. F. (2013). Hydrate formation and particle distributions in gas–water systems. *Chemical Engineering Science, 104*, 177-188.

Al-Sabagh, A. M., Nasser, N. M., Farag, A. A., Migahed, M. A., Eissa, A. M., & Mahmoud, T. (2013). Structure effect of some amine derivatives on corrosion inhibition efficiency for carbon steel in acidic media using electrochemical and quantum theory methods. *Egyptian Journal of Petroleum, 22*(1), 101-116.

Al-Warhi, T. I., Al-Hazimi, H. M., & El-Faham, A. (2012). Recent development in peptide coupling reagents. *Journal of Saudi Chemical Society, 16*(2), 97-116.

AlHarooni, K., Pack, D., Iglauer, S., Gubner, R., Ghodkay, V., & Barifcani, A. (2017). Effects of thermally degraded monoethylene glycol with methyl diethanolamine and film-forming corrosion inhibitor on gas hydrate kinetics. *Energy & Fuels, 31*(6), 6397-6412.

Aman, Z. M., Akhfash, M., Johns, M. L., & May, E. F. (2014). Methane hydrate bed formation in a visual autoclave: cold restart and Reynolds number dependence. *Journal of Chemical & Engineering Data, 60*(2), 409-417.

Aman, Z. M., & Koh, C. A. (2016). Interfacial phenomena in gas hydrate systems. *Chemical Society Reviews, 45*(6), 1678-1690.

Amani, M., & Hjeij, D. (2015). *A comprehensive review of corrosion and its Inhibition in the oil and gas industry.* Paper presented at the SPE Kuwait Oil and Gas Show and Conference.

Anderson, R., Mozaffar, H., & Tohidi, B. (2011). *Development of a crystal growth inhibition based method for the evaluation of kinetic hydrate inhibitors.* Paper presented at the Proceedings of the 7th International Conference on Gas Hydrates.

Arthur, D. E., Jonathan, A., Ameh, P. O., & Anya, C. (2013). A review on the assessment of polymeric materials used as corrosion inhibitor of metals and alloys. *International Journal of Industrial Chemistry, 4*(1), 2.

Ballard, A. (2006). *Flow-assurance lessons: the Mica tieback.* Paper presented at the Offshore Technology Conference.

Ben-Naim, A. (1975). Hydrophobic interaction and structural changes in the solvent. *Biopolymers, 14*(7), 1337-1355.

Bidle, K. A., Kastner, M., & Bartlett, D. H. (1999). A phylogenetic analysis of microbial communities associated with methane hydrate containing marine fluids and sediments in the Cascadia margin (ODP site 892B). *FEMS Microbiology Letters, 177*(1), 101-108.

Brondel, D., Edwards, R., Hayman, A., Hill, D., Mehta, S., & Semerad, T. (1987). Corrosion in the oil industry. *Journal of Petroleum Technology, 39*, 756-762.

Burgazli, C., Navarrete, R., & Mead, S. (2005). New dual purpose chemistry for gas hydrate and corrosion inhibition. *Journal of Canadian Petroleum Technology, 44*(11).

Carroll, J. (2009). *Natural gas hydrates: A guide for engineers*: Gulf Professional Publishing.

Cha, M., Shin, K., Seo, Y., Shin, J.-Y., & Kang, S.-P. (2013). Catastrophic growth of gas hydrates in the presence of kinetic hydrate inhibitors. *The Journal of Physical Chemistry A, 117*(51), 13988-13995.

Christiansen, R. L., & Sloan, E. D. (1994). Mechanisms and kinetics of hydrate formation. *Annals of the New York Academy of Sciences, 715*(1), 283-305.

Chua, P. C., Kelland, M. A., Hirano, T., & Yamamoto, H. (2012a). Kinetic hydrate inhibition of poly(N-isopropylacrylamide)s with different tacticities. *Energy & Fuels, 26*(8), 4961-4967.

Chua, P. C., Kelland, M. A., Ishitake, K., Satoh, K., Kamigaito, M., & Okamoto, Y. (2012b). Kinetic hydrate inhibition of poly(N-isopropylmethacrylamide)s with different tacticities. *Energy & Fuels, 26*(6), 3577-3585.

Clark, L. W., Frostman, L. M., & Anderson, J. (2005). *Low dosage hydrate inhibitors (LDHI): Advances in flow assurance technology for offshore gas production systems.* Paper presented at the International Petroleum Technology Conference.

Cochran, S. (2003). *Hydrate control and remediation best practices in deepwater oil developments.* Paper presented at the Offshore Technology Conference.

Cox, J. L. (1983). *Natural gas hydrates: Properties, occurrence and recovery*. Boston: Butterworth Pub.

Dariva, C. G., & Galio, A. F. (2014). Corrosion inhibitors – principles, mechanisms and applications *Developments in corrosion protection*: InTech.

Dashti, H., Yew, L. Z., & Lou, X. (2015). Recent advances in gas hydrate-based CO 2 capture. *Journal of Natural Gas Science and Engineering, 23*, 195-207.

Del Villano, L., & Kelland, M. A. (2011). An investigation into the laboratory method for the evaluation of the performance of kinetic hydrate inhibitors using superheated gas hydrates. *Chemical Engineering Science, 66*(9), 1973-1985.

Denniel, S., Perrin, J., & Felix-Henry, A. (2004). *Review of flow assurance solutions for deepwater fields.* Paper presented at the Offshore Technology Conference.

Dhapte, V., & Mehta, P. (2015). Advances in hydrotropic solutions: an updated review. *St. Petersburg Polytechnical University Journal: Physics and Mathematics, 1*(4), 424-435.

Di Lorenzo, M., Aman, Z. M., Sanchez Soto, G., Johns, M., Kozielski, K. A., & May, E. F. (2014). Hydrate formation in gas-dominant systems using a single-pass flowloop. *Energy & Fuels, 28*(5), 3043-3052.

Dirdal, E. G., Arulanantham, C., Sefidroodi, H., & Kelland, M. A. (2012). Can cyclopentane hydrate formation be used to rank the performance of kinetic hydrate inhibitors? *Chemical Engineering Science, 82*, 177-184.

Duchateau, C., Glénat, P., Pou, T.-E., Hidalgo, M., & Dicharry, C. (2009a). Hydrate precursor test method for the laboratory evaluation of kinetic hydrate inhibitors. *Energy & Fuels, 24*(1), 616-623.

Duchateau, C., Peytavy, J.-L., Glénat, P., Pou, T.-E., Hidalgo, M., & Dicharry, C. (2009b). Laboratory evaluation of kinetic hydrate inhibitors: a procedure for enhancing the repeatability of test results. *Energy & Fuels, 23*(2), 962-966.

Duchateau, C., Pou, T.-E., Hidalgo, M., Glénat, P., & Dicharry, C. (2012). Interfacial measurements for laboratory evaluation of kinetic hydrate inhibitors. *Chemical Engineering Science, 71*, 220-225.

Duncan, K. E., Perez-Ibarra, B. M., Jenneman, G., Harris, J. B., Webb, R., & Sublette, K. (2014). The effect of corrosion inhibitors on microbial communities associated with corrosion in a model flow cell system. *Applied microbiology and biotechnology, 98*(2), 907-918.

Durnie, W., De Marco, R., Jefferson, A., & Kinsella, B. (1999). Development of a structure-activity relationship for oil field corrosion inhibitors. *Journal of the Electrochemical Society, 146*(5), 1751-1756.

Eduok, U., Faye, O., & Szpunar, J. (2016). Corrosion inhibition of X70 sheets by a film-forming imidazole derivative at acidic pH. *RSC Advances, 6*(110), 108777-108790.

Edwards, A., Osborne, C., Webster, S., Klenerman, D., Joseph, M., Ostovar, P., & Doyle, M. (1994). Mechanistic studies of the corrosion inhibitor oleic imidazoline. *Corrosion Science, 36*(2), 315-325.

Englezos, P. (1993). Clathrate hydrates. *Industrial & Engineering Chemistry Research, 32*(7), 1251-1274.

Englezos, P., Kalogerakis, N., Dholabhai, P. D., & Bishnoi, P. R. (1987). Kinetics of formation of methane and ethane gas hydrates. *Chemical Engineering Science, 42*(11), 2647-2658.

English, N. J., & MacElroy, J. (2015). Perspectives on molecular simulation of clathrate hydrates: Progress, prospects and challenges. *Chemical Engineering Science, 121*, 133-156.

Feng, Y., Billon, L., Grassl, B., Khoukh, A., & François, J. (2002). Hydrophobically associating polyacrylamides and their partially hydrolyzed derivatives prepared by post-modification. 1. Synthesis and characterization. *Polymer, 43*(7), 2055-2064.

Finšgar, M., & Jackson, J. (2014). Application of corrosion inhibitors for steels in acidic media for the oil and gas industry: A review. *Corrosion Science, 86*, 17-41.

Franks, F., Pedley, M., & Reid, D. S. (1976). Solute interactions in dilute aqueous solutions. Part 1.—Microcalorimetric study of the hydrophobic interaction. *Journal of the Chemical Society, Faraday Transactions 1: Physical Chemistry in Condensed Phases, 72*, 359-367.

Free, M. L. (2002). Understanding the effect of surfactant aggregation on corrosion inhibition of mild steel in acidic medium. *Corrosion Science, 44*(12), 2865-2870.

Frostman, L., Gallagher, C., Ramachandran, S., & Weispfennig, K. (2001). *Ensuring systems compatibility for deepwater chemicals.* Paper presented at the SPE International Symposium on Oilfield Chemistry.

Frostman, L., Thieu, V., Crosby, D., & Downs, H. (2003). *Low-dosage hydrate inhibitors (LDHIs): Reducing costs in existing systems and designing for the future.* Paper presented at the International Symposium on Oilfield Chemistry.

Fu, B. (2007). *Development of non-interfering corrosion inhibitors for sour gas pipelines with co-injection of kinetic hydrate inhibitors.* Paper presented at the CORROSION 2007.

Fu, S., Cenegy, L., & Neff, C. (2001). *A summary of successful field applications of a kinetic hydrate inhibitor.* Paper presented at the SPE International Symposium on Oilfield Chemistry.

Fuchs-Godec, R. (2006). The adsorption, CMC determination and corrosion inhibition of some N-alkyl quaternary ammonium salts on carbon steel surface in 2M H2SO4. *Colloids and Surfaces A: Physicochemical and Engineering Aspects, 280*(1), 130-139.

Gao, S. (2008). Investigation of interactions between gas hydrates and several other flow assurance elements. *Energy & Fuels, 22*(5), 3150-3153.

Gbaruko, B., Igwe, J., Gbaruko, P., & Nwokeoma, R. (2007a). Gas hydrates and clathrates: Flow assurance, environmental and economic perspectives and the Nigerian liquified natural gas project. *Journal of Petroleum Science and Engineering, 56*(1), 192-198.

Gbaruko, B. C., Igwe, J. C., Gbaruko, P. N., & Nwokeoma, R. C. (2007b). Gas hydrates and clathrates: Flow assurance, environmental and economic perspectives and the Nigerian liquified natural gas project. *Journal of Petroleum Science and Engineering, 56*(1), 192-198.

Gece, G. (2008). The use of quantum chemical methods in corrosion inhibitor studies. *Corrosion Science, 50*(11), 2981-2992.

Geethanjali, R., Sabirneeza, A., & Subhashini, S. (2014). Water-soluble and biodegradable pectin-grafted polyacrylamide and pectin-grafted polyacrylic acid: electrochemical investigation of corrosion-inhibition behaviour on mild steel in 3.5% NaCl media. *Indian Journal of Materials Science, 2014*.

Gjertsen, L. H., & Fadnes, F. H. (2000). Measurements and predictions of hydrate equilibrium conditions. *Annals of the New York Academy of Sciences, 912*(1), 722-734.

Gregg, M., & Ramachandran, S. (2004). *Review of corrosion inhibitor developments and testing for offshore oil and gas production systems.* Paper presented at the CORROSION 2004.

Greim, H., Bury, D., Klimisch, H.-J., Oeben-Negele, M., & Ziegler-Skylakakis, K. (1998). Toxicity of aliphatic amines: Structure-activity relationship. *Chemosphere, 36*(2), 271-295.

Hammerschmidt, E. (1934). Formation of gas hydrates in natural gas transmission lines. *Industrial & Engineering Chemistry, 26*(8), 851-855.

Hansen, C. M. (2007). *Hansen solubility parameters: A user's handbook*. United States: Taylor & Francis Group.

Hatch, G. B., & Ralston, P. H. (1969). United States Patent No. 3483133A.

Hawtin, R. W., Quigley, D., & Rodger, P. M. (2008). Gas hydrate nucleation and cage formation at a water/methane interface. *Physical Chemistry Chemical Physics, 10*(32), 4853-4864.

Hemmingsen, P. V., Li, X., & Kinnari, K. (2008). *Hydrate plugging potential in underinhibited systems*. Paper presented at the 6th International Conference on Gas Hydrates, Vancouver, British Columbia, Canada.

Hluchan, V., Wheeler, B., & Hackerman, N. (1988). Amino acids as corrosion inhibitors in hydrochloric acid solutions. *Materials and corrosion, 39*(11), 512-517.

hoon Sohn, Y., Kim, J., Shin, K., Chang, D., Seo, Y., Aman, Z. M., & May, E. F. (2015). Hydrate plug formation risk with varying watercut and inhibitor concentrations. *Chemical Engineering Science, 126*, 711-718.

Hoppe, R., Martin, R. L., Pakulski, M. K., & Schaffer, T. D. (2006). *Corrosion mitigation with gas hydrate inhibitors.* Paper presented at the SPE Gas Technology Symposium.

Hoseinzadeh, A., Danaee, I., Maddahy, M., & Avei, M. R. (2014). Taurine as a green corrosion inhibitor for Aisi 4130 steel alloy in hydrochloric acid solution. *Chemical Engineering Communications, 201*(3), 380-402.

Huang, C., Fennema, O., & Powrie, W. (1966). Gas hydrates in aqueous-organic systems: II. Concentration by gas hydrate formation. *Cryobiology, 2*(5), 240-245.

Hunt, A. (1996). Fluid properties determine flow line blockage potential. *Oil and Gas journal, 94*(29), 62-66.

Igboanusi, U. P., & Opara, A. C. (2011). The advancement from thermodynamic inhibitors to kinetic inhibitors and anti-agglomerants in natural gas flow assurance. *International Journal of Chemical and Environmental Engineering, 2*(2), 131-134.

Jacobson, L. C., Hujo, W., & Molinero, V. (2010). Amorphous precursors in the nucleation of clathrate hydrates. *Journal of the American Chemical Society, 132*(33), 11806-11811.

Jones, R., Morales, N., Anthony, J., Webber, P. A., & Harrington, R. (2013). *Development of a novel kinetic hydrate inhibitor and corrosion inhibitor package for wet gas application.* Paper presented at the OTC Brasil.

Jordan, M., Sjuraether, K., Collins, I., Feasey, N., & Emmons, D. (2001). *Life cycle management of scale control within subsea fields and its impact on flow assurance, Gulf of Mexico and the North Sea basin.* Paper presented at the SPE Annual Technical Conference and Exhibition.

Joshi, S. V., Grasso, G. A., Lafond, P. G., Rao, I., Webb, E., Zerpa, L. E., . . . Sum, A. K. (2013). Experimental flowloop investigations of gas hydrate formation in high water cut systems. *Chemical Engineering Science, 97*, 198-209.

Jovancicevic, V., Ramachandran, S., & Prince, P. (1999). Inhibition of carbon dioxide corrosion of mild steel by imidazolines and their precursors. *Corrosion, 55*(5), 449-455.

Kadiri, M. (2010). *Physicochemical changes to soil and sediment in managed realignment sites following tidal inundation.* Queen Mary University of London.

Kanu, A., Al-Hajri, N., Messaoud, Y., & Ono, N. (2014). *Mitigating hydrates in subsea oil flowlines: Consider production flow monitoring and control.* Paper presented at the IPTC 2014: International Petroleum Technology Conference.

Ke, W., & Kelland, M. A. (2016). Kinetic hydrate inhibitor studies for gas hydrate systems: A review of experimental equipment and test methods. *Energy & Fuels, 30*(12), 10015-10028.

Ke, W., Svartaas, T. M., & Abay, H. K. (2011). *An experimental study on sI hydrate formation in presence of methanol, PVP and PVCap in an isochoric cell.* Paper presented at the Proceedings of the 7th International Conference on Gas Hydrates.

Kelland, M. A. (2006). History of the development of low dosage hydrate inhibitors. *Energy & Fuels, 20*(3), 825-847.

Kelland, M. A. (2009). *Production chemicals for the oil and gas industry*. Boca Raton: CRC Press.

Kelland, M. A. (2011). *A review of kinetic hydrate inhibitors: Tailor-made water-soluble polymers for oil and gas industry applications* (Vol. 8). New York: Nova Science Publishers, Inc.

Kelland, M. A. (2014). *Production chemicals for the oil and gas industry*. Boca Raton: CRC press.

Kelland, M. A., & Iversen, J. E. (2010). Kinetic hydrate inhibition at pressures up to 760 bar in deep water drilling fluids. *Energy & Fuels, 24*(5), 3003-3013.

Kelland, M. A., Svartaas, T. M., Øvsthus, J., & Namba, T. (2000). A new class of kinetic hydrate inhibitor. *Annals of the New York Academy of Sciences, 912*, 281-293.

Kermani, M., & Harrop, D. (1996). The impact of corrosion on oil and gas industry. *SPE Production & Facilities, 11*(03), 186-190.

Kim, E., Lee, S., Lee, J. D., & Seo, Y. (2016). Enclathration of tert-butyl alcohol in sII hydrates and its implications in gas storage and CO2 sequestration. *Fuel, 164*, 237-244.

Kim, J., Shin, K., Seo, Y., Cho, S. J., & Lee, J. D. (2014). Synergistic hydrate inhibition of monoethylene glycol with poly (vinylcaprolactam) in thermodynamically underinhibited system. *The Journal of Physical Chemistry B, 118*(30), 9065-9075.

Klomp, U., & Mehta, A. (2007). *Validation of kinetic inhibitors for sour gas fields.* Paper presented at the IPTC 2007: International Petroleum Technology Conference.

Koh, C. A. (2002). Towards a fundamental understanding of natural gas hydrates. *Chemical Society Reviews, 31*(3), 157-167.

Koh, C. A., Sloan, E. D., Sum, A. K., & Wu, D. T. (2011). Fundamentals and applications of gas hydrates. *Annual Review of Chemical and Biomolecular Engineering, 2*, 237-257.

Koh, C. A., Sum, A. K., & Sloan, E. D. (2012). State of the art: Natural gas hydrates as a natural resource. *Journal of Natural Gas Science and Engineering, 8*, 132-138.

Koh, C. A., Westacott, R., Zhang, W., Hirachand, K., Creek, J., & Soper, A. (2002). Mechanisms of gas hydrate formation and inhibition. *Fluid Phase Equilibria, 194*, 143-151.

Kuang, W., & Gao, C. (2014). Synthesis and characterization of novel twin-tailed hydrophobically associated copolymers and their applications to Cr (III) removal from aqueous solutions. *Journal of Applied Polymer Science, 131*(21).

Kumar, A., Sakpal, T., Linga, P., & Kumar, R. (2013). Influence of contact medium and surfactants on carbon dioxide clathrate hydrate kinetics. *Fuel, 105*, 664-671.

Kumar, V. S., Raja, C., & Jayakumar, C. (2014). A review on solubility enhancement using hydrotropic phenomena. *International journal of Pharmacy and Pharmaceutical Sciences, 6*(6), 1-7.

Kunz, W., Holmberg, K., & Zemb, T. (2016). Hydrotropes. *Current Opinion in Colloid & Interface Science, 22*, 99-107.

Kutz, M. (2015). *Mechanical engineers' handbook, volume 1: Materials and engineering mechanics*. Hoboken, New Jersey: John Wiley & Sons.

Kvamme, B. (1996). A new theory for kinetics of hydrate formation. *Proceedings of the 2nd International Conference on Natural Gas Hydrates*, 139–146.

Kvenvolden, K. A., & McMenamin, M. A. (1980). Hydrates of natural gas: a review of their geologic occurrence. Arlington, VA: U.S. Geological Survey.

Lauricella, M., Meloni, S., English, N. J., Peters, B., & Ciccotti, G. (2014). Methane clathrate hydrate nucleation mechanism by advanced molecular simulations. *The Journal of Physical Chemistry C, 118*(40), 22847-22857.

Lee, J., Hampton, B. J., Alapati, R. R., Sanford, E. A., & O'Brien, S. (2009). *Flow assurance: innovative technique for flowline plug remediation.* Paper presented at the Offshore Technology Conference.

Lee, J., Park, S., & Sung, W. (2010). An experimental study on the productivity of dissociated gas from gas hydrate by depressurization scheme. *Energy Conversion and Management, 51*(12), 2510-2515.

Lervik, J. K., Kulbotten, H., & Klevjer, G. (1997). *Prevention of hydrate formation in pipelines by electrical methods.* Paper presented at the The Seventh International Offshore and Polar Engineering Conference.

Li, X.-S., Xu, C.-G., Zhang, Y., Ruan, X.-K., Li, G., & Wang, Y. (2016). Investigation into gas production from natural gas hydrate: A review. *Applied Energy, 172*, 286-322.

Lone, A., & Kelland, M. A. (2013). Exploring kinetic hydrate inhibitor test methods and conditions using a multicell steel rocker rig. *Energy & Fuels, 27*(5), 2536-2547.

Long, j., Lederhos, j., Sum, A., Christiansen, R., & Sloan, E. D. (1994). *Kinetic inhibitors of natural gas hydrates*. Paper presented at the 73rd Annual GPA Convention, New Orleans, Louisiana.

Loveday, J., Nelmes, R., Guthrie, M., & Belmonte, S. (2001). Stable methane hydrate above 2 GPa and the source of Titan's atmospheric methane. *Nature, 410*(6829), 661.

Lucas, E. F., Spinelli, L. S., & Khalil, C. N. (2002). Polymers applications in petroleum production. *Encyclopedia of Polymer Science and Technology*.

Mady, M. F., & Kelland, M. A. (2014). N, N-Dimethylhydrazidoacrylamides. Part 1: Copolymers with N-Isopropylacrylamide as novel high-cloud-point kinetic hydrate inhibitors. *Energy & Fuels, 28*(9), 5714-5720.

Mady, M. F., & Kelland, M. A. (2015). N, N-Dimethylhydrazidoacrylamides. Part 2: High-cloud-point kinetic hydrate inhibitor copolymers with N-Vinylcaprolactam and effect of pH on performance. *Energy & Fuels, 29*(2), 678-685.

Maeda, N. (2014). Measurements of gas hydrate formation probability distributions on a quasi-free water droplet. *Review of Scientific Instruments, 85*(6), 065115.

Maeda, N., Fong, C., Sheng, Q., Silveira, K. C. d., Tian, W., Seeber, A., . . . Wood, C. D. (2016). High-throughput testing of kinetic hydrate inhibitors. *Energy & Fuels, 30*(7), 5432-5438.

Maeda, N., Wells, D., Becker, N. C., Hartley, P. G., Wilson, P. W., Haymet, A. D., & Kozielski, K. A. (2011). Development of a high pressure automated lag time apparatus for experimental studies and statistical analyses of nucleation and growth of gas hydrates. *Review of Scientific Instruments, 82*(6), 065109.

Maege, I., Jaehne, E., Henke, A., Adler, H.-J. P., Bram, C., Jung, C., & Stratmann, M. (1998). Self-assembling adhesion promoters for corrosion resistant metal polymer interfaces. *Progress in Organic Coatings, 34*(1), 1-12.

Makogon, Y., Makogon, T., & Holditch, S. (2000a). Kinetics and mechanisms of gas hydrate formation and dissociation with inhibitors. *Annals of the New York Academy of Sciences, 912*(1), 777-796.

Makogon, Y. F. (1981). *Hydrates of natural gas*. Tulsa, OKlahoma: PennWell Publishing Company.

Makogon, Y. F. (1997). *Hydrates of hydrocarbons*. Tulsa, Oklahoma: Pennwell Publishing Company.

Makogon, Y. F., Makogon, T. Y., & Holditch, S. A. (2000b). Kinetics and mechanisms of gas hydrate formation and dissociation with inhibitors. *Annals of the New York Academy of Sciences, 912*(1), 777-796.

Mao, W. L., Mao, H.-k., Goncharov, A. F., Struzhkin, V. V., Guo, Q., Hu, J., . . . Zhao, Y. (2002). Hydrogen clusters in clathrate hydrate. *Science, 297*(5590), 2247-2249.

Martínez, D., Gonzalez, R., Montemayor, K., Juarez-Hernandez, A., Fajardo, G., & Hernandez-Rodriguez, M. (2009). Amine type inhibitor effect on corrosion–erosion wear in oil gas pipes. *Wear, 267*(1), 255-258.

May, E. F., Wu, R., Kelland, M. A., Aman, Z. M., Kozielski, K. A., Hartley, P. G., & Maeda, N. (2014). Quantitative kinetic inhibitor comparisons and memory effect

measurements from hydrate formation probability distributions. *Chemical Engineering Science, 107*, 1-12.
Meakins, R. (1963). Alkyl quaternary ammonium compounds as inhibitors of the acid corrosion of steel. *Journal of Applied Chemistry, 13*(8), 339-345.
Mehta, A., Hebert, P., Cadena, E., & Weatherman, J. (2002). *Fulfilling the promise of low dosage hydrate inhibitors: journey from academic curiosity to successful field implementation.* Paper presented at the Offshore Technology Conference.
Mercer, A., & Lumbard, E. (1995). Corrosion of mild steel in water. *British Corrosion Journal, 30*(1), 43-55.
Mokhatab, S., & Poe, W. A. (2012). *Handbook of natural gas transmission and processing*. United States: Gulf Professional Publishing.
Mokhatab, S., Wilkens, R. J., & Leontaritis, K. J. (2007). A review of strategies for solving gas-hydrate problems in subsea pipelines. *Energy Sources, Part A: Recovery, Utilization, and Environmental Effects, 29*(1), 39-45.
Moloney, J., Mok, W. Y., & Gamble, C. G. (2009). *Compatible corrosion and kinetic hydrate inhibitors for wet sour gas transmission lines.* Paper presented at the CORROSION 2009.
Moon, C., Taylor, P. C., & Rodger, P. M. (2003). Molecular dynamics study of gas hydrate formation. *Journal of the American Chemical Society, 125*(16), 4706-4707.
Moore, J., Vers, L. V., & Conrad, P. (2009). *Flow assurance: Understanding kinetic hydrate inhibitor and corrosion inhibitor interactions.* Paper presented at the Offshore Technology Conference.
Moussa, M., El-Far, A., & El-Shafei, A. (2007). The use of water-soluble hydrazones as inhibitors for the corrosion of C-steel in acidic medium. *Materials chemistry and physics, 105*(1), 105-113.
Mulet, X., Conn, C. E., Fong, C., Kennedy, D. F., Moghaddam, M. J., & Drummond, C. J. (2013). High-throughput development of amphiphile self-assembly materials: fast-tracking synthesis, characterization, formulation, application, and understanding. *Accounts of chemical research, 46*(7), 1497-1505.
Musa, O. M., & Lei, C. (2016). United States Patent No. 9493598B2.
Musa, O. M., Lei, C., & Narayanan, K. S. (2011). United Stated Patent No. 20110277844A1.
Nakarit, C., Kelland, M. A., Liu, D., & Chen, E. Y.-X. (2013). Cationic kinetic hydrate inhibitors and the effect on performance of incorporating cationic monomers into N-vinyl lactam copolymers. *Chemical Engineering Science, 102*, 424-431.
Needham, R. B., & Doe, P. H. (1987). Polymer flooding review. *Journal of Petroleum Technology, 39*(12), 1,503-501,507.
Nimmo, B., & Hinds, G. (2003). Beginners guide to corrosion. NPL., UK.
O'Reilly, R., Ieong, N. S., Chua, P. C., & Kelland, M. A. (2011). Crystal growth inhibition of tetrahydrofuran hydrate with poly (N-vinyl piperidone) and other poly (N-vinyl lactam) homopolymers. *Chemical Engineering Science, 66*(24), 6555-6560.
O'Reilly, R., Ieong, N. S., Chua, P. C., & Kelland, M. A. (2011). Missing poly (N-vinyl lactam) kinetic hydrate inhibitor: High-pressure kinetic hydrate inhibition of structure II gas hydrates with poly (N-vinyl piperidone) and other poly (N-vinyl lactam) homopolymers. *Energy & Fuels, 25*(10), 4595-4599.
Obanijesu, E., Gubner, R., Barifcani, A., Pareek, V., & Tade, M. (2014). The influence of corrosion inhibitors on hydrate formation temperature along the subsea natural gas pipelines. *Journal of Petroleum Science and Engineering, 120*, 239-252.
Obanijesu, E. O., Pareek, V., Gubner, R., & Tade, M. O. (2010). Corrosion education as a tool for the survival of natural gas industry. *Nafta, 61*(12), 541-554.
Okafor, P., Liu, X., & Zheng, Y. (2009). Corrosion inhibition of mild steel by ethylamino imidazoline derivative in CO 2-saturated solution. *Corrosion Science, 51*(4), 761-768.
Palmer, J. W., Hedges, W., & Dawson, J. L. (2004). The use of corrosion inhibitors in oil and gas production *European Fedration of Corrosoin Publications NUMBER 39*. London, UK: Maney Publishing.

Park, J., Kim, H., Sheng, Q., Wood, C. D., & Seo, Y. (2017a). Kinetic hydrate inhibition performance of poly(vinyl caprolactam) modified with corrosion inhibitor groups. *Energy & Fuels, 31*(9), 9363-9373.

Park, J., Silveira, K. C. d., Sheng, Q., Wood, C. D., & Seo, Y. (2017b). Performance of poly(N-isopropylacrylamide)-based kinetic hydrate inhibitors for nucleation and growth of natural gas hydrates. *Energy & Fuels, 31*(3), 2697-2704.

Park, S.-N., Park, J.-C., Kim, H. O., Song, M. J., & Suh, H. (2002). Characterization of porous collagen/hyaluronic acid scaffold modified by 1-ethyl-3-(3-dimethylaminopropyl) carbodiimide cross-linking. *Biomaterials, 23*(4), 1205-1212.

Pattee, F., & Kopp, F. (2000). *Impact of electrically-heated systems on the operation of deep water subsea oil flowlines.* Paper presented at the Offshore Technology Conference.

Perrin, A., Musa, O. M., & Steed, J. W. (2013). The chemistry of low dosage clathrate hydrate inhibitors. *Chem Soc Rev, 42*(5), 1996-2015.

Peytavy, J.-L., Glenat, P., & Bourg, P. (2007). *Kinetic hydrate inhibitors-sensitivity towards pressure and corrosion inhibitors.* Paper presented at the International Petroleum Technology Conference.

Pickering, P. F., Edmonds, B., Moorwood, R. A. S., Szczepanski, R., & Watson, M. J. (2001). *Evaluating new chemicals and alternatives for mitigating hydrates in oil and gas production* Paper presented at the IIR Conference, Aberdeen, Scotland.

Popoola, L. T., Grema, A. S., Latinwo, G. K., Gutti, B., & Balogun, A. S. (2013). Corrosion problems during oil and gas production and its mitigation. *International Journal of Industrial Chemistry, 4*(1), 35.

Purwanto, Y. A., Oshita, S., Seo, Y., & Kawagoe, Y. (2001). Concentration of liquid foods by the use of gas hydrate. *Journal of Food Engineering, 47*(2), 133-138.

Pyzer-Knapp, E. O., Suh, C., Gómez-Bombarelli, R., Aguilera-Iparraguirre, J., & Aspuru-Guzik, A. (2015). What is high-throughput virtual screening? A perspective from organic materials discovery. *Annual Review of Materials Research, 45*, 195-216.

Qin, H.-B., Sun, Z.-F., Wang, X.-Q., Yang, J.-L., Sun, C.-Y., Liu, B., . . . Chen, G.-J. (2015). Synthesis and evaluation of two new kinetic hydrate inhibitors. *Energy & Fuels, 29*(11), 7135-7141.

Radhakrishnan, R., & Trout, B. L. (2002). A new approach for studying nucleation phenomena using molecular simulations: application to CO2 hydrate clathrates. *The Journal of Chemical Physics, 117*(4), 1786-1796.

Ree, L. H., Kelland, M. A., Roth, P. J., & Batchelor, R. (2016). First investigation of modified poly (2-vinyl-4, 4-dimethylazlactone) s as kinetic hydrate inhibitors. *Chemical Engineering Science, 152*, 248-254.

Ree, L. H., Mady, M. F., & Kelland, M. A. (2015). N, N-dimethylhydrazidoacrylamides. Part 3: Improving kinetic hydrate inhibitor performance using polymers of N, N-dimethylhydrazidomethacrylamide. *Energy & Fuels, 29*(12), 7923-7930.

Ribeiro, C. P., & Lage, P. L. C. (2008). Modelling of hydrate formation kinetics: State-of-the-art and future directions. *Chemical Engineering Science, 63*(8), 2007-2034.

Ripmeester, J., & Davidson, D. (1977). Some new clathrate hydrates. *Molecular Crystals and Liquid Crystals, 43*(3-4), 189-195.

Roy, B., & Moulik, S. (2003). Effect of hydrotropes on solution behaviour of amphiphiles. *Current Science*, 1148-1155.

Sami, N. A., Sangwai, J. S., & Balasubramanian, N. (2013). Gas hydrate applications and problems in oil and gas industry. *International Journal of Scientific & Engineering Research, 4*(8).

Sassen, R., & MacDonald, I. R. (1994). Evidence of structure H hydrate, Gulf of Mexico continental slope. *Organic Geochemistry, 22*(6), 1029-1032.

Sefidroodi, H., Abrahamsen, E., & Kelland, M. A. (2013). Investigation into the strength and source of the memory effect for cyclopentane hydrate. *Chemical Engineering Science, 87*, 133-140.

Sehgal, D., & Vijay, I. K. (1994). A method for the high efficiency of water-soluble carbodiimide-mediated amidation. *Analytical biochemistry, 218*(1), 87-91.

Seo, Y., Kang, S.-P., & Jang, W. (2009). Structure and composition analysis of natural gas hydrates: 13C NMR spectroscopic and gas uptake measurements of mixed gas hydrates. *The Journal of Physical Chemistry A, 113*(35), 9641-9649.

Shahnazar, S., Bagheri, S., Termeh Yousefi, A., Mehrmashhadi, J., Sayuti Abd Karim, M., & Adib Kadri, N. (2018). Structure, mechanism, and performance evaluation of natural gas hydrate kinetic inhibitors. *Reviews in Inorganic Chemistry, 38*(1), 1-19.

Sharifi, H., Walker, V. K., Ripmeester, J., & Englezos, P. (2014). Insights into the behavior of biological clathrate hydrate inhibitors in aqueous saline solutions. *Crystal Growth & Design, 14*(6), 2923-2930.

Sheng, Q., Silveira, K. C. d., Tian, W., Fong, C., Maeda, N., Gubner, R., & Wood, C. D. (2017). Simultaneous hydrate and corrosion inhibition with modified poly (vinyl caprolactam) polymers. *Energy & Fuels, 31*(7), 6724-6731.

Sheng, Q., Tian, W., Lapierre, F., Gao, S., Mulder, R. J., Zhu, Y., . . . Wood, C. D. (2014). Arrays of polyacrylamide hydrogels using a carbodiimide-mediated crosslinking reaction. *Journal of Applied Polymer Science, 131*(12), 40416.

Shtanko, N. I., Lequieu, W., Goethals, E. J., & Du Prez, F. E. (2003). pH- and thermo-responsive properties of poly(N-vinylcaprolactam-co-acrylic acid) copolymers. *Polymer International, 52*(10), 1605-1610.

Silveira, K. C. d., Sheng, Q., Tian, W., Fernandes Lucas, E., & Wood, C. D. (2015). Libraries of modified polyacrylamides using post-synthetic modification. *Journal of Applied Polymer Science, 132*(47), 42797.

Silveira, K. C. d., Sheng, Q., Tian, W., Fong, C., Maeda, N., Lucas, E. F., & Wood, C. D. (2017). High throughput synthesis and characterization of PNIPAM-based kinetic hydrate inhibitors. *Fuel, 188*, 522-529.

Sinquin, A., Palermo, T., & Peysson, Y. (2004). Rheological and flow properties of gas hydrate suspensions. *Oil & gas science and technology, 59*(1), 41-57.

Sira, J., Patil, S., & Kamath, V. (1990). *Study of hydrate dissociation by methanol and glycol injection.* Paper presented at the SPE Annual technical conference and exhibition.

Sloan, E. D. (2000). *Hydrate engineering (Digital Edition)*. Richardson, TX, USA: Society of Petroleum Engineers.

Sloan, E. D. (2003). Fundamental principles and applications of natural gas hydrates. *Nature, 426*(6964), 353-363.

Sloan, E. D. (2010). *Natural gas hydrates in flow assurance*: Gulf Professional Publishing.

Sloan, E. D., & Earle, D. (1995). United States Patent No. 5432292A.

Sloan, E. D., & Fleyfel, F. (1991). A molecular mechanism for gas hydrate nucleation from ice. *AIChE Journal, 37*(9), 1281-1292.

Sloan, E. D., & Koh, C. (2007). *Clathrate hydrates of natural gases*. Boca Raton, FL: CRC Press/Taylor & Francis.

Sloan, E. D., Koh, C. A., & Sum, A. (2010). *Natural gas hydrates in flow assurance*: Gulf Professional Publishing.

Sowa, B., & Maeda, N. (2015). Statistical study of the memory effect in model natural gas hydrate systems. *The Journal of Physical Chemistry A, 119*(44), 10784-10790.

Stern, L. A., Kirby, S. H., & Durham, W. B. (1996). Peculiarities of methane clathrate hydrate formation and solid-state deformation, including possible superheating of water ice. *Science, 273*(5283), 1843.

Sun, M., Hu, R., Yu, H., Zhao, B., & Ren, H. (2015, 15-17 Oct. 2015). *Intracranial hemorrhage detection by 3D voxel segmentation on brain CT images.* Paper presented at the 2015 International Conference on Wireless Communications & Signal Processing (WCSP).

Sun, Z.-G., Fan, S.-S., Guo, K.-H., Shi, L., Guo, Y.-K., & Wang, R.-Z. (2002). Gas hydrate phase equilibrium data of cyclohexane and cyclopentane. *Journal of Chemical & Engineering Data, 47*(2), 313-315.

Tang, C., Dai, X., Du, J., Li, D., Zang, X., Yang, X., & Liang, D. (2010). Kinetic studies of gas hydrate formation with low-dosage hydrate inhibitors. *Science China Chemistry, 53*(12), 2622-2627.

Tariq, M., Rooney, D., Othman, E., Aparicio, S., Atilhan, M., & Khraisheh, M. (2014). Gas hydrate inhibition: A review of the role of ionic liquids. *Industrial & Engineering Chemistry Research, 53*(46), 17855-17868.

Taylor, K. C., & Nasr-El-Din, H. A. (1998). Water-soluble hydrophobically associating polymers for improved oil recovery: A literature review. *Journal of Petroleum Science and Engineering, 19*(3), 265-280.

Ting, S. G., & Crestwood, M. (1974). United States Patent No. 3819328A.

Tiu, B. D. B., & Advincula, R. C. (2015). Polymeric corrosion inhibitors for the oil and gas industry: design principles and mechanism. *Reactive and Functional Polymers, 95*, 25-45.

Tohidi, B. (2014). Advances in avoiding gas hydrate problems. *Centre for Gas Hydrate Research & Hydrafact Ltd., Institute of Petroleum Engineering, Heriot-Watt University*, 1-47.

Tohidi, B., Burgass, R., Danesh, A., Østergaard, K., & Todd, A. (2000). Improving the accuracy of gas hydrate dissociation point measurements. *Annals of the New York Academy of Sciences, 912*(1), 924-931.

Tohidi Kalorazi, B. A., Ross; Azarinezhad -Mohammadi, Roghieh; Chapoy, Antonin; Valko, Ivan. (2008). Novel techniques in addressing gas hydrates and flow assurance: cold flow/hydraflow. *Paper presented at Africa/Middle East Oil and Gas Flow Assurance Summit, Cairo, Egypt*.

Tse, N. M., Kennedy, D. F., Moffat, B. A., Kirby, N., Caruso, R. A., & Drummond, C. J. (2012). High-throughput preparation of hexagonally ordered mesoporous silica and gadolinosilicate nanoparticles for use as MRI contrast agents. *ACS combinatorial science, 14*(8), 443-450.

Udachin, K. A., Ratcliffe, C. I., & Ripmeester, J. A. (2001). A dense and efficient clathrate hydrate structure with unusual cages. *Angewandte Chemie, 113*(7), 1343-1345.

Udachin, K. A., & Ripmeester, J. A. (1999). A complex clathrate hydrate structure showing bimodal guest hydration. *Nature, 397*, 420.

Valeur, E., & Bradley, M. (2009). Amide bond formation: beyond the myth of coupling reagents. *Chemical Society Reviews, 38*(2), 606-631.

Veluswamy, H. P., Kumar, S., Kumar, R., Rangsunvigit, P., & Linga, P. (2016). Enhanced clathrate hydrate formation kinetics at near ambient temperatures and moderate pressures: Application to natural gas storage. *Fuel, 182*, 907-919.

Walker, V. K., Zeng, H., Ohno, H., Daraboina, N., Sharifi, H., Bagherzadeh, S. A., . . . Englezos, P. (2015). Antifreeze proteins as gas hydrate inhibitors. *Canadian Journal of Chemistry, 93*(8), 839-849.

Wallwork, K. S., Kennedy, B. J., & Wang, D. (2007). *The high resolution powder diffraction beamline for the Australian Synchrotron.* Paper presented at the AIP Conference Proceedings.

Walsh, M. R., Koh, C. A., Sloan, E. D., Sum, A. K., & Wu, D. T. (2009). Microsecond simulations of spontaneous methane hydrate nucleation and growth. *Science, 326*(5956), 1095-1098.

Warrier, P., Khan, M. N., Srivastava, V., Maupin, C. M., & Koh, C. A. (2016). Overview: Nucleation of clathrate hydrates. *The Journal of Chemical Physics, 145*(21), 211705.

Woie, K. (2011). *A study of the interaction between a kinetic hydrate inhibitor and selected corrosion inhibitors.* University of Stavanger, Norway.

Wu, M., Wang, S., & Liu, H. (2007). A study on inhibitors for the prevention of hydrate formation in gas transmission pipeline. *Journal of Natural Gas Chemistry, 16*(1), 81-85.

Yagasaki, T., Matsumoto, M., & Tanaka, H. (2015). Adsorption mechanism of inhibitor and guest molecules on the surface of gas hydrates. *Journal of the American Chemical Society, 137*(37), 12079-12085.

Yan, X., Zou, C., & Qin, Y. (2014). A new sight of water-soluble polyacrylamide modified by β-cyclodextrin as corrosion inhibitor for X70 steel. *Starch-Stärke, 66*(11-12), 968-975.

Yang, M., Ma, B., Shao, H., Clark, A. M., & Wells, A. (2016). Macrophage phenotypic subtypes diametrically regulate epithelial-mesenchymal plasticity in breast cancer cells. *BMC Cancer, 16*(1), 419.

Zerpa, L. E., Salager, J.-L., Koh, C. A., Sloan, E. D., & Sum, A. K. (2010). Surface chemistry and gas hydrates in flow assurance. *Industrial & Engineering Chemistry Research, 50*(1), 188-197.

Zhang, D.-q., Gao, L.-x., Zhou, G.-d., & Lee, K. Y. (2008). Undecyl substitution in imidazole and its action on corrosion inhibition of copper in aerated acidic chloride media. *Journal of Applied Electrochemistry, 38*(1), 71-76.

Zhang, G., Rogers, R. E., French, W. T., & Lao, W. (2007). Investigation of microbial influences on seafloor gas-hydrate formations. *Marine chemistry, 103*(3), 359-369.

Zhang, H.-h., Pang, X., Zhou, M., Liu, C., Wei, L., & Gao, K. (2015). The behavior of pre-corrosion effect on the performance of imidazoline-based inhibitor in 3wt.% NaCl solution saturated with CO 2. *Applied Surface Science, 356*, 63-72.

Zhang, Z., Chen, S., Li, Y., Li, S., & Wang, L. (2009). A study of the inhibition of iron corrosion by imidazole and its derivatives self-assembled films. *Corrosion Science, 51*(2), 291-300.

Zhu, Z., Jian, O., Paillet, S., Desbrières, J., & Grassl, B. (2007). Hydrophobically modified associating polyacrylamide (HAPAM) synthesized by micellar copolymerization at high monomer concentration. *European polymer journal, 43*(3), 824-834.